Aus dem Max von Pettenkofer-Institut für Hygiene und Medizinische Mikrobiologie
Lehrstuhl: Bakteriologie
der Ludwig-Maximilians-Universität München

Kommissarische Leitung: Prof. Dr. Rainer Haas

Development and Application of a Novel Cag Type IV Secretion Reporter Assay in *Helicobacter pylori*

Dissertation
zum Erwerb des Doktorgrades der Naturwissenschaften
an der Medizinischen Fakultät
der Ludwig-Maximilians-Universität München

vorgelegt von
Franziska Maria Schindele
aus Kempten (Allgäu)

2016

Mit Genehmigung der Medizinischen Fakultät
der Universität München

Betreuer:	Prof. Dr. Rainer Haas
Zweitgutachter:	Prof. Dr. Andreas Ladurner
Dekan:	Prof. Dr. med. dent. Reinhard Hickel
Tag der mündlichen Prüfung:	30.03.2017

Eidesstattliche Versicherung

Ich, Franziska Maria Schindele, erkläre hiermit an Eides statt, dass ich die vorliegende Dissertation mit dem Thema

Development and Application of a Novel Cag Type IV Secretion Reporter Assay in *Helicobacter pylori*

selbständig verfasst, mich außer der angegebenen keiner weiteren Hilfsmittel bedient und alle Erkenntnisse, die aus dem Schrifttum ganz oder annähernd übernommen sind, als solche kenntlich gemacht und nach ihrer Herkunft unter Bezeichnung der Fundstelle einzeln nachgewiesen habe.
Ich erkläre des Weiteren, dass die hier vorgelegte Dissertation nicht in gleicher oder in ähnlicher Form bei einer anderen Stelle zur Erlangung eines akademischen Grades eingereicht wurde.

Ort, Datum Unterschrift

Teile dieser Arbeit wurden veröffentlicht unter folgendem Titel:

- **Schindele F**, Weiss E, Haas R, & Fischer W (2016) Quantitative analysis of CagA type IV secretion by *Helicobacter pylori* reveals substrate recognition and translocation requirements. *Mol Microbiol* 100(1):188-203.

Weitere Publikationen im Promotionszeitraum, die nicht in dieser Arbeit enthalten sind:

- Zhong Y, Anderl F, Kruse T, **Schindele F**, Jagusztyn-Krynicka EK, Fischer W, Gerhard M, & Mejías-Luque R (2016) *Helicobacter pylori* HP0231 influences bacterial virulence and is essential for gastric colonization. *PLoS One* 11(5):e0154643.
- Kaspar D, Auer F, Schardt J, **Schindele F**, Ospina A, Held C, Ehrenreich A, Scherer S, & Müller-Herbst S (2014) Temperature- and nitrogen source-dependent regulation of GlnR target genes in *Listeria monocytogenes*. *FEMS Microbiol Lett* 355(2):131-141.

CONTENTS

ABSTRACT

The gastric pathogen *Helicobacter pylori* infects approximately half of the world population. It colonizes the gastric mucosa persistently, causing various diseases including gastric cancer. As *H. pylori* becomes increasingly resistant to the current therapeutic antibiotics, alternative treatment strategies are urgently required. The development of gastric disorders is at least partly due to the *H. pylori* Cag type IV secretion system. This molecular machine transfers the bacterial oncoprotein CagA (cytotoxin-associated gene product A) into gastric cells. Inside the host cell, CagA hijacks intracellular signaling cascades, finally promoting gastric carcinogenesis. This work aimed to elucidate mechanisms of CagA translocation as well as to find substances which inhibit this process.

As alternative methods for analyzing CagA translocation are time-consuming and labor-intensive, a novel reporter system was established, which is based on the fusion of a TEM-1 β-lactamase to full-length CagA (TEM-CagA). TEM-CagA translocation by *H. pylori* into target cells can be monitored by TEM-1-mediated cleavage of the fluorescent β-lactam derivative CCF4. This fast, sensitive and highly specific method enables quantitative CagA translocation analysis by any fluorescence-assisted device. Applying this assay, CagA translocation dynamics as well as the type IV signal recognition and secretion process were investigated. Specifically, the impact of partially uncharacterized Cag components on CagA translocation efficiency was determined, and the stabilizing role of the CagA chaperone, CagF, further defined. It could be shown that the C-terminal secretion signal of CagA is defined rather by its minimal length than by a distinct signal sequence. A contribution of the foremost CagA N-terminus for signal recognition was excluded, while an extensive internal CagA domain was indispensable for CagA delivery. Moreover, CagA translocation was proven to depend on bacterial *de novo* protein synthesis and active host cellular processes.

To prevent CagA-induced carcinogenesis, anti-infectives which directly block CagA translocation into host cells would be most effective. Hence, the TEM-CagA assay was downscaled for screenings of compound libraries to identify specific Cag type IV secretion inhibitors for usage as therapeutic pathoblockers. This procedure resulted in preliminary identification of two related compounds that were able to specifically inhibit CagA translocation *in vitro*. In addition, these screening studies yielded other substances which were shown to specifically inhibit *H. pylori* growth *in vitro* by targeting its respiratory chain, and two of these substances were provisionally validated as potential new antibiotics. Thus, this work did not only contribute novel mechanistic insights into CagA translocation, but further revealed two promising approaches to treat infection with *H. pylori*.

ZUSAMMENFASSUNG

Etwa die Hälfte der Weltbevölkerung ist mit dem Magenkeim *Helicobacter pylori* infiziert. Dieses Bakterium persistiert in der Magenschleimhaut und ist Auslöser verschiedener Krankheiten, einschließlich Magenkrebs. Da *H. pylori* zunehmend Resistenzen gegen die derzeitigen therapeutischen Antibiotika ausbildet, werden alternative Behandlungsstrategien dringend benötigt. Ein maßgeblicher Faktor für die Entstehung der *H. pylori*-assoziierten Krankheitsbilder ist das Cag-Typ IV-Sekretionssystem. Diese molekulare Maschine transferiert das bakterielle Onkoprotein CagA (Zytotoxin-assoziiertes Genprodukt A) in Magenzellen. CagA übernimmt innerhalb der Wirtszelle die Kontrolle über intrazelluläre Signalkaskaden, was schließlich zur Karzinogenese führt. Diese Arbeit hatte zum Ziel, die Mechanismen der CagA-Translokation weiterführend aufzuklären und Substanzen zu finden, die diesen Prozess hemmen.

Bisherige Methoden zur Analyse der CagA-Translokation sind sehr zeit- und arbeitsintensiv. Daher wurde ein neues Reportersystem etabliert, welches auf einer Fusion der TEM-1 β-Laktamase an das CagA-Protein basiert (TEM-CagA). Die Translokation von TEM-CagA aus *H. pylori* in Zielzellen kann mittels der Spaltung des fluoreszierenden β-Laktam-Derivats CCF4 durch TEM-1 verfolgt werden. Dieses Prinzip ermöglicht eine Quantifizierung der CagA-Translokation durch Fluoreszenzmessung auf eine schnelle, sensitive und hochspezifische Weise. Mit Hilfe dieses Verfahrens wurden die Dynamik der CagA-Translokation und der Typ IV-Signalerkennungs- und Sekretionsprozess untersucht. Dabei wurde der Einfluss einiger wenig charakterisierter Komponenten auf die CagA-Translokation überprüft und die stabilisierende Rolle des CagA Chaperons CagF weitergehend definiert. Es konnte gezeigt werden, dass das C-terminale Sekretionssignal von CagA eher durch eine minimale Länge als durch eine spezifische Signalsequenz bestimmt wird. Eine Beteiligung des äußersten N-terminus von CagA bei der Signalerkennung wurde ausgeschlossen, während die Notwendigkeit eines ausgedehnten internen CagA-Bereichs für die CagA-Sekretion gezeigt wurde. Zudem wurde nachgewiesen, dass die Translokation von CagA von der bakteriellen *de novo*-Proteinsynthese und von aktiven Wirtszellprozessen abhängt.

Neue Anti-Infektiva, welche die CagA-Übertragung in die Wirtszelle unterbinden, könnten eine äußerst effiziente Maßnahme gegen die von CagA induzierte Karzinogenese sein. Zur Identifizierung derartiger therapeutischer Pathoblocker wurde das TEM-CagA-Reportersystem zum Screening von Substanzbibliotheken verwendet. Dabei wurden zwei verwandte Substanzen gefunden, welche den CagA-Translokationsprozess gezielt *in vitro* blockieren. Zudem wurden während des Screeningprozesses weitere Substanzen entdeckt, die spezifisch

das Wachstum von *H. pylori* hemmen. Diese Inhibition wurde auf eine Beeinträchtigung der bakteriellen Atmung zurückgeführt, und zwei dieser Substanzen wurden vorläufig als potentielle neue Antibiotika validiert. Diese Arbeit hat daher nicht nur zu neuen Erkenntnissen im Hinblick auf die CagA-Translokation geführt, sondern auch zu zwei möglichen Behandlungsansätzen der Infektion mit *H. pylori* beigetragen.

I. INTRODUCTION

1. *Helicobacter pylori*: a gastric pathogen

1.1 Discovery of *H. pylori* and epidemiology of infection

Helicobacter pylori is a gram-negative, microaerophilic bacterium that colonizes the human gastric mucosa persistently, which leads to various malignancies including gastric cancer. Modern research of *H. pylori* started in the early 1980s by the Australian pathologists Robin Warren and Barry J. Marshall. They were the first to isolate *H. pylori* [1] and the first to establish a link between infection with this bacterium and gastritis as well as peptic ulcers [2]. However, at this time, the gastric environment was assumed to be sterile due to its harsh acidic conditions. To finally convince the medical community, Marshall performed a self-experiment and drank a *H. pylori* suspension which actually caused an acute gastritis [3]. Since then, *H. pylori* is in the worldwide focus of medical research and to honor its discovery, Marshall & Warren were awarded the Nobel Prize for Medicine and Physiology in 2005.

Approximately 50% of the world population is chronically infected with *H. pylori*. The prevalence of infection varies immensely between countries. While the infection rate in many developing countries is over 80%, the prevalence in industrialized countries ranges between 20 to 40% [4, 5]. However, *H. pylori* infections seem to decrease in Western countries with the socioeconomic development including higher hygiene standards. It is assumed that *H. pylori* is transmitted via the oral-oral or fecal-oral route during early childhood and persists without antibiotic treatment for a life-time in its gastric niche [4, 5]. *H. pylori* strains can be divided in various populations with distinct geographical distribution which plays a major role in tracing ancient human migration [6]. Hence, it has been suggested that *H. pylori* has been present in humans for at least 100,000 years [7] and accompanied the migration of modern humans out of Africa about 58,000 years ago [8].

1.2 *H. pylori*-induced diseases

Infection with *H. pylori* increases the risk for various gastric diseases. A comprehensive overview of disease progression is presented in Figure 1. The initial infection phase during childhood has a predominantly subclinical outcome and is accompanied by an acute gastritis and a profound, but transient, hypochlorhydria [9]. During the course of persistent colonization with *H. pylori*, the infection elicits a gastric mucosal inflammatory response in virtually all infected persons [10]. This chronic gastritis is mainly asymptomatic but a major

risk factor for sequelae, and 10% of infected persons develop peptic ulcers, 1-2% gastric adenocarcinoma and a few mucosa-associated lymphoid tissue (MALT)-lymphoma [11].

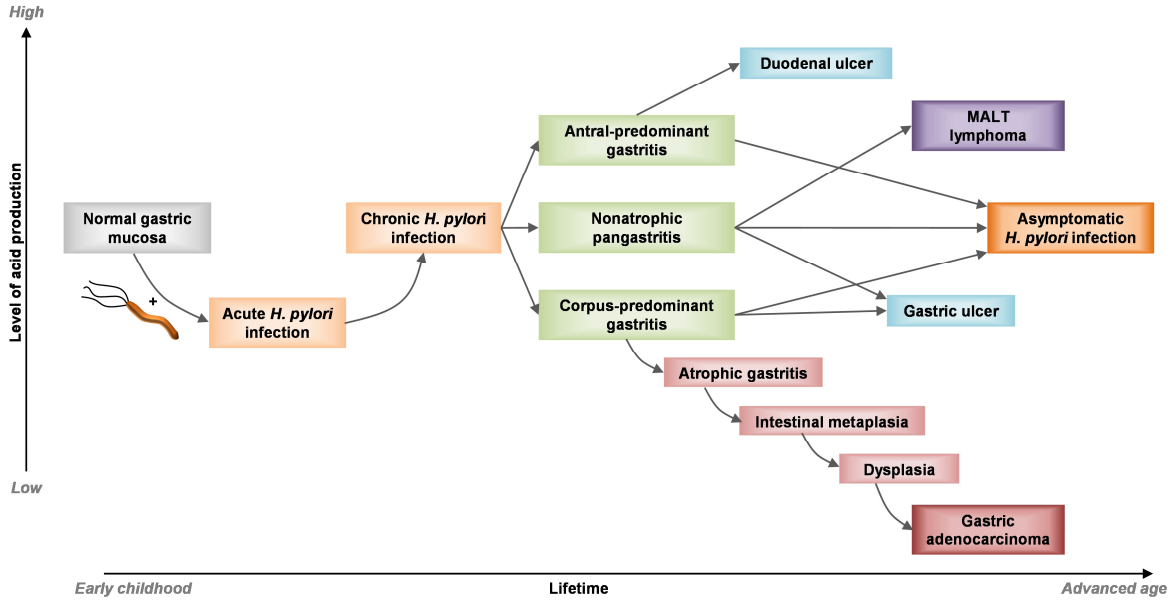

Figure 1: *H. pylori*-induced disease progression
See text for further information. MALT: Mucosa-associated lymphoid tissue. Modified from [11].

In the majority of infected patients, *H. pylori*-induced gastritis is more common in the antrum than in the corpus of the stomach (antral-predominant gastritis) [9]. This phenomenon is mostly attributed to high local acid concentrations in the corpus which favors a colonization of the antrum by *H. pylori*. In agreement, a corpus-predominant pattern of gastritis is observed in individuals with low gastric acid output, which is mainly attributed to a genetic predisposition of the host [12]. The different gastritis forms promote two types of peptic ulceration: duodenal and gastric ulcers. Patients with antral-predominant gastritis are susceptible to duodenal ulcers, as this type of gastritis causes hypergastrinemia (high gastrin secretion levels) and increased acid leakage from the stomach to the duodenum [13]. The duodenum develops gastric metaplasia in response to the high acid load, and can be subsequently colonized by *H. pylori*, which leads to subsequent inflammation and duodenal ulceration [13]. Gastric ulcers are associated with pan- or corpus-predominant gastritis, related to normal or low acid levels, and the ulceration forms at the junction of antral and corpus mucosa [9, 13]. Duodenal ulcers occur in middle age, while gastric ulcers affect older people [14].

Infection with *H. pylori* significantly increases the risk for gastric MALT-lymphoma. MALT-lymphoma originates from marginal zone B cells of mucosa-associated lymphoid tissue. As MALT is usually absent in an uninfected stomach, its acquisition seems to depend on

H. pylori infection, and the transformation into MALT-lymphoma usually arises from pan-gastric inflammation [15, 16].

The most serious *H. pylori*-induced disease is gastric cancer, and 90% of new cases worldwide are attributed to infection with the bacterium [17]. Gastric adenocarcinoma is classified into a more common intestinal and a less common diffuse type. Diffuse-type carcinoma derives from individually infiltrating neoplastic cells, but underlying mechanisms have not been studied extensively [14]. Intestinal-type gastric adenocarcinoma describes a malignant epithelial tumor that originates from the glandular epithelium. The development of this adenocarcinoma can be considered as the long-term consequence of progression from gastritis to gastric atrophy (loss of specialized cell types such as parietal and chief cells), intestinal metaplasia (replacement of gastric mucosa by intestinal-type epithelium), and dysplasia (neoplasia of lining epithelial cells), collectively called the Correa pathway [18, 19]. The decisive step in this cascade is the development of atrophy, as progression to cancer can only be prevented when *H. pylori* is eradicated prior to atrophy formation [14, 20]. Gastric adenocarcinoma is predisposed by pan- or corpus-predominant gastritis and a resulting hypochlorhydria, which might explain why persons with duodenal ulcers (associated with antral-predominant gastritis and increased acid production) are partially protected from this kind of cancer [21]. Gastric cancer is one of the leading causes of cancer-related deaths worldwide [22]. As infection with *H. pylori* increases the risk for gastric cancer approximately 10-fold [23, 24], *H. pylori* has been classified as a class 1 carcinogen by the World Health Organization´s (WHO) International Agency for Research into Cancer (IARC) [25].

In general, antibiotic therapy can drastically decrease the risk for *H. pylori*-linked gastric malignancies and will be specified in Chapter 5.

2. Colonization of the gastric mucosa: virulence factors

The disease outcomes described above are strongly influenced by the genetic predisposition of the host, environmental parameters and the molecular repertoire of *H. pylori* [26, 27]. *H. pylori* is highly adapted to survive and colonize the human stomach. Within its small genome (1.67 megabases), *H. pylori* encodes, besides a minimal set of metabolic genes [28], various virulence factors that enable the bacterium not only to persist in but also to exploit the gastric environment. Studies in various rodent models have revealed more than 100 bacterial genes that are required for gastric colonization [29, 30]. An overview of some selected virulence factors will be given in the following section and a simplified schematic is shown in

Figure 2. The major virulence factor cytotoxin-associated gene product A (CagA) together with the Cag type IV secretion system (Cag-T4SS) will not be focused on in this chapter, but described in detail in Chapters 3 & 4.

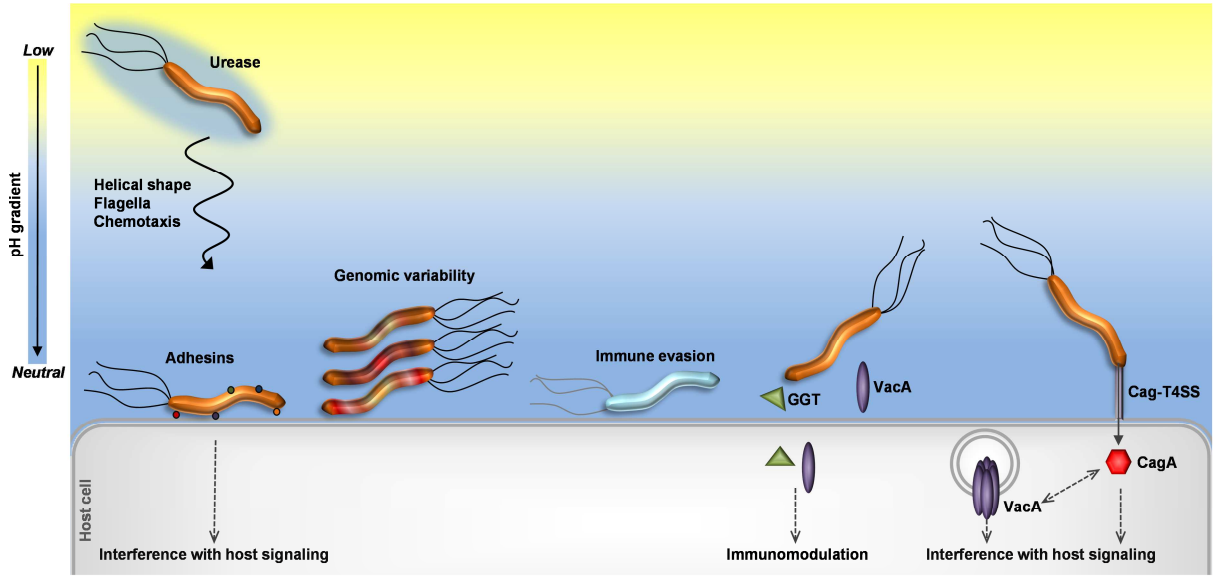

Figure 2: Strategies of *H. pylori* for persistent stomach colonization
H. pylori survives the gastric acidity by production of urease, and quickly moves to the neutral mucus layer responding to chemotactic cues, which is assisted by its helical shape and flagella (Chapter 2.1.1). Adherence to the mucus and gastric epithelial cells is mediated by various outer membrane proteins (Chapter 2.1.2). *H. pylori* exhibits a high genomic variability for adaptation during long-term colonization (Chapter 2.2.1). This also facilitates evasion from the innate host immune response (Chapter 2.2.2). Adaptive immunity is modulated by secreted GGT and VacA proteins (Chapter 2.2.2). Further interference with host cell signaling is achieved by type IV secretion-injected CagA protein (see Chapters 3 & 4). CagA: cytotoxin-associated gene product A, Cag-T4SS: Cag type IV secretion system, GGT: γ-glutamyl transpeptidase, VacA: vacuolating toxin A. Modified after [31].

2.1 Initial steps of stomach colonization

2.1.1 From the acidic lumen to the neutral mucosa

First of all, *H. pylori* has to deal with the acidity of the stomach lumen (pH 1-2). *H. pylori* is neither an acidophilic nor an acid-tolerant organism, and thus has to move as fast as possible from the lumen to the thick gastric mucus layer, where it is protected from the acidic milieu. *H. pylori* resists the initial luminal acid exposure through production of urease, which converts urea into ammonia generating a neutral environment on the bacterial surface [32]. In addition, the increased local pH facilitates motility through the mucus, because the gel-like mucin layer is pH-dependently transformed into a solution where the bacterium can freely swim [33]. Moreover, *H. pylori* possesses a unique helical shape for rotational cork-screw like movement through the viscous environment and indeed, modifications regarding the cell shape inhibit colonization in animal studies [34]. Motility is enabled by up to six unipolar

flagella and crucial at early stages of infection [35, 36]. However, motility is irreversibly lost within one minute in the acidic lumen [37]. Hence, movements are strictly regulated by chemotaxis, which alters flagellar activity and is pivotal for a successful infection [38]. For localization of the epithelium, *H. pylori* uses the mucus pH gradient for orientation [39]. Furthermore, the energy sensor TlpD is essential for initial infection and persistence of *H. pylori* in animal models of infection [40]. Responding to chemotactic cues, injured gastric sites are preferred which might be attributed to a higher nutrient availability [41].

2.1.2 Adhesion in the gastric mucosa

Another crucial step in gastric colonization of *H. pylori* is its ability to adhere to the human gastric epithelium and mucosa. This prevents shedding of *H. pylori* by peristalsis and enables proximity to the host cells for direct interaction and nutrient availability. Adhesion is mediated by outer membrane proteins (OMPs) that can bind to distinct host cell components and are accordingly termed adhesins. The genome of *H. pylori* contains about 60 genes that are predicted to encode OMPs [42]. The first adhesin that was discovered was BabA (blood group antigen-binding adhesin), which can adhere to the carbohydrate moiety of the fucosylated Lewis b (Le^b) histo-blood group antigen on the surface of gastric epithelial cells [43]. Moreover, adhesins are also linked to the induction of host cell signal transduction pathways. For example AlpA and AlpB (Adherence associated lipoproteins A and B [44]) are homologous proteins that bind to the extracellular matrix protein laminin on the basolateral side of host epithelial cells [45]. Infection experiments in Mongolian gerbils with respective deletion mutants revealed a severe inflammation and suggested abrogation of anti-inflammatory signaling mediated by the *alp*AB locus [46]. In addition, *H. pylori* infection can induce the expression of several receptors like sialyl-dimeric-Lewis x glycosphingolipid, which are bound by the SabA (Sialic acid-binding) adhesin [47]. Just recently, a novel bacterial adhesin, termed LabA (HopD) was identified and characterized to bind specifically to MUC5AC mucins [48]. The high diversity of adhesin binding partners underscores the capability of the bacterium to initially establish various interactions that promote its persistence in the gastric mucosa in close proximity to the host cells.

2.2 Long-term persistence

2.2.1 Generation of genetic diversity

For adequate adaptation to changing environmental conditions, *H. pylori* is highly efficient in generating genetic diversity by its high mutational rate [49]. Individuals are often infected with more than one distinct *H. pylori* strain. Due to the natural competence of the bacterium (ability for exogenous DNA uptake), conjugation systems and subsequent recombination events, the genetic repertoire can broadened further [50, 51]. Consequently, strains undergo a rapid microevolution and drastically vary their genome during long-term colonization [52]. One well-studied example is the gene conversion and phase variation of the earlier described adhesins. In particular, 5´- and 3´-end regions of the *omp* genes are highly conserved which allows gene conversion, and distinct dinucleotide repeats in the 5´ regions enable slipped-strand mispairing, resulting in phase variation. This leads to modifications in OMP sequence or expression levels, which makes an adapted adherence capability as well as immune evasion possible [53, 54].

2.2.2 Manipulation of the host immune response

Infection with *H. pylori* elicits a humoral and cellular immune response, and leukocytes infiltrate the stomach tissue upon persistent colonization [10, 55]. Nevertheless, the host immune response is not effective in eradicating *H. pylori*, which is mainly attributed to manipulation of the innate and adaptive immune system.

The modulation of the innate immunity is mainly based on target modification or subversion of innate recognition pathways [31]. Target modification is facilitated by the above-described high genomic plasticity. Moreover, *H. pylori* avoids detection by several pattern recognition receptors (PRRs) that are crucial for identification of pathogen-associated molecular patterns (PAMPs) in other bacterial pathogens. For example, the LPS (lipopolysaccharide) of *H. pylori* is 1000-fold less biologically active than the LPS of *E. coli* [56] due to a dephosphorylation of the lipid A domain [57]. This provides not only resistance to host antimicrobial peptides but also subverts activation of the PRR Toll-like receptor 4 (TLR4), and results in the inhibition of pro-inflammatory cascades. Besides, *H. pylori* flagellin is not recognized by Toll-like receptor 5 (TLR5) due to modifications in the N-terminal TLR5 recognition domain and hence protected from host clearance [58]. In contrast, *H. pylori* non-LPS ligands (e.g. lipoproteins) are identified by Toll-like receptor 2 (TLR2), and this recognition triggers the expression of anti-inflammatory genes [59]. In conclusion, the innate immune response is

mainly subverted by reduced activation of pro-inflammatory cascades or manipulation/activation of anti-inflammatory cascades [31].

Manipulation of the adaptive immunity is mainly achieved by two secreted virulence factors: vacuolating toxin A (VacA) and γ-glutamyl transpeptidase (GGT) [31]. VacA is a multifunctional toxin (reviewed in [60, 61]) and was first described for its ability to induce vacuoles in eukaryotic cells upon *H. pylori* infection [62]. To do so, VacA is secreted via an auto-transporter mechanism, binds to the host cell and, after internalization, forms hexameric anion-selective channels in the endosomal membrane [63]. Generally, most VacA-induced cellular alterations are attributed to its capacity to form pores in cell membranes. For example, VacA inserts into the inner mitochondrial membrane which triggers apoptosis [64]. Moreover, VacA causes functional alterations in a variety of immune cells. Upon infection of macrophages with *H. pylori*, phagosome maturation is VacA-dependently inhibited and thus bacterial clearance prevented [65]. Also, an inhibition of antigen presentation of B-lymphocytes by VacA has been described [66]. The interference of VacA with T-lymphocytes is of major importance. VacA enters T-lymphocytes by binding to the β2 (CD18) integrin [67] and suppresses an immune response by blocking proliferation via suppression of IL-2 transcription [68]. In addition, T-lymphocyte function is modified by GGT. GGT induces cell-cycle arrest of T-cells by glutamine deprivation at the site of infection [69, 70]. Moreover, T-cell-mediated clearance of *H. pylori* is indirectly suppressed by synergistic action of VacA and GGT. Both virulence factors promote a preferential differentiation of naive T-cells into regulatory T-cells, and thus prevent them from maturation into T-helper 1 (Th1) and T-helper 17 (Th17) lymphocytes which could control or even eliminate *H. pylori* infection [71].

Furthermore, regulation of the activity of distinct virulence factors facilitates gastric persistence. For example, the pathophysiological actions of VacA are attenuated by the presence of CagA and vice versa [72, 73]. In summary, *H. pylori* uses various strategies to persist in the gastric mucosa which are mainly based on a dynamic adaption to the environment and distinct mechanisms to evade elimination by the host immune system.

3. The Cag type IV secretion system: virulence determinant with unique features

The injection of the *H. pylori* oncoprotein CagA into host cells constitutes the key event in various infection-associated malignancies. CagA is delivered through a type IV secretion system-mediated process, and represents the only known translocated effector protein [74-76].

This section describes this CagA translocation machinery, the Cag type IV secretion system (Cag-T4SS) (schematically depicted in Figure 2). As the architecture of the Cag-T4SS is only partly elucidated, a prototypical gram-negative type IV secretion system is first depicted.

3.1 Prototypes of bacterial type IV secretion systems

Type IV secretion systems (T4SS) designate multiprotein complexes that span the inner and outer membrane and are found in various bacteria. T4SS can be functionally divided into three subfamilies [77]: DNA conjugation machineries, DNA uptake/release systems and effector translocator systems. DNA conjugation systems constitute the largest family and enable transport of DNA substrates within and across bacterial species as well as into eukaryotic target cells. Conjugation is responsible for the spread of antibiotic resistance and virulence traits among bacteria, and *H. pylori* uses this type of T4SS for horizontal gene transfer as well [78]. Less common systems are substrate uptake/release T4SS that import or export DNA fragments or proteins independently of any cell contact. One such T4SS, the ComB competence system, is also produced by *H. pylori* and enables exogenous DNA import [79]. Effector translocator systems transport bacterial proteins into eukaryotic cells. This group incorporates, apart from the Cag-T4SS of *H. pylori*, other T4SS of human pathogens that are linked to disease including those of *Brucella*, *Bartonella*, *Coxiella*, *Rickettsia spp.*, or *Legionella pneumophila* [80].

A prototypical T4SS is the VirB/VirD4 system of the phytopathogen *Agrobacterium tumefaciens*. This system acts both as a conjugation machine and as an effector translocator which delivers the oncogenic T-DNA and/or several effector proteins into plant cells, eliciting the tumorous crown-gall disease. The VirB/VirD4 T4SS apparatus consists of 12 proteins (11 VirB proteins and VirD4) and most other T4SS consist of a conserved VirB/VirD4 protein set [77]. The general architecture of a prototypic T4SS apparatus is presented in Figure 3A. The system is composed of four functional machine subassemblies [77, 81, 82]: a type IV coupling protein, an inner membrane complex (cytoplasmic membrane translocon, IMC), an outer membrane complex (core complex, OMC), and an external pilus. The coupling protein is an ATPase (VirD4) that binds substrates and initiates transfer to the cytoplasmic membrane translocon. This complex is composed of two further ATPases (VirB4, VirB11), two polytopic membrane proteins (VirB3 and VirB6) and one bitopic protein (VirB8) which facilitate substrate transfer across the inner membrane. VirD4 forms, together with the VirB4 and VirB11 ATPases, a motor complex at the translocation channel entrance that is assumed to drive T4SS biogenesis and any ATP-dependent translocation step. Substrate passage across

the periplasm is enabled by the core complex, which is composed of two outer membrane-associated proteins (VirB9 and the lipoprotein VirB7) and the cell-envelope-spanning subunit VirB10. The translocation channel extending through the core complex might be composed of the major pilin subunit VirB2 and parts of VirB8 and VirB9 [83-85]. It is suggested that the pilus constitutes the extended part of the transfer channel [83]. The pilus itself is an extracellular organelle for contact initiation with recipient cells. It is composed of VirB2, forming the shaft, and the pilus-associated adhesin VirB5. Moreover, a lytic transglycosylase (VirB1) that hydrolyzes the peptidoglycan layer is crucial for pilus biogenesis [77, 81, 82].

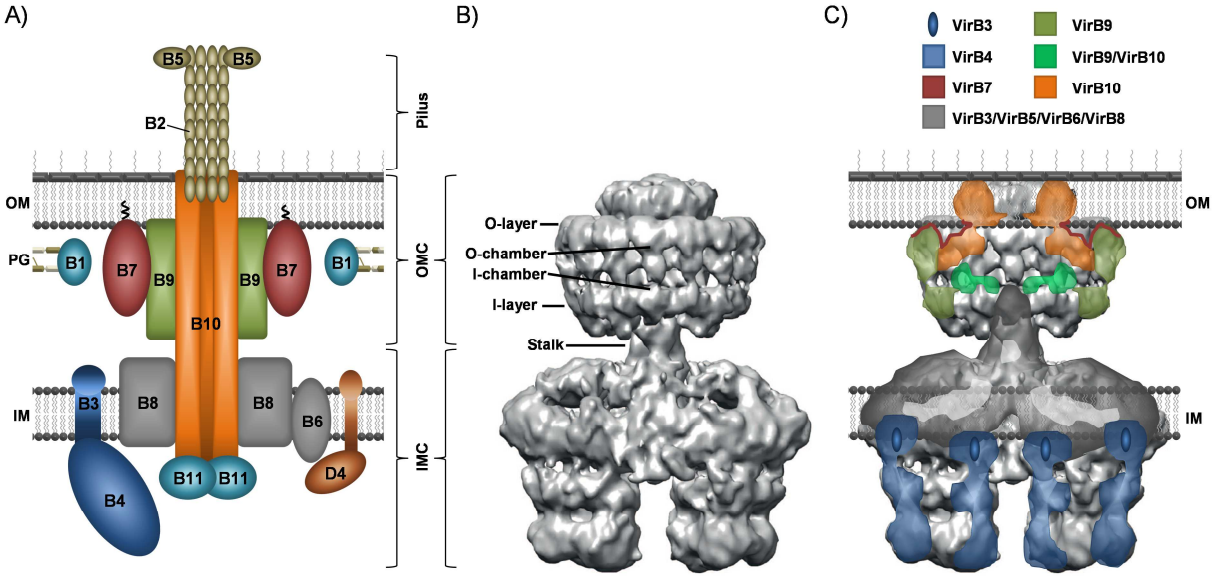

Figure 3: Models of a prototypical type IV secretion system
A) Schematic model of a T4SS according to the nomenclature of the VirB/VirD4 T4SS of *Agrobacterium tumefaciens*. Colors refer to the components highlighted in C).
B) Electron density map reconstruction of eight components of an *E. coli* T4SS (copied from [86]).
C) Localization of known components and position of cell membranes in the map from B).
I-: inner, IM: inner membrane, IMC: inner membrane complex, O-: outer, OM: outer membrane, OMC: outer membrane complex, PG: peptidoglycan, T4SS: type IV secretion system.

A relevant advance in T4SS research has been achieved by the structure elucidation of the core unit of a T4SS apparatus from plasmid R388 of *E. coli* [86], which is presented in Figure 3B. The structure revealed a 3 MDa assembly of eight VirB/VirD4 homologue subunits (highlighted in Figure 3C) consisting of an IMC (composed of VirB4 ATPase subunits as well as VirB3, VirB6 and VirB8), an OMC spanning the periplasm as well as a flexible central stalk linking both components. In accordance with prior studies [84, 85], the core complex assembles as a large barrel and is composed of 14 copies each of VirB10, VirB7 and VirB9 homologues. These are arranged in symmetric inner and outer layers (I- and O-layers) that form chambers divided by a central middle platform. Importantly, the T4SS core structure shows no continuous central channel. Thus, apart from a one-step translocation, a two-step

process could be assumed as well, where substrates access the core complex secretion chambers from the periplasm [86].

3.2 Delivery of the oncoprotein CagA by a type IV secretion system

The Cag type IV secretion system (Cag-T4SS) is evolutionarily related to other T4SS and harbors various Vir homologues. However, the Cag-T4SS markedly differs from the prototypical *A. tumefaciens* VirB/VirD4 T4SS.

3.2.1 The *cag* pathogenicity island

The Cag-T4SS is, together with its effector protein CagA, encoded on the *cag* pathogenicity island (*cag*PAI), schematically depicted in Figure 4. This chromosomal insertion element incorporates an approximately 37 kb locus containing 27-31 genes [87, 88]. Of importance, the presence of the *cag*PAI increases the risk of cancer development, and *H. pylori* strains are divided into highly virulent *cag*PAI-positive (type-1) and less virulent *cag*PAI-negative (type-2) strains [89]. Apart from strains carrying a complete *cag*PAI, some contain an incomplete *cag*PAI lacking one or more genes, or one that was disrupted by chromosomal rearrangements. Nevertheless, *cag*PAI-encoded genes are highly conserved, thus it has been suggested that the pathogenicity island was acquired about 60,000 years ago and might confer an evolutionary advantage [90].

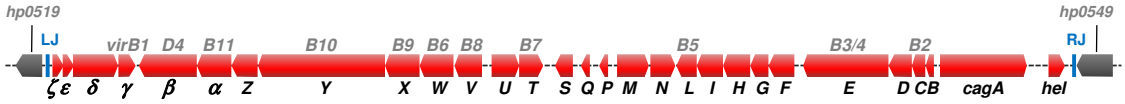

Figure 4: Scheme of the *cag* pathogenicity island (*cag*PAI)
The *cag*PAI is integrated at a defined chromosomal locus flanked by genes *hp0519* and *hp0549*. Gene designations are indicated below, and putative Vir protein homologies above the boxes. LJ: left junction, RJ: right junction. Adapted from [87].

3.2.2 Assembly model of the Cag type IV secretion system

For all prototypical VirB/D4 components, respective Cag counterparts with sequence similarities can be found and are listed in Figure 5A [87, 91]. However, most of these Cag components exhibit domain structures distinct from their Vir counterparts. For example, the VirB10 homologue CagY has only a small C-terminal region similar to VirB10, is considerably larger and contains additional domains composed of repeat regions [92]. Moreover, the Cag-T4SS incorporates additional components with unique structures that are

essential for functionality (see Chapter 3.2.3). Nevertheless, according to Vir homologies and various protein-protein interaction studies, a model of the Cag-T4SS has been established and is presented in Figure 5B [87].

A)

Vir	Cag
VirB1	Cagγ
VirB2	CagC
VirB3/4	CagE
VirB5	CagL
VirB6	CagW
VirB7	CagT
VirB8	CagV
VirB9	CagX
VirB10	CagY
VirB11	Cagα
VirD4	Cagβ

B)

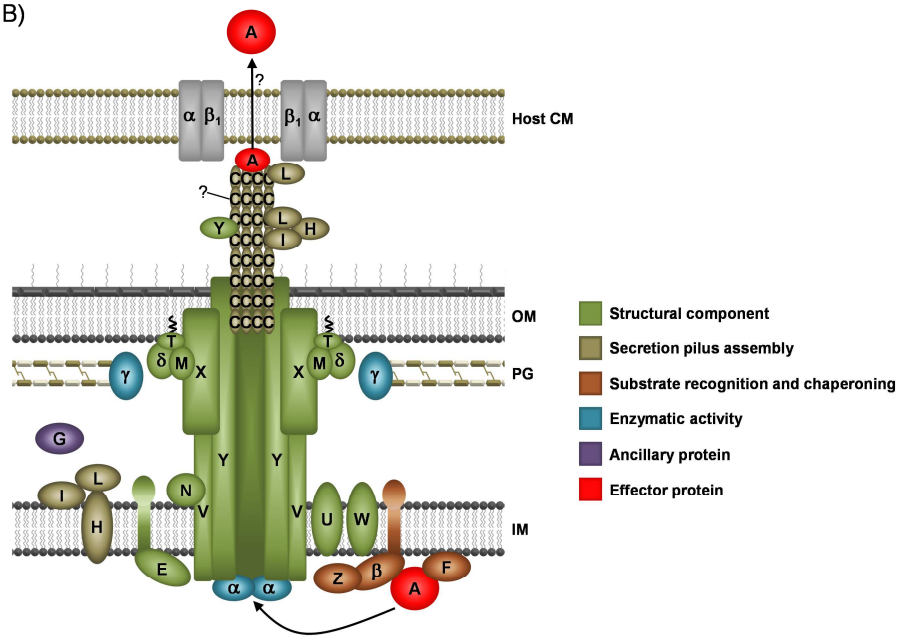

Figure 5: Model of the Cag type IV secretion apparatus of *H. pylori*
A) Vir and Cag component similarities according to [87, 91].
B) Schematic model of the Cag type IV secretion system. Components refer to the Cag nomenclature and are divided into several functional classes (color schemes indicated at the right side). CM: cytoplasmic membrane, IM: inner membrane, OM: outer membrane, PG: peptidoglycan. Modified from [87].

The coupling protein (VirD4) homologue Cagβ is predicted to be located in the inner membrane [93] and its cytoplasmic part has been shown to interact with the effector protein CagA as well as with CagZ [94, 95]. It has been hypothesized that Cagβ and CagZ form a signal recognition receptor complex where CagA is additionally stabilized by its membrane-associated chaperone CagF [87]. The energy for biogenesis and translocation processes is delivered by two more ATPases, Cagα (VirB11) and CagE (VirB3/4). It has been shown that the cytoplasmic protein Cagα assembles into dynamic hexamers and is catalytically active [96]. CagE exhibits sequence similarities to the VirB4 ATPase and possesses a VirB3-like extension at the N-terminus [93]. Hence, the cytoplasmic membrane translocon might be composed of CagE, and the inner membrane proteins CagW (polytopic, VirB6 [93]) and CagV (bitopic, VirB8 [97]) [88]. The integral membrane proteins CagU and CagH might be associated with the inner membrane complex as well, but functional studies are lacking [87]. The core complex is built up by the membrane spanning VirB10 homologue CagY, CagX (VirB9) and CagT (VirB7, lipoprotein). Accordingly, direct interactions between CagX and CagY [93], as well as between CagX and CagT [98], have been reported. In addition, CagM

[93] and Cagδ [99] are outer membrane-associated and co-assemble into an extended core complex [100]. In various studies, pilus-like surface structures associated with the Cag-T4SS could be identified [101-103]. Although the major pilin (VirB2) homologue CagC is supposed to be involved in pilus formation [104], a *cagC* deletion mutant was found to produce pili as the wild-type [105]. Staining of pili with antibodies identified the VirB5-like adhesin CagL as well as CagY, CagX and CagT localizing to the pilus surface or to the base of the pilus [101, 102]. This seems to be reasonable for CagL, which has been shown to bind to host cell integrins (see Chapter 3.2.4), but inconsistent for the putative core complex components. Moreover, CagL has been shown to interact with CagI and CagH [103, 106], and such an assembly might also associate with pili as all subunits are involved in pilus formation (see Chapter 3.2.3). In addition, CagH is predicted to be an integral cytoplasmic membrane protein [93], and a subassembly of CagH, CagI and CagL at the periplasmic face of the inner membrane is speculated. As *cagG* is genetically organized together with *cagH*, *I* and *L*, a functional connection of CagG to this subcomplex could also be imagined [106]. Accordingly, CagG is supposed to be located in the periplasm (see Figure 5B) and various interactions with other Cag components are assumed [94]. Also for the enzymatically-active peptidoglycan hydrolase Cagγ (VirB1 [107]), a periplasmic location is postulated. CagN is probably anchored in the cytoplasmic membrane [108] and has been shown to interact with CagY [93]. However, specific localization of Cag-T4SS components might be speculative, but studies deciphering Cag-T4SS functionalities give additional insights and are described in the next section.

3.2.3 Role of Cag components on Cag type IV secretion system function

Mutagenesis studies with isogenic deletion mutants of *cag*PAI-encoded genes identified various Cag components essential for Cag-T4SS function. To validate the functionality of the Cag-T4SS, examination of various phenotypes can be considered: CagA phosphorylation and induction of IL-8 secretion upon *in vitro* infection as well as bacterial pilus formation. After delivery into host cells, CagA gets tyrosine-phosphorylated immediately by cellular kinases [74-76]. This phosphorylation event can be analyzed via immunoblotting using specific antibodies. Besides CagA translocation, one consequence of Cag-T4SS activity is the upregulation of pro-inflammatory cytokine secretion including IL-8 [109, 110]. The larger part of IL-8 induction is independent of CagA translocation and proves functionality of the T4SS apparatus. It should be mentioned that IL-8 secretion might be triggered by T4SS-delivered peptidoglycan which is recognized by NOD1 [111], although these results are

controversial as another study showed peptidoglycan delivery by outer membrane vesicles [112]. Moreover, the presence of pili is directly linked to Cag-T4SS function as mutants that fail to produce pili are defective in CagA translocation and IL-8 induction [103, 105, 113, 114]. But on the contrary, mutants that form pili do not necessarily translocate CagA or induce IL-8 secretion (e.g. *cagα*). The outcome of several studies focusing on the above-mentioned phenotypes is summarized in Table 1.

Table 1: Overview of characteristics and functions of *cag*PAI-encoded proteins
Gene designations and protein sizes refer to [28]. CagA-P: CagA phosphorylation. +/- refers to phenotype characteristics of respective deletion mutants with -: abolished, +: weak, ++: moderate, +++: unchanged, ++++: increased. AF: accessory factor, IM: inner membrane, IL-8: interleukin-8, OM: outer membrane, SA: secretion apparatus component, SC: supportive component, TF: translocation factor. Modified from [87] and [88].

Gene	**Protein** **Size [kDa]**	**Effect of gene deletion**			**Proposed function**
		CagA-P	**IL-8**	**Pilus**	
hp0520	Cagζ (13)	+++	+++	*n.d.*	AF
hp0521	Cagε (10)	+++	+++	*n.d.*	AF
hp0522	Cagδ (50)	-	-	-	OM complex, SA
hp0523	Cagγ (18)	-	-	*n.d.*	VirB1, peptidoglycan hydrolase, SA
hp0524	Cagβ (80)	-	+++	+++	VirD4, coupling factor, TF
hp0525	Cagα (35)	-	-	+++	VirB11, ATPase, SA
hp0526	CagZ (21)	++	++	*n.d.*	Cagβ stabilization, SC
hp0527	CagY (220)	-	-	-	VirB10, core complex, integrin binding, SA
hp0528	CagX (55)	-	-	-	VirB9, core complex, SA
hp0529	CagW (55)	-	-	*n.d.*	VirB6, IM translocon, SA
hp0530	CagV (27)	-	-	-	VirB8, IM translocon, SA
hp0531	CagU (23)	-	-	*n.d.*	SA
hp0532	CagT (30)	-	-	-	VirB7, core complex, OM lipoprotein, SA
hp0534	CagS (21)	+++	+++	*n.d.*	AF
hp0535	CagQ (14)	+++	+++	*n.d.*	AF
hp0536	CagP (13)	+++	+++	*n.d.*	AF
hp0537	CagM (40)	-	-	-	OM complex, SA
hp0538	CagN (32)	+	+	*n.d.*	SC
hp0539	CagL (26)	-	-	-	VirB5, pilus biogenesis, integrin targeting, SA
hp0540	CagI (40)	-	-/+++	-	Pilus biogenesis, integrin targeting, SA or TF*
hp0541	CagH (39)	-	-	++++	Pilus biogenesis, SA
hp0542	CagG (16)	+	++	*n.d.*	SC
hp0543	CagF (29)	-	+++	*n.d.*	CagA chaperone, TF
hp0544	CagE (100)	-	-	-	VirB3 / VirB4, ATPase, SA
hp0545	CagD (22)	-/+	+	*n.d.*	SC or TF**
hp0546	CagC (13)	-	-	+++	VirB2, pilus subunit (?), SA
n.d.	CagB (8)	*n.d.*	*n.d.*	*n.d.*	*n.d.*
hp0547	CagA (125)	-	+++	+++[#]	Effector protein

*conflicting data with respect for requirement for IL-8 induction [89, 115, 116].
**conflicting data with respect for requirement for CagA translocation [115, 117].
[#]derived from [123].

In general, Cag components can be discriminated into four factor classes [87]: secretion apparatus components (SA), translocation factors (TF), supportive components (SC) and accessory factors (AF). Secretion apparatus components are necessary for CagA phosphorylation (CagA-P) as well as IL-8 induction. In total, 14 *cag*PAI genes have been identified to be essential components [115, 116] and include all proposed Vir homologues (except Cagβ) as well as several Cag-T4SS-specific components. Following this, the Vir counterparts are likely to fulfill the same essential role in the Cag-T4SS as in the prototypical T4SSs. For example, core complex components such as CagT and CagX or proposed inner membrane complex forming CagE and CagV proteins are essential for both Cag-T4SS functions as well as pilus formation. Apart from the VirB homologues, essential Cag-T4SS-specific components include the outer membrane complex-associated proteins Cagδ and CagM as well as the above-mentioned inner membrane translocon-related CagU. Moreover, CagI and CagH are indispensable for a functional Cag-T4SS which is in accordance with a reported involvement in pilus formation, and *cagH* deletion even leads to a hyperpiliated phenotype [103]. This again stresses the requirement of all these unique Cag components for full function of Cag type IV secretion. So-called translocation factors designate Cag components that are exclusively required for CagA phosphorylation but dispensable for functional IL-8 induction. These include the putative coupling protein Cagβ, the chaperone CagF, and CagD, albeit conflicting data exist regarding the latter protein [115, 117]. The exclusive requirement of Cagβ for CagA delivery seems reasonable as the integrity of the T4SS machinery should be independent of the coupling protein. Moreover, CagF is supposed to support CagA delivery to the coupling complex by protection of CagA from premature degradation [118-120]. Some Cag-T4SS components, like CagZ, CagN and CagG, are not necessary but their absence clearly reduces functional phenotypes. They are thus denominated supportive components. For example CagG, the absence of which reduces CagA phosphorylation and IL-8 induction, is proposed to be functionally associated with the essential secretion apparatus components CagH, CagL and CagI [106], and a lack of this connection upon *cagG* deletion is likely the reason for the weak phenotypes. The last group is constituted by accessory factors including Cagζ, Cagε, CagS, CagQ and CagP. These factors do not seem to contribute to function but transcription of respective genes has been shown [121]. Of these, *cagP* is transcribed together with a non-coding upstream RNA, CncR1. This small RNA has been shown to inversely modulate bacterial motility and adhesion to host cells attributing a major regulatory function to the *cagP* locus [122].

Overall, CagA translocation underlies a complex regulation and is also influenced by *cag*PAI-

independent factors. For example, a functional dependence between HopQ, an outer membrane protein, and the Cag-T4SS has been reported [124]. Moreover, pilus formation seems to be highly dependent on environmental conditions. Following this, iron limitation has been shown to induce T4SS pili and increase CagA phosphorylation [125], while zinc depletion reduced T4SS pili and CagA translocation [126].

3.2.4 A mechanistic view on CagA translocation

The exact CagA delivery mechanism into host cells is only poorly understood. Host cell contact is assumed to be mediated by binding to $\alpha_5\beta_1$ integrin via the pilus-located proteins CagL, CagY, CagI as well as CagA [113, 114]. All components have been shown to directly bind to β_1 integrins, while CagL might act as the major tip adhesin. The VirB5 homologue CagL is described to bind via an RGD motif to β_1 integrins, leading to an integrin activation that induces CagA translocation and subsequent tyrosine phosphorylation [113]. But the requirement of this binding event for CagA translocation is controversial [114]. However, blocking of integrins inhibits CagA translocation, supposing a role of $\alpha_5\beta_1$ integrins as target receptors for the Cag-T4SS, and importantly, the CagA protein itself exhibits the strongest binding capability to β_1 integrin compared to the other Cag components [114, 127]. As CagA has been localized at or near the tips of Cag-T4SS pili [113, 128], it is suggested that this pilus-exposed CagA protein constitutes a translocation intermediate following a multistep translocation process, as has already been proposed for other T4SS (see Chapter 3.1). Moreover, CagA has been shown to be located on the bacterial surface in a T4SS-dependent manner [129]. Thus, it is not clear whether CagA is delivered through the pilus shaft or if the pilus is just necessary to mediate direct cell contact. However, CagA protein does not enter cells autonomously and translocation is strictly dependent on a functional Cag-T4SS. Also, the uptake process of CagA into the host cell cytoplasm is not fully understood. It has been shown that CagA binds to phosphatidylserine at the outer leaflet of the host cell membrane which is speculated to be crucial for uptake [129]. In addition, treatment of cells with various cellular inhibitors, like actin cytoskeleton modulators, block CagA phosphorylation [114, 129]. But a definite contribution of host cellular processes or pore formation in the host cell membrane is still a matter of debate.

4. The CagA protein: insights into its carcinogenic potential

CagA is a unique bacterial oncoprotein and considered as the major virulence determinant of *H. pylori*. How CagA has evolved its cancer-promoting properties will be described in the following sections.

4.1 Structural and translocation-relevant domains

Depending on the *H. pylori* strain, CagA has a size of ~120-145 kDa. CagA exhibits a unique fold without obvious similarity to other proteins and can be divided into a structured N-terminal region (70%) and an intrinsically disordered C-terminal tail (30%). Crystallographic studies could thus only elucidate the structure of C-terminal truncated CagA [127, 130]. The structure derived from Hayashi *et al.* [130] is presented in Figure 6A. The N-terminal region can be divided in domain D1-3. The N-terminal D1 domain is, besides a small interaction surface area with D2, structurally isolated from the other domains and consists predominantly of α-helices that constitute a single folded compact domain with multiple tertiary contacts in between. D2 comprises anti-parallel strands forming a single layer β-sheet (SLB) region and two independent subdomains (D2´ and D2´´, see Figure 6B). D3 consists of a long α-helix and a four-helix bundle at the carboxyl-terminal part (also entitled as D4 according to [127]). Besides the unstructured C-terminus, also the N-terminal portion comprises short disordered stretches including the first 23 amino acids, an unstructured part between D1 and D2 as well as two internal stretches in D2 [130]. Moreover, an intramolecular interaction between the N-terminal D3 domain and the C-terminus via an N-terminal binding sequence (NBS) and a C-terminal binding sequence (CBS) is assumed [130] (see Figure 6B). The above-mentioned SLB region within D2 constitutes the binding site for β_1 integrin, which was shown to be crucial for CagA delivery into host cells [127]. The D2 middle domain also harbors positively charged regions (“basic patch”) that are important for the binding to host cell phosphatidylserine (PS) via electrostatic interactions, which are necessary for translocation [129]. Many T4SS substrates carry secretion signals in the C-terminus and often charged amino acids play a major role [77]. Indeed, deletion of the C-terminal 20 amino acids of CagA rendered the protein translocation-incompetent [131]. However, site-specific mutations of C-terminal charged amino acids did not result in any impact on translocation, and a specific secretion signal of CagA has not been defined yet [131]. Additionally, an intact N-terminus has been revealed to be important for translocation [131]. As mentioned earlier, also the interaction with the secretion-assisting chaperone CagF is important for delivery [118, 119].

Although at first a distinct CagF binding domain of ~100 amino acids in the C-terminal CagA region was assigned [119] (Figure 6B), recent data suggests that multiple copies of CagF form various CagA domain contacts to maintain CagA in a translocation-competent and protease-resistant conformation [120]. Whether CagA is translocated in an unfolded or folded state is still unclear. Indeed, folded N-terminal CagA would fit through the estimated diameter of the Cag-T4SS channel [101, 130], assuming that CagA uses this transport route (see Chapter 3.2.4). In another study, spontaneous refolding of recombinant expressed D2/3 and C-terminal CagA could be observed after denaturation, while the N-terminal D1 domain did not. Thus, it was speculated that CagA delivery is performed in an unfolded state where the C-terminus, crucial for substrate recognition, is transported first and assists N-terminal refolding afterwards [132].

In general, the intrinsically disordered C-terminal tail as well as flexible linkers in the N-terminal domain offer diverse surfaces for host cell interactions and will be described next.

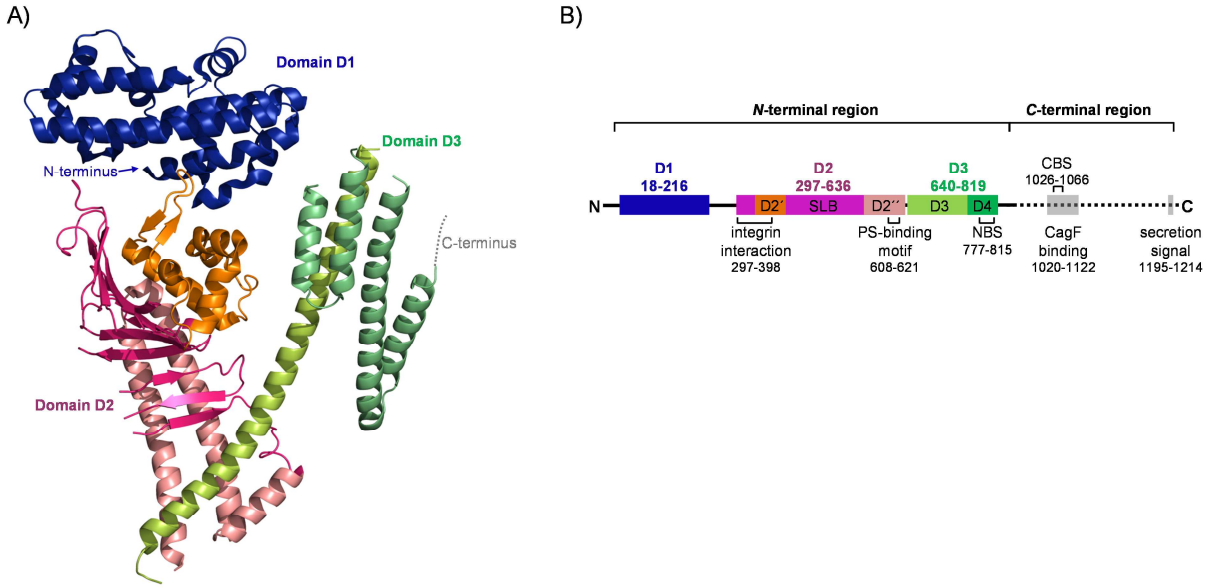

Figure 6: Structure of the CagA N-terminal region
A) Cartoon diagram of the CagA N-terminal region from *H. pylori* 26695. The region is composed of domain D1-3 with D1 in blue, D2 in red tones and D3 in green tones. The N-terminus and the beginning of the unstructured C-terminus are indicated. The structure was copied and modified from [130].
B) Schematic representation of CagA. Colors refer to the domains in A) and numbers to the amino acid positions of CagA from *H. pylori* P12. CBS: C-terminal binding sequence, NBS: N-terminal binding sequence, PS: phosphatidylserine, SLB: single layer β-sheet.

4.2 Interference with host cell signaling

For a better overview, a schematic of the CagA structural domains and functional regions is given in Figure 7 (adapted from [133]). Once inside the host cell, CagA is tethered to the inner leaflet of the cell membrane via the above-described interactions with

phosphatidylserine (PS) in polarized epithelial cells [129], while the EPIYA sequence motif is responsible for membrane association in nonpolarized cells [134]. EPIYA (glutamate-proline-isoleucine-tyrosine-alanine) motifs are located in the C-terminal region and are rapidly tyrosine-phosphorylated by the oncogenic Src family (Src family kinases (SRK)) as well as c-Abl kinases [135, 136]. The phosphorylation of EPIYA motifs constitutes the previously described phosphorylation event which can be detected via immunoblotting (see Chapter 3.2.3). Four distinct EPIYA motifs can be distinguished, EPIYA-A to D, that are classified on the basis of their surrounding amino acid sequence. *H. pylori* strains from East Asian countries harbor East Asian-type CagA including EPIYA-A, EPIYA-B and one EPIYA-D motifs, whereas strains from Western countries carry Western-type CagA containing EPIYA-A, EPIYA-B and one or multiple EPIYA-C motifs [137]. This variation in EPIYA motifs also affects CagA action, and a higher number of EPIYA motifs promotes binding to intracellular targets enhancing the activity within host cells [138, 139], which ultimately correlates with the severity of *H. pylori*-induced disease outcome [140, 141]. In particular, phosphorylated EPIYA segments are able to interact with SH2-domain (Src homology 2 domain)-containing proteins, as for example the SHP-2 tyrosine phosphatase [142]. SHP-2 constitutes a bona fide oncoprotein and mutations are linked to various cancer types [143]. CagA-induced deregulation of SHP-2 leads to the dephosphorylation of various host cellular proteins, which triggers pro-oncogenic cell signaling. One phenotypically observable consequence of this is the induction of an elongated cell shape known as the hummingbird phenotype [144]. Adjacent to the EPIYA motif are one or more MKI motifs (MARK kinase inhibitor or multimerization motif CM). This motif participates in interaction with the activated c-Met receptor (hepatocyte growth factor receptor), which leads to sustained activation of NF-kB causing an increased pro-inflammatory signaling [145]. The MKI motif also specifically interacts with the PAR1b/MARK2 kinase by mimicking substrates thereby inhibiting its activity which leads to disruption of tight junctions and loss of cellular polarity [146, 147]. Moreover, binding to the Par1b/MARK2 homodimers mediates CagA dimerization via the MKI motif, which at the same time stabilizes the binding of CagA and SHP-2. Thus it is assumed that the CagA dimer simultaneously builds a complex with SHP-2 and PAR1 sustaining CagA pathophysiological activity [146]. In addition, the intramolecular interaction of CagA between the C-terminus and N-terminal D3 mediated by CBS and NBS exposes the EPIYA / MKI region and brings the disordered C-terminus in a rigid formation, further stabilizing interactions [130]. Also, the N-terminal region is involved in various interactions. For example, D1 and the linker region between D1 and D2 interact with the gastric tumor

suppressor RUNX3 mediating its degradation [148], and indeed, RUNX3 is frequently inactivated in gastric cancer. Moreover, a CagA-mediated degradation of the p53 tumor suppressor, via association of domain D1 with apoptosis stimulating protein of p53 (ASPP2), has been described and further contributes to an anti-apoptotic effect [149].

Overall, CagA has been shown to interact with more than 20 host cell proteins (reviewed in [133, 150]). Generally, CagA hijacks intracellular signaling cascades in an either phosphorylation-dependent (via EPIYA motifs) or phosphorylation-independent manner. In the course of this, various changes including the induction of uncontrolled cell growth, disruption of epithelial integrity as well as sustained pro-inflammatory signaling are mediated which promote gastric carcinogenesis.

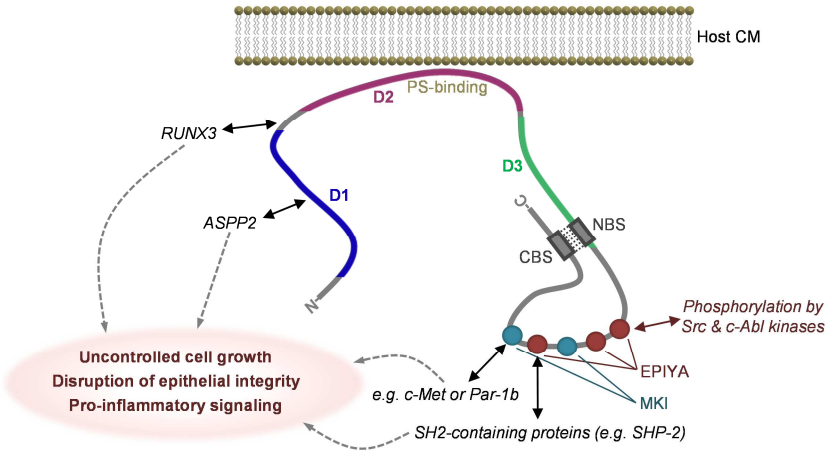

Figure 7: Schematic of CagA domains and host interaction sites
CagA physically interacts with various host cell proteins which mediates the modulation of cell signaling promoting gastric carcinogenesis. D1, D2, D3 refer to structural N-terminal domains (compare Figure 6). CBS: C-terminal binding site, CM: cytoplasmic membrane, MKI: MARK kinase inhibitor motif, NBS: N-terminal binding site, PS: phosphatidylserine. See text for further details. Adapted from [133].

4.3 Evidence for a link between CagA and cancer

The risk for developing disease upon infection with *H. pylori* is influenced by various parameters but with CagA being the greatest risk factor (reviewed in [26, 27]). In addition to the above-mentioned studies on the molecular level, various *in vivo* data also underscore the disease-promoting activity of CagA. For example, upon infection of Mongolian gerbils with *H. pylori*, the strength of inflammation increases and gastric malignancies including adenocarcinoma develop in a CagA-dependent manner [125, 152, 153]. Moreover, transgenic mice expressing CagA form malignancies [154] and in a transgenic Zebrafish model, intestinal carcinogenesis is enhanced upon CagA expression [155]. Also various epidemiological studies show a significantly higher prevalence of gastric diseases including

gastric cancer in individuals that are infected with *cagA*- or *cag*PAI-positive strains compared to persons infected with *cag*PAI-negative *H. pylori* strains [156-158]. These observations strikingly suggest that the CagA-mediated cellular deregulation, together with a general inflammatory response to the infection, marks the pathological progression towards gastric cancer.

5. Treatment of *H. pylori* infection: the increasing failure

Successful eradication of *H. pylori* infection results in regression of ulcers as well as MALT lymphoma and prevents gastric cancer development if atrophy has not evolved yet (see also Chapter 1.2) [159, 160]. In general, only symptomatic individuals are treated with at least two antibiotics in combination with a proton pump inhibitor (PPI). PPI are concomitantly prescribed in order to increase the gastric pH which augments the solubility and local concentration of the antibiotic. However, due to the increasing antibiotic resistance rates [161, 162], treatment efficacy of *H. pylori* infection has decreased drastically with eradication rates often below 50% [163]. According to the latest therapy recommendations [163], first-line therapies should be either composed of a nonbismuth quadruple therapy (PPI, amoxicillin, metronidazole, clarithromycin) or a bismuth quadruple therapy (PPI, bismuth, metronidazole, tetracycline), while the classical triple therapy (PPI, clarithromycin, amoxicillin or metronidazole) should be restricted to areas with low clarithromycin resistance or high eradication rates. Although several other antibiotic combinations are available (second and third line), the problem of the worldwide spreading antibiotic resistances will further deteriorate in the future, and therapies are predicted to fail at increasing rates. Vaccine developments against *H. pylori* infection have been in progress for years, and various pre-clinical and some clinical trials have been performed, but only with limited success [164]. So far, no complete sterilizing immunity was achieved which is mainly attributed to an insufficient induction of a humoral immune response due to the various immune evasion strategies of the bacterium (see Chapter 2.2.2) [165]. The most promising clearance effects were observed in trials where a T-helper cell response could be induced but the efficacy of these approaches is hampered by *H. pylori* persistence mechanisms that subvert adaptive immunity (see Chapter 2.2.2) [133, 164].

However, most people tolerate the presence of *H. pylori* without any adverse effects, and some epidemiological studies even documented an inverse association of *H. pylori* infection with allergic and chronic inflammatory diseases, which is suggested to rely on the *H. pylori*-immunomodulatory effects [14, 166]. Thus, new therapies might be aimed at preventing

H. pylori-induced pathology, rather than to achieve a complete eradication. Indeed, regarding the increasing failure of traditional antibiotic therapy, novel approaches to combat the disease progression upon *H. pylori* infection are urgently needed.

6. Aims of this work

H. pylori becomes increasingly resistant to the current therapeutic antibiotics and the development of new treatment strategies is a challenging issue. Novel antibacterial approaches try to target bacterial virulence factors instead of bacterial viability [167, 168]. So-called pathoblockers provide moreover the benefits of reduced resistance development due to a missing selective pressure, as well as a preservation of the gut microbiome [168]. In the case of *H. pylori*, novel anti-infectives that directly block type IV secretion-mediated CagA translocation into host cells would be most effective to prevent CagA-induced carcinogenesis (see Chapter 4). Hence, studying exact CagA translocation mechanisms as well as strategies to inhibit this process are of major interest. Once inside the host cell, CagA is rapidly phosphorylated by host cell kinases, a process which is routinely analyzed via immunoblotting. As this method is time-consuming and labor-intensive, a novel reporter system should be established that allows fast, sensitive and quantitative CagA translocation analysis. This assay should then be used to study CagA translocation dynamics as well as the type IV signal recognition and secretion process. Moreover, the assay system should be applied to high-throughput screening of different compound libraries to identify specific Cag type IV secretion inhibitors. Compounds discovered during these screenings should be further characterized for their action on *H. pylori*.

II. MATERIALS & METHODS

1. Materials

1.1 Cell lines

Cell lines used in this work are listed in Table 2.

Table 2: Overview of cell lines
FCS: fetal calf serum, Gln: L-glutamine

Cell line	Description	Culture conditions	Source or reference
AGS	Human gastric epithelial adenocarcinoma cell line	RPMI / 10% FCS; 37°C / 5% CO_2	ATCC CRL-1739
HEK-293	Human embryonic kidney epithelial cell line	DMEM / 15% FCS / 2 mM Gln; 37°C / 5% CO_2	ATCC CRL-1573
HEK-293 CEA	Human embryonic kidney epithelial cell line, expressing CEA	DMEM / 15% FCS / 2 mM Gln / 0.5 µg/mL G418; 37°C / 5% CO_2	[169]
J774A.1	Murine macrophage cell line	DMEM / 10% FCS / 2 mM Gln; 37°C / 10% CO_2	ATCC TIB-67
Kato III	Human gastric carcinoma cell line	DMEM / 20% FCS / 2 mM Gln; 37°C / 5% CO_2	ATCC HTB-103
L929	Murine fibroblast cell line	DMEM / 10% FCS/ 2 mM Gln; 37°C / 5% CO_2	ATCC CCL-1

1.2 Bacterial strains

1.2.1 *H. pylori* strains

A list of *H. pylori* strains used or generated in this work is presented in Table 3.

Table 3: Overview of *H. pylori* strains
Expression of *(tem)-cagA* in various mutants is under control of the endogenous promoter within the *cagA* locus, if not otherwise specified. Plasmids are described in detail in Table 5.

Strain	Internal ID	Genotype/properties	Source or reference
26695	WSP86/TIGR	Wild-type; first *H. pylori* strain to be completely sequenced	[28]

Strain	Internal ID	Genotype/properties	Source or reference
B8	EL5	Wild-type; adapted to Mongolian gerbils	[170]
P12	WSP12	Wild-type; clinical isolate (888-0) of the University of Hamburg	[171]
P12 CagA-KKK→A	WSP607	P12[pWS321] transformed with pWS349; Cm^R; CagA-$K_{1203,1208,1213}$→A expression	This work
P12 CagA-REEHKKK→A	WSP620	P12[pWS321] transformed with pWS350; Cm^R; CagA-$R_{1195}E_{1196,1199}H_{1200}K_{1203,1208,1213}$→A expression	This work
P12 CagAΔ5C	WSP805	P12[pWS321] transformed with pWS497; Cm^R; CagAΔ1210-1214 expression	This work
P12 CagAΔ6C	WSP661	P12[pWS321] transformed with pWS387; Cm^R; CagAΔ1209-1214 expression	This work
P12 CagAΔ7C	WSP991/WSP343	P12[pWS321] transformed with pWS502; Cm^R; CagAΔ1208-1214 expression	This work
P12 CagAΔ8C	WSP662	P12[pWS321] transformed with pWS388; Cm^R; CagAΔ1207-1214 expression	This work
P12 CagAΔ9C	WSP1000	P12[pWS321] transformed with pWS580; Cm^R; CagAΔ1206-1214 expression	This work
P12 CagAΔ10C	WSP663	P12[pWS321] transformed with pWS389; Cm^R; CagAΔ1205-1214 expression	This work
P12 CagAΔ10C-GSK	FSP75	P12[pWS321] transformed with pFS12; Cm^R; CagAΔ10C-GSK expression	This work
P12 CagAΔ10C-Myc	FSP76	P12[pWS321] transformed with pFS13; Cm^R; CagAΔ10C-Myc expression	This work
P12 CagAΔ12C	WSP1001	P12[pWS321] transformed with pWS581; Cm^R; CagAΔ1204-1214 expression	This work
P12 CagAΔ181C	WSP558	P12 transformed with pWS321; Cm^R; CagAΔ1034-1214 expression	This work
P12 CagAΔ17N	WSP849	P12[pWS373] transformed with pWS522; Cm^R; CagAΔ1-17 expression	This work
P12 CagAΔD1	WSP979	P12[pWS373] transformed with pWS571; Cm^R; CagAΔ18-284 expression	This work

Strain	Internal ID	Genotype/properties	Source or reference
P12 CagAΔEPIYA	WSP999	P12[pWS373] transformed with pWS579; Cm^R; CagAΔ868-1019 expression	This work
P12 Δ*cagA*	WSP649	P12 transformed with pWS373; Kan^R; deletion of *cagA*	This work
P12 Δ*cagI*	WSP556	P12 transformed with pWS320; Erm^R; deletion of *cagI*	[106]
P12 TEM-CagA	FSP1	P12[pWS373] transformed with pWS486; Cm^R; TEM-CagA expression	This work
P12 TEM-CagA & CagA	WSP874	P12[pWS486] transformed with pJP104; Cm^R, Kan^R; TEM-CagA expression, CagA expression (*cagA* encoded in *recA* locus)	This work
P12 TEM-CagA & CagAΔ20C	FSP74	P12[pWS486] transformed with pWS178; Cm^R; Kan^R; TEM-CagA expression, CagAΔ20C expression (*cagA*Δ20C encoded in *recA* locus)	This work
P12 TEM-CagA; Δ*cagF*	FSP71/WSP943	P12[WS486] transformed with pWS474; Cm^R, Erm^R; TEM-CagA expression, deletion of *cagF*	This work
P12 TEM-CagA; Δ*cagG*	WSP925	P12[WS486] transformed with pWS428; Cm^R, Erm^R; TEM-CagA expression, deletion of *cagG*	This work
P12 TEM-CagA; Δ*cagH*	WSP927	P12[WS486] transformed with pWS423; Cm^R, Erm^R; TEM-CagA expression, deletion of *cagH*	This work
P12 TEM-CagA; Δ*cagI*	FSP2	P12[pWS486] transformed with pWS320; Cm^R, Erm^R; TEM-CagA expression, deletion of *cagI*	This work
P12 TEM-CagA; Δ*cagP*	WSP926	P12[WS486] transformed with pWS503; Cm^R, Erm^R; TEM-CagA expression, deletion of *cagP*	This work
P12 TEM-CagA-GSK	LKP1	P12[pWS486, pWS321] transformed with pWS491; Cm^R; TEM-CagA-GSK expression	This work
P12 TEM-CagA-M45	WSP809	P12[pWS486, pWS321] transformed with pWS500; Cm^R; TEM-CagA-M45 expression	This work
P12 TEM-CagA-KKK→A	WSP821	P12[pWS486, pWS321] transformed with pWS349; Cm^R; TEM-CagA-$K_{1203,1208,1213}$→A expression	This work
P12 TEM-CagA-REEHKKK→A	WSP820	P12[pWS486, pWS321] transformed with pWS350; Cm^R; TEM-CagA-R_{1195},$E_{1196,1199}$,H_{1200},$K_{1203,1208,1213}$→A expression	This work
P12 TEM-CagAΔ5C	WSP808/824	P12[pWS486, pWS321] transformed with pWS497; Cm^R; TEM-CagAΔ1210-1214 expression	This work

Strain	Internal ID	Genotype/properties	Source or reference
P12 TEM-CagAΔ6C	WSP992	P12[pWS486, pWS321] transformed with pWS387; Cm^R; TEM-CagAΔ1209-1214 expression	This work
P12 TEM-CagAΔ7C	WSP857	P12[pWS486, pWS321] transformed with pWS502; Cm^R; TEM-CagAΔ1208-1214 expression	This work
P12 TEM-CagAΔ8C	WSP993	P12[pWS486, pWS321] transformed with pWS388; Cm^R; TEM-CagAΔ1207-1214 expression	This work
P12 TEM-CagAΔ9C	WSP1002	P12[pWS486, pWS321] transformed with pWS580; Cm^R; TEM-CagAΔ1206-1214 expression	This work
P12 TEM-CagAΔ10C	WSP994	P12[pWS486, pWS321] transformed with pWS389; Cm^R; TEM-CagAΔ1205-1214 expression	This work
P12 TEM-CagAΔ10C-GSK	FSP77	P12[pWS486, pWS321] transformed with pFS12; Cm^R; TEM-CagAΔ10C-GSK expression	This work
P12 TEM-CagAΔ10C-Myc	FSP78	P12[pWS486, pWS321] transformed with pFS13; Cm^R; TEM-CagAΔ10C-Myc expression	This work
P12 TEM-CagAΔ12C	WSP1003	P12[pWS486, pWS321] transformed with pWS581; Cm^R; TEM-CagAΔ1204-1214 expression	This work
P12 TEM-CagAΔ181C	WSP801	P12[pWS486] transformed with pWS321; Kan^R; TEM-CagAΔ1034-1214 expression	This work
P12 TEM-CagAΔ17N	WSP955	P12[pWS373] transformed with pWS559; Cm^R; TEM-GSGGGS-CagAΔ1-17 expression	This work
P12 TEM-CagAΔD1	WSP996/997	P12[pWS373] transformed with pWS575; Cm^R; TEM-CagAΔ18-284 expression	This work
P12 TEM-CagAΔD2-D3-EPIYA	WSP1007	P12[pWS373] transformed with pWS586; Cm^R; TEM-CagAΔ260-1019 expression	This work
P12 TEM-CagAΔEPIYA	WSP806	P12[pWS373] transformed with pWS498; Cm^R; TEM-CagAΔ868-1019 expression	This work

1.2.2 *E. coli* and other strains

E. coli and other bacterial strains used in this work are listed in Table 4.

Table 4: *E. coli* and other bacterial strains

Strain	Genotype/description	Source or reference
E. coli DH5α	F-Φ80d *lac*Z Δ*M15* Δ(*lac*ZYA-*arg*F) U169 *deo*R *recA*1 *endA*1 *hsd*R17 (*rK*-, *mK*+) *pho*A *sup*E44 λ-*thi*-l *gyr* A96 *rel*A1	Life Technologies [172]
E. coli TOP10	F-*mcrA* Δ(*mrr-hsd*RMS-*mcr*BC) Φ80*lac*ZΔ*M15* Δ*lac*O74 *rec*A1 *ara*Δ139 Δ(*ara-leu*)7697 *gal*U *gal*K *rps*L (StrR) *end*A1 *nup*G	Life Technologies [173]
C. jejuni	C31	W. Fischer
S. aureus	*Staphylococcus aureus* subsp. *aureus* Rosenbach	ATCC 29213

1.3 Plasmids

Plasmids used in this work are listed in Table 5.

Table 5: Overview of plasmids
Genomic DNA of *H. pylori* P12 served as template for PCRs if not otherwise stated. Numbering of CagA refers to codon positions. Corresponding primers are listed in Table 6.

Name	Purpose	Backbone/modification	Source or reference
pBluescript II KS	Cloning vector		Agilent Technologies
pCX340	Template for *tem* (*blaM*) sequence		[174]
pFS12	Construction of (*tem*)-*cagA*Δ10C-*gsk*	pWS336; replacement of *Xba*I/*Kpn*I fragment by PCR product with primers WS237 & FS8	This work
pFS13	Construction of (*tem*)-*cagA*Δ10C-*myc*	pWS336; replacement of *Xba*I/*Kpn*I fragment by PCR product with primers WS237 & FS10	This work
pJP104	Insertion of *cagA* in *recA* locus		[175]
pUC18	Cloning vector		Life Technologies

Name	Purpose	Backbone/modification	Source or reference
pWS178	Insertion of *cagA*Δ20C in *recA* locus		[131]
pWS320	Deletion of *cagI* locus, Δ*cagI*::*rpsL-erm*		[106]
pWS321	Deletion of *cagA* 3´ region, Δ*cagA* 3´::*aphA-3*	pBluescript II KS; insertion of a *cagA* downstream fragment amplified with primers WS390 & WS391 into *Bam*HI/*Not*I site and an *aphA-3* kanamycin resistance cassette; insertion of an internal *cagA* fragment (codons 847-1033) amplified with primers WS423 & WS424 into *Xho*I/*Cla*I site	This work
pWS336	*cagA* reconstitution plasmid for 3´ modifications	pUC18; insertion of a *cagA* downstream fragment amplified with primers WS390 & WS391 into *Bam*HI/*Not*I site and a cat_{GC} chloramphenicol resistance cassette; insertion of the *cagA* 3´ region (codons 847-1214) amplified with WS423 & WS425 into *Sal*I/*Pst*I site	This work
pWS349	Construction of (*tem*)-*cagA*-KKK→A	pWS336; replacement of *Xba*I/*Kpn*I fragment by PCR product with primers WS237 & RL5	This work
pWS350	Construction of (*tem*)-*cagA*-REHHKKK→A	pWS336; replacement of *Xba*I/*Kpn*I fragment by PCR product with primers WS237 & RL6	This work
pWS373	Deletion of *cagA* gene, Δ*cagA*::*aphA-3*	pBluescript II KS; insertion of a *cagA* downstream fragment amplified with primers WS390 & WS391 into *Bam*HI/*Not*I site and an *aphA-3* kanamycin resistance cassette; insertion of a *cagA* upstream fragment amplified with primers hp546r & WS400 into *Xho*I/*Bam*HI site	This work
pWS387	Construction of (*tem*)-*cagA*Δ6C	pWS336; replacement of *Xba*I/*Kpn*I fragment by PCR product with primers WS237 & WS477	This work
pWS388	Construction of (*tem*)-*cagA*Δ8C	pWS336; replacement of *Xba*I/*Kpn*I fragment by PCR product with primers WS237 & WS281	This work
pWS389	Construction of (*tem*)-*cagA*Δ10C	pWS336; replacement of *Xba*I/*Kpn*I fragment by PCR product with primers WS237 & WS479	This work
pWS403	*cagA* reconstitution plasmid	pUC18; insertion of a *cagA* downstream fragment amplified with primers WS390 & WS391 into *Bam*HI/*Not*I site and a cat_{GC} chloramphenicol resistance cassette; insertion of *cagA* amplified with WS370 & WS425 into *Nde*I/*Pst*I site and insertion of *cagA* upstream region amplified with primers hp546r & WS242 into *Sal*I/*Nde*I site	This work

Name	Purpose	Backbone/modification	Source or reference
pWS423	Deletion of *cagH* gene, Δ*cagH::rpsL-erm*		W. Fischer
pWS428	Deletion of *cagG* gene, Δ*cagG::rpsL-erm*		W. Fischer
pWS474	Deletion of *cagF* gene, Δ*cagF::rpsL-erm*		W. Fischer
pWS476	Plasmid intermediate for construction of *tem-cagA* (*blaM-cagA*)	pWS403; insertion of *tem* (*blaM*) amplified with WS553 & WS428 into *Nde*I/*Bgl*II site and pCX340 as template	This work
pWS486	Construction of *tem-cagA* (*blaM-cagA*)	pWS476; insertion of full-length *cagA* amplified with WS265 & WS425 into *Bgl*II and *Kpn*I site	This work
pWS491	Construction of *tem-cagA-gsk*	pWS336; replacement of *Xba*I/*Kpn*I fragment by PCR product with primers WS237 & WS597	This work
pWS497	Construction of (*tem*)-*cagA*Δ5C	pWS336; replacement of *Xba*I/*Kpn*I fragment by PCR product with primers WS237 & WS177	This work
pWS498	Construction of *tem-cagA*Δ868-1019	pWS476; insertion of PCR product with primer WS265 & WS318 into *Bgl*II	This work
pWS500	Construction of *tem-cagA-m45*	pWS336; replacement of *Xba*I/*Kpn*I fragment by PCR product with primers WS237 & WS267	This work
pWS502	*Construction of* (*tem*)-*cagA*Δ7C	pWS336; replacement of *Xba*I/*Kpn*I fragment by PCR product with primers WS237 & WS281	This work
pWS503	Deletion of *cagP* gene, Δ*cagP::rpsL-erm*		W. Fischer
pWS508	Construction of (*tem*)-*cagA*Δ20C	pWS336; replacement of *Xba*I/*Kpn*I fragment by PCR product with primers WS237 & WS178	This work
pWS522	Construction of *cagA*Δ1-17	pWS403; replacement of *Nde*I/*Kpn*I fragment by PCR product of primers WS611 & WS425	This work
pWS559	Construction of *tem*-GSGGGS-*cagA*Δ1-17	pWS476; replacement of *Bgl*II/*Kpn*I fragment by PCR product with primers WS652 & WS425	This work
pWS571	Construction of *cagA*Δ18-284	pWS403; replacement of *Nde*I/*Kpn*I fragment by overlap extension PCR product with primers WS370, WS613, WS612 & WS425	This work

Name	Purpose	Backbone/modification	Source or reference
pWS575	Construction of *tem-cagA*Δ18-284	pWS476; replacement of *Bgl*II/*Kpn*I fragment with PCR product with WS265 & WS425 and pWS571 as template	This work
pWS579	Construction of *cagA*Δ868-1019	pWS403; replacement of *Nde*I/*Bgl*II fragment by PCR product with primers WS370 & WS318	This work
pWS580	Construction of (*tem*)-*cagA*Δ9C	pWS336; replacement of *Xba*I/*Kpn*I fragment by PCR product with primers WS237 & WS704	This work
pWS581	Construction of (*tem*)-*cagA*Δ12C	pWS336; replacement of *Xba*I/*Kpn*I fragment by PCR product with primers WS237 & WS291	This work
pWS586	Construction of *tem-cagA*Δ260-1019	pWS476; insertion of PCR product with primers WS265 & WS705 into *Bgl*II site	This work

1.4 Oligonucleotides

Salt-free oligonucleotides were purchased from Biomers.net or Metabion. Oligonucleotides were dissolved in ddH_2O to a stock concentration of 100 pmol/µL and diluted to a final working concentration of 10 pmol/µL. Oligonucleotides were stored at -20°C. Primer design, specificity and amplicon length was determined with the CLC DNA workbench software. All primers used in this work are summarized in Table 6.

Table 6: Overview of oligonucleotides
Recognition sites of restriction enzymes are underlined.

Name	Sequence (5´ → 3´)	Restriction enzyme
FS8	GGGGTACCTTATGATTCTGCAAAACTTGTAGTTCGAGGTCGGCC AGACATCTCGAGATTCTTGATTCCATGCTCTGCAT	*Kpn*I
FS10	GGGGTACCTTACAGATCCTCTTCTGAGATGAGTTTTTGTTCATTC TTGATTCCATGCTCTGCAT	*Kpn*I
hp546r	ACCGCTCGAGTGTAAAAAATTTCATGCGTT	*Xho*I
RL5	CCGGTACCTTAAGATGCTTGGAAACCACCTGCTGTATTAACATT CGCGATTCCATGC	*Kpn*I
RL6	CCGGTACCTTAAGATGCTTGGAAACCACCTGCTGTATTAACATT CGCGATTCCAGCCGCTGCATTTGCCGCCGCCAAGCAG	*Kpn*I
WS177	GGGGTACCTTAACCTTTTGTATTAACATTC	*Kpn*I
WS178	CTGGTACCTTACGCCAAGCAGTAATATCCT	*Kpn*I
WS237	AATCTAGAGCAAACGATAGAC	*Xba*I

Name	Sequence (5´ → 3´)	Restriction enzyme
WS242	ACCGCTCGAGCATATGTTCTCCTTACTAACTAGTTTC	*Nde*I
WS265	CAGGATCCGACTAACGAAACCATTAACC	*Bam*HI
WS267	GGGGTACCTTATAAGATCCTGGTTTCTGTTTCAAAAGGCGGCAA ACGATCCCTGCTCCTGTCGACAGATTTTTGGAAACCACCTTTTG	*Kpn*I
WS281	CGGGTACCTTATGTATTAACATTCTTGATTC	*Kpn*I
WS291	GCGGTACCTTAGATTCCATGCTCTGCATTTTC	*Kpn*I
WS318	CGGGATCCGAAAAGTTTTTAGAAAG	*Bam*HI
WS370	AGCATATGACTAACGAAACCATTAAC	*Nde*I
WS390	CGGGATCCTAAAGGATTAAGGAATACC	*Bam*HI
WS391	ACCTGCGGCCGCTAAAGTGGAATTTCATGCG	*Not*I
WS400	GCGGATCCCATATGTTCTCCTTACTAACTAGTTTC	*Bam*HI
WS423	ACCGCTCGAGAACCCTAGTCGGTAATGGG	*Xho*I
WS424	ATATCGATTTAAGCCAATTTTTGATTCCTTG	*Cla*I
WS425	ACCGCTGCAG GGTACCTTAAGATTTTTGGAAACCAC	*Pst*I *&Kpn*I
WS428	GAAGATCTCCCCAATGCTTAATCAGTGAGGCACC	*Bgl*II
WS477	CGGGTACCTTATTTTGTATTAACATTCTTGATTC	*Kpn*I
WS478	CGGGTACCTTAATTAACATTCTTGATTCCATG	*Kpn*I
WS479	CGGGTACCTTAATTCTTGATTCCATGCTCTGC	*Kpn*I
WS553	ACGCGTCGACCATATGCACCCAGAAACGCTGGTGAAAG	*Nde*I
WS597	GGGGTACCTTATGATTCTGCAAAACTTGTAGTTCGAGGTCGGCC AGACATCTCGAGAGATTTTTGGAAACCACCTTTTG	*Kpn*I
WS611	ACCGTACATATGGATCCGCAGCAATTTATCAATAATC	*Nde*I
WS612	GGCTTTTAACCCTAATTACAAGTTCAACCAATTATTGATTC	
WS613	GTTGAACTTGTAATTAGGGTTAAAAGCCGCTTCGGTTTG	
WS652	ACCGTACATATGGATCCGGGATCTGGGGGTGGGTCTGGTCCGCA GCAATTTATCAATAATC	*Bam*HI
WS704	CGGGTACCTTAAACATTCTTGATTCCATGCTC	*Kpn*I

Name	Sequence (5´ → 3´)	Restriction enzyme
WS705	GCGGATCCTCAAGTAAATCTCTAGCTTCAGG	*Bam*HI

1.5 Chemicals and standard buffers

Chemicals were purchased from Roth, Merck, or Sigma-Aldrich if not otherwise specified. In general, distilled water (dH_2O) was used for the preparation of buffer or media, while ultrapure water (ddH_2O, Roth) was used for any molecular biological reaction. Cell culture grade DPBS (Dulbecco's PBS without calcium and magnesium, Life Technologies) was used for experiments with living bacteria or cells, and self-prepared PBS for all other purposes.

Self-prepared PBS (phosphate-buffered saline)

2.7 mM	Potassium chloride (KCl)
138 mM	Sodium chloride (NaCl)
1.5 mM	Monopotassium phosphate (KH_2PO_4)
8 mM	Disodium phosphate (Na_2HPO_4)

1.6 Cultivation media and additives

1.6.1 Liquid media and supplements

Liquid media and supplements used for cultivation of bacteria and eukaryotic cells are listed in Table 7.

Table 7: List of liquid media and supplements

Media	Supplier	Comment
Brucella broth (BB)	Becton Dickinson	for BB liquid media, 28 g/L
Dulbecco´s Modified Eagle media with sodium pyruvate and pyridoxine (DMEM)	Life Technologies	
Fetal calf serum (FCS)	Life Technologies	heat inactivated (56°C, 20 min)
G418	Sigma-Aldrich	
Lennox-L-Medium (Luria-Bertani broth, LB)	Invitrogen	for LB liquid media, 20 g/L
L-glutamine	Life Technologies	
RPMI 1640 media with L-glutamine	Life Technologies	

1.6.2 Agar plates

Lennox-L agar (32 g/L, Invitrogen) and GC agar base (36 g/L, Oxoid) were used for LB agar and GC agar (serum) plates, respectively. Serum plates were additionally supplemented with 8% horse serum (PAA) and 1% vitamin mix after autoclaving and cooling down below a temperature of 55°C. If necessary, antibiotics (see Table 8) were added. Plates were stored at 4°C.

GC agar plates (serum plates) *formula per 0.455 L dH_2O*

18 g	GC agar base
40 mL	Horse serum (8%)
5 mL	Vitamin mix (1%) consisting of 100 g/L α-D-glucose, 10 g/L L-glutamine, 26 g/L L-cysteine, 1.1 g/L L-cystine, 0.15 g/L L-arginine, 0.1 g/L cocarboxylase, 20 mg/L iron(III)nitrate, 3 mg/L thiamine, 13 mg/L p-aminobenzoic acid, 0.25 g/L nicotinamide adenine dinucleotide, 10 mg/L vitamin B12, 1 g/L adenine, 30 mg/L guanine, 0.5 g/L uracil

1.6.3 Antibiotics

Antibiotics were dissolved in respective solvents, sterile filtrated (0.22 µm) and stored in aliquots at -20°C. Additional information is listed in Table 8.

Table 8: List of antibiotics

Antibiotic	Supplier	Solvent	Final concentration in media/agar plate	
			H. pylori	***E. coli***
Ampicillin	Sigma-Aldrich	Water	-	100 mg/L
Chloramphenicol	Fluka	Ethanol	6 mg/L	30 mg/L
Erythromycin	AppliChem	Ethanol	10 mg/L	250 mg/L
Kanamycin	Sigma-Aldrich	Water	8 mg/L	50 mg/L
Streptomycin	Sigma-Aldrich	Water	250 mg/L	250 mg/L

1.7 Compounds for high-throughput screenings and follow-up studies

For high-throughput screening assays, compound libraries as well as any resupply were derived from the Helmholtz Center for Infection research (Braunschweig). The libraries comprised purified natural products from the HZI (Saarbrücken) and IMIT (Tübingen), chemically synthesized molecules from the SPECS company, and pharmacologically active substances from Sigma-Aldrich´s LOPAC library. Further substances, used as reference substances in follow-up studies, are listed in Table 9.

Table 9: Commercial compounds for follow-up studies

Compound	Solvent	Supplier
Antimycin A from *Streptomyces* sp.	Ethanol	Sigma-Aldrich
Carbonyl cyanide *m*-chlorophenyl hydrazone (CCCP)	DMSO	Sigma-Aldrich
Rotenone	DMSO	Sigma-Aldrich

1.8 Antibodies

All antibodies including the applied final concentration are listed in Table 10.

Table 10: List of antibodies
AP: alkaline phosphatase, POX: horseradish peroxidase, α: anti-

Antibody	Internal-ID	Antigen (origin)	Final concentration	Supplier or reference
Primary antibodies				
α CagA	AK257	Polyclonal antibody against C-terminal part of CagA (rabbit)	1:5000 (AP) 1:50000 (POX)	[74]
α CagA	AK268	Polyclonal antibody against N-terminal part of CagA (rabbit)	1:1000 (AP)	[131]
α CagF	AK284	Polyclonal antibody against CagF (rabbit)	1:1000 (AP)	[119]
α CagI	AK293	Polyclonal antibody against C-terminal part of CagI (rabbit)	1:2000 (AP)	[106]
α IL-8		Monoclonal antibody against human interleukin-8 (mouse)	ELISA/coating	BD Pharmingen
α IL-8 biotin		Monoclonal antibody against human interleukin-8, biotin conjugated	ELISA/detection	BD Pharmingen
α M45		Polyclonal antibody against the M45-epitope (mouse)	1:1000 (AP)	[176]
α Myc tag		Monoclonal antibody against the Myc epitope tag (mouse)	1:5000 (AP)	Cell Signaling Technology, Inc.
α P-GSK		Polyclonal antibody against phospho-GSK(glycogen synthase kinase)-3β (rabbit)	1:1000 (POX)	Cell Signaling Technology, Inc.
α P-Tyr	4G10	Monoclonal antibody against tyrosine-phosphorylated proteins (mouse)	1:5000 (POX)	Merck Millipore

Antibody	Internal-ID	Antigen (origin)	Final concentration	Supplier or reference
Primary antibodies				
α P-Tyr	PY99	Monoclonal antibody against tyrosine-phosphorylated proteins (mouse)	1:5000 (POX)	Santa Cruz Biotechnologies
α RecA	AK263	Polyclonal antibody against RecA (rabbit)	1:1000 (AP)	[177]
α TEM-1		Monoclonal antibody against TEM type β-lactamases from *E. coli* (mouse)	1:2500 (AP)	Abcam
α Tubulin		Monoclonal antibody against tubulin (mouse)	1:50000 (POX)	Abcam
Secondary antibodies				
Protein A-AP		AP coupled to protein A (*S. aureus*)	1:5000	Sigma-Aldrich
α mouse-AP		AP-coupled polyclonal antibody against mouse-IgG (goat)	1:1000	Sigma-Aldrich
α mouse-POX		POX-coupled polyclonal antibody against mouse-IgG (goat)	1:10000	Sigma-Aldrich
α rabbit-POX		POX-coupled polyclonal antibody against rabbit-IgG (goat)	1:10000	Sigma-Aldrich

2. Methods

2.1 Microbiological methods

2.1.1 Cultivation of *H. pylori*

H. pylori was streaked onto serum plates from glycerol stock cultures (2.1.3) and incubated for at least 48 h at 37°C under microaerobic conditions (5% O_2, 10% CO_2, 85% N_2). Grown cultures were passaged onto fresh serum plates every day or at least once before experiments and again cultivated for about 24 h. For liquid cultures, BB supplemented with 10% FCS (BB/FCS) was inoculated and incubated in an anaerobic pot under microaerobic atmosphere (see above) while shaking (85 rpm).

2.1.2 Cultivation of *E. coli* and other bacteria

E. coli and *S. aureus* were pre-cultured from glycerol stocks on LB agar plates. Plates were stored at 4°C for maximal 2 weeks. For overnight cultures, LB medium was inoculated with one single colony and incubated at 37°C while shaking (150 rpm). If necessary, LB was supplemented with respective antibiotics (see Table 8). *C. jejuni* was always freshly streaked out from glycerol stock culture (2.1.3) on serum plates followed by incubation for 24 h at 37°C / 10% CO_2.

2.1.3 Maintenance of bacterial cultures

For long-term storage, bacterial strains were frozen in a glycerol emulsion to prevent any cell damage. To do so, freshly grown bacteria were suspended in a so-called freezing media (70% BB containing 10% FCS and 20% glycerol) and stored at -80°C in cryogenic tubes (Nalgene, Thermo Fisher Scientific).

2.1.4 Determination of the optical density of bacterial suspensions

The concentration of bacterial suspensions was determined by measuring the amount of light scattered by the culture at a wavelength of 550 nm (OD_{550}) with a spectrophotometer (DR 2000, Hach). Bacteria were derived directly from liquid cultures or resuspended from agar plates in medium or buffer using a sterile cotton swab. An OD_{550} of 0.1 was estimated to correspond to approximately 2.5 x 10^7 cfu/mL.

2.1.5 Growth curves

H. pylori and *C. jejuni* grown on serum plates or *E. coli* and *S. aureus* derived from liquid cultures (2.1.1 and 2.1.2) were diluted to an OD_{550} of 0.075 (2.1.4) and subcultured in 96-well microtiter plates (clear, flat-bottom, Costar, Corning Inc.), which were then sealed with a gas-permeable membrane (Breathe-Easy® sealing membrane, Diversified Biotech). Plates were incubated at 37°C (while shaking) in the Clariostar plate reader (BMG Labtech), and the optical density at 550 nm was automatically monitored. Thereby, for *H. pylori* and *C. jejuni* a microaerobic environment (5% O_2 / 10% CO_2 or 18% O_2 / 10% CO_2) was generated by an atmospheric control unit (ACU, BMG Labtech). Measurements were conducted until the stationary phase was reached. Growth curves were analyzed and processed using the MARS Data Analysis software 3.10 R5 (BMG Labtech). Percental growth was expressed as [(ΔOD_{sample} / $\Delta OD_{control}$) x 100], while ΔOD corresponded to "$OD_{stationary\ phase} - OD_{lag\ phase}$".

2.1.6 Generation of genetically manipulated bacteria

Transformation describes the direct uptake of exogenous DNA into bacterial cells, occurring when bacteria are in a competent state. For the introduction of plasmid DNA into *E. coli*, competence was artificially induced by a chemical pre-treatment to permeabilize the cell membrane. In the case of *H. pylori*, the natural competence of the bacterium was exploited for genetic manipulation.

Preparation and transformation of rubidium chloride (RbCl) competent E. coli cells

For preparation of rubidium chloride (RbCl) competent *E. coli* (modified after [173]), 200 mL of LB medium was inoculated with 20 mL of the respective *E. coli* overnight pre-culture (2.1.2). The cell suspension was incubated at 37°C and grown to an optimal OD_{550} of about 0.56, which corresponds to the logarithmic growth phase. Cultures were transferred in pre-chilled falcon tubes and harvested by centrifugation (3000 x g, 10 min, 4°C). The LB medium was decanted and cells were resuspended in 80 mL of ice-cold TfbI. After a rest on ice for 5 min, cells were pelleted again (3000 x g, 10 min, 4°C) and the supernatant discarded. Finally, the cell pellet was resuspended in 8 mL of ice-cold TfbII solution. Aliquots of 50 µL were dispensed, immediately frozen in liquid nitrogen and stored at -80°C.

TfbI buffer *in dH_2O*

30 mM	Potassium acetate
100 mM	Rubidium chloride (RbCl)
10 mM	Calcium chloride ($CaCl_2$)
50 mM	Manganese chloride ($MnCl_2$)

Glycerol was added to a final concentration of 15% (v/v), pH adjusted to 5.8 and sterile-filtrated.

TfbII buffer *in dH_2O*

10 mM	3-(*N*-morpholino)propanesulfonic acid (MOPS)
75 mM	$CaCl_2$
10 mM	RbCl

Glycerol was added to a final concentration of 15% (v/v), pH adjusted to 6.5 and sterile-filtrated.

For effective transformation (protocol adapted from [178]), 15 µL of a ligation reaction mixture (2.4.9) was added to frozen RbCl competent *E. coli*. Then, the bacterial cells were thawed rapidly by warming between hands, gently swirled and immediately placed on ice for 30 min. Cells were heat shocked for 90 s at 42°C (Thermoblock, Eppendorf) and instantly transferred on ice again for 2 min. 1 mL of LB medium was added and bacteria were incubated for at least 1 h at 37°C while shaking to allow expression of antibiotic resistance. The culture suspension was centrifuged (2500 x g, 5 min), the supernatant decanted, the cell pellet resuspended in the remaining medium and gently plated on LB agar plates containing

respective antibiotics (Table 8). Incubation was performed at 37°C for 24 h.

Natural transformation of H. pylori cells

H. pylori was harvested from serum plates and suspended in BB/FCS (modified after [179]). Cells were adjusted to an OD_{550} of 0.2 and dispended in a 24-well plate with a total volume of 1 mL per transformation reaction. *H. pylori* was incubated for 1-2 h at 37°C / 10% CO_2 to increase motility and transformation competence. After addition of 5-10 µL plasmid DNA, suspensions were incubated for another 4-6 h. Bacteria were collected by centrifugation (1000 x g / 5 min), resuspended in the remaining medium and plated on selective serum plates. For detection of single colonies, *H. pylori* was incubated for at least 3 days at 37°C under microaerobic conditions (5% O_2, 10% CO_2, 85% N_2).

2.2 Cell culture

2.2.1 Cultivation and maintenance of cell lines

Cell lines were cultivated in 75 cm^2 tissue culture flasks (BD Falcon®) under standard conditions (see Table 2) and subcultured every 2-3 days. In detail, adherent cells (except J774) were washed with Dulbecco´s buffered saline (DPBS, Life Technologies), treated with 3 mL of 0.05% Trypsin-EDTA (TE, Life Technologies) and incubated for 5 min at 37°C to detach the cells. This reaction was stopped by adding culture medium supplemented with FCS, cells were diluted in fresh media and further cultured. J744 were washed with DPBS, scraped off with a cell scraper and transferred into fresh media. For cell counting, cells were resolved in solution, live/dead stained with trypan blue (Life Technologies) and applied to a Neubauer counting chamber. For experiments, cells were dispended in 6-, 12-, 24-, 48 or 384-well plates (tissue culture-treated, Costar, Corning Inc.), and in 96-well plates (black, transparent bottom, tissue culture-treated, 4titude®) or 386-well plates (black, transparent bottom, tissue culture-treated, Corning Inc.) for fluorescence-assisted plate reader applications.

2.2.2 Freezing and thawing of cell lines

For long-term storage, cells were collected by centrifugation (about 10^6 cells) and resuspended in freezing medium (50% culture medium, 45% FCS, 5% DMSO). Stocks were stored in cryogenic tubes (Nalgene, Thermo Fisher Scientific) for at least 24 h at -70°C and

then transferred to liquid nitrogen tanks. For thawing of cells, frozen stocks were incubated at 37°C, washed twice with pre-warmed culture medium (250 x g, 10 min) and cultivated under recommended conditions (see Table 2).

2.3 *In vitro* infections

To mimic the infection process of *H. pylori* with eukaryotic cells, *in vitro* infections were carried out. When *H. pylori* was cultured on plates, bacteria were first suspended in DPBS containing 10% FCS (DPBS/FCS), diluted to an OD_{550} appropriate for the later multiplicity of infection (MOI) (2.1.4), and then incubated for about 2 h at 37°C / 10% CO_2 to increase fitness and motility of bacteria. Eukaryotic cells, grown to a confluency of ~80% (2.2.1), were infected with *H. pylori* with an MOI of 100, if not otherwise specified. The infection was incubated for 2.5 h at 37°C / 5% CO_2 (only J774 cells at 37°C / 10% CO_2), if not otherwise stated. Further analysis was carried out via tyrosine/GSK phosphorylation assay (2.5.4), immunoprecipitation (2.5.5), ELISA (2.5.6), or with the TEM-CagA assay (2.8).

2.4 DNA methods

2.4.1 Preparation of genomic DNA

For isolation of genomic *H. pylori* DNA (gDNA), the QIAmp DNA Mini Kit (Qiagen) was employed. Briefly, *H. pylori* was collected from serum plates and suspended in 180 µL ATL buffer. After addition of 20 µL proteinase K, the suspension was incubated at 56°C for at least 3 h while shaking for efficient cell lysis. Then, 200 µL of AL buffer was added and heated at 70°C for 10 min. After the precipitation of nucleic acids, 200 µL of ethanol was added and the mixture was applied to a column which was followed by several washing steps according to the manufacturer´s instructions. Finally, gDNA bound to the column matrix was dissolved in ddH_2O to a concentration suitable for further experimentation and stored at -20°C.

2.4.2 Preparation of plasmid DNA

Plasmids derived from *E. coli* were either purified with the QIAprep Spin Miniprep Kit (Qiagen) for highly pure plasmid preparations or by a rather impure boiling procedure (adapted from [180]).

The commercial kit was performed following the spin protocol. For this purpose, liquid overnight cultures were harvested by centrifugation or bacteria grown on plates were directly

suspended in P1 buffer, then lysed, applied to the column and the DNA bound to the silica-based membrane. Remaining contaminates were removed by washing steps and plasmid DNA was eluted with 40 µL ddH_2O.

For the plasmid preparation by boiling, bacteria were first resuspended in 300 µL STET buffer. After the addition of 15 µL lysozyme (10 mg/mL in STET buffer), the suspension was left on ice for at least 5 min. To break the cells further down, the suspension was cooked for 1 min and centrifuged (20,000 x g / 10 min) for the removal of cell debris. The supernatant was mixed with 200 µL isopropanol and incubated at -20°C for at least 10 min to increase precipitation of DNA. The DNA was pelleted by centrifugation and washed with 70% ethanol, dried and resuspended in 50 µL ddH_2O. Purified DNA was stored at -20°C.

STET buffer *in dH_2O*	
50 mM	Tris/HCl, pH 8.0
50 mM	Ethylenediaminetetraacetic acid (EDTA)
8%	Saccharose
5%	Triton X-100

2.4.3 Nucleic acid concentration determination

Nucleic acid samples were routinely controlled for their concentration and purity by measuring optical densities (at 260, 280 and 230 nm) with the NanoDrop ND-1000 spectrophotometer (PeqLab). For this purpose, 1 µL of nucleic acid in the respective solvent was applied on the sample column and the OD_{260}, which is proportional to the nucleic acid concentration (Lambert-Beer law), was determined. OD_{260}/OD_{280} as well as OD_{260}/OD_{230} ratios were recorded to assess impurities with proteins or other organic components.

2.4.4 Polymerase chain reaction (PCR)

Polymerase chain reaction (PCR) is a common technique for *in vitro* enzymatic amplification of a specific segment of DNA. For amplification of DNA with cloning purposes, the *ExTaq* DNA polymerase (Takara, Clontech) was applied. This polymerase exhibits a 3'→5' exonuclease (proofreading) activity that enables the polymerase to correct nucleotide incorporation errors, resulting in high fidelity [181]. For conventional gene amplification (e.g. mutant screening) the *PanScript* Polymerase (pan-biotech), lacking this proofreading ability, was used. A 1:50 dilution of genomic (2.4.1) or plasmid DNA (2.4.2) served as template. In general, annealing temperatures were adjusted to primer specifity and elongation time was adapted to the amplicon size. Reactions were carried out in a thermal cycler (Thermo Hybaid Px2, Thermo Fisher Scientific; Mastercycler personel, Eppendorf).

PCR mix for *ExTaq* polymerase	
50 µL volume	
14.9 µL	ddH_2O
5 µL	10x *ExTaq* buffer
5 µL	Magnesium chloride ($MgCl_2$, 25 mM)
10 µL	3´-Oligonucleotide (10 pmol/µL)
10 µL	5´-Oligonucleotide (10 pmol/µL)
4 µL	dNTP-Mix (2.5 mM)
0.1 µL	*ExTaq* polymerase
1 µL	DNA template

PCR mix for *PanScript* polymerase	
50 µL volume	
13.4 µL	ddH_2O
5 µL	10x *PanScript* NH4-buffer
2.5 µL	$MgCl_2$ (50 mM)
10 µL	3´-Oligonucleotide (10 pmol/µL)
10 µL	5´-Oligonucleotide (10 pmol/µL)
8 µL	dNTP-Mix (1.25 mM)
0.1 µL	*PanScript* polymerase
1 µL	DNA template

	PCR Cycling program		
		ExTaq	*PanScript*
	Initial denaturation	94°C / 5 min	
30 times	Denaturation	94°C / 30 s	
30 times	Annealing	50 – 52°C / 30 s	
30 times	Elongation	68°C / 2 kb/min	72°C / 1 kb/min
	Final elongation	68°C / 5 min	72°C / 5 min

2.4.5 Agarose gel electrophoresis

In order to separate and purify DNA fragments derived from PCR amplification (2.4.4) or restriction enzyme digest (2.4.7), agarose gel electrophoresis was performed. DNA (negatively charged) migrates in an electric field from the cathode to the anode. Thus, DNA fragments of different length can be easily separated, as shorter DNA fragments move faster through the agarose matrix than longer fragments. Gels were prepared by heating 1-2% (w/v) agarose in 1x tris-acetate-EDTA (TAE) buffer, until the agarose was completely dissolved. This mixture was put into a filling device and pockets were formed with a comb. Prior to loading the gel pockets, DNA samples were premixed with GEBS buffer. A DNA ladder (Generuler^{TM} 1kb DNA Ladder, Thermo Fisher Scientific) served as reference. Gels were run in horizontal gel chambers (Bio-Rad) in 1x TAE buffer with a constant voltage of up to 15 V/cm gel length for 30 to 60 min to achieve optimal separation of DNA fragments. Staining of analytic gels was performed in ethidium bromide (1 mg/L) for 45 min and gels were photographed under ultraviolet (UV) light using a gel documentation system (Molecular Imager Gel Dox XR System, Bio-Rad). Preparative gels were stained with a 0.1% methylene blue solution. After destaining with tab water, DNA bands were cutted with a scalpel and purified (2.4.6).

1x tris-acetate-EDTA (TAE) buffer	
in dH_2O	
40 mM	Tris/HCl, pH 8
20 mM	Acetic acid
1 mM	EDTA

GEBS buffer	
20% (v/v)	Glycerine
50 mM	EDTA
0,05% (w/v)	Bromphenol blue
0,5% (w/v)	N-Laurylsarcosyl

2.4.6 Purification of DNA fragments

To guarantee a high purity of DNA fragments for any downstream application, impurities in DNA samples (derived from enzymatic reaction or agarose gel) had to be removed. Therefore, the illustra GFX PCR DNA and Gel Band Purification Kit (GE Healthcare) was employed following the manufacturer´s recommendations.

2.4.7 Digestion of DNA with restriction enzymes

DNA was digested with restriction enzymes (RE) from Thermo Fisher Scientific or Roche Applied Science following the manufacturer´s instructions. Briefly, Plasmid DNA or PCR amplicon DNA was incubated with the respective enzyme in the recommended reaction buffer for 2-3 h at 37°C. Therefore, 1-2 µg DNA were used for preparative and 30-100 ng DNA for analytic restrictions. DNA fragments were either first purified via agarose gel electrophoresis (2.4.5) or directly re-buffered after every digestion step (2.4.6). Purified DNA was eluted in ddH_2O and stored at -20°C.

Digestion mix e.g. *10 µL volume*	
8 µL	Plasmid/insert diluted in ddH_2O
1 µL	10x RE-specific buffer
1 µL	RE

2.4.8 Dephosphorylation of DNA plasmid ends

To prevent recirculation of vector DNA plasmids after restriction digest (2.4.7), a shrimp alkaline phosphatase (SAP, Roche Applied Science) treatment was conducted. Together with a SAP-specific buffer, the reaction mixture was incubated for 1 h at 37°C and plasmids were re-purified afterwards (2.4.6).

Dephosphorylation mix *100 µL volume*	
88 µL	Digested plasmid
10 µL	10x SAP buffer
2 µL	SAP

2.4.9 Ligation

For ligation of restriction enzyme-generated DNA fragments, the T4 DNA Ligase (Fermentas) was employed. Respective amounts of inserts and vector DNA were determined following a molar ratio of 3:1 for cloning PCR products in plasmid vectors and equimolar amounts for DNA fragments of similar length. Reaction mixtures were incubated overnight at RT and then used for transformations (2.1.6).

Ligation mix *20 µL volume*	
20-100 ng	Linear vector DNA
1:1 or 1:3	Insert DNA
(molar ratio of insert : vector)	
2 µL	10x Ligase buffer
1 µL	T4 DNA Ligase
to 20 µL	ddH_2O

2.4.10 *In silico* cloning and DNA sequence analysis

In silico cloning was performed with the CLC DNA Workbench 6 software in order to determine and monitor the base pair length of various DNA fragments (generated during digestion and amplification steps). For analysis of DNA sequences, 10-20 ng/µL of purified PCR products or 50 ng/µL of plasmid DNA were subjected to sequencing by the GATC Biotech AG. Evaluation of sequences was performed with the CLC DNA Workbench 6 software.

2.5 Protein biochemistry methods

2.5.1 Production of bacterial lysates

To produce bacterial lysates, the OD_{550} (2.1.4) of a bacterial suspension was determined and the desired amount sedimented by centrifugation (1500 x g, 5 min). The supernatant was discarded and the cell pellet resuspended in SDS sample buffer (see 2.5.2). Samples were cooked for 10 min at 95°C and finally analyzed via SDS-PAGE (2.5.2) and subsequent Immunoblotting (2.5.3).

2.5.2 Sodium dodecyl sulfate polyacrylamide gel electrophoresis (SDS-PAGE)

SDS-PAGE (modified from [182]) enables analytical separation of proteins. Prior to SDS-PAGE, proteins are denatured by heating in the presence of thiols and SDS. Proteins bind SDS in a constant weight ratio, and the negatively charged SDS-protein complexes are separated according to their molecular size when migrating through the gel matrix in response to an electrical field. To increase the resolution during separation, a discontinuous gel was applied [178]. This consisted of an upper stacking gel with a low polyacrylamide concentration (5%) and slightly acidic pH, and a resolving gel which is more basic and has a higher polyacrylamide content. To do so, resolving gel solutions (6-12%) were filled into slab mini-gel polymerization cassettes up to 1.5 cm beneath the glass plate edge and overlaid with water to provide a barrier to oxygen (that inhibits polymerization) as well as to form a flat

interface. After polymerization (about 1 h), the water layer was poured off and the stacking gel solution applied. A comb was inserted to form sample wells and polymerization was allowed for about 1 h. Gels were either directly clambed to the *Mini-PROTEAN® 3 Cell* chamber (Bio-Rad) or stored at 4°C.

Before performing electrophoresis, samples had to be diluted in SDS sample buffer and heated for 10 min at 95°C to break up cells and denature secondary and tertiary protein structures. Then, 2-10 µL of sample volume was loaded into the gel pockets. As a size reference, 5 µL of Page Ruler™ Prestained Protein Ladder (Fermentas) was used. Electrophoresis was conducted in SDS-running buffer with a voltage of 100 V until the tracking dye entered the resolving gel. Then, voltage was increased up to 140 V until the dye had reached the bottom of the separating gel.

SDS-polyacrylamide gel composition *sufficient for 1 minigel*

	Resolving gel				Stacking gel
	6%	**8%**	**10%**	**12%**	
dH_2O	2.6 mL	2.3 mL	1.9 mL	1.6 mL	0.68 mL
Acrylamide (Rotiphorese® Gel 30 (37.5:1))	1.0 mL	1.3 mL	1.7 mL	2.0 mL	0.17 mL
1.5 M Tris/HCl, pH 8.8	1.3 mL	1.3 mL	1.3 mL	1.3 mL	-
1.0 M Tris/HCl, pH 6.8	-				0.13 mL
10% (w/v) SDS	50 µL				10 µL
10% (w/v) Ammonium peroxide sulfate (APS)	50 µL				10 µL
Tetramethylethylenediamine (TEMED)*)	4 µL	3 µL	2 µL	2 µL	1 µL

*) starts polymerization of acrylamide and was added last

SDS-running buffer

250 mM	Glycine
0.1% (w/v)	SDS
25 mM	Tris/HCl, pH 8.3

Gels were either analyzed via immunoblotting (2.5.3) or stained with Coomassie Brilliant Blue solution (according to [183]) for 2 h while slightly agitating. After incubation in destaining solution for 24 h, gels were photographed with the ChemiDoc MP device (Bio-Rad).

Coomassie Brilliant Blue staining solution

0.275% (w/v)	Coomassie Brilliant Blue R250
7.5% (v/v)	Acetic acid
50% (v/v)	Methanol

Destaining solution

7.5% (v/v)	Acetic acid
10% (v/v)	Ethanol
10% (v/v)	Methanol

2.5.3 Immunoblot (Western blot)

Immunoblotting is a common technique for the detection of proteins that are immobilized on a membrane and visualized with specific antibodies. Therefore, protein samples are first

electrophoretically separated by SDS-PAGE and then transferred onto a membrane applying an electric field.

Blotting procedure

A piece of PVDF (polyvinylidene fluoride) membrane (9 x 6 cm, Bio-Rad) was activated by wetting in 100% methanol for 15 s. Subsequently, the membrane was transferred to a container of anode II buffer for at least 2 min to equilibrate the membrane. Using a semi-dry blot system [184], two thick sheets of anode I saturated whatman filter paper and two thin sheets saturated with anode II buffer were placed into the blotting chamber (Biotec-Fischer). The SDS-PAGE gel (2.5.2) together with the membrane was put on top followed by two thin and two thick sheets soaked with cathode buffer. For transfer of the proteins from the gel onto the blot, a current of 1.25 mA/cm^2 was applied for 70-80 min. Afterwards, the membrane was dried on a clean filter paper for at least 1 h, reactivated in 100% methanol and equilibrated in anode II buffer. All subsequent steps, except chemiluminescent development, were performed while slightly agitating on a rocking platform.

Anode I buffer	
300 mM	Tris/HCl, pH 10.4
10%	Methanol

Cathode buffer	
25 mM	Tris/HCl, pH 9.6
40 mM	6-Amino caproic acid
10%	Methanol

Anode II buffer	
25 mM	Tris/HCl, pH 10.4
10%	Methanol

Detection of immobilized proteins with antibodies

At first, remaining binding sites on the membrane were blocked by incubation in blocking solution (consisting of 5% milk powder in TBST) overnight at 4°C. The membrane was then incubated for 2 h with the first antibody in TBST/1% milk powder in the respective dilution (see Table 10). To remove unspecifically bound antibodies, washing steps were performed (5x 5 min with 1x TBST). A second antibody (conjugated with POX or AP, see Table 10) in TBST/1% milk powder was incubated with the membrane for 1 h and extensively washed afterwards (at least 5x 5 min with TBST). For chromogenic development of AP activity, membranes were incubated with 5 mL AP detection solution until desired bands were visible, and the reaction was stopped with tab water. For chemiluminescent detection of POX-coupled antibodies, the membrane was immersed for 2 min in a substrate solution containing luminol (Immobilon Chemiluminescent HRP Substrate, Millipore) and luminescence was detected in a ChemiDoc MP device (Bio-Rad). Further analysis, including densitometric evaluation for

relative quantification of signal bands, was conducted with the Image Lab software (Bio-Rad).

10x TBS *in dH_2O*	
1.5 M	NaCl
200 mM	Tris/HCl, pH 7.5

TBS-Tween buffer (TBST)	
100 mL	10x TBS
1 mL	Tween 20
up to 1 L	dH_2O

AP detection solution	
100 mM	Tris/HCl, pH 9.6
7 mM	$MgCl_2$
50 mg/L	5-Bromo-4-chloro-3-indolyl phosphate (BCIP)
0.1 g/L	Nitro blue tetrazolium (NBT)

Membrane stripping

After chemiluminescent development, membranes could be re-used by soaking in an acid solution (25 mM glycine/HCl, 1% SDS, pH 2) for 60 min to remove bound antibody complexes. Prior to re-incubation with antibodies, membranes were extensively washed with tab water and again saturated in TBST/1% milk powder.

2.5.4 Tyrosine and GSK phosphorylation assay

H. pylori is able to inject its CagA protein into eukaryotic host cells. As the protein itself or a GSK-tag, genetically fused to CagA, gets phosphorylated inside the target cell, the analysis of these phosphorylation events are routinely used as proof of CagA translocation. For this, AGS cells were infected with *H. pylori* following the standard protocol (2.3) and then chilled on ice. To remove dead cell debris and unbound bacteria, cells were washed two times with pre-chilled PBS and AGS cells were scraped off on ice in PBS, which was supplemented with a protease and phosphatase inhibitors mixture (PBS*). Cells were sedimented by centrifugation and either directly resuspended in SDS sample buffer for SDS-PAGE (2.5.2) or first in RIPA buffer for an upstream pull-down assay (2.5.5). After immunoblotting (2.5.3), bacterial CagA protein or CagA fused to a phosphorylatable GSK-tag was visualized with specific antibodies (see Table 10).

Inhibitor mixture for PBS*	
1 mM	Phenylmethylsulfonyl fluoride (PMSF)
1 mM	Sodium vanadate
1 µM	Leupeptin
1 µM	Pepstatin
1 per 10 mL	*PhosSTOP tablet (only for GSK assay, Roche Applied Science)*

2.5.5 Immunoprecipitation (Pull-down assay)

Pull-down experiments were conducted to concentrate and purify specific proteins, including corresponding interacting proteins, from a bacteria or bacteria-cell lysate. First, bacteria grown on agar plates (2.1.1) or infected AGS cells (2.3) were washed twice with PBS. In the latter case, cells were scraped off as described in the previous chapter (2.5.4). Bacteria, or cells with adherent bacteria, were resuspended in radioimmunoprecipitation (RIPA) buffer and lysed by sonication (50% duty cycle, output control 3, three 10 s intervals followed by 10 s rest; Sonifier 250, Branson). Cell debris was removed by centrifugation (10 min / 15,000 x g) and a 1:500 dilution of a respective antiserum was added to the supernatant. After an overnight incubation at 4°C while slightly agitating, 50 µL of pre-washed protein G-agarose (Roche Applied Science) was added to the samples, and incubation was continued for at least another 2 h to achieve maximal absorption of antibody-bound proteins to the agarose beads. To remove unspecific bound proteins, the beads were washed three times with RIPA buffer and proteins were eluted by boiling for 10 min in SDS-PAGE sample buffer. Samples were analyzed via SDS-PAGE (2.5.2) and subsequent immunoblotting (2.5.3).

RIPA buffer

50 mM	Tris/HCl, pH 8.0
150 mM	NaCl
1 mM	EDTA
1% (v/v)	Nonidet P-40
0.25% (w/v)	Sodium deoxycholate
+	Inhibitor mixture (see 2.5.4)

2.5.6 ELISA for interleukin-8 (IL-8) quantification

AGS cells release IL-8 in response to infection with *H. pylori*. To quantify this, supernatants of *in vitro* infections (see 2.3) were analyzed by ELISA (Enzyme Linked Immunosorbent Assay). For this purpose, the wells of an immunoabsorbent 96-well plate (Nunc) were coated with 100 µL IL-8 antibody (see Table 10) diluted in coating buffer (3 µg/mL in 100 mM Na_2HPO_4, pH 9.0), and incubated overnight at 4°C. Wells were washed three times with washing buffer (PBS with 0.05% Tween-20) and saturated in 200 µL blocking buffer (washing buffer with 10% FCS) for 2-4 h at RT. Wells were again washed three times and 100 µL of diluted supernatant samples (in RPMI / 10% FCS) were added. To enable quantitative analysis, a dilution series of human IL-8 (BD Pharmingen) in RPMI / 10% FCS was established, ranging from concentrations of 0 to 800 µg/mL, and added to the wells. After an overnight incubation at 4°C, wells were four times washed to remove unbound antigens,

and 100 µL of biotinylated anti-IL-8 antibody (0.5 µg/mL in blocking buffer, see Table 10) was added. After incubating at RT for 2 h and washing four times, 100 µL of a Streptavidin-Biotin-POX solution (Peroxidase Standard, Biozol) was added and incubated for another hour. The wells were extensively washed in six washing cycles, 100 µL of TMB substrate solution (BD OptEla^{TM}, BD Biosciences) was added to each well and incubated for 30 min in the dark at RT. The chromogenic development was stopped with 50 µL 1 M sulfuric acid (H_2SO_4) per well. Subsequently, the optical density at 450 nm was determined (Clariostar, BMG Labtech) and a standard calibration curve was computed using OD_{450} values of the IL-8 standard dilutions. IL-8 concentrations were determined with the standard curve function and multiplied by the dilution factor.

Streptavidin-Biotin-POX solution *per 96-well microtiter plate*

1.5 µL	Solution A
1.5 µL	Solution B
mixed in 200 µL	50 mM Tris/HCl, pH 7.6

After incubation for 30 min at RT, the mixture was filled up to 10 mL with 50 mM Tris/HCl, pH 7.6

2.6 Brightfield and phase-contrast microscopy

Bacteria, cells or cells infected with *H. pylori* were routinely checked via brightfield or phase-contrast microscopy using a WILOVERT S (Hund Wetzlar) or a LEICA DM IRB (Leica) microscope. Pictures were taken using the latter one with the SPOT Insight 2Mp Monochrome FireWire digital camera system (Diagnostic instruments).

2.7 Flow cytometry (FACS)

In flow cytometry, bacterial or eukaryotic cell suspensions are hydrodynamically focused before entering a laser beam, and the emitted light signals are detected by photomultiplier tubes (PMT) (including a forward angle light scatter detector (FSC), a side-scatter detector (SSC), and multiple fluorescence emissions detectors). Signals are then digitized for computer analysis. FACS measurements were applied for examination of TEM-1 activity (2.8.1), bacterial membrane potential (2.10), and permeability (2.11). Briefly, cell populations were first defined by means of the FSC (as a measure for volume) and SSC (as a measure for granularity) detector signals, and the fluorescence emission of at least 10,000 cell counts was recorded. All measurements were conducted with the FACS CantoII instrument (BD Biosciences, Heidelberg), and data was evaluated using the FACSDiva software or the FlowJo software (Tree Star).

2.8 TEM-CagA translocation assay

The TEM-CagA translocation assay is a novel method to analyze *H. pylori* CagA translocation into eukaryotic cells. The test principle is in detail described in the results section (1.1). Briefly, eukaryotic cells were infected with *H. pylori* P12 harboring a TEM-CagA fusion (2.3). After infection, cells were loaded with the fluorescent substrate CCF4-AM in the corresponding loading solution (Live-BLAzer-FRET B/G loading kit, Invitrogen) which was supplemented with 1 mM probenecid (Sigma-Aldrich).

1x CCF4-AM loading solution *for 1 mL volume*	
1 µL	Solution A (= 1 mM CCF4-AM)
10 µL	Solution B
156 µL	Solution C
5 µL	Probenecid (200 mM)
828 µL	DPBS

2.8.1 Analysis by flow cytometry

For flow cytometry applications (see 2.7), cells were incubated in the staining solution for 90 min in the dark at RT. Stained cells were washed three times with DPBS, finally suspended in 200 µL DPBS and subjected to FACS analysis. CagA translocation was expressed as the ratio of the Pacific Blue to the AmCyan emission channels (Blue-to-Green). Percental CagA translocation rates were determined following [(Blue-to-Green$_{(\text{sample-negative control})}$ / Blue-to-Green$_{(\text{positive control-negative control})}$) x 100] with P12[TEM-CagA] as positive, and P12[TEM-CagA]Δ*cagI* as negative control.

2.8.2 Analysis by fluorescence-assisted plate reading

For fluorescence quantification by plate reading, infected cells were incubated with the loading solution at RT in the dark for at least 120 min and directly measured with a Clariostar reader (BMG Labtech) using an excitation wavelength of 405 nm (10 nm bandwidth). Emission was detected with 460 nm (20 nm bandwidth, blue fluorescence) and 530 nm (15 nm bandwidth, green fluorescence) filters. CagA translocation was defined as the emission ratio at 460 nm$_{(\text{sample-blank})}$ divided by that at 530 nm$_{(\text{sample-blank})}$ (Blue-to-Green), where the blank wells contained only CCF4-AM loading solution, but no cells or bacteria. Relative CagA translocation levels were calculated using the formula described in 2.8.1.

2.8.3 Analysis by fluorescence microscopy

For the detection of TEM-1 activity by fluorescence microscopy, infected AGS cells were

covered with CCF4-AM in the respective loading solution, and examined with a Leica TCS SP5 confocal microscope. Routine image processing was performed with ImageJ v1.45h (US National Institutes of Health).

2.9 High-throughput screening of compound libraries

Compound libraries were derived from the Helmholtz Center for Infection Research (Braunschweig). For screening analysis with the TEM-CagA assay (2.8.2), compounds were pre-pipetted in 384-well plates (low volume, sterile, Corning Inc.), and each well content was sufficient for a 20 µL test volume. In detail, 20 µl of bacterial cells (OD_{550} of 0.075 in DPBS/FCS) were added into each well and incubated for 30 min at 37°C / 10% CO_2. Then, 17 µL of the bacteria-compound mixture was gently pipetted up and down, and transferred onto AGS cells which were seeded in 384-well plates (low volume, sterile, Corning Inc.; see also 2.2.1). Infection proceeded following standard conditions (2.3), and TEM-1 activity was determined via plate reading (2.8.2). For screening analysis via growth curves, compounds were derived in 96-well plates (half-volume, sterile, Corning Inc.). Per well, 50 µL of bacterial suspension was dispended and the OD_{550} automatically monitored (see 2.1.5).

2.10 Measurement of bacterial membrane potential

To evaluate the effect of various compounds on *H. pylori* membrane potential, the *Bac*Light™ Bacterial Membrane Potential Kit (Molecular Probes), which contains the carbocyanine dye $DiOC_2(3)$ (3,3′-diethyloxacarbocyanine iodide), was used. $DiOC_2(3)$ exhibits green fluorescence in the bacterial cytosol, but larger membrane potential causes self-association of the dye, leading to a fluorescence shift towards red emission. First, 75 µL of a *H. pylori* suspension (OD_{550} of 0.075 in BB/FCS) was incubated in the presence of the respective compound for 3 h at 37°C / 10% CO_2. Thereby, 10 µM of the protonophore CCCP (carbonyl cyanide 3-chlorophenylhydrazone) was applied as a membrane potential destroying control. 12.5 µL of the suspension was then transferred into 200 µL DPBS (supplemented with 1 mM EDTA and 15 µM $DiOC_2(3)$), and incubated for another 30 min at 37°C / 10% CO_2. Bacterial cells were analyzed by flow cytometry with the FITC- and PE-fluorescence emission detectors (see 2.7), and the red to green fluorescence ratio was determined.

2.11 Measurement of bacterial membrane permeability

Increased membrane permeability leads to the destruction of the membrane potential. To assess the influence of several compounds on membrane permeability, which would explain the effect on membrane potential, the fluorescent dye propidium iodide (PI, Miltenyi Biotec) was applied. PI is membrane impermeant and can only enter permeabilized cells. Once PI is in the cell, it intercalates into the DNA which leads to an increase in red fluorescence. For this analysis, a *H. pylori* suspension was incubated with respective compounds as described in the previous section (2.10). Then, 12.5 µL of the suspension was added to 200 µL DPBS (containing 1 mM EDTA and 4 µL PI), and incubated at RT for 1 h in the dark. The red fluorescence shift was analyzed via flow cytometry in the PE emission channel (see 2.7) and expressed as median fluorescence intensity (MFI).

2.12 Quantification of bacterial ATP content

The influence of several compounds on cellular ATP content of *H. pylori* was determined using the ATP bioluminescence assay Kit CLS II (Roche Applied Science). Thereby, even low concentrations of ATP can be detected due to the ATP dependency of the light emitting oxidation of luciferin. To do so, 450 µL of bacterial cell suspension (OD_{550} of 0.15 in BB/FCS) was first exposed to the compounds of interest for 5 min at 37°C / 10% CO_2. Bacteria were collected by centrifugation (10,000 x g / 5 min), the supernatant discarded, and the pellet was resuspended in 75 µL 100 mM Tris/HCl (containing 4 mM EDTA, pH 7.75). This suspension was cooked for 2 min at 95°C, the cell debris removed by centrifugation (10,000 x g / 1 min) and 50 µL of the supernatant was added into a 96-well plate (black, transparent bottom, tissue culture-treated, 4titude®). In addition, the ATP calibration stock (provided by the kit) was solved in 100 mM Tris/HCl (containing 4 mM EDTA, pH 7.75), serially diluted in the range of 10^{-5} to 10^{-10} M, and added to the wells. The plate was left on ice until measurement. After the addition of 50 µL of the luciferase reagent to the samples/standards by automated injection, bioluminescence development was recorded with a 1 s delay plus signal integration time of 10 s in the Clariostar plate reader (BMG Labtech). The blank control (standard without ATP) was subtracted and the ATP concentrations were calculated from a log-log plot of the standard curve data. Percental concentrations relate to $[1-((ATPcontent_{untreated\ control\ -\ sample} / ATPcontent_{untreated\ control}) \times 100)]$.

2.13 Determination of bacterial oxygen consumption

To test the influence of specific substances on *H. pylori* oxygen consumption, OxoPlates® (96-well microtiter plates, round bottom, PreSens), which have an integrated chemical optical oxygen sensor, were applied. For this, 140 µL of *H. pylori* suspensions (OD_{550} of 1.0 in DPBS) together with the test substances, were added into the wells. Besides, freshly-prepared oxygen-free water (cal0, 300 µL per well, sealed with a strip of adhesive foil) and air-saturated water (cal100, 200 µL per well) were used as calibration standards.

Oxygen-free water = cal0
0.15 g Sodium sulfite (Na_2SO_3)
in 15 mL dH_2O
A 15 mL falcon vessel with a tightly fitting screw top was used for preparation.

Air-saturated water = cal100
20 mL dH_2O
in a 50 mL falcon tube
The water was vigorously shaken for at least 2 min.

Organic acids *in DPBS, pH 7.4*

	Injected volume
500 mM Pyruvate	2 µL
500 mM D,L-Lactate	2 µL
500 mM α-Ketoglutarate	4 µL
250 mM Succinate	4 µL

Before starting the measurement, the plate was incubated for at least 10 min at 37°C in the pre-warmed plate reader (FluoStar Optima, BMG Labtech) in order to equilibrate the samples and standards. Fluorescence was recorded every 2 min using a 550 nm excitation filter, and emission was detected with a 660 nm (indicator fluorescence, $I_{indicator}$) and 590 nm filter (reference fluorescence, $I_{reference}$). With it, the time-resolved mode was applied with an integration start at 0 µs and integration time of 500 µs. After the third measurement cycle, an organic acid solution was automatically injected to the samples and the fluorescence detection proceeded for at least 10 more cycles. For each well the reference signal "$I_R = I_{indicator} / I_{reference}$" was calculated. The oxygen partial pressure pO_2 (in % air saturation) was calculated for each measurement point following pO2[% air sat.] = [100 x $((k_0/I_R - 1) / (k_0/k_{100} - 1))$], where k_0 is the I_R of cal0 and k_{100} the I_R of cal100, respectively.

2.14 Evaluation of cellular cytotoxicity

The effect of several compounds on eukaryotic cell proliferation and viability was assessed with the Cell Proliferation Reagent WST-1 (Roche Applied Science). This assay is based on the cleavage of the tetrazolium salt WST-1 to formazan by mitochondrial dehydrogenases. Thus, the color change correlates with the number of metabolically active cells in culture. At

first, 30 µL of cell suspensions were seeded into 384-well plates (black, clear bottom, Corning Inc.) and cultivated at respective conditions (see Table 2) but using a phenol red-free culture medium (for reduction of background in the later measurement). On the following day, test substances were added in corresponding dilutions and incubation was continued for three days. Then, 2.5 µL of WST-1 solution was added to each well and further incubated for at least 60 min. The absorbance of the formazan product at OD_{450} and a reference wavelength at 690 nm (OD_{690nm}) were recorded in the Clariostar plate reader (BMG Labtech). For evaluation, the difference of OD_{450nm} and OD_{690nm} was determined, and the blank control (only medium and WST-1) was subtracted, resulting in OD_{norm}. Percental cytotoxicity was expressed as the OD_{norm} of the sample divided by OD_{norm} of the corresponding DMSO control, and IC_{50} values were determined by non-linear regression analysis.

2.15 Statistical analysis

Statistical analysis was performed with the GraphPad prism 5 software. Experimental data sets shown are generally average values resulting from at least three independent measurements including the standard error of the mean. The significance of differences was determined using either Student´s t-test, one-way ANOVA with Tukey post hoc test, or two-way ANOVA with Bonferroni post hoc test.

III. RESULTS

1. Development of a novel Cag type IV secretion reporter

H. pylori translocates its oncogenic protein CagA via type IV secretion into eukaryotic cells. Once inside, CagA gets phosphorylated immediately at several tyrosine residues (EPIYA motifs) via host cell kinases [74-76]. For years, CagA translocation has been routinely checked by detection of this phosphorylation event via immunoblotting. However, this method gives only insights into the rate of CagA phosphorylation, but not the translocation process itself. Moreover, it is stringently dependent on the presence of the EPIYA region and hence, also limits CagA translocation evaluation of specific mutants. To overcome these restrictions, a phosphorylatable GSK-tag was fused to CagA [131], which allowed an extended evaluation of CagA translocation via phospho-GSK specific antibodies. But still, immunoblotting constitutes a labor-intensive and time-consuming procedure with limited sensitivity and quantifiability. Thus, a phosphorylation-independent reporter that enables not only fast but also quantitative analysis should be developed.

1.1 Principle of a β-lactamase (TEM-1)-dependent translocation assay

In other bacterial pathogens such as *Escherichia coli*, *Yersinia pestis* or *Legionella pneumophila*, the translocation of various effector proteins has been studied via fusion of a 29 kDa TEM-1 β-lactamase [174, 185, 186]. This compact enzyme, which is originally the product of an *E. coli* plasmid-encoded ampicillin resistance gene, can efficiently cleave β-lactam antibiotics including penicillins and (first generation) cephalosporins. Thus, a modified version of TEM-1 (lacking the endogenous secretion signal) has been found to be an excellent reporter tag. A general schematic how this should work as a type IV secretion reporter in *H. pylori* is depicted in Figure 8. Briefly, *H. pylori* translocates the TEM-1 (β-lactamase)-CagA fusion protein into the host cell cytosol, where the enzymatic activity of the reporter tag is detected via conversion of the cell-permeable fluorescence substrate CCF4 (Figure 8A). The structure of CCF4 is shown in Figure 8B. This FRET (Fluorescence Resonance Energy Transfer)-based fluorescent substrate consists of a cephalosporin core linking a 7-hydroxycoumarin to a fluorescein. The esterified form of CCF4 (CCF4-AM) is non-fluorescent but when entering the cell, esters get cleaved off by endogenous esterases and the intact molecule produces a green fluorescence signal due to the FRET-excited fluorescein molecule. Upon cleavage of the β-lactam ring of the cephalosporin core, the two fluorophores get spatially separated, the FRET disrupted, and only the blue fluorescence of the coumarin

can be detected. This permits a ratiometric read-out of the Blue-to-Green fluorescence by any fluorescence-assisted device allowing quantitative analysis of translocated CagA protein.

In the following sections, the transfer of this method into *H. pylori* for quantitative Cag type IV secretion analysis will be described.

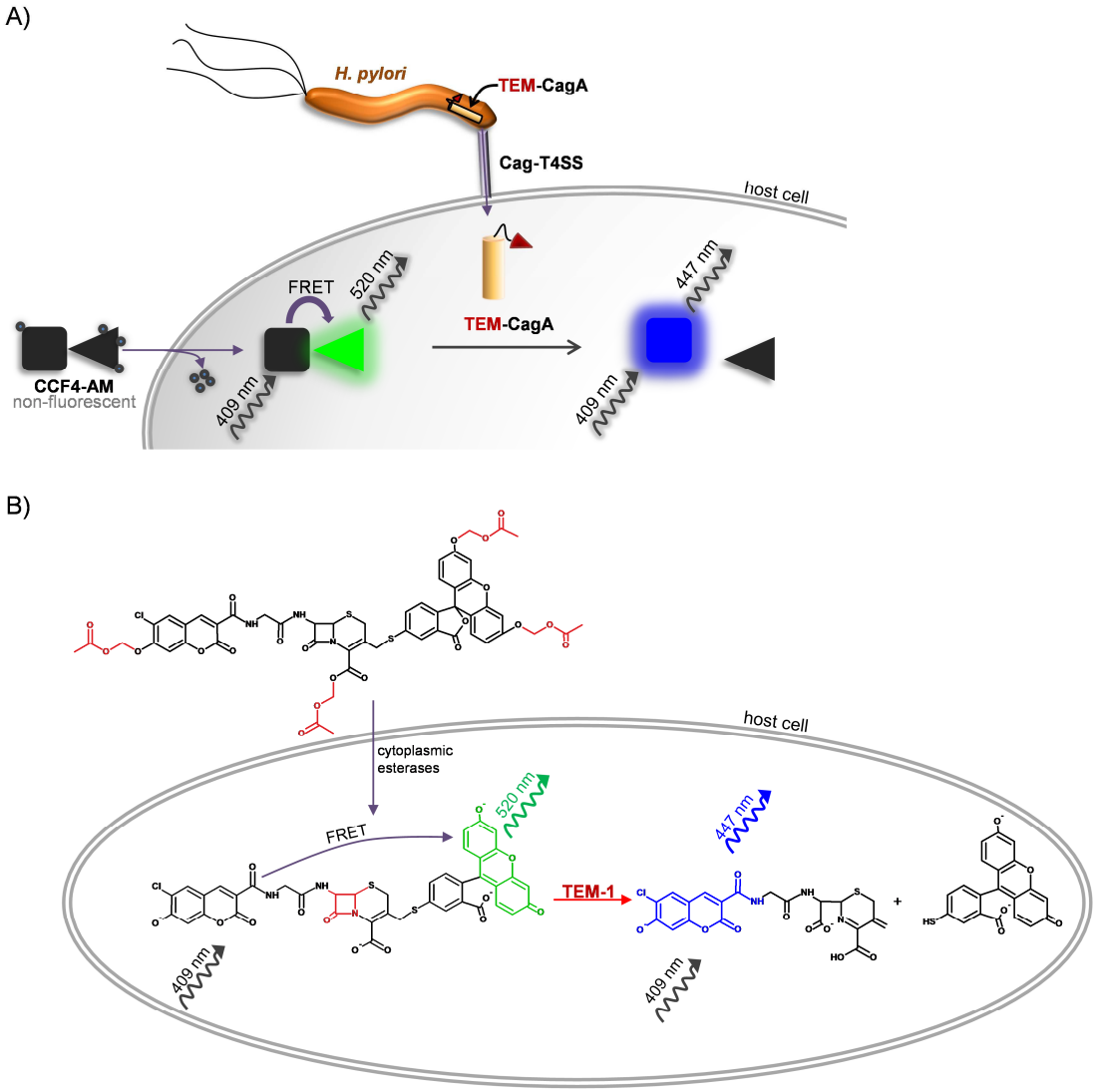

Figure 8: Principle of a β-lactamase (TEM-1)-dependent CagA translocation reporter
A) *H. pylori* translocates the TEM-1 (β-lactamase)-CagA fusion protein (TEM-CagA) into the eukaryotic host cell. Enzymatic activity of the TEM-1 reporter tag can be monitored by conversion of the β-lactam derivative CCF4. The intact molecule emits green fluorescence, while after enzymatic cleavage of CCF4, blue fluorescence is emitted. The ratio of Blue-to-Green fluorescence serves as a measure of CagA translocation (adapted from [174]).
B) The lipophilic, esterified form of CCF4 (CCF4-AM) enters the cell and ester moieties get cleaved off by endogenous cytoplasmic esterases converting the molecule into a negatively charged substrate, which is retained in the cytosol. CCF4 consists of a cephalosporin core linking a 7-hydroxycoumarin to a fluorescein. In the absence of TEM-1 activity, excitation of the coumarin (at 409 nm) in the intact CCF4 results in FRET to the fluorescein, emitting a green fluorescence signal (at 520 nm). In the presence of TEM-1, enzymatic cleavage of CCF4 spatially separates the two fluorophores and disrupts FRET, with the result that excitation of the coumarin (at 409 nm) leads to a blue fluorescence signal (450 nm). CCF4-AM structure is derived from [187].
FRET: Fluorescence Resonance Energy Transfer, T4SS: type IV secretion system.

1.2 Construction and evaluation of TEM-CagA-expressing reporter strains

For construction of TEM-CagA-expressing reporter strains, a chromosomal *cagA* reconstitution system was established that only introduced minimal changes into the wild-type. Hence, expression of variant *cagA* genes should be enabled in the *cagA* locus itself under control of the endogenous *cagA* promoter. For this purpose (see Figure 9A), the wild-type *cagA* gene in *H. pylori* P12 was exchanged by transformation using pWS373 with an *aphA-3* kanamycin resistance cassette (P12[pWS373]). Subsequently, the TEM-1 β-lactamase gene (*tem-1* or *blaM*), lacking its N-terminal secretion signal, was fused in-frame to the 5´ end of P12 wild-type *cagA* (*tem-1-cagA*), and the corresponding construct (pWS486) was introduced into P12[pWS373] via homologous recombination (P12[pWS486] or P12[TEM-CagA]).

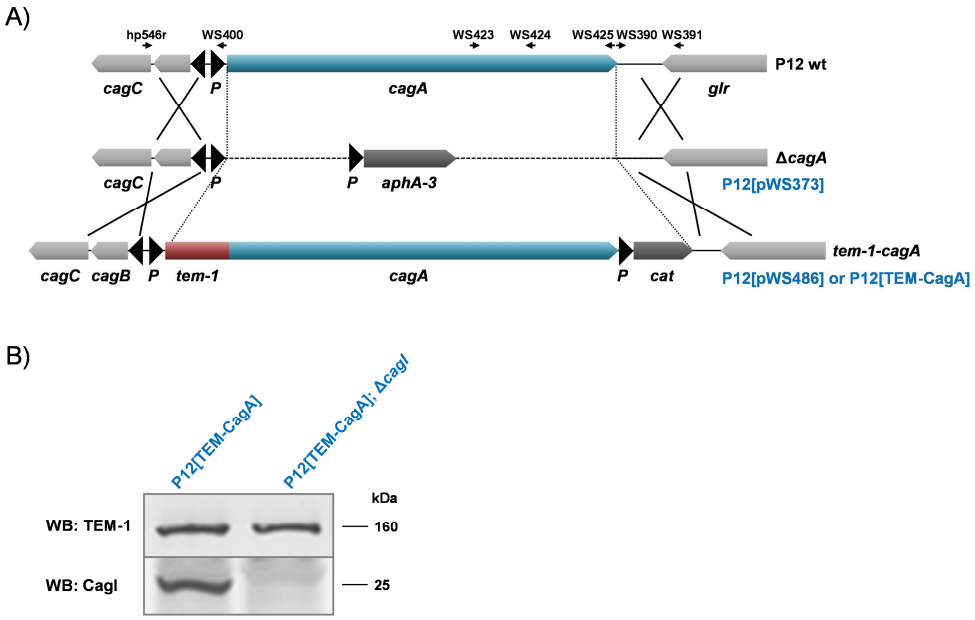

Figure 9: Construction of TEM-CagA-expressing reporter strains
A) Chromosomal reconstitution strategy for generation of *H. pylori* P12 strains expressing the TEM-CagA fusion protein. The *cagA* gene was deleted via insertion of an *aphA-3* cassette by transformation with pWS373. The *tem-1-cagA*-encoding plasmid pWS486 including a *cat* resistance cassette as selection marker was subsequently introduced via homologous recombination. Arrows depict primer binding sites used for construction of deletion and reconstitution plasmids (see Materials & Methods section for details).
B) Immunoblot (WB) of a bacterial lysate showing the stable expression of the TEM-CagA fusion protein using a TEM-1 antibody. Generation of an isogenic *cagI* deletion mutant of the TEM-CagA producing strain served as a type IV secretion-defective control.

Bacterial lysates of P12[TEM-CagA] were analyzed via immunoblotting using a TEM-1 antibody (see Figure 9B) and stable expression of the TEM-CagA fusion protein was detected. In addition, a negative control reporter strain was engineered by deletion of the *cagI* gene locus (with plasmid pWS320) in P12[TEM-CagA]. Although *cagI* deletion mutants are

defective in type IV secretion [106], a stable TEM-CagA expression is still guaranteed (see Figure 9B).

To determine whether the TEM-CagA-producing reporter strain is able to translocate the fusion protein into host cells, AGS cells (~2 x 10^7) were infected, lysed and TEM-CagA was immunoprecipitated using CagA antiserum as well as TEM-1 antibody. Fractions were analyzed via immunoblot using CagA and phosphotyrosine-specific antibodies (shown in Figure 10A) and a clear phosphorylation of the TEM-CagA protein was observed, indicating translocation of the reporter-tagged protein into the host cells. In contrast, the isogenic *cagI* deletion mutant yielded no tyrosine-phosphorylated TEM-CagA upon infection, further confirming that phosphorylation depends on functionality of the type IV secretion machinery. However, phosphorylation of the native CagA protein was much higher as compared to TEM-CagA. This might be either due to the lower expression level of TEM-CagA, or to a less effective phosphorylation by host cell kinases.

To independently prove translocation of the TEM-CagA protein, a phosphorylatable GSK-tag was genetically fused to the C-terminus of TEM-CagA (P12[TEM-CagA-GSK]). This reporter tag gets phosphorylated independently of EPIYA motifs and was also applied in previous studies to monitor CagA translocation [131]. AGS cells (~10^6) were infected with P12[TEM-CagA-GSK] or P12[TEM-CagA] and analyzed by Western blotting with a TEM-1 and a phospho-GSK-specific antibody (Figure 10B). Phosphorylation of the GSK-tag could be detected for the TEM-CagA-GSK fusion protein but not for TEM-CagA or uninfected cells. Because of the known unspecific background binding of the phospho-GSK antibody to the unphosphorylated GSK tag, lysates of TEM-CagA-(GSK)-producing bacteria were applied as controls. Although a weak cross-reaction could be detected for TEM-CagA-GSK, the signal was much lower than upon AGS cell infection, thus verifying the translocation of TEM-CagA-GSK.

For evaluation of TEM-CagA-induced cytokine secretion, supernatants derived from infected AGS cells were analyzed by ELISA for IL-8 concentration (Figure 10C). The IL-8 level induced by translocated TEM-CagA protein was the same as for the native CagA protein, while infections with type IV secretion-deficient strains (Δ*cagI*) yielded similar IL-8 baseline values. Hence, it was concluded that TEM-CagA induces IL-8 secretion upon infection to the same rate as the native protein. In addition, an induction of the hummingbird phenotype in AGS cells was examined (see Figure 10D). As expected, after 4 h infection with P12 wild-type, a strong hummingbird phenotype was induced (left picture, Figure 10D). In contrast, infection with P12[TEM-CagA] produced no morphological differences of AGS cells in

comparison to uninfected cells. Hence, the TEM-CagA fusion was not able to stimulate a hummingbird phenotype, which could be either due to relatively low levels of TEM-CagA or to an incapability of the fusion protein to interact with host cell components that are responsible for the morphological changes.

Taken together, although some pathophysiological properties of CagA were impaired by fusion to TEM-1, translocation of TEM-CagA into the cells via type IV secretion could be clearly demonstrated.

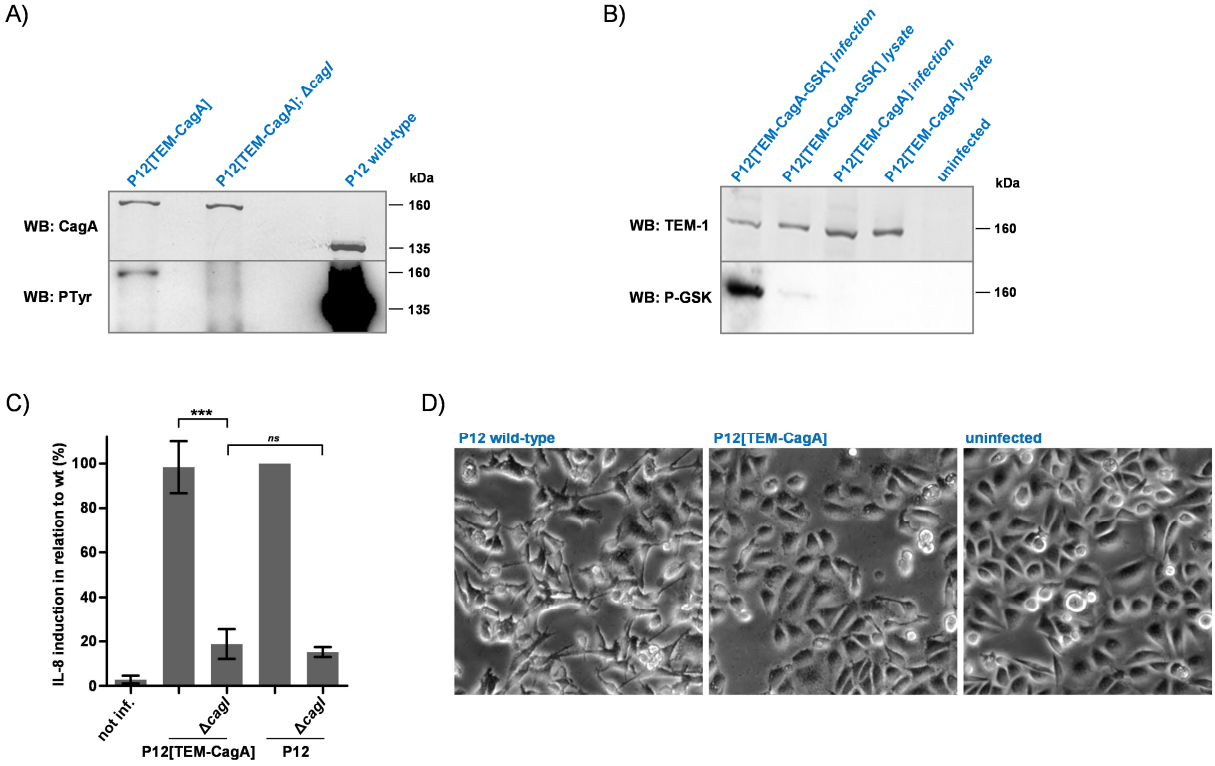

Figure 10: Evaluation of TEM-CagA-producing reporter strains

A) Analysis of immunoprecipitation fractions with CagA and phosphotyrosine immunoblots (WB). AGS cells were infected with the reporter strains P12[TEM-CagA], its isogenic *cagI* deletion mutant and the P12 wild-type strain. Infected cells were lysed and subjected to immunoprecipitation using the polyclonal CagA antiserum AK257 and a monoclonal TEM-1 antibody.

B) Immunoblot analysis (WB) of AGS cells infected with P12[TEM-CagA-GSK] and P12[TEM-CagA] reporter strains as well as corresponding bacterial lysates using TEM-1 and phospho-GSK specific antibodies.

C) Quantitative IL-8 determination in supernatants of AGS cells infected with P12[TEM-CagA], the P12 wild-type and corresponding *cagI* deletion mutants. All values were normalized to the IL-8 values found in the supernatants of P12 wild-type-infected cells, and are indicated as mean values with standard errors of the mean from four independent infections. ANOVA (one-way, Tukey post hoc test), ***: $p<0.001$, *ns*: non-significant.

D) Phase-contrast microscopy to detect the hummingbird phenotype of AGS cells after infection with P12 wild-type and P12[TEM-CagA].

1.3 Determination of TEM-CagA-mediated hydrolysis of CCF4

Having proven that TEM-CagA is translocated into cells, the next step of assay establishment incorporated the monitoring of TEM-CagA-mediated hydrolysis of the CCF4 substrate via fluorescence-assisted devices (summarized in Figure 11). For visualization with fluorescence microscopy, AGS cells were infected with P12[TEM-CagA] or its isogenic *cagI* deletion mutant as a negative control, fixed and covered with the CCF4-AM substrate solution. Blue and green fluorescence signals were recorded and are shown in Figure 11A. For translocated TEM-CagA protein (left panel), a clear blue fluorescence signal was detected due to CCF4 hydrolysis, while the weak green fluorescence signal derived from uncleaved CCF4. In contrast, cells infected with the negative control (right panel) exhibited solely a strong green fluorescence signal, which demonstrates that CCF4 does not hydrolyze spontaneously.

For flow cytometry analysis, AGS cells were incubated with CCF4-AM substrate after infection, washed and fluorescence emission was recorded with the Pacific Blue (blue) and AmCyan (green) channels, and blue-to-green fluorescence ratios were calculated for each individual cell (see Figure 11B). As expected, cells left uninfected or infected with the P12 wild-type did not exhibit any shift in the blue fluorescence channel (upper panel, Figure 11B), but only green fluorescence showing that CCF4-AM entered the cells. Accordingly, only a very low blue-to-green fluorescence ratio (lower panel, Figure 11B) was detectable. In contrast, infection with P12[TEM-CagA] yielded a strong shift of cells in the Pacific Blue channel and a considerable increase of the blue-to-green fluorescence ratio. Of importance, no signal was detected for cells infected with the translocation-deficient reporter strain in the Pacific Blue detector and the corresponding blue-to-green fluorescence ratio was at a background level. To exclude unspecific lysis of CCF4 at the cell surface, AGS cells were also incubated with ultrasonicated P12[TEM-CagA] lysates. No blue fluorescence increase and thus no blue-to-green fluorescence ratio above background level could be observed, further proving that CCF4 gets exclusively hydrolyzed by type IV secretion-translocated TEM-CagA. Moreover, CCF4 seems to only enter and get cleaved in eukaryotic cells but not in the *H. pylori* cytoplasm, as the background signal of translocation-deficient, but TEM-CagA-expressing strains, did not differ in blue or green fluorescence signals compared to infection with P12 wild-type or cells left uninfected.

To show that analysis can also be conducted via fluorescence-assisted plate reading, infected cells were incubated with CCF4 loading solution for 120 min and subsequently measured (Figure 11C). In accordance with the previous analysis, a strong blue-to-green signal could be observed after infection with P12[TEM-CagA] while only a low background signal was

detectable upon infection with the Δ*cagI* mutant. To test whether the CagA translocation process is stopped after addition of CCF4 substrate, cells were directly infected with P12[TEM-CagA] in CCF4-AM substrate solution (CCF4 infection, Figure 11C). In this case, only a blue-to-green background signal was observed, indicating that type IV secretion-mediated CagA translocation is interrupted upon addition of CCF4 and respective incubation conditions. This offers the possibility to stop CagA delivery at defined time points and hence control the infection duration.

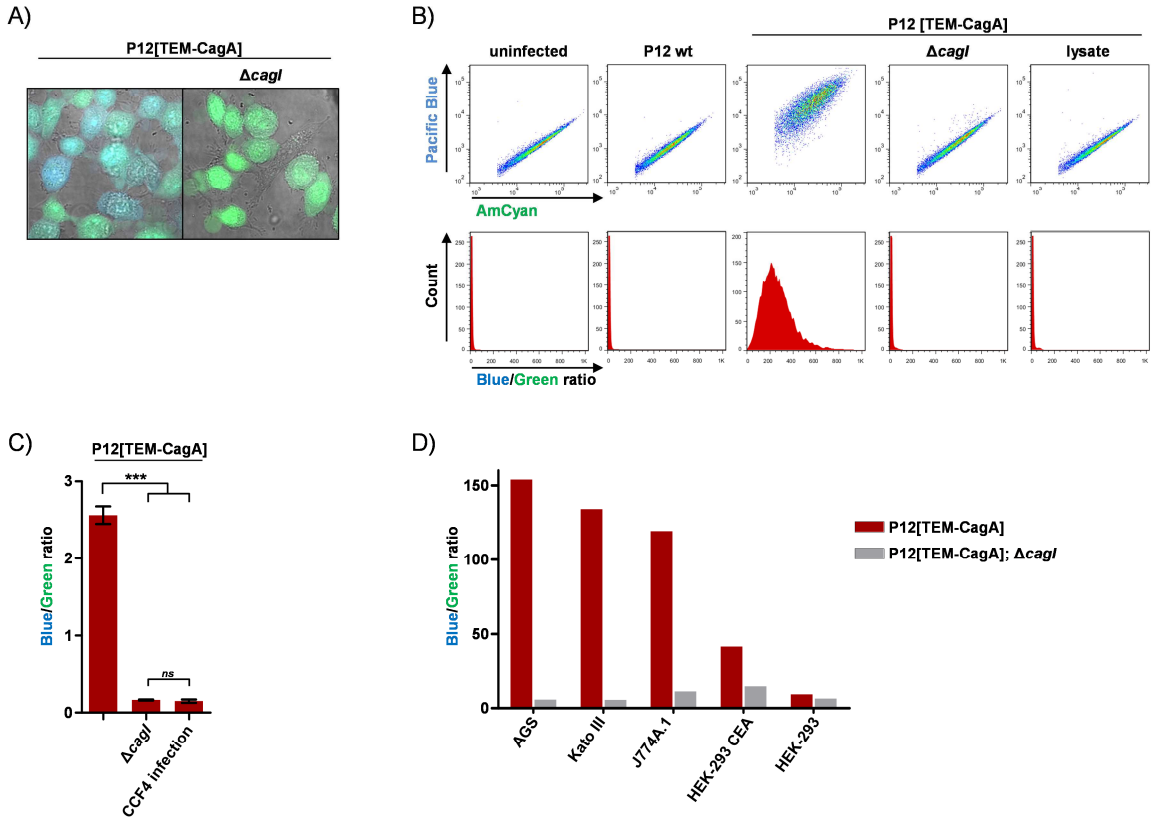

Figure 11: Determination of CCF4 hydrolysis by type IV secretion-translocated TEM-CagA
A) Fluorescence microscopy of infected AGS cells. Cells were infected with P12[TEM-CagA] or its isogenic *cagI* deletion mutant, fixed and incubated with the CCF4-AM substrate solution. Blue and green fluorescence signals were recorded.
B) Flow cytometry analysis of infected AGS cells. Cells were either left uninfected or infected with wild-type P12, P12[TEM-CagA] or its isogenic *cagI* deletion mutant. As a control, cells were treated with a lysate of ultrasonicated P12[TEM-CagA]. After incubation with CCF4-AM, turn-over of CCF4 by translocated TEM-CagA was monitored in the AmCyan (green) or Pacific Blue (blue) fluorescence channels (upper panels). Ratios of blue-to-green fluorescence calculated for each individual cell are plotted in the lower panels.
C) Plate reader analysis of infected AGS cells. Cells were infected with P12[TEM-CagA] or its isogenic *cagI* deletion mutant for 2.5 h and subsequently incubated with CCF4-AM. As a control, P12[TEM-CagA] was added to cells together with the CCF4-AM substrate solution (CCF4 infection). Values shown are mean blue-to-green ratios with standard errors of the mean of three independent measurements. ANOVA (one-way, Tukey post hoc test), ***: $p<0.001$, *ns*: no significant difference.
D) Flow cytometry analysis of different cell lines. Cells were infected with P12[TEM-CagA] or its isogenic *cagI* deletion mutant and loaded with CCF4-AM. Depicted values correspond to blue-to-green fluorescence ratios.

To test the applicability of the assay with other cell lines besides gastric epithelial AGS cells, gastric carcinoma cells (Kato III), murine macrophage cells (J774A.1), and embryonic kidney epithelial cells either expressing CEACAM 5 receptors (HEK-293 CEA) or not (HEK-293) were infected with P12[TEM-CagA] or its isogenic Δ*cagI* mutant. Flow cytometry analysis (see Figure 11D) revealed high blue-to-green fluorescence ratios for Kato III and J774A.1 upon infection with P12[TEM-CagA] as well as low background signals for the negative controls, and signals were comparable to those of infected AGS cells. HEK-293 CEA cells infected with the TEM-CagA-expressing reporter strain produced a lower blue-to-green fluorescence ratio, but nevertheless yielded a clear difference to cells infected with the Δ*cagI* mutant. Only weak background signals were detected for HEK-293 cells after infection with the translocation-competent and -deficient strains, as it has been shown that CagA can only be translocated into these cells when they express CEACAM receptors (R. Haas, personal communication).
In summary, turn-over of CCF4 by translocated TEM-CagA is a highly specific event and can be detected in various cell types where CagA translocation is possible.

To determine the dynamics of CCF4 turnover and hence the optimal incubation time with the CCF4-AM substrate solution, AGS cells infected with P12[TEM-CagA] and the isogenic *cagI* deletion mutant were loaded with the substrate solution and fluorescence development was immediately recorded in a plate reader every 5 min for about 16 h. Respective curves of blue and green fluorescence as well as blue-to-green signals are presented in Figure 12. The blue fluorescence emission (=CCF4 hydrolysis by translocated TEM-CagA; Figure 12A) of cells infected with P12[TEM-CagA] increased the first 6 h in a linear fashion before the signal started to saturate. Importantly, the fluorescence values at MOI 100 and 7 differed significantly, indicating that the bacterial load correlates with amounts of translocated TEM-CagA, which would allow quantitative analysis of CagA translocation. In addition, no blue fluorescence signal was detected for cells infected with translocation-deficient controls, further highlighting that even after a long incubation time (at least 16 h), CCF4 was specifically hydrolyzed by translocated TEM-CagA. The increase of green fluorescence (=intact CCF4 that entered the cell; Figure 12B) was strongest in the first 2 h and only slightly augmented afterwards, indicating substrate saturation. As expected, the level of green fluorescence was higher for infection with the negative control, because under this condition intact CCF4 accumulates inside the cell. According to the blue fluorescence development (Figure 12C), the blue-to-green ratio increased over time, and reliable signals were observed after 60 min. Again, the signal of cells infected at MOI 100 was remarkably higher than at

MOI 7, further supporting the possibility of quantitative analysis. As expected, only background signals of blue-to-green fluorescence were observed for corresponding *cagI* deletion mutants. Taken together, a minimal incubation time of 60 min with CCF4-AM solution should be chosen and determination of the blue-to-green ratio seems to be possible for up to 14 h. Moreover, calculation of the blue-to-green fluorescence ratio (Figure 12C) constitutes a ratiometric analysis, because the CCF4 uptake rate of every single cell is taken into account, as free CCF4 in the substrate solution is esterified (CCF4-AM) and non-fluorescent (also see Figure 8).

In summary, detection of valid blue-to-green fluorescence ratios is possible by any fluorescence-assisted device. All experimental set-ups confirmed the feasibility of the assay to monitor CagA translocation in a specific, sensitive and even quantitative way. The latter applicability was examined in more detail and is presented in the following chapter.

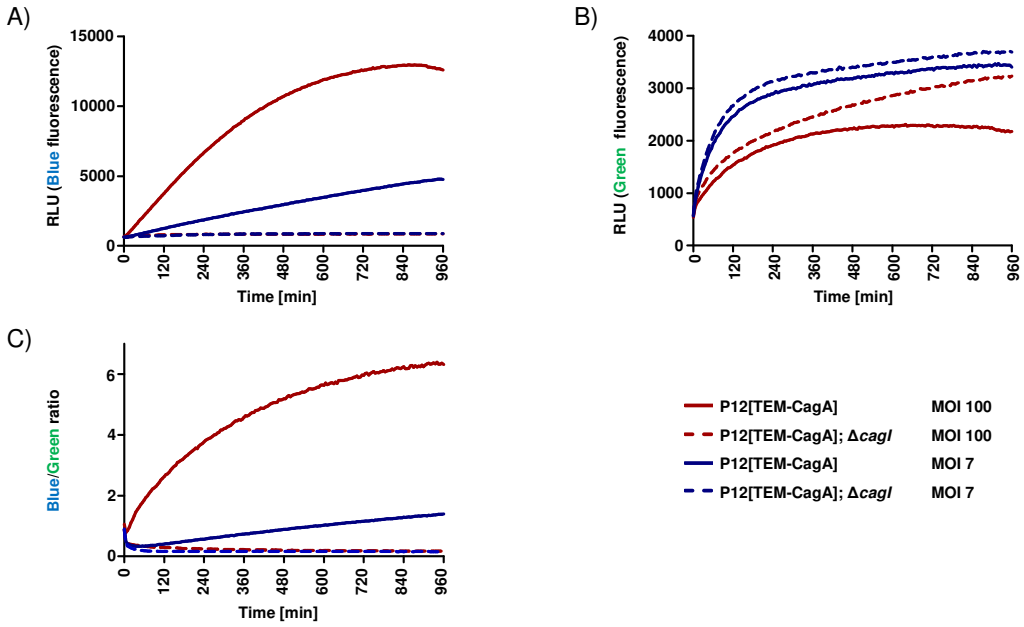

Figure 12: Kinetic analysis of CCF4 turnover by translocated TEM-CagA protein
AGS cells were infected with P12[TEM-CagA] or its isogenic *cagI* deletion mutant for 2.5 h at an MOI of 100 and 7. Cells were loaded with CCF4-AM and fluorescence development was recorded in a plate reader every 5 min at room temperature. MOI: multiplicity of infection, RLU: relative light unit.
A) Blue fluorescence development over time expressed as RLU.
B) Green fluorescence development over time expressed as RLU.
C) Blue-to-green fluorescence ratios over time after subtraction of corresponding blank control values.

1.4 Quantification of TEM-CagA translocation

For validation of the novel established TEM-CagA translocation reporter to quantify relative amounts of translocated CagA protein, several experimental set-ups were tested.

First, AGS cells were infected at various MOIs (up to 400) with the P12[TEM-CagA] reporter strain for 2.5 h and the turnover of CCF4 was monitored by flow cytometry in the green (AmCyan) and blue (Pacific Blue) emission channels (Figure 13A). With increasing MOI, the cell population was subject to augmented shifting in the blue channel, while first signals were detectable at MOI 6 and seemed to stagnate at MOIs higher than 100. In accordance with the data of the previous chapter (1.3, Figure 12), higher MOIs resulted in increased blue-to-green fluorescence ratios which highly suggests a correlation between translocated CagA amounts and fluorescence signals.

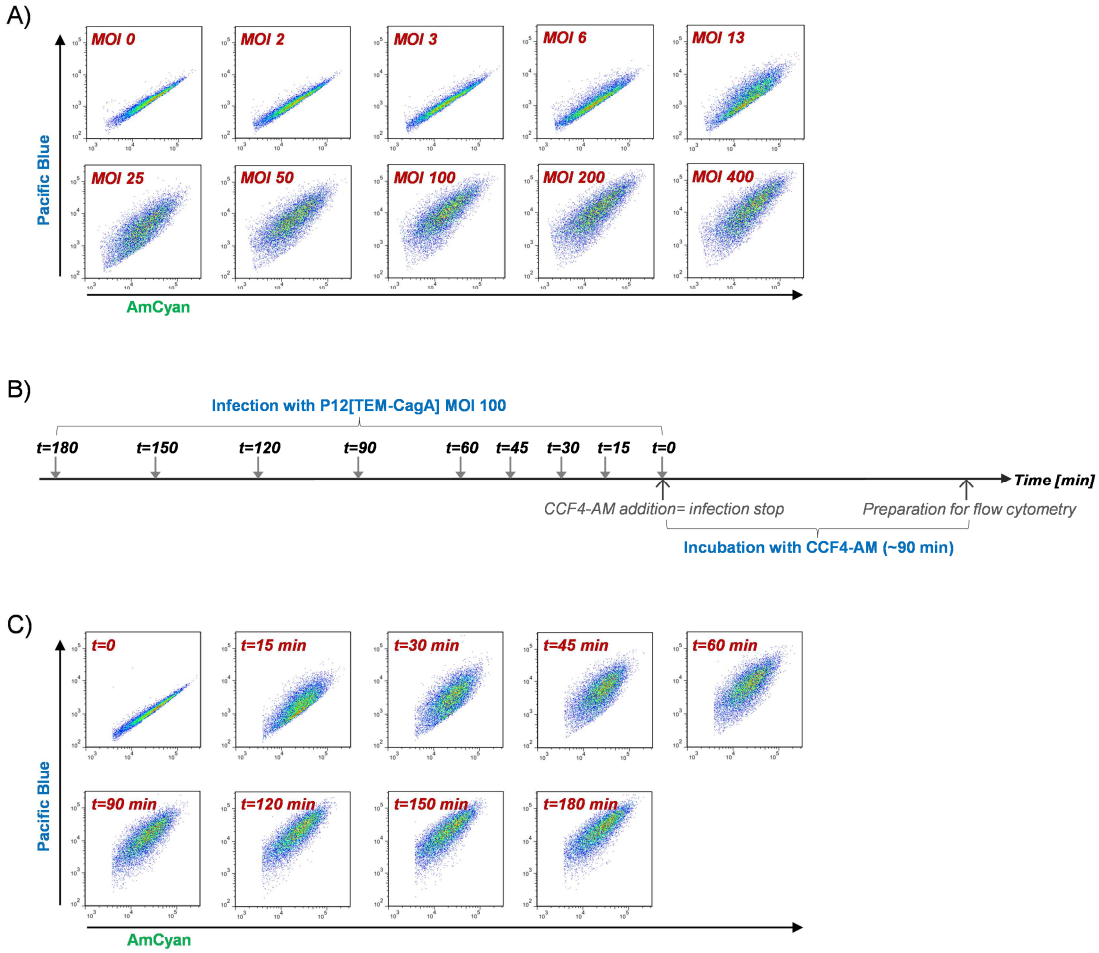

Figure 13: Flow cytometry analysis of cells infected at increasing MOIs and infection duration
A) Scatter plots of infected cells in the blue (Pacific Blue) and green (AmCyan) channels. AGS cells were infected with P12[TEM-CagA] at increasing MOIs for 2.5 h.
B) Timescale for a time-course infection set-up. AGS cells were infected with P12[TEM-CagA] at defined time points. Infection was stopped by CCF4-AM addition and after loading, cells were analyzed.
C) Scatter plots of infected cells in the blue (Pacific Blue) and green (AmCyan) channels during time-course infection at MOI 100.
MOI: multiplicity of infection.

To further prove this relationship, AGS cells were infected for various time spans with the P12[TEM-CagA] reporter strain. An overview of the infection set-up is given in Figure 13B. Briefly, the *H. pylori* reporter strain was added at defined time points to the cells at an MOI of 100, and the infection was stopped by CCF4-AM addition (see also 1.3, Figure 11C). After loading with the substrate for 90 min, cells were analyzed by flow cytometry in the blue and green fluorescence detectors. Corresponding scatter plots (Figure 13C) showed a drastic shift of cells already after 15 min of infection. This shifting further increased and finally stagnated after approximately 120 min. Again, the signal increment can be associated to enhanced amounts of translocated CagA that accumulate during longer infection time spans. These observations further strengthen the applicability of the assay as a quantitative tool. In addition, signals are detectable at very low MOIs as well as after very short infection durations, emphasizing the high sensitivity of this method.

As time-course analysis of AGS cell infections showed consistent shifts of cell populations, quantitative analysis of CagA translocation (expressed as blue-to-green ratio) as well as percental amounts of injected cells were quantified from independent measurements via flow cytometry (summarized in Figure 14). For this purpose, AGS cells were infected with P12[TEM-CagA] at various time points with an MOI of 100, 50 or 25, and blue-to-green ratios were recorded. As presented in Figure 14A, overall blue-to-green ratios increased with longer infection duration and with higher MOI. Surprisingly, the signal stagnated after 2.5 h infection independent of the MOI, suggesting that *H. pylori* stops translocation of CagA into the cells under these infection conditions. In a next step, a gate was defined within the Pacific Blue and AmCyan scatter plots (Figure 14B, shown in red) to define only the cell population that had received a TEM-CagA injection. Subsequently, the percentage of cells that shifted into this gate over time is depicted in Figure 14C. For MOI 50 and 100, 50% of the cell population got already injected with TEM-CagA after 15 min, and virtually the whole population shifted into the red gate after 60 min. For cells infected with MOI 25, the proportion in the red gate also incremented with longer infection duration but stagnated at about 60%. Hence, it appears that in an *in vitro* cell culture experiment every cell gets injected with CagA as long as the applied MOI is high enough. Additionally, blue-to-green ratios of the cells in the red gate were determined (Figure 14D). The calculated ratios were similar to the values for the ungated population (Figure 14A), although a more sensitive blue-to-green signal increase was detectable in the first minutes of infection which is attributed to the pre-definition of the CagA-injected cell population.

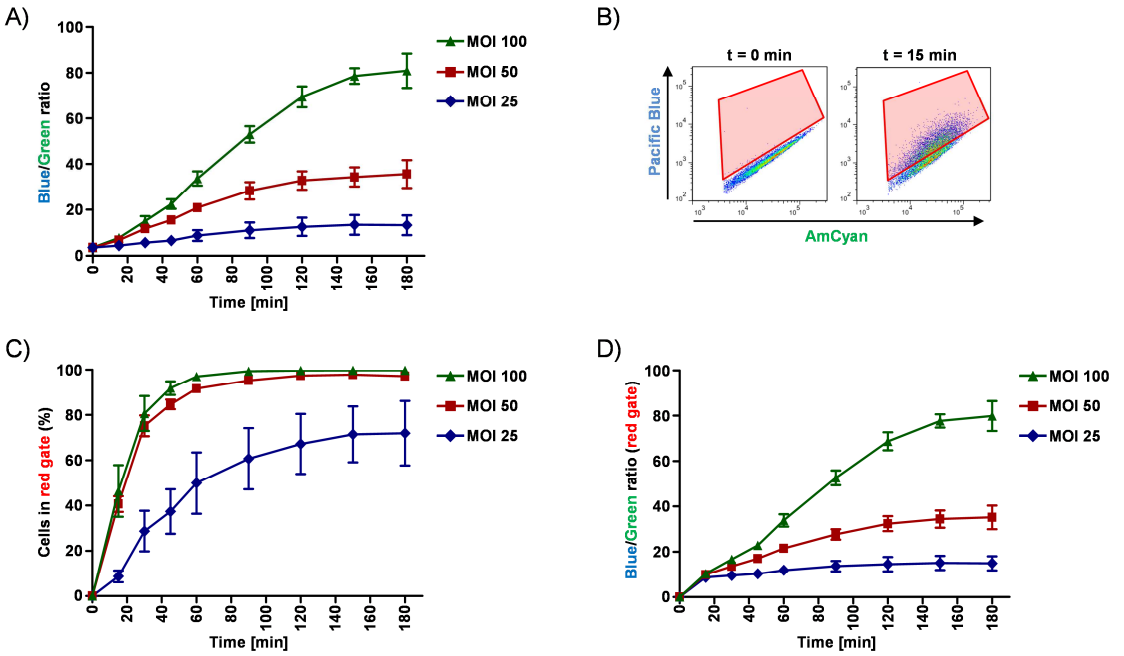

Figure 14: Quantitative analysis of TEM-CagA translocation by flow cytometry
AGS cells were infected with P12[TEM-CagA] with an MOI of 100, 50 or 25 at distinct time points. All depicted values represent mean values of three independent measurements with standard errors of the mean. MOI: multiplicity of infection.
A) Quantification of translocated TEM-CagA during time-course experiments expressed as blue-to-green ratios.
B) Gating of cells. Cells from the data shown in A) were gated in the AmCyan-Pacific Blue scatter plot as indicated (red gate).
C) Percentage of cells that shifted into the red gate.
D) Quantification of translocated TEM-CagA during time-course experiments expressed as blue-to-green ratios of cells that shifted into the red gate.

In addition to flow cytometry, TEM-CagA translocation was evaluated by fluorescence-assisted plate reading (Figure 15), for which AGS cells were infected with increasing amounts of P12[TEM-CagA] for 2.5 h similar to the experiment shown in Figure 13A. In accordance with these previous results, blue-to-green ratio signals were detectable at very low MOIs (~6), increased with rising MOIs and stagnated at an MOI of 100 (Figure 15A). Indeed, fluorescence signals even dropped at MOIs higher than 100, which might be attributable to the high bacterial load that damaged the cells or actually distorted fluorescence measurement. Moreover, time-course experiments with AGS cells that were infected with P12[TEM-CagA] at an MOI of 100, 50 or 7 at defined time points (Figure 15B), revealed similar results as those obtained with flow cytometry (Figure 14). Briefly, ratios increased after longer infection durations as well as with higher MOIs, and the signal stagnated again after approximately 2.5 h, indicating a stoppage of CagA translocation. Overall, blue-to-green fluorescence signals were lower in the dataset of Figure 15A compared to B. While the MOI titration (Figure 15A) was conducted in 384-well plates, the time-course experiments (Figure 15B) were performed in 96-well plates. This is in accordance with other datasets where the signal ratio in 384-well plates was usually lower compared to values derived in 96-well plates (data

not shown). In general, although gating of cells is not possible for plate reading analysis, results were comparable to flow cytometry.

In summary, the newly established TEM-CagA translocation reporter assay allows quantitative analysis of CagA translocation with reproducible results and only little variation. Furthermore, an MOI of 100 and infection duration of 2.5 h assure a high blue-to-green signal ratio and were used as infection parameters for subsequent studies throughout this work.

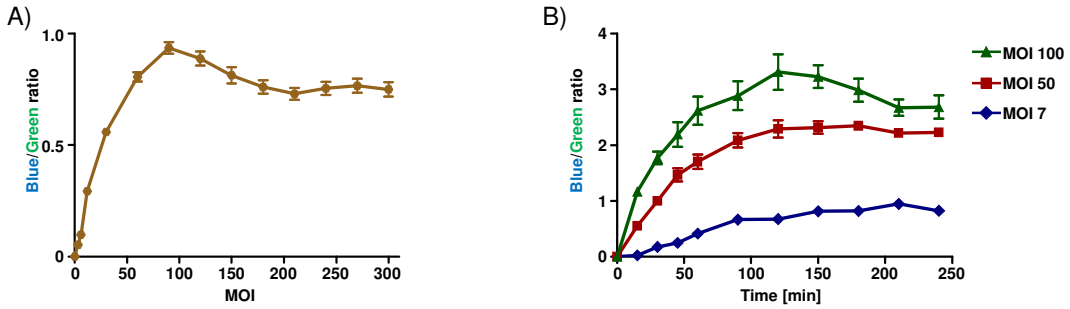

Figure 15: Quantitative analysis of TEM-CagA translocation by fluorescence-assisted plate reading
Blue-to-green fluorescence ratios indicated represent mean values of three independent measurements with standard errors of the mean. MOI: multiplicity of infection
A) Quantification of translocated TEM-CagA after infection with increasing MOIs. AGS cells were infected with P12[TEM-CagA] at increasing MOIs for 2.5 h in 384-well plates.
B) Quantification of translocated TEM-CagA after time-course experiments. AGS cells were infected with P12[TEM-CagA] at an MOI of 100, 50 or 7 for defined time spans in 96-well plates.

2. Characterization of CagA translocation and substrate recognition parameters

Validation of the TEM-1-dependent Cag type IV secretion reporter demonstrated that this method allows a fast, sensitive and quantitative analysis of CagA translocation. Thus, the TEM-CagA assay was utilized to characterize various parameters of CagA translocation and substrate recognition.

2.1 Influence of *cag*PAI-encoded proteins on translocation efficiency

The *cag*PAI of *H. pylori* encodes various proteins that are structural components or accessory proteins of the type IV secretion system as well as the translocated effector protein CagA. Although this system has been intensively studied in the last decades, not all functions of particular components are known. In a prior study [115], the influence of various *cag*PAI-encoded proteins on CagA phosphorylation was demonstrated by systematic mutagenesis. In this work, using the novel phosphorylation-independent TEM-CagA assay, it was investigated which influence specific Cag components have on the CagA translocation rate and whether

there are differences between phosphorylation and translocation rates, with the aim to finally obtain quantitative rates of CagA translocation. Besides the well-described CagA chaperone CagF [118, 119] and the CagH protein, important for pilus biogenesis [103], also the partially undescribed accessory proteins CagG and CagP were taken into focus; the respective encoding genes are highlighted in red in Figure 16A. Previous data showed an essential function of CagF and CagH for CagA phosphorylation, while the *cagG* deletion mutant had reduced CagA phosphorylation upon infection and no influence for CagP was observed [115]. To evaluate the influence on TEM-CagA translocation, P12[TEM-CagA] was transformed with plasmids to generate isogenic deletion mutants, namely Δ*cagF* (with pWS474), Δ*cagG* (with pWS428), Δ*cagH* (with pWS423) and Δ*cagP* (with pWS503).

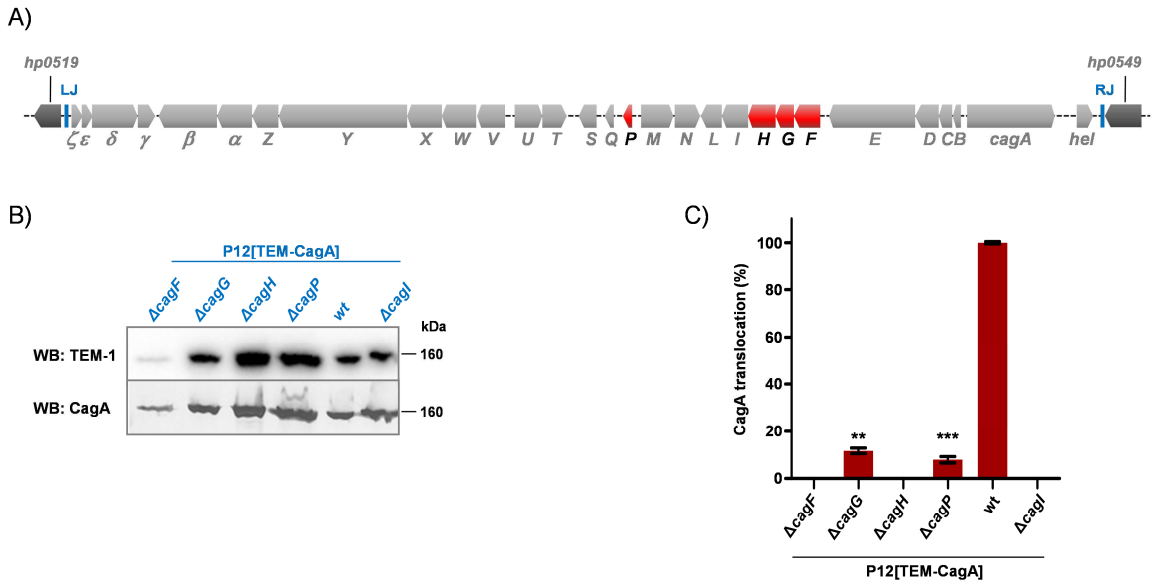

Figure 16: Influence of *cag*PAI-encoded proteins on TEM-CagA translocation
A) Schematic overview of the *cag*PAI; *cag* genes of interest are highlighted in red.
B) Immunoblot (WB) of bacterial lysates analyzing TEM-CagA protein expression using a TEM-1 and a CagA (AK268) antibody, respectively.
C) Quantification of TEM-CagA translocation rates by plate reading. AGS cells were infected with P12[TEM-CagA] and its isogenic *cagF*, *cagG*, *cagH*, *cagP* and *cagI* deletion mutants. The average blue-to-green ratios of each infection were normalized to the mean ratio of P12[TEM-CagA]-infected cells, and are shown as mean percentages of five independent experiments with standard errors of the mean. t-test (one-tailed, unpaired) comparing to wild-type, **: $p<0.005$, ***: $p<0.0005$.

Analysis by Western blotting using TEM-1 and CagA-specific antibodies (see Figure 16B), confirmed expression of TEM-CagA for all generated mutants, although the expression rate of the Δ*cagF* deletion mutant was relatively low. A reduced CagA expression has already been observed for other Δ*cagF* deletion mutants and might be attributed to the chaperone-like stabilizing effect of CagF on CagA expression [119]. Quantification of CagA translocation using the TEM-CagA assay (translocation efficiency defined as wild-type = 100% and Δ*cagI* mutant = 0%; Figure 16C) revealed no translocation for P12[TEM-CagA]Δ*cagF* as well as

the Δ*cagH* deletion mutant. This is in accordance with the corresponding CagA phosphorylation data where both *cag*PAI components were indispensable for a functional phosphorylation [115, 119]. The CagA translocation rate of the Δ*cagG* deletion mutant exhibited a translocation rate of 12%, which is in agreement with previous data, where only a very weak CagA phosphorylation was detectable [115], albeit not quantified. In contrast, the translocation rate of P12[TEM-CagA]Δ*cagP* reached about 8%, contrary to the reported phosphorylation capability of 100% for the *cagP* mutant [115]. In that previous study, experiments were carried out with the *H. pylori* strain 26695 and not the P12 strain used here, which could be the reason for this discrepancy.

In conclusion, it could be shown that specific *cag*PAI-encoded proteins drastically influence CagA translocation or even completely abolish the process. Moreover, applying the novel TEM-CagA assay, even low translocation rates are quantifiable in a reproducible manner.

2.2 Investigations on the C-terminal CagA secretion signal

Apart from the influence of various type IV secretion-associated proteins on CagA translocation efficiency, CagA sequences themselves also play a remarkable role in the translocation process. Type IV-secreted substrates are generally recognized via C-terminal signal sequences [188] and indeed, previous studies indicated that CagA translocation is dependent on its C-terminus, as C-terminal amino acid deletions rendered the protein translocation-incompetent [131]. In this study, distinct mutants with variations and deletions in the C-terminus were constructed to further decipher and define this CagA secretion signal. Therefore, plasmid pWS321 was used for deletion of the *cagA* 3´ region in P12 or P12[TEM-CagA], and modified versions of the pWS336 plasmid were used as reconstitution plasmids that recombined in the *cagA* 3´ region only (see Materials & Methods section for further details).

2.2.1 Influence of C-terminal amino acid sequence extensions

At first, it was analyzed whether extensions of the CagA C-terminus had any influence on translocation. Therefore, TEM-CagA variants with additional C-terminal GSK or M45 tags were constructed (TEM-CagA-GSK, TEM-CagA-M45; see Figure 17A). Immunoblot analysis of the corresponding bacterial lysates (Figure 17B) showed protein expression levels comparable to P12[TEM-CagA], indicating that C-terminal tags in combination with an N-terminal TEM-1 tag are well tolerated. GSK-tag phosphorylation of TEM-CagA-GSK upon

AGS cell infection has already been shown in Figure 10B. In addition, translocation rates of P12[TEM-CagA-GSK] and P12[TEM-CagA-M45] were quantitatively determined using the TEM-CagA assay (translocation efficiency defined as P12[TEM-CagA] = 100% and Δ*cagI* mutant = 0%; Figure 17C). Both mutants exhibited a reduced CagA translocation to the same extent (about 70%), although the amino acid composition differed immensely between the two tags. Hence, the Cag type IV secretion system seems to tolerate C-terminal amino acid extensions, and these elongations do not seem to interfere with substrate recognition.

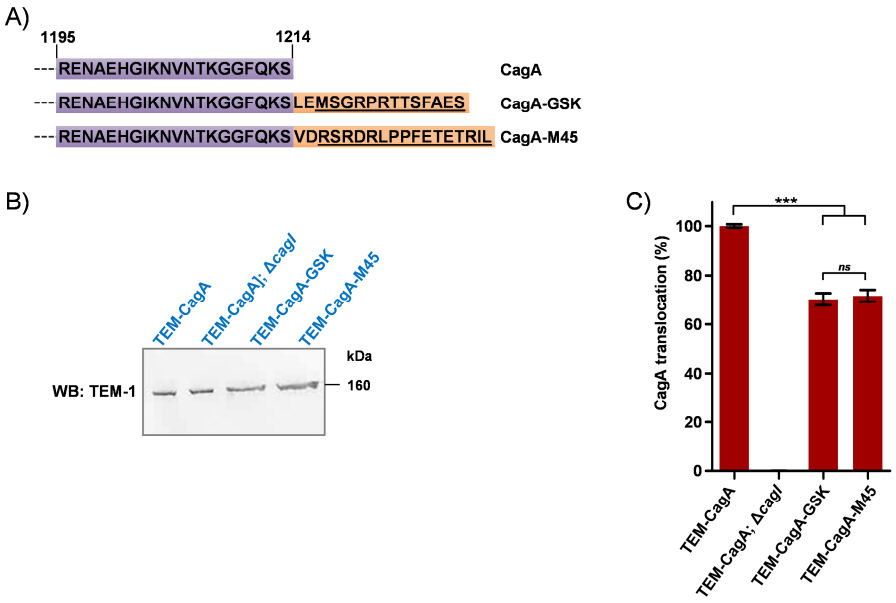

Figure 17: Influence of C-terminal tag fusions on CagA translocation
A) Schematic overview of the C-terminal amino acid composition of CagA and variants with GSK or M45 tag extensions. The CagA amino acid sequence is highlighted in purple and additional amino acids in orange while underlined sequences are corresponding to the tag sequence.
B) Immunoblot (WB) of bacterial lysates analyzing TEM-CagA or TEM-CagA variant expression using a TEM-1 antibody.
C) Quantification of TEM-CagA translocation rates by plate reading. AGS cells were infected with P12[TEM-CagA] or the indicated mutants. The average blue-to-green ratios of each infection were normalized to the mean ratio of P12[TEM-CagA]-infected cells, and are shown as mean percentages of four independent experiments with standard errors of the mean. ANOVA (one-way, Tukey post hoc test), ***: $p<0.001$, *ns*: no significant difference.

2.2.2 Influence of sequential C-terminal amino acid truncations

Prior studies showed that C-terminal truncations of 20 amino acids rendered the CagA protein translocation-deficient, while shorter truncations of up to 5 amino acids did not display a significant reduction of CagA phosphorylation [131]. To further specify this, CagA and TEM-CagA variants were generated lacking 5-12 amino acids from the C-terminus (see Figure 18A). At first, AGS cells were infected with P12 wild-type and the corresponding variants and analyzed by phosphotyrosine and CagA immunoblots (Figure 18B). As previously shown, truncations of 5 amino acids did not influence CagA phosphorylation. In addition,

truncations of 6 amino acids also did not result in any decrease in phosphorylation. Interestingly, these two CagA variants even appeared to exhibit increased phosphorylation signals, which might be attributed to higher CagA expression levels. For CagA variants with 7 or 8 C-terminal amino acid deletions, only a very weak phosphorylation band was detectable (highlighted by arrowheads, Figure 18B), and longer truncations completely abolished phosphorylation (10, 12 or 20 amino acids; Figure 18B or data not shown).

To control the functionality of the type IV secretion apparatus, which is able to trigger IL-8 secretion independently of CagA translocation, supernatants of co-cultured AGS cells were analyzed via ELISA for IL-8 concentration (Figure 18C). Interestingly, IL-8 induction upon infection with an isogenic Δ*cagA* deletion mutant was reduced to about 60% in comparison to P12 wild-type-infected cells. This observation has also been reported previously [119], and might be due to a strain-specific NF-κB activation by translocated CagA leading to higher IL-8 secretion [189]. IL-8 levels induced by CagAΔ5C and CagAΔ6C were as high as the wild-type control, which was in accordance with the unaffected CagA phosphorylation. For CagA variants with deletions of 7 or more amino acids, IL-8 induction was at the same level as for the Δ*cagA* deletion mutant. Although slightly higher levels for CagAΔ7C and CagAΔ8C mutants were expected because of the weak CagA phosphorylation, the sensitivity of the IL-8 ELISA might be limited. Nevertheless, it clearly demonstrated functionality of the Cag type IV secretion system in all variants.

Moreover, corresponding P12[TEM-CagA] variants were generated and the TEM-CagA expression levels analyzed, depicted in Figure 18D. Expression levels were equivalent to the unmodified TEM-CagA control. AGS cells were infected with these variants and percental CagA translocation rates were determined using the TEM-CagA assay (translocation efficiency defined as P12[TEM-CagA] = 100% and Δ*cagI* mutant = 0%; Figure 18E). With this assay, TEM-CagA variants lacking 5 or 6 amino acids exhibited translocation rates comparable to the full-length protein, TEM-CagAΔ7C about 40%, and variants lacking 8 or 9 amino acids displayed 20% translocation. Variants with longer truncations (10, 12 or 20 amino acids) were not detectably translocated (Figure 18E or data not shown). In general, these results were consistent with the data for the tyrosine phosphorylation but allowed a more precise, sensitive and quantitative translocation analysis. Furthermore, these observations demonstrate that the C-terminal type IV secretion signal does not require the final 6 amino acids and tolerates C-terminal deletions of up to nine amino acids.

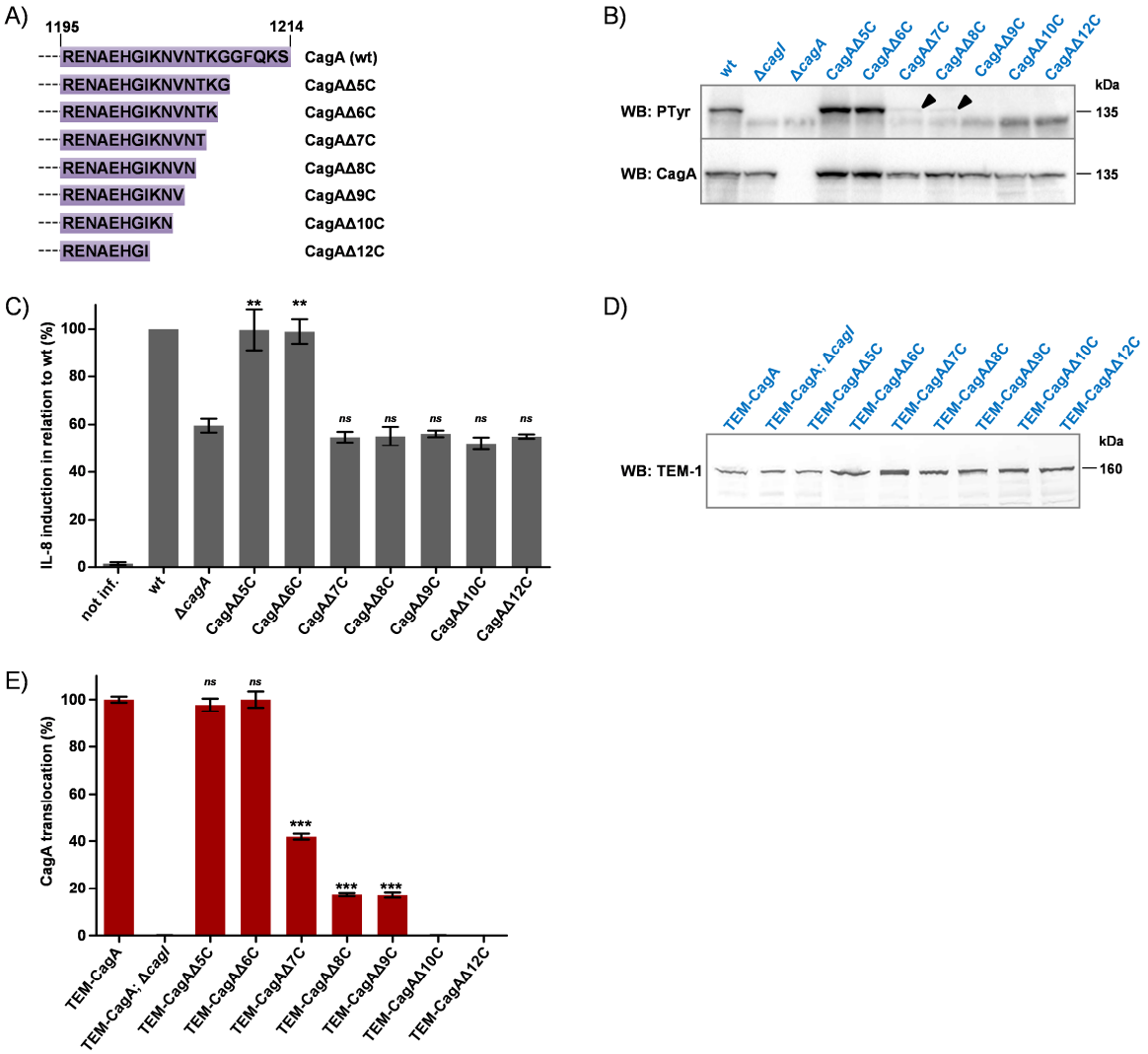

Figure 18: Influence of C-terminal truncations on CagA translocation
A) Schematic overview of the C-terminal amino acid composition of CagA and variants with sequential truncations.
B) Immunoblot analysis of infected AGS cells with phosphotyrosine (4G10) and CagA (AK257) antibodies. Cells were infected with P12 wild-type or the indicated mutants and analyzed via Western blotting (WB). The arrowheads highlight weak phosphorylation bands for CagAΔ7C and CagAΔ8C.
C) Analysis of co-culture supernatants derived from B) for IL-8 secretion via sandwich ELISA. All values were normalized to the IL-8 values found in the supernatants of P12 wild-type-infected cells, and are indicated as mean values with standard errors of the mean from at least three independent infections. t-test (one-tailed, unpaired) comparing to Δ*cagA*, **: p<0.01, *ns*: no significant difference.
D) Immunoblot (WB) of bacterial lysates analyzing TEM-CagA or TEM-CagA variant expression using a TEM-1 antibody.
E) Quantification of TEM-CagA translocation rates by plate reading. AGS cells were infected with P12[TEM-CagA] or the indicated mutants. The average blue-to-green ratios of each infection were normalized to the mean ratio of P12[TEM-CagA]-infected cells, and are shown as mean percentages of four independent experiments with standard errors of the mean. t-test (one-tailed, unpaired) comparing to TEM-CagA, ***: p<0.0001, *ns*: no significant difference.

2.2.3 Influence of charged amino acids located in the C-terminus

In addition to examinations focusing on the length of the C-terminus, the role of charged amino acids located in the C-terminal tail was investigated. For other type IV secretion systems, charged amino acids play a major role in the substrate recognition process [190,

191]. However, it has been reported that the two lysine residues close to the CagA C-terminus are not essential for translocation [131]. In addition, alanine scanning mutagenesis of the CagA C-terminus exchanging various acidic or basic residues with alanine as well as charge reversal of single amino acids did not impair CagA phosphorylation [192]. To finally rule out any influence of charges on CagA translocation, two variants were constructed where either exclusively lysine residues or all charged amino acids were mutated to alanines within the last 20 amino acids of CagA (CagA-KKK→A and CagA-REEHKKK→A, respectively; see Figure 19A).

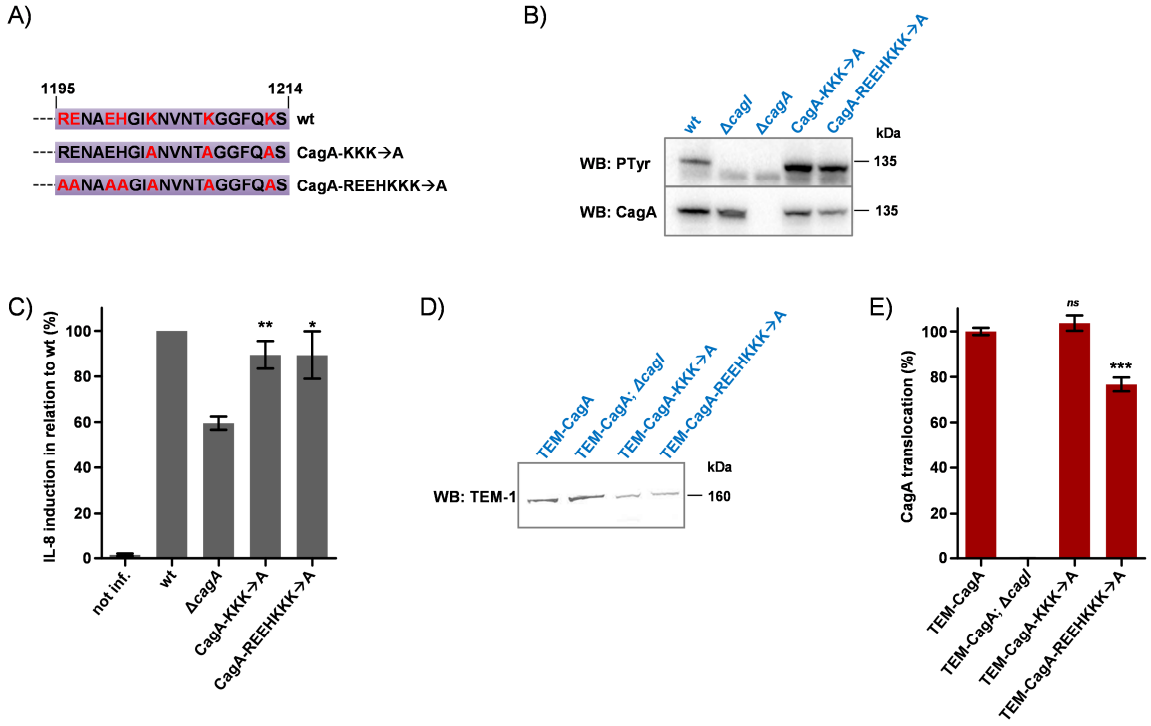

Figure 19: Influence of C-terminal charged amino acids on CagA translocation
A) Schematic overview of the C-terminal amino acid composition of CagA and variants with alanine mutagenesis. Charged amino acids or respective alanine substitutions are highlighted in red.
B) Immunoblot analysis of infected AGS cells with phosphotyrosine (4G10) and CagA (AK257) antibodies. Cells were infected with P12 wild-type or the indicated mutants and analyzed via Western blotting (WB).
C) Analysis of co-culture supernatants derived from B) for IL-8 secretion via sandwich ELISA. All values were normalized to the IL-8 values found in the supernatants of P12 wild-type-infected cells, and are indicated as mean values with standard errors of the mean from at least three independent infections. t-test (one-tailed, unpaired) comparing to Δ*cagA*, *: $p<0.05$, **: $p<0.01$.
D) Immunoblot (WB) of bacterial lysates analyzing TEM-CagA or TEM-CagA variant expression using a TEM-1 antibody.
E) Quantification of TEM-CagA translocation rates by plate reading. AGS cells were infected with P12[TEM-CagA] or the indicated mutants. The average blue-to-green ratios of each infection were normalized to the mean ratio of P12[TEM-CagA]-infected cells, and are shown as mean percentages of six independent experiments with standard errors of the mean. t-test (one-tailed, unpaired) comparing to TEM-CagA, ***: $p<0.001$, *ns*: no significant difference.

Tyrosine phosphorylation immunoblots of mutant-infected AGS cells did not show any difference in comparison to the wild-type (Figure 19B). Consistently, analysis of IL-8

secretion exhibited no impairment for these variants (Figure 19C). Nevertheless, corresponding TEM-CagA variants were constructed to evaluate weak changes in CagA translocation rates. Although TEM-CagA protein was expressed slightly less than the full-length equivalent (Figure 19D), AGS cells were infected with TEM-CagA-expressing variants and percental CagA translocation rates were determined using the TEM-CagA assay (translocation efficiency defined as P12[TEM-CagA] = 100% and Δ*cagI* mutant = 0%; Figure 19E). P12[TEM-CagA-KKK→A] exhibited the same amounts of translocated CagA as the positive control, albeit being lower expressed. This implies that only a minor proportion of the usually high CagA protein levels gets translocated into the cells, which was also recently reported [193]. For the variant with a complete exchange of all charged amino acids to alanine (TEM-CagA-REEHKKK→A), a slight reduction of CagA translocation (~77%) could be observed. This further suggested that charged amino acids are not essential for the substrate recognition process.

In summary, it could be demonstrated that the C-terminal secretion signal is defined by a minimal length rather than the presence of charged amino acids. Moreover, applying the novel TEM-CagA assay, subtle changes can be easily quantified.

2.2.4 Exchange of the C-terminus with arbitrary tags

Hitherto, it was convincingly demonstrated that the C-terminus should comprise a minimal length of amino acids for efficient CagA translocation. Precisely, CagA translocation tolerates a removal of up to nine amino acids, whereas no translocation is observed for CagAΔ10C variants. In addition, removal of charges in the C-terminal region does not influence translocation rates, implying that a defined signal sequence is lacking. To further specify this hypothesis, CagA variants were genetically engineered where the last ten natural amino acids were replaced by two tags, the GSK- and Myc-tag (CagAΔ10C-GSK, CagAΔ10C-Myc; shown in Figure 20A). AGS cells were infected with these mutants and the tyrosine phosphorylation as well as CagA expression levels were analyzed via immunoblotting (Figure 20B). Interestingly, a very weak signal could be detected for the CagAΔ10C-GSK variant, while CagA expression levels were slightly reduced. In contrast, no CagA phosphorylation was detectable for CagAΔ10C-Myc, although it was expressed at levels comparable to the wild-type. To evaluate the functionality of the type IV secretion system, supernatants of respective co-cultures were analyzed for IL-8 content (Figure 20C). P12[CagAΔ10C-GSK] and P12[CagAΔ10C-Myc]-infected cells secreted IL-8 to a similar level as cells infected with an isogenic Δ*cagA* mutant, which is in accordance with the weak or abolished CagA

phosphorylation of the variants. To quantify CagA translocation rates, corresponding TEM-CagA fusion variants were constructed. Analysis of TEM-CagA expression revealed similar levels compared to the wild-type control (Figure 20D). Quantification by TEM-CagA assay (translocation efficiency defined as P12[TEM-CagA] = 100% and Δ*cagI* mutant = 0%; Figure 20E) showed only a slight reduction of the TEM-CagAΔ10C-GSK variant (~87%) compared to the native fusion protein. Surprisingly, a weak translocation was observed upon infection with P12[TEM-CagAΔ10C-Myc] (~6%), which could not be detected applying the tyrosine phosphorylation assay, further stressing the sensitivity of the novel TEM-CagA assay.

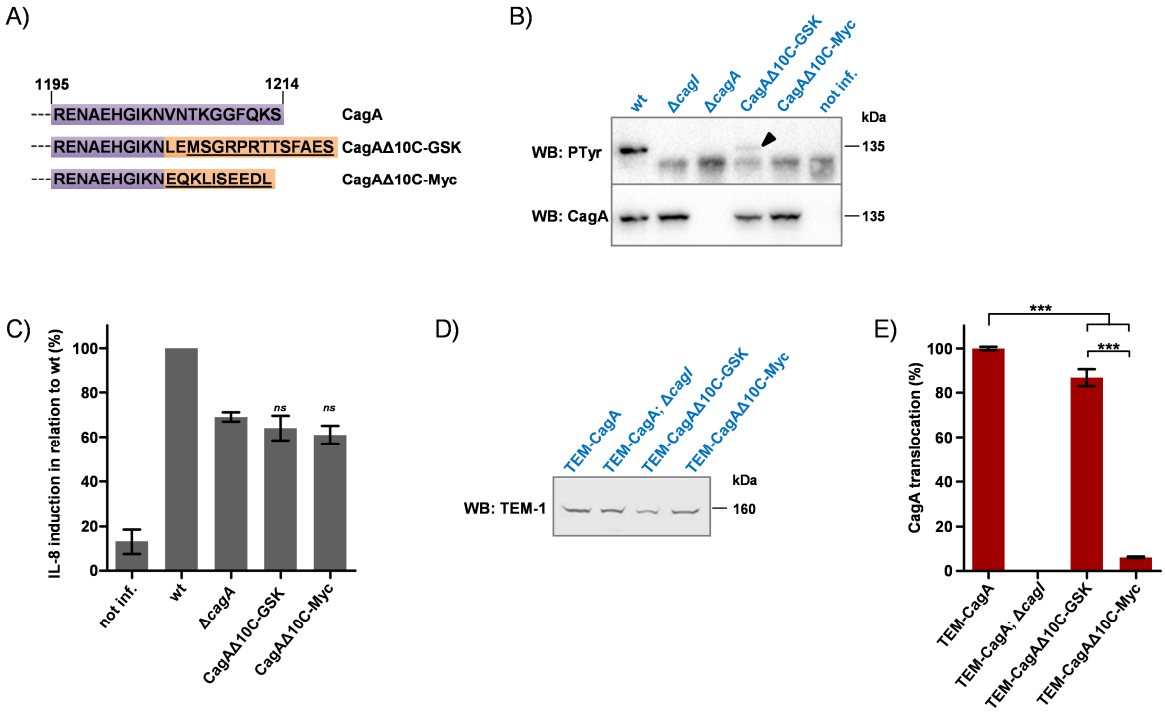

Figure 20: Reconstitution of CagA translocation by arbitrary C-terminal tags
A) Schematic overview of the C-terminal amino acid composition of CagA and CagAΔ10C variants with GSK or Myc tag extension. CagA amino acid sequence is highlighted in purple and additional amino acids in orange while underlined sequences are corresponding to the tag sequence.
B) Immunoblot analysis of infected AGS cells with phosphotyrosine (4G10) and CagA (AK257) antibodies. Cells were infected with P12 wild-type or the indicated mutants, and analyzed via Western blot (WB). The arrowhead highlights a weak phosphorylation band for CagAΔ10C-GSK.
C) Analysis of co-culture supernatants derived from B) for IL-8 secretion via sandwich ELISA. All values were normalized to the IL-8 values found in the supernatants of P12 wild-type-infected cells, and are indicated as mean values with standard errors of the mean from at least three independent infections. t-test (one-tailed, unpaired) comparing to Δ*cagA*, *ns*: no significant difference.
D) Immunoblot (WB) of bacterial lysates analyzing TEM-CagA or TEM-CagA variant expression using a TEM-1 antibody.
E) Quantification of TEM-CagA translocation rates by plate reading. AGS cells were infected with P12[TEM-CagA] or the indicated mutants. The average blue-to-green ratios of each infection were normalized to the mean ratio of P12[TEM-CagA]-infected cells, and are shown as mean percentages of five independent experiments with standard errors of the mean. ANOVA (one-way, Tukey post hoc test), ***: $p<0.001$.

Taken together, it is possible to reconstitute CagA translocation by substitution of the last ten amino acids with unrelated amino acid sequences. This observation strengthens the

hypothesis, that the type IV secretion machinery just requires any arbitrary C-terminal amino acid sequence for substrate recognition. However, the remarkable differences in translocation rates delivered by P12[TEM-CagAΔ10C-GSK] and P12[TEM-CagAΔ10C-Myc] indicate that the C-terminal amino acid composition can determine efficiency of translocation, although a specific signal cannot be defined.

2.3 Influence of N-terminal and internal domains on CagA translocation

In addition to C-terminal signal sequences, other regions of individual type IV-secreted effector proteins can be involved in the recognition and translocation process as well [77]. For the CagA protein, preliminary studies demonstrated that minor N-terminal deletions render the protein translocation-incompetent [131]. However, the respective plasmid-encoded CagA variants were only weakly expressed within these studies, hampering translocation analysis via tyrosine phosphorylation due to the low sensitivity of this technique. Hence, CagA variants with N-terminal and also internal domain deletions under control of the endogenous *cagA* promoter were constructed. Briefly, as for the generation of P12[TEM-CagA] (see also Figure 9), plasmid pWS373 was used for deletion of the *cagA* region in *H. pylori* P12, and subsequently, diverse plasmids, carrying modified *cagA* versions, were employed as reconstitution plasmids that recombined in the *cagA* region (see Materials & Methods section for further details).

According to the crystal structure of CagA, the protein can be divided into a structured N-terminal region consisting of 3-4 domains and a rather unstructured C-terminal tail [130]. Within the N-terminal region, domain D1 has very little interaction surface with the other domains, and it seemed possible to delete this domain without any structural influence on other CagA regions. In addition, the first 17 amino acids were unstructured in the crystal [130]. Thus, variants lacking the first 17 amino acids of CagA (CagAΔ17N) as well as a mutant lacking domain D1 (amino acids 18-284, CagAΔD1) were constructed (Figure 21A). Moreover, a variant lacking the whole EPIYA region was engineered (CagAΔEPIYA) to investigate the role of this tyrosine phosphorylatable domain onto translocation (Figure 21A). After infection of AGS cells with these mutants, a very weak phosphorylation band of CagAΔ17N could be detected via immunoblotting (Figure 21B, highlighted by an arrowhead), while the signal for CagAΔD1 could not be evaluated due to high background signals. As expected, no signal for the EPIYA deletion variant was detectable as the read-out of this assay is based on detection of the tyrosine phosphorylation within this region. Analysis of

respective co-culture supernatants revealed a significant increase of IL-8 secretion (~80%) upon infection with P12[CagAΔ17N] compared to the Δ*cagA* deletion mutant (Figure 21C), that correlated with the detectable CagA phosphorylation. No increase in IL-8 concentration was observed in the supernatants of cells infected with the P12[CagAΔD1] or P12[CagAΔEPIYA] variants.

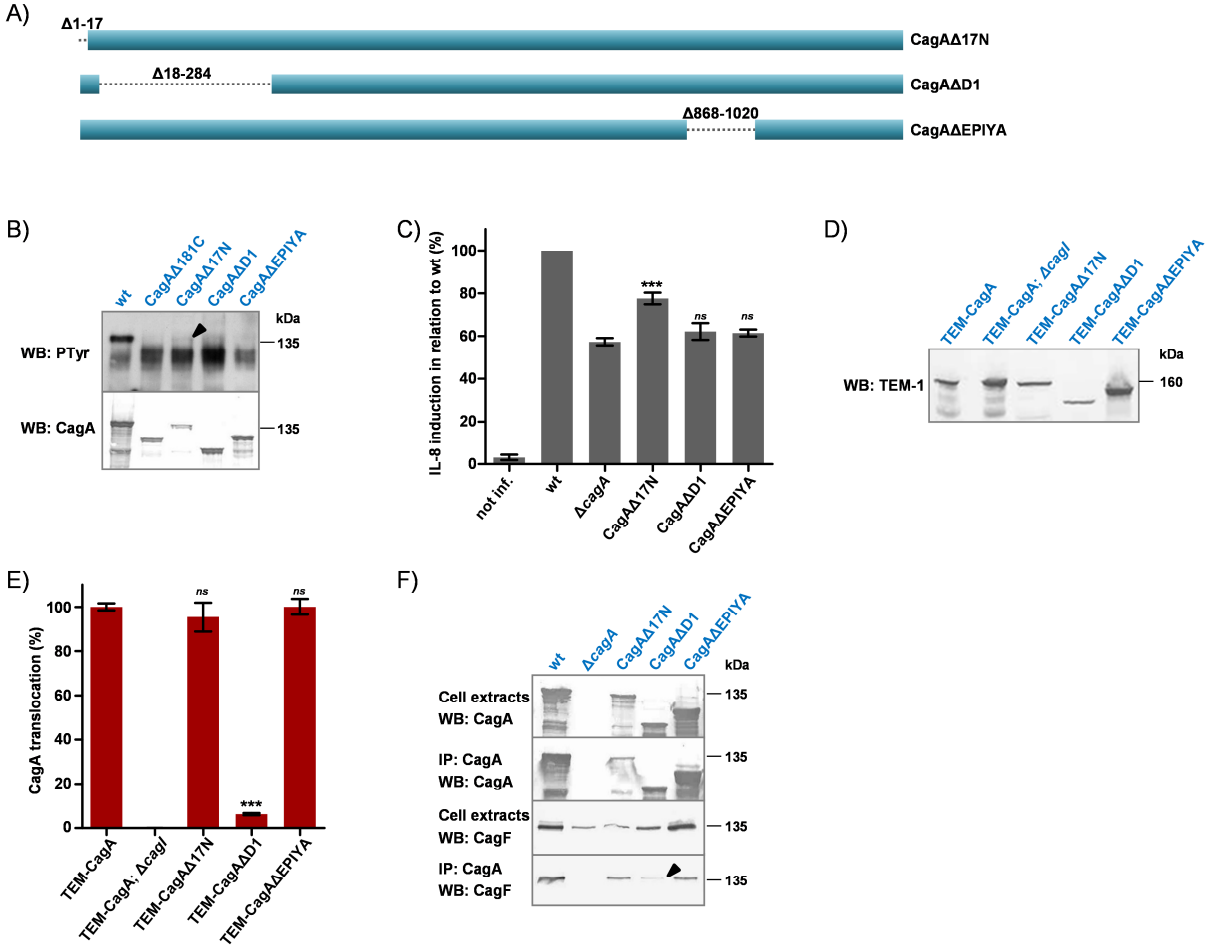

Figure 21: Influence of N-terminal and internal domain deletions on CagA translocation

A) Schematic overview of N-terminal and internal CagA deletion variants.

B) Immunoblot analysis of infected AGS cells with phosphotyrosine (4G10) and CagA (AK257) antibodies. Cells were infected with P12 wild-type or the indicated mutants and subjected to Western blotting (WB). The arrowhead highlights a weak phosphorylation band of CagAΔD1.

C) Analysis of co-culture supernatants derived from B) for IL-8 secretion via sandwich ELISA. All values were normalized to the IL-8 values found in the supernatants of P12 wild-type-infected cells, and are indicated as mean values with standard errors of the mean from at least three independent infections; t-test (one-tailed, unpaired) comparing to Δ*cagA*, ***, $p<0.0005$, *ns*: no significant difference.

D) Immunoblot (WB) of bacterial lysates analyzing TEM-CagA or TEM-CagA variant expression using a TEM-1 antibody.

E) Quantification of TEM-CagA translocation rates by plate reading. AGS cells were infected with P12[TEM-CagA] or the indicated mutants. The average blue-to-green ratios of each infection were normalized to the mean ratio of P12[TEM-CagA]-infected cells, and are shown as mean percentages from at least four independent experiments with standard errors of the mean. t-test (one-tailed, unpaired) comparing to TEM-CagA, ***, $p<0.0001$, *ns*: no significant difference.

F) Analysis of co-immunoprecipitation (IP) fractions with CagA and CagF immunoblots (WB). AGS cells were infected with P12 wild-type or the indicated mutants, then lysed and subjected to immunoprecipitation using the polyclonal CagA antiserum AK257. The arrowhead highlights a weak CagF band for CagAΔD1.

To quantify CagA translocation rates, corresponding TEM-fusion variants were constructed and exhibited protein expression levels comparable to the wild-type (Figure 21D). Evaluation using the TEM-CagA assay (translocation efficiency defined as P12[TEM-CagA] = 100% and Δ*cagI* mutant = 0%; Figure 21E) surprisingly showed translocation rates of TEM-CagAΔ17N of about 100% which could not be concluded from immunoblot analysis (Figure 21B) and clearly proves that the N-terminus is not involved in substrate recognition. Moreover, a slight translocation of TEM-CagAΔD1 could be detected (~6%), indicating a role of the D1 domain for efficient translocation. Regarding TEM-CagAΔEPIYA, the translocation rate was as high as for the wild-type, suggesting no contribution of this region to substrate recognition of the type IV secretion system. Nevertheless, no difference in IL-8 induction was observed upon infection for this variant in comparison to the Δ*cagA* deletion mutant (Figure 21C). This was consistent with previously published data, where a necessity of the EPIYA region for CagA-dependent IL-8 induction was reported [189].

To investigate the drastically reduced CagA translocation of the D1 deletion variant in more detail, immunoprecipitation experiments were performed to evaluate the binding efficiency of the modified CagA protein to its secretion chaperone CagF (Figure 21F). CagF was co-precipitated from cell extracts of the wild-type, but not the Δ*cagA* mutant, proving the specificity of this immunoprecipitation. CagF was also detectable in cell extracts of CagAΔ17N, CagAΔD1 and the CagAΔEPIYA variant, but the precipitation efficiency of CagAΔD1 was clearly reduced compared to the other mutants (highlighted with an arrowhead, Figure 21F). This is consistent with prior studies [120], where an interaction of CagF with various CagA domains (including D1) could be shown. Moreover, the data presented here might extend this finding, as the CagF and D1 interaction appears to be crucial for efficient delivery of CagA. Nevertheless, a role of the N-terminal D1 domain for direct CagA substrate recognition by the type IV secretion apparatus cannot be excluded.

According to the data presented in this and prior chapters, CagA translocation seems to be highly dependent on the presence of its C-terminus and strongly influenced by the N-terminal D1 domain, while the first 17 N-terminal amino acids as well as the EPIYA region do not have a function for this process. For further experiments, a TEM-CagA fusion variant was constructed that incorporated translocation-promoting regions like the N-terminal D1 domain or C-terminus, but completely lacked the N-terminal D2 and D3 domain as well as the EPIYA region (amino acids 260-1019, TEM-CagAΔD2-D3-EPIYA; Figure 22A). As an additional negative control, a variant lacking the last 181 amino acids (TEM-CagAΔ181C) was used. CagA expression profiles of the mutants revealed a relatively low expression level of TEM-

CagAΔD2-D3-EPIYA (Figure 22B). Therefore, it is obvious that the removal of large sequence parts might influence stability and structure of CagA. Nevertheless, the TEM-CagA translocation assay was conducted, depicted in Figure 22C (translocation efficiency defined as P12[TEM-CagA] = 100% and Δ*cagI* mutant = 0%). As expected, no signal was observed for TEM-CagAΔ181C and moreover, no translocation was detectable for TEM-CagAΔD2-D3-EPIYA. This observation could be due to the rather low TEM-CagA expression of the mutant, although prior data demonstrated full translocation rates even for less well-expressed fusions (compare Figure 19E). In fact, it seems more likely that deletion of the N-terminal D2 domain renders the protein translocation-incompetent as this region directly interacts with the host cell integrins that are crucial for delivery into the cell [127].

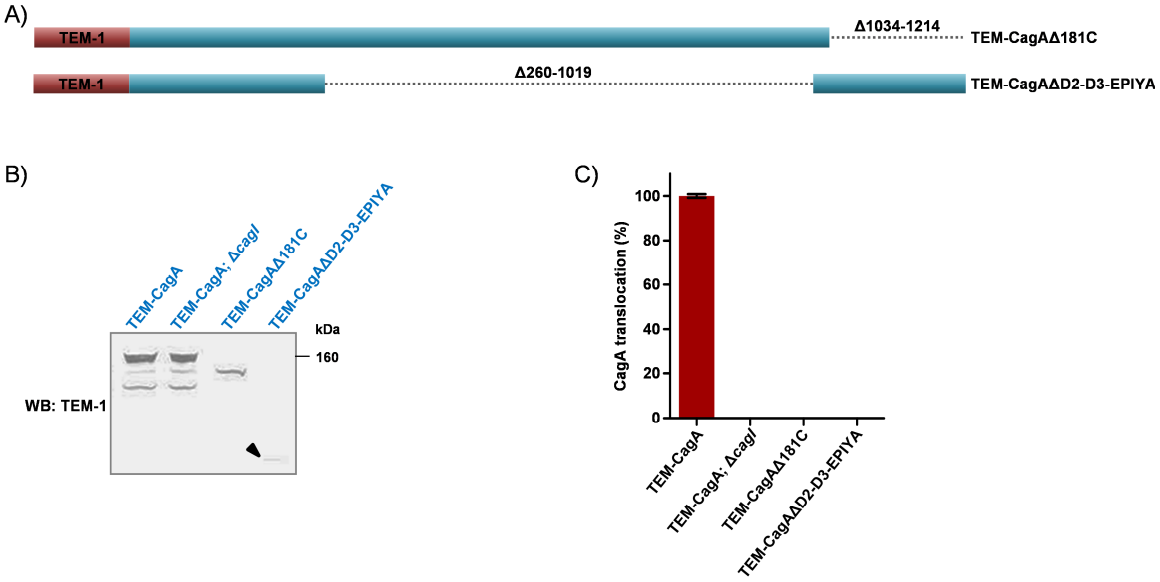

Figure 22: Influence of an internal domain deletion on CagA translocation
A) Schematic overview of investigated CagA deletion variants.
B) Immunoblot (WB) of bacterial lysates analyzing TEM-CagA or TEM-CagA variant expression using a TEM-1 antibody.
C) Quantification of TEM-CagA translocation rates by plate reading. AGS cells were infected with P12[TEM-CagA] or the indicated mutants. The average blue-to-green ratios of each infection were normalized to the mean ratio of P12[TEM-CagA]-infected cells, and are shown as mean percentages from four independent experiments with standard errors of the mean.

2.4 Impact of protein expression on CagA translocation

As another translocation parameter, the influence of protein expression on CagA translocation was characterized. For this purpose, firstly it was examined how the co-expression of two CagA variants influences the total translocation rate and secondly, whether the CagA translocation process requires freshly synthesized proteins.

2.4.1 Analysis of CagA and TEM-CagA co-expressing strains

The consistent results regarding tyrosine phosphorylation of CagA and translocation of TEM-CagA suggested that both proteins are recognized by the same machinery. To obtain further data on the efficiency of this process, mutants were constructed that expressed wild-type or variant CagA together with TEM-CagA protein. For this purpose, P12[TEM-CagA] was transformed with *cagA* reconstitution plasmids that integrated into the *recA* locus [175].

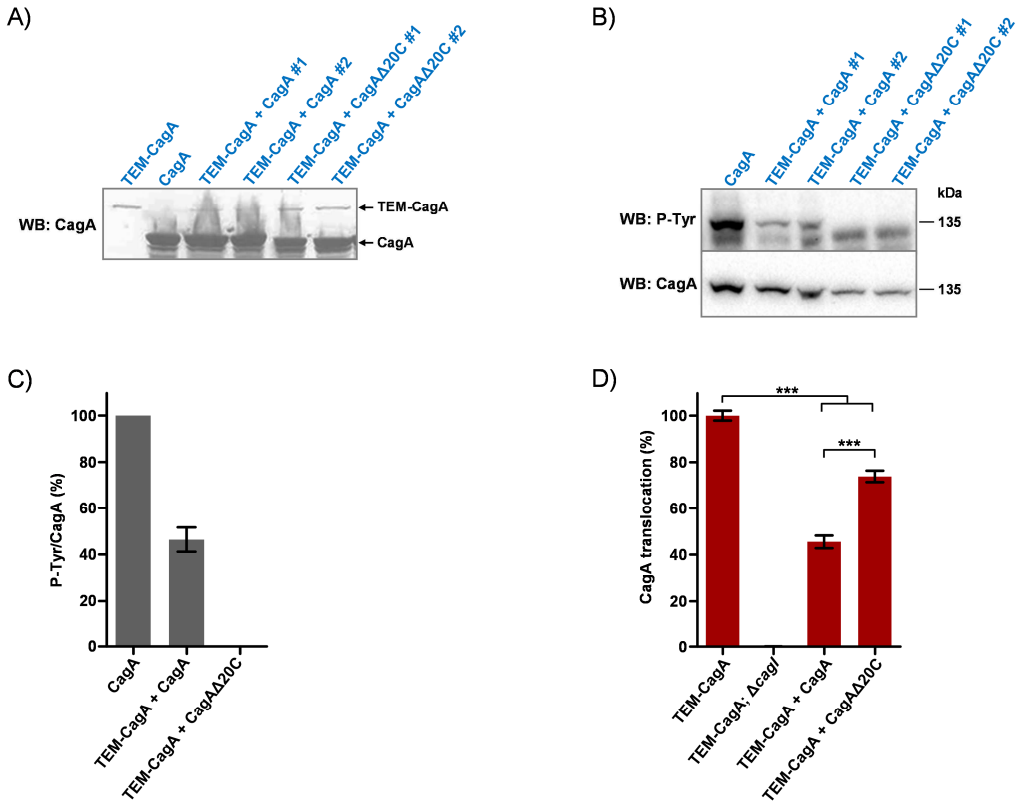

Figure 23: Analysis of CagA and TEM-CagA co-expressing strains
A) Immunoblots (WB) analyzing CagA and TEM-CagA expression in co-producing strains using a CagA antibody (AK268).
B) Immunoblot analysis of infected AGS cells with phosphotyrosine (PY99) and CagA (AK268) antibodies. Cells were infected with P12 wild-type or the indicated mutants and analyzed via Western blotting (WB).
C) Tyrosine phosphorylation levels of CagA (exemplarily shown in B) were estimated by quantitative immunoblot analysis and are indicated as mean densitometric ratios of phosphotyrosine to CagA protein bands normalized to P12 wild-type from three independent experiments, with standard errors of the mean.
D) Quantification of TEM-CagA translocation rates by plate reading. AGS cells were infected with P12[TEM-CagA] or co-producing mutants. The average blue-to-green ratios of each infection were normalized to the mean ratio of P12[TEM-CagA]-infected cells, and are shown as mean percentages of four independent experiments with standard errors of the mean; ANOVA (one-way, Tukey post hoc test), ***: $p<0.001$.

The immunoblot presented in Figure 23A depicts expression of TEM-CagA and wild-type CagA or a CagA variant lacking the last 20 amino acids (TEM-CagA + CagA and TEM-CagA + CagAΔ20C). Although the TEM-CagA fusion protein was expressed less than wild-type CagA, phosphotyrosine analysis (see Figure 23B) showed a decrease of CagA phosphorylation for the TEM-CagA + CagA co-producing mutant. This was additionally

verified by quantification of phosphorylated CagA in relation to total CagA protein amounts following a densitometric determination from independent experiments (see Figure 23C). In detail, a reduction of phosphorylated CagA to about 46% was observed for P12[TEM-CagA + CagA] compared to the wild-type. Conversely, the percental CagA translocation (translocation efficiency defined as P12[TEM-CagA] = 100% and Δ*cagI* mutant = 0%; see Figure 23D), determined via CCF4 cleavage by translocated TEM-CagA, was equally reduced to about 46%, indicating that both proteins are competitively recognized and translocated to the same amounts by the type IV secretion apparatus. As expected, no tyrosine phosphorylation was observed for CagAΔ20C lacking the C-terminal secretion signal (see Figure 23B). Surprisingly, TEM-CagA translocation from a strain co-producing CagAΔ20C did not reach 100%, although it was significantly increased in comparison to the wild-type CagA co-producing variant (Figure 23D). This observation might be based on the fact that competition for recruitment to the secretion apparatus depends on, but is not restricted to, the C-terminal secretion signal.

Taken together, the data proves that CagA and TEM-CagA are translocated with the same efficiency, although expressed to different amounts. Again, the data implicates that not all CagA molecules present in the cell are translocated and that even high amounts of wild-type CagA are not able to completely block delivery of TEM-CagA. This raises further speculations that exclusively newly synthesized CagA protein is recruited by the translocation machinery irrespective of the amounts already present, which will be investigated in the next section.

2.4.2 Direct and secondary inhibition of protein synthesis

To examine whether only freshly synthesized CagA protein is translocated into host cells, an antibiotic directly inhibiting protein synthesis was used and as control one with bacteriolytic activity. For this purpose, three different protocol layouts were designed, which are summarized in Figure 24A. Within these layouts, *H. pylori* was either pre-incubated with the antibiotic and washed before infection, or the washing step was skipped and AGS cells were directly infected with the *H. pylori*-antibiotic mixture after a short pre-incubation. As a control, solely the AGS cells were exposed to the antibiotic prior to infection to exclude any cell-specific effects. Following these protocols, various concentrations of erythromycin were employed in order to evaluate the effect of direct protein biosynthesis inhibition on CagA translocation, and percental rates were determined using the TEM-CagA assay (Figure 24B). Translocation was completely abolished using 10 mg/L erythromycin and also strongly

influenced at lower concentrations. In addition, growth curves of bacteria were performed in the presence of erythromycin, and the expected bacteriostatic effect correlated with the translocation inhibition (Figure 24C). In contrast, treatment of *H. pylori* with ampicillin did not influence CagA translocation as strongly as erythromycin (Figure 24D), although growth analysis in the presence of ampicillin revealed curves typical for this bactericidal antibiotic (Figure 24E). Ampicillin blocks protein synthesis only as a secondary effect, hence, the stronger effects of erythromycin on CagA translocation might be based on a direct deprivation of freshly synthesized proteins from the type IV secretion machinery. No influence on CagA translocation was observed for conditions where only cells were exposed to the antibiotics and thus, unspecific cytotoxic effects could be excluded (Figure 24B/D).

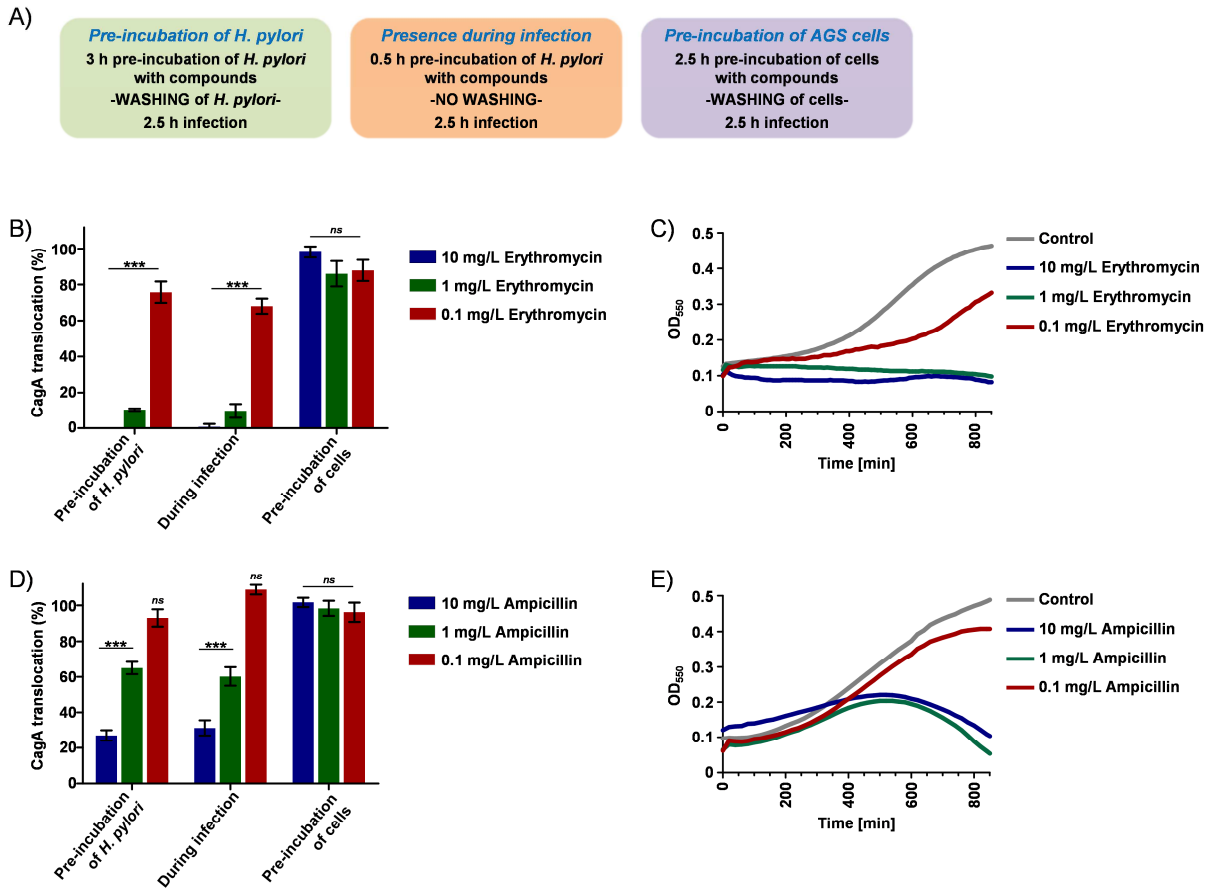

Figure 24: Influence of direct and secondary protein synthesis inhibition on CagA translocation
A) Layout protocols for infections with inhibiting compounds.
B) Quantification of TEM-CagA translocation rates by plate reading. AGS cells were infected with P12[TEM-CagA] in the presence of erythromycin according to the protocols described in A). The average blue-to-green ratios of each infection were normalized to the mean ratio of P12[TEM-CagA]-infected cells, and are shown as mean percentages of at least four independent experiments with standard errors of the mean. ANOVA (one-way, Turkey post hoc test) referring to untreated controls, ***: $p<0.001$, *ns*: no significant difference.
C) Growth analysis of *H. pylori* in the presence of erythromycin. OD_{550} was recorded every 5 min for at least 16 h and experiments were independently repeated at least 3 times. The figure depicts a representative growth curve.
D) Quantification of TEM-CagA translocation rates by plate reading in the presence of ampicillin. Experiments were performed as described in B).
E) Growth analysis of *H. pylori* in the presence of ampicillin. Experiments were performed as described in C).

Together with the time-course experiments (Chapter 1.4), the data generated from co-producing mutants in the previous section (Chapter 2.4.1) as well as the clear inhibitory competence of erythromycin on CagA translocation, a dynamic model is conceivable in which only freshly synthesized CagA is introduced into the type IV secretion machinery.

2.5 Influence of metal ions on CagA translocation competence

It has been published that sequestration of specific metal ions has a high impact on CagA translocation competence [125, 126]. Indeed, this might be crucial for host colonization and the interplay of *H. pylori* with the immune system. In this work, data concerning the influence of metal ions should be confirmed and extended, applying the novel TEM-CagA translocation assay.

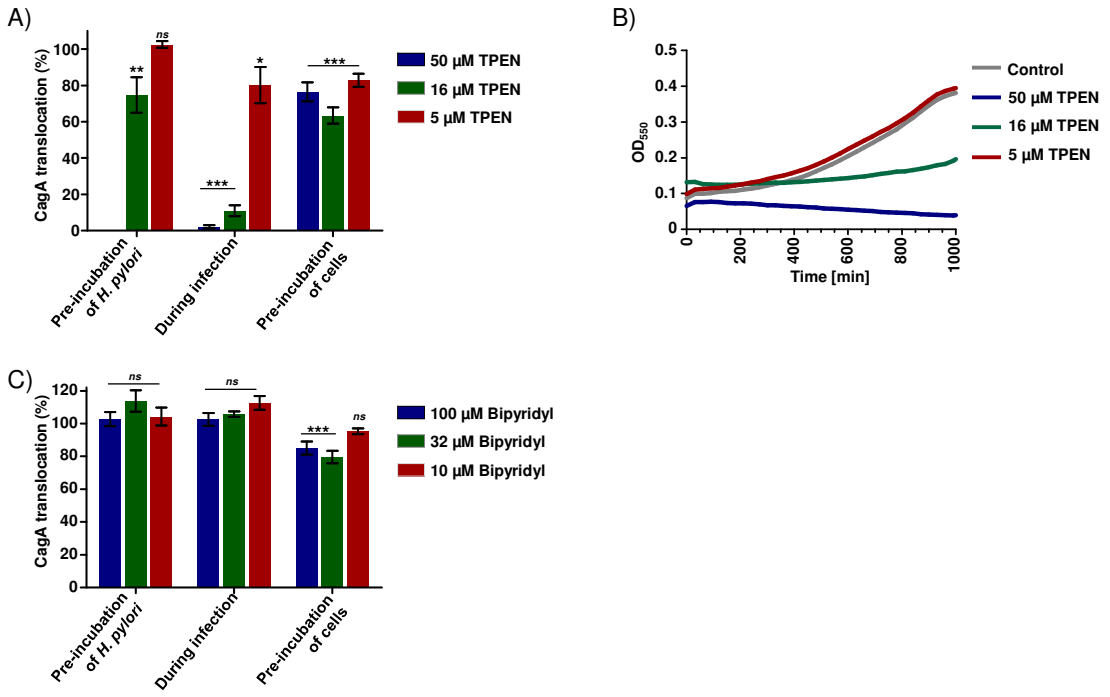

Figure 25: Influence of metal ion sequestration on CagA translocation
A) Quantification of TEM-CagA translocation rates by plate reading. AGS cells were infected with P12[TEM-CagA] with various concentrations of TPEN according to the protocols described in Figure 24A). The average blue-to-green ratios of each infection were normalized to the mean ratio of P12[TEM-CagA]-infected cells, and are shown as mean percentages of at least four independent experiments with standard errors of the mean. ANOVA (one-way, Tukey post hoc test) referring to untreated controls, *: $p<0.05$, **: $p<0.01$, ***: $p<0.001$, *ns*: no significant difference.
B) Growth analysis of *H. pylori* in the presence of TPEN. OD_{550} was recorded every 5 min for at least 16 h and experiments were independently repeated at least 3 times. The figure depicts a representative growth curve.
C) Quantification of TEM-CagA translocation rates by plate reading in the presence of various concentrations of bipyridyl. Experiments were performed as described in A).

At first, the proposed inhibitory effect of zinc sequestration on Cag type IV secretion activity [126] was investigated. For this purpose, TPEN (N,N,N',N'-tetrakis(2-pyridylmethyl)

ethylenediamine), a high-affinity zinc chelator, was applied and experiments were performed as depicted in Figure 24A. Following this, P12[TEM-CagA], AGS cells or the co-culture were exposed to various concentrations of TPEN and percental translocation rates were examined via the TEM-CagA assay (Figure 25A). Translocation was dose-dependently inhibited when *H. pylori* was either pre-incubated with TPEN or TPEN was present during infection. Nonetheless, growth analysis of *H. pylori* revealed a high antimicrobial activity of TPEN (Figure 25B). In addition, translocation rates were also reduced when only cells were in contact with TPEN (pre-incubation of cells, Figure 25A). This indicated a toxic effect on the cells and in fact, zinc sequestration induces apoptosis in eukaryotic cells [194]. For this reason, the effects of TPEN on translocation might be ascribed to an antimicrobial effect against *H. pylori* and a cytotoxic effect on the cells rather than to a specific decrease in Cag type IV secretion activity as recently reported [126].

Moreover, it has been reported that low iron conditions can induce hypervirulent *H. pylori* strains *in vivo* by means of increased CagA injection into the host cell [125, 195]. To confirm this hypothesis with the novel TEM-CagA assay, bipyridyl, a high-affinity chelator for iron, was applied according to the three different protocol layouts described in Figure 17A. Contrary to the published results, no increase of CagA translocation could be observed (Figure 18C). However, translocation rates were decreased (~80%) for the condition were only cells got in contact with bipyridyl, indicating a cytotoxic effect on the cells. Like for zinc, the proposed hypothesis could not be supported.

2.6 Inhibition of CagA translocation by modulation of cellular structures

Hitherto, experiments focused on possibilities to influence CagA translocation by directly acting on *H. pylori*. Delivery of CagA is not only dependent on a functional type IV secretion system, but also on host cell machineries. To characterize several host cell contributions in more detail, cells as well as *H. pylori* as control were treated with specific inhibitors following the experimental set-ups depicted in Figure 24A. In general, corresponding data on tyrosine phosphorylation of CagA was prior reported and should be extended employing the phosphorylation-independent TEM-CagA reporter assay.

2.6.1 Modulation of the cytoskeleton and lipid rafts

At first, the influence of the actin cytoskeleton on CagA translocation was investigated using various concentrations of cytochalasin D, a potent inhibitor of actin polymerization. Infection of cells with P12[TEM-CagA] exhibited an impairment of translocation (~50%) as long as AGS cells were in contact with the inhibitor (Figure 26A). No dose-dependency was observed, indicating a saturated inhibition by cytochalasin D. In contrast, only a slight effect was detected for pre-incubation with *H. pylori* (~80% translocation at 2 µM), suggesting a specific action on the actin cytoskeleton (Figure 26A). In addition, similar results were obtained for another actin polymerization inhibitor (latrunculin B, data not shown) and in accordance with previous reports investigating CagA phosphorylation [129].

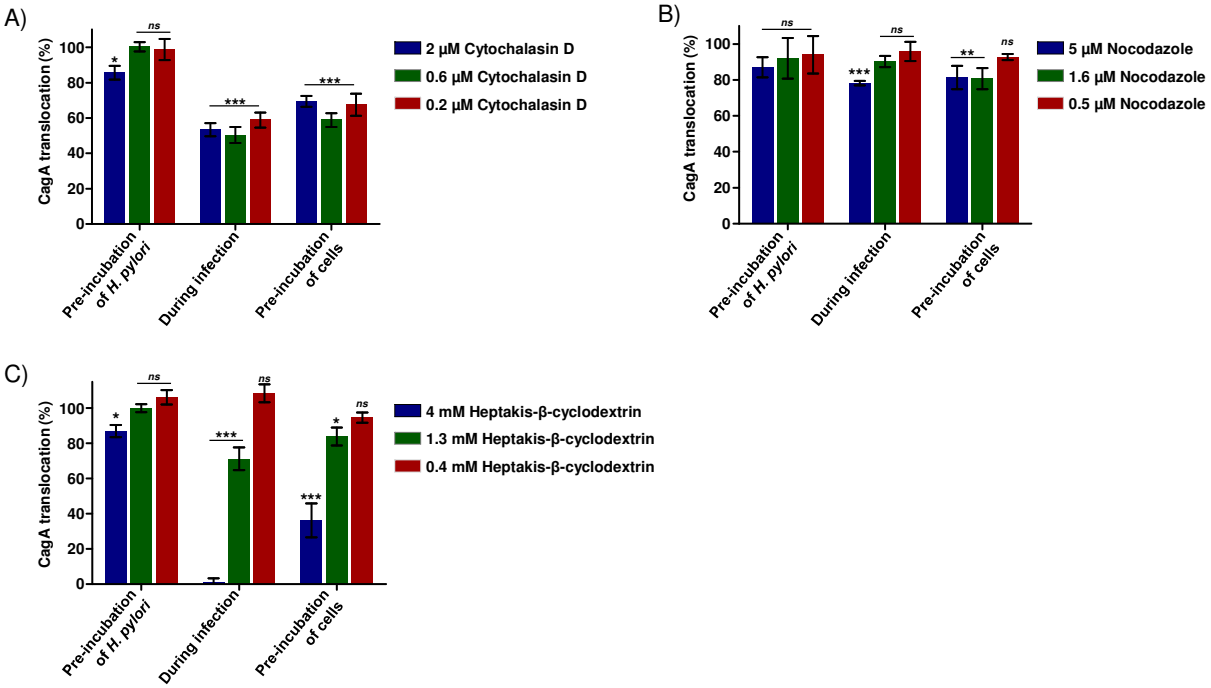

Figure 26: Impact of structural cell modifications on CagA translocation
A) Quantification of TEM-CagA translocation rates by plate reading. AGS cells were infected with P12[TEM-CagA] with various concentrations of cytochalasin D according to the protocols described in Figure 24A). The average blue-to-green ratios of each infection were normalized to the mean ratio of P12[TEM-CagA]-infected cells, and are shown as mean percentages of at least four independent experiments with standard errors of the mean. ANOVA (one-way, Tukey post hoc test) referring to untreated controls, *: $p<0.05$, **: $p<0.01$, ***: $p<0.001$, *ns*: no significant difference.
B) Quantification of TEM-CagA translocation rates by plate reading in the presence of various concentrations of nocodazole. Experiments were performed as described in A).
C) Quantification of TEM-CagA translocation rates by plate reading in the presence of various concentrations of heptakis-β-cyclodextrin. Experiments were performed as described in A).

Also, the impact of the microtubule (filament) system on CagA translocation was examined. Nocodazole was applied to disrupt microtubule filaments, and effects on translocation are summarized in Figure 26B. No influence was observed when bacteria were pre-incubated with nocodazole prior to infection and a slight but significant inhibitory effect was observed

when cells were in contact with the substance for the highest concentrations applied (~80% translocation at 5 or 1.6 µM). Thus far, no effect on CagA phosphorylation was described in response to the inhibition of tubulin polymerization, which might be owed to the low sensitivity for detecting weak changes via tyrosine phosphorylation analysis.

In order to study the influence of host cell membrane composition on CagA translocation, heptakis(2,6-di-O-methyl)-β-cyclodextrin was used. This substance exhibits a high affinity for cholesterol and is able to deplete cholesterol from the membrane, leading to the disruption of lipid raft microdomains [196]. Measurement of CagA translocation in the presence of heptakis-β-cyclodextrin showed the strongest effects when applied during infection or for pre-incubation of AGS cells (Figure 26C). Effects were most severe in the latter set-up suggesting that constant cholesterol depletion is necessary for preventing CagA translocation. These results are consistent with prior data, where an inhibiting effect of heptakis-β-cyclodextrin on CagA phosphorylation was observed [114, 129, 197].

Taken together, experiments presented in this chapter not only confirm but further extend previously described data by using three different experimental set-ups together with quantification of CagA translocation in a phosphorylation-independent manner.

2.6.2 Inhibition of eukaryotic kinases

As a last parameter, the influence of cellular kinases on CagA translocation was analyzed. Once inside the host cell, CagA rapidly gets tyrosine-phosphorylated by kinases, which constitutes a crucial step for CagA interaction with host proteins and its interference with corresponding signal transduction pathways. Inhibition of this phosphorylation step was examined in various studies using either PP2, a specific inhibitor of Src-family kinases, or genistein, a general tyrosine kinase inhibitor [74, 198]. However, kinase inhibition is not compatible with measurement of CagA phosphorylation, and thus no information is available whether CagA can enter the cells upon inhibitor treatment. Hence, the newly developed phosphorylation-independent TEM-CagA translocation reporter was applied using various concentrations of PP2 or genistein (see Figure 27A&B) in combination with the different experimental set-ups described in Figure 24A. Pre-treatment of cells with inhibitors affected CagA translocation only weakly for PP2 (~80% translocation at 10 µM) and not at all for genistein, which confirms that CagA was still delivered into the cells. In contrast, when bacteria were exposed to the substances (either pre-incubated or during infection, Figure 27A&B), a translocation inhibition by PP2 and an even stronger reduction by genistein was observed. Growth analysis in the presence of PP2 and genistein (Figure 27C&D) revealed an

antimicrobial activity against *H. pylori*, and growth suppression correlated with translocation inhibition. In fact, an anti-*H. pylori* activity of genistein has been described before [199]. Hence, the potential susceptibility of *H. pylori* towards supposedly exclusive eukaryotic inhibitors should not be neglected in future experimental set-ups.

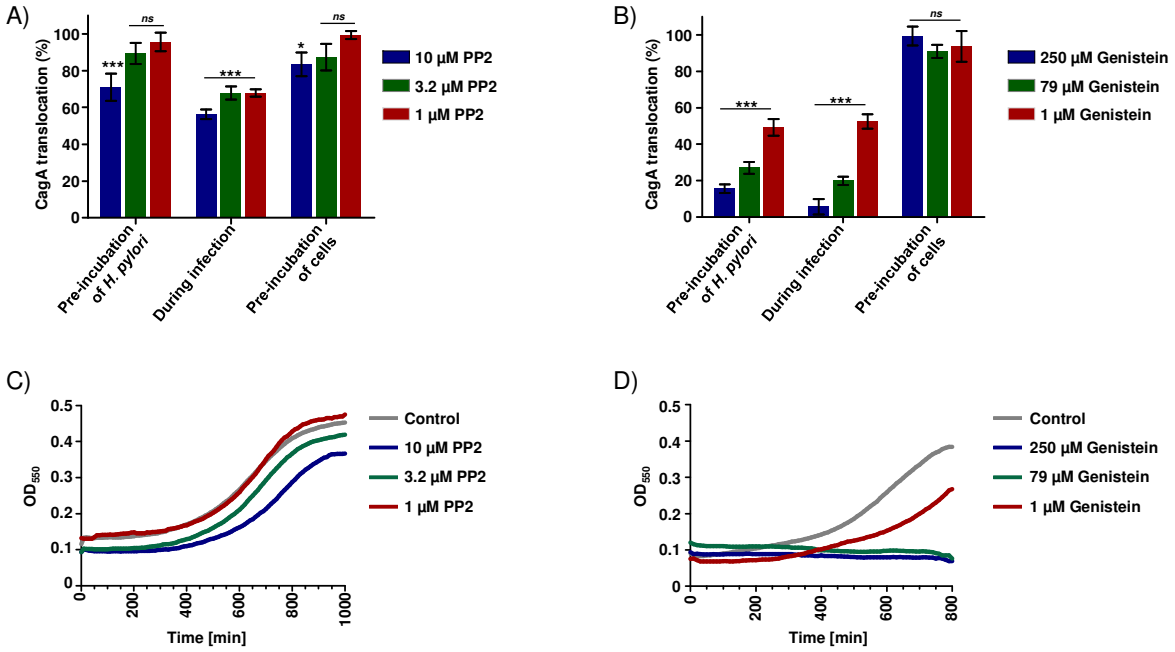

Figure 27: Influence of the inhibition of eukaryotic kinases on CagA translocation
A) Quantification of TEM-CagA translocation rates by plate reading. AGS cells were infected with P12[TEM-CagA] with various concentrations of PP2 according to the protocols described in Figure 24A). The average blue-to-green ratios of each infection were normalized to the mean ratio of P12[TEM-CagA]-infected cells, and are shown as mean percentages of at least four independent experiments with standard errors of the mean. ANOVA (one-way, Tukey post hoc test) referring to untreated controls, ***: $p<0.001$, *ns*: no significant difference.
B) Quantification of TEM-CagA translocation rates by plate reading in the presence of various concentrations of genistein. Experiments were performed as described in A).
C) Growth analysis of *H. pylori* in the presence of PP2. OD_{550} was recorded every 5 min for at least 16 h and experiments were independently repeated at least 3 times. The figure depicts a representative growth curves.
D) Growth analysis of *H. pylori* in the presence of genistein. Experiments were performed as described in C).

3. High-throughput screening for CagA translocation inhibitors

Infection with *H. pylori* leads to various malignancies including gastric or duodenal ulcer disease, gastric adenocarcinoma, and mucosa-associated lymphoid tissue (MALT) lymphoma [11, 13, 18, 19, 23, 24]. Antibiotic treatment of *H. pylori* infection increasingly fails due to resistance development [161, 162] and thus, alternative strategies are urgently needed. As the delivery of CagA into the host cell constitutes a key event in the induction of the above-mentioned diseases [137, 156-158], one promising approach could be to directly inhibit the CagA translocation process. Thereby, the cancerogenic effects of the CagA protein could be dampened and at the same time the risk for resistance development diminished. The search

for such specific inhibitors was a main part of this work and will be described in the following sections.

3.1 Experimental set-up for a high-throughput screening platform

To increase the probability for the identification of specific CagA translocation inhibitors, a high-throughput screening platform had to be established. For quick identification of substances blocking the translocation process, the newly established TEM-CagA assay was applied and miniaturized to the 384-well format. A chart of the final screening workflow including follow-up studies is presented in Figure 28.

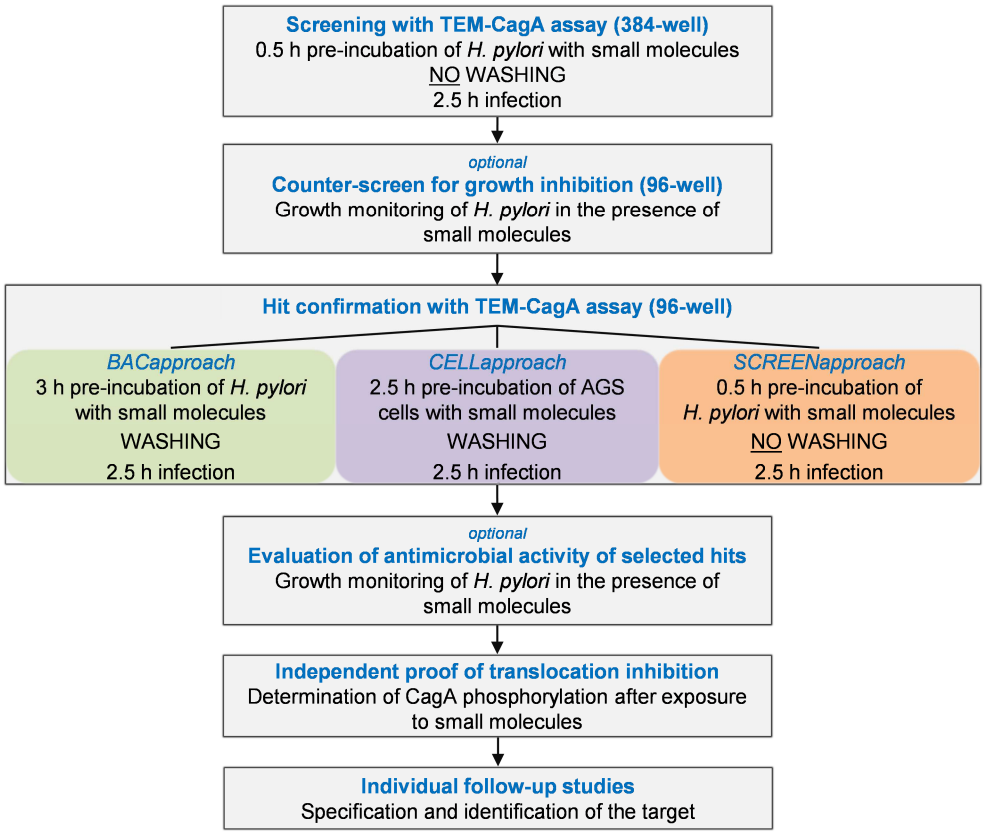

Figure 28: Workflow of the high-throughput screening platform
See text for further details to individual steps.

For the initial TEM-CagA assay screening step, small-molecule libraries were derived in 384-well plates. Briefly, the reporter strain *H. pylori* P12[TEM-CagA] was pre-incubated with small-molecule compounds, the bacteria-compound mixture transferred onto AGS cells and after 2.5 h infection, percental CagA translocation rates were determined. To subsequently identify compounds with an anti-*H. pylori* effect, a counter-screening for growth inhibition was conducted in 96-well plates. The influence on growth was analyzed via growth curve analysis and expressed as the percental OD_{550} increase compared to an untreated control. This

step was optional and not executed for every library. Promising hit compounds that displayed high translocation inhibition were confirmed employing the TEM-CagA assay in the 96-well format. For this purpose, three different experimental set-ups were applied to quickly identify whether the compounds exhibited an effect on *H. pylori*, the cells or even both. To do so, either *H. pylori* (BACapproach) or AGS cells (CELLapproach) were pre-treated with compounds prior to infection. In addition, a set-up equal to the initial screening conditions (SCREENapproach) was applied. Antimicrobial activity of selected compounds was examined, if no counter-screen for growth inhibition had been performed before. To independently verify CagA translocation inhibition, tyrosine phosphorylation assays were performed following the above-mentioned protocols. Depending on the compounds favorized, individual follow-up studies were conducted that will be specified in detail in the respective sections.

3.2 Evaluation of the TEM-CagA assay for high-throughput screenings

Before describing the single library screenings in detail, a summary of all screenings is depicted in Figure 29A.

A)

Library	Number	Source	Properties	Statistics		
				Z´-Factor	S/N-Ratio	S/B-Ratio
Extended natural compound library (ExNCL)	340	IMIT (Tübingen)	Natural products (antibiotics)	0.64	51.09	7.74
LOPAC	1267	Sigma-Aldrich	Pharmacologically active substances	0.68	219.48	18.16
Natural compound library (NCL)	259	HZI (Saarbrücken)	Natural products from *Myxobacteriaceae*	0.61	46.41	14.52
SPECS-selected	1120	SPECS company	Chemically synthesized	0.80	151.57	18.50
SPECS-random	1120	SPECS company	Chemically synthesized	0.59	86.49	11.96
TOTAL	**4106**			**0.66**	**119.46**	**15.29**

B)

$$Z' - \text{Factor} = 1 - \frac{3(\sigma_{Positive\ Control} + \sigma_{Negative\ Control})}{|\mu_{Positive\ Control} - \mu_{Negative\ Control}|}$$

$$S/N - \text{Ratio} = \frac{\mu_{Positive\ Control} - \mu_{Negative\ Control}}{\sigma_{Negative\ Control}}$$

$$S/B - \text{Ratio} = \frac{\mu_{Positive\ Control}}{\mu_{Negative\ Control}}$$

C)

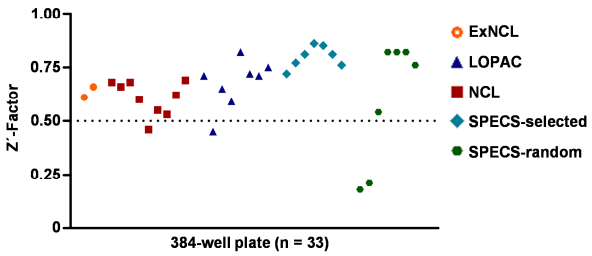

Figure 29: Summary of screened libraries and corresponding statistical parameters
A) Table summarizing all libraries screened including the number of compounds, source, properties and statistics of the TEM-CagA assay screening procedure. Values printed in bold either denote the total amount of screened compounds or mean values of statistical parameters. S/N = signal to noise, S/B = signal to background.
B) Formulas of statistical parameters shown in A) according to [200]. μ: mean value, σ: standard deviation, positive control: blue-to-green fluorescence signal of untreated P12[TEM-CagA], negative control: blue-to-green fluorescence signal of P12[TEM-CagA]Δ*cagI*.
C) Overview of Z´-factors determined for individual 384-well plates screened with the TEM-CagA assay.

Library-specific properties ranged from purified natural products to chemically synthesized compounds. Of importance, statistical parameters of TEM-CagA reporter screenings in 384-well plates are listed, and corresponding formulas are shown in Figure 29B (according to [200]). The most important parameter is the Z´-factor, which is a widespread measure for the quality of high-throughput screening assays. In this context, values above 0.5 comply with an excellent screening performance [200]. Following this, an average Z´-factor of 0.66 was calculated for all TEM-CagA reporter screenings, which validates the experimental procedure. However, when analyzing Z´-factors of every single 384-well plate screened (n = 33, Figure 29C), 4 plates exhibited values below 0.5. In addition, the parameters "signal to noise" (S/N) and "signal to background" (S/B) are listed. Values of these parameters cannot be classified in certain ranges and are considered as the higher the value the higher the screening validity. Especially the S/B-ratio is less important because no signal variation is included. Values of S/N-ratios varied strongly (46-219) and further confirm the trustworthiness of the more constant Z´-factor. Considering the average Z´-factor above 0.5, the TEM-CagA reporter assay was successfully evaluated as a valid high-throughput screening method.

3.3 Screening of the ExNCL library

At first, the extended natural compound library (ExNCL) was screened. This library was derived from the Interfaculty Institute of Microbiology and Infection Medicine (IMIT, Tübingen) and comprised 340 purified natural compounds with unique structures and mainly antibacterial bioactivities. For screening of TEM-CagA translocation inhibition a compound concentration of 5 µM was employed. A total number of 39 compounds were detected that revealed a translocation rate lower than 50% (see Figure 30A). A subsequent counter-screening for growth inhibition identified 157 compounds that reduced *H. pylori* growth by more than 50% (see Figure 30B). This higher hit rate was expected, as for growth screening double concentrations (10 µM) were applied and the library consisted mainly of antibiotics. To filter compounds that demonstrated CagA translocation inhibition without major anti-*H. pylori* effects, translocation rates were plotted against the respective growth rates (see Figure 30C). In total, 181 compounds displayed no or weak effects on translocation and growth (both parameters >50%). A group of 37 compounds blocked translocation (<50%) and also influenced growth (<50%), suggesting that translocation inhibition was due to an antibacterial effect. Accordingly, many of these substance groups were already described to exhibit anti-*H. pylori* activities, such as several angucyclinone derivates (rabelomycin, tetrangomycin,

frigocyclinone) [201, 202]. Also various macrolide antibiotics (e.g. different mycinamicin derivates or picromycin), a substance class that can be used for *H. pylori* treatment, inhibited translocation and growth [203]. Surprisingly, also some antibiotics that were originally thought to be active exclusively against gram-positive bacteria, such as naphtocyclinons [204] or avilamycins [205], showed strong effects against *H. pylori*.

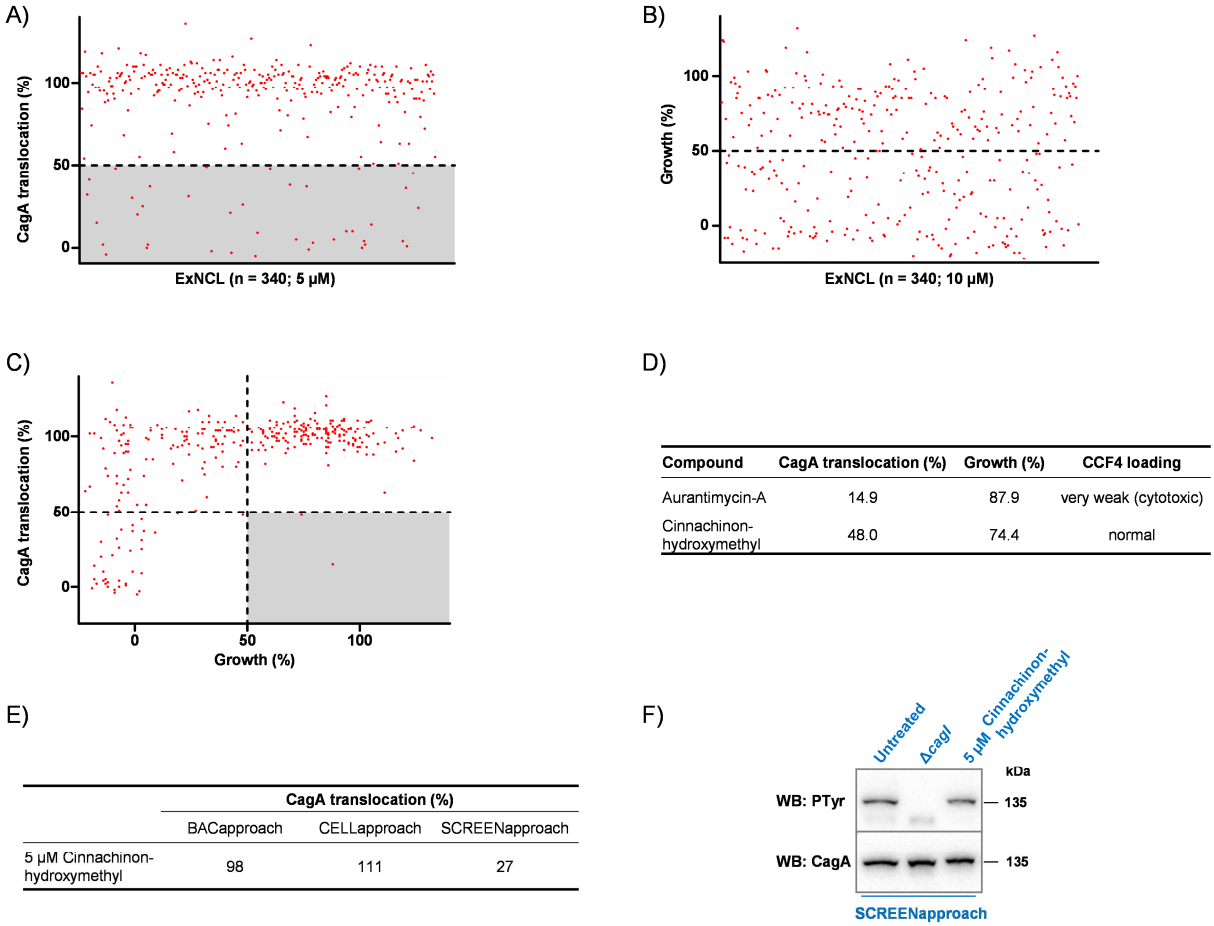

Compound	CagA translocation (%)	Growth (%)	CCF4 loading
Aurantimycin-A	14.9	87.9	very weak (cytotoxic)
Cinnachinon-hydroxymethyl	48.0	74.4	normal

	CagA translocation (%)		
	BACapproach	CELLapproach	SCREENapproach
5 µM Cinnachinon-hydroxymethyl	98	111	27

Figure 30: Summary of ExNCL library screening
A) Screening for CagA translocation inhibition using the TEM-CagA reporter assay. Each dot represents the effect of a compound on translocation at 5 µM.
B) Screening for *H. pylori* growth inhibition via growth curve analysis. Each dot represents the effect of a compound on growth at 10 µM.
C) Plot summarizing CagA translocation versus growth inhibition for every compound, represented by a red dot.
D) Overview of compounds exhibiting a translocation rate lower than 50% and a growth rate higher than 50%. CCF4 loading refers to green fluorescence signals recorded in the TEM-CagA assay, and low values indicate eukaryotic cytotoxicity.
E) Confirmation of the effect of cinnachinon-hydroxymethyl on CagA translocation. Translocation was quantified using the TEM-CagA assay according to the protocol layouts described in Figure 28. Values are derived from two independent measurements.
F) Immunoblot analysis of infected AGS cells with phosphotyrosine (4G10) and CagA (AK257) antibodies. Cells were infected with P12 wild-type in the presence of cinnachinon-hydroxymethyl following the protocol layout described in E), and analyzed via Western blot (WB).

However, only two compounds, namely aurantimycin-A and cinnachinon-hydroxymethyl, displayed CagA translocation rates below 50% and growth rates above 50% (summarized in

Figure 30D). Of these, aurantimycin-A exhibited the best inhibitory profile (CagA translocation: 15%, growth: 88%). Unfortunately, raw data of the TEM-CagA translocation assay revealed only weak loading of AGS cells with the CCF4 substrate (expressed as green fluorescence value, data not shown), which indicates a strong cytotoxic effect on the cells. In fact, aurantimycin-A was described to be cytotoxic [206], and was thus excluded as a promising hit candidate for specific translocation inhibition. Cinnachinon-hydroxymethyl did not show an abnormal CCF4 loading, but its inhibitory capability on translocation was weak (48% translocation), and the compound was also slightly active against *H. pylori* (74% growth). However, the compound was investigated in follow-up studies and the TEM-CagA assay was repeated following the protocol layouts described in Figure 28. Corresponding percental CagA translocation rates are presented in Figure 30E. An inhibition of translocation could be reproduced when cinnachinon-hydroxymethyl was present during infection (27% translocation in SCREENapproach), but not applying the BAC- or CELLapproach, excluding an antibacterial or cytotoxic effect of the substance. The observed effect in the SCREENapproach was confirmed with the orthogonal CagA tyrosine phosphorylation assay, and the corresponding immunoblot is depicted in Figure 30F. Unfortunately, no decrease of phosphorylation in the presence of cinnachinon-hydroxymethyl could be detected, which suggested that the compound exhibits an inhibitory effect on the TEM-CagA assay. Hence, the substance was excluded as a specific translocation inhibitor candidate.

3.4 Screening of the LOPAC library

Next, the LOPAC library (Sigma-Aldrich) was screened. This library comprised 1267 pharmacologically active compounds including various drug-like molecules from the fields of neuroscience and cell signaling, as summarized in Figure 31A.

Screening for TEM-CagA translocation inhibition at 50 µM compound concentration revealed 151 substances that were able to block translocation by more than 50% (see Figure 31B). Within a subsequent growth counter-screen, even more compounds (n = 422) were identified to lower *H. pylori* growth below 50% (see Figure 31C), which might be due to the higher compound concentration of 100 µM. Remarkably, 290 of these substances completely blocked *H. pylori* growth. However, neither for translocation nor for growth inhibitors, a clear action spectrum of the different drug classes could be deduced. For a better overview, the influence of every compound on translocation was compared to its impact on growth (see Figure 31D). More than 65% of all compounds (n = 835, >50% for both parameters) did not exhibit an influence on translocation or growth. 141 compounds were able to reduce

translocation (<50%), but inhibited bacterial growth at the same time (Figure 31D). Thus, for these substances an unspecific effect on translocation due to antibacterial activity was concluded. In total, ten substances yielded translocation rates below 50% and percental growth above 50%; they are listed together with their mode of action and indication in Figure 31E. Among these hits, related compounds were identified, such as LLH-1 and LLH-2, as well as cantharadin and its corresponding acid.

A)

Application	%
Neurotransmission	58
Phosphorylation	8
Cell Stress	4
Lipids	4
Ion Channels	6
G Protein	3
Gene Regulation	3
Hormones	3
Apoptosis/Cell Cycle	2
Others (cell signaling)	9

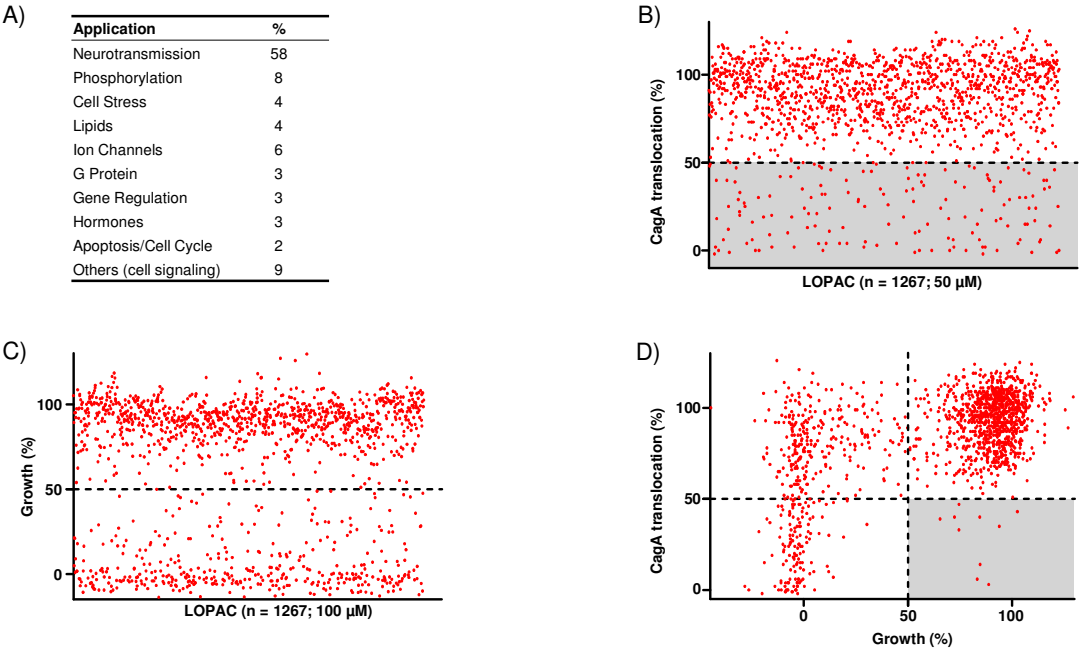

E)

Compound	CagA translocation (%)	Growth (%)	CCF4 loading	Mode of action	Indication
LLH-1	13.7	84.9	ok		
LLH-2	3.4	88.8	ok		
Cantharidic acid	40.1	84.7	slightly reduced	phosphatase inhibitor	
Cantharidin	32.7	74.6	slightly reduced	phosphatase inhibitor	skin lesions; aphrodisiac (but highly toxic)
Dihydroergocristine methanesulfonate	39.7	72.5	ok	agonist at dopaminergic and adrenergic receptors; antagonist at serotonergic receptors	dementia
Iodoacetamide	47.3 (inconsistent)	74.7	ok	alkylating agent	
Methysergide maleate	5.7	83.3	ok	serotonin receptor antagonist	migraine (strong side effects)
NF449 octasodium salt	42.9	102.7	ok	G protein antagonist	
Propantheline bromide	38.7	65.6	ok	blocking of acetylcholine	hyperhidrosis; cramps or spasms of the intestinal tract
Wortmannin	35.1	94	ok	phosphatidylinositol 3-kinase inhibitor	none, high liver toxicity

Figure 31: Summary of LOPAC library screening
A) Drug targets of compounds in the LOPAC library. Classification according to Sigma-Aldrich LOPAC®1280 database.
B) Screening for CagA translocation inhibition using the TEM-CagA reporter assay. Each dot represents the effect of a compound on translocation at 50 µM.
C) Screening for *H. pylori* growth inhibition via growth curve analysis. Each dot represents the effect of a compound on growth at 100 µM.
D) Plot summarizing CagA translocation versus growth inhibition for every compound, represented by a red dot.
E) Overview of compounds exhibiting a translocation rate lower than 50% and a growth rate higher than 50%. CCF4 loading refers to the green fluorescence signals recorded in the TEM-CagA assay, and low values indicate eukaryotic cytotoxicity. Mode of actions and indications are also summarized.

To confirm and extend the results of the screenings, the TEM-CagA assay was repeated with these ten substances following the protocol layouts described in Figure 28. Corresponding percental CagA translocation rates are summarized in Figure 32A. Unfortunately, the inhibitory activities of dihydroergocristine methanesulfonate, methysergide maleate, NF449 octasodium salt and propantheline bromide could not be reproduced with the same suppressive potential that was observed in the initial screening; so these compounds were excluded from further experimentations. In addition, cantharidin and cantharidic acid revealed a high cytotoxic effect in the CELL- and SCREENapproaches (Figure 32A), as assessed by deficient CCF4 loading. This was also observed in the screening (see Figure 31E), and might be the reason for the discovered inhibition. Also wortmannin caused a reduced CCF4 loading when added to cells, and was thus omitted from future studies. A complete translocation blockage was discovered for iodoacetamide employing the BACapproach and an inhibition of approximately 50% when present during infection (SCREENapproach), which is in accordance with the screening results. In addition, a strong translocation inhibition was reproduced for the related compounds LLH-1 and LLH-2, but only when present during infection (33% and 8% translocation at 35 µM, SCREENapproach), indicating neither an antibacterial nor a cytotoxic effect of the substances.

To independently prove the results of the TEM-CagA assay for iodoacetamide, LLH-1 and LLH-2, the alternative CagA tyrosine phosphorylation assay was performed; corresponding immunoblots are shown in Figure 32B. For iodoacetamide, the strong effect observed in the BACapproach could not be shown by CagA phosphorylation analysis (left blots, Figure 32B), suggesting that the compound might interfere with the TEM-CagA assay. Anyway, iodoacetamide would not have any potential for therapeutic application due to its rather unspecific alkylating activity. In contrast, LLH-1 reduced CagA phosphorylation drastically, and LLH-2 even completely abolished phosphorylation applying the SCREENapproach (right blots, Figure 32B), which confirmed the results of the TEM-CagA assay. Analysis of respective co-culture supernatants revealed a substantial decrease of IL-8 secretion upon LLH-1 and LLH-2 treatment (80% and 50% IL-8 induction, respectively; see Figure 32C), and corresponded to the strength of the translocation decline. Even so, the induction of a basal IL-8 secretion verified a functional Cag-T4SS despite the impaired CagA translocation ability. To further exclude an antibacterial effect on *H. pylori*, growth curves were performed in the presence of LLH-1 and LLH-2 (see Figure 32D). As in the primary growth screening, no adverse effects on *H. pylori* growth could be observed.

Taken together, the related LLH-1 and LLH-2 compounds seem to specifically inhibit CagA

translocation, which was proven by the TEM-CagA as well as the tyrosine phosphorylation assay. Of importance, the substances do not exhibit an anti-*H. pylori* effect, as was demonstrated via BACapproach testing and growth analysis. Thus, LLH-1 and LLH-2 constitute promising lead substances for specific CagA translocation inhibition and should be investigated in future studies.

A)

Compound	CagA translocation (%)					
	BACapproach		CELLapproach		SCREENapproach	
	35 µM	50 µM	35 µM	50 µM	35 µM	50 µM
LLH-1	131	87	99	105	33	59
LLH-2	105	88	100	114	8	0
Cantharidic acid	76	*n.d.*	no CCF4 loading	*n.d.*	no CCF4 loading	*n.d.*
Cantharidin	109	*n.d.*	no CCF4 loading	*n.d.*	no CCF4 loading	*n.d.*
Dihydroergocristine methanesulfonate	70	*n.d.*	89	*n.d.*	80	80
Iodoacetamide	0	*n.d.*	101	*n.d.*	49	*n.d.*
Methysergide maleate	124	*n.d.*	87	*n.d.*	90	57
NF449 octasodium salt	82	*n.d.*	79	*n.d.*	103	75
Propantheline bromide	82	*n.d.*	86	*n.d.*	84	84
Wortmannin	102	*n.d.*	49 (low CCF4 loading)	*n.d.*	63 (low CCF4 loading)	*n.d.*

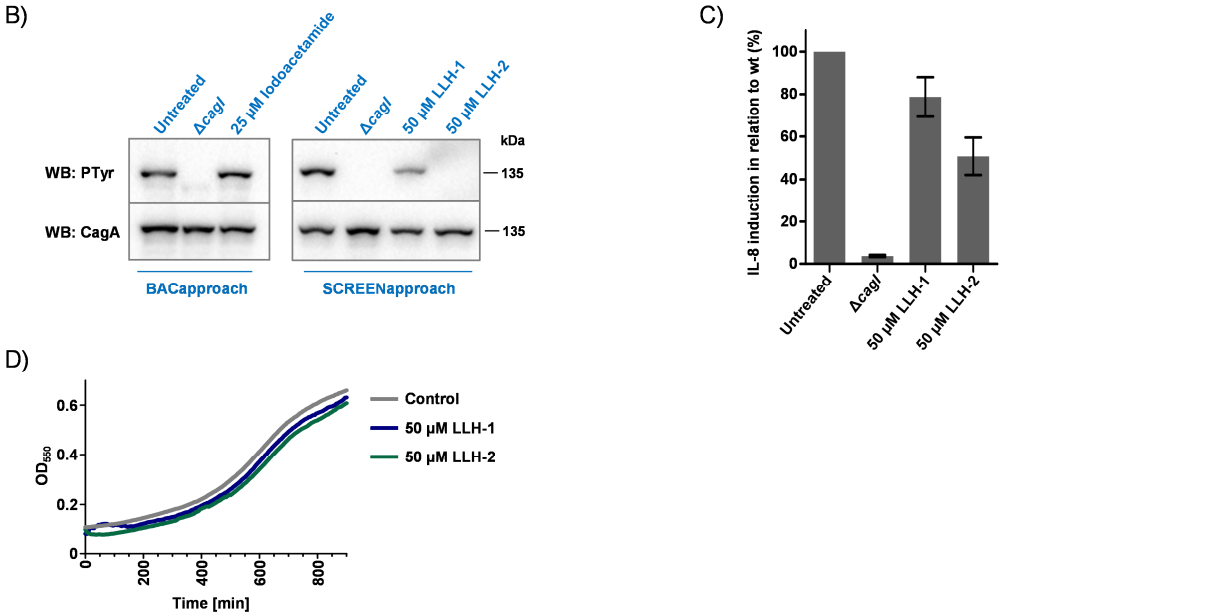

Figure 32: Confirmation of LOPAC screening results

A) Confirmation of LOPAC hits. Translocation was quantified using the TEM-CagA assay according to the protocol layouts described in Figure 28. Compound concentrations are indicated, and values are derived from maximally two measurements. CCF4 loading refers to the green fluorescence signals recorded in the TEM-CagA assay, and low values indicate eukaryotic cytotoxicity.

B) Immunoblot analysis of infected AGS cells with phosphotyrosine (4G10) and CagA (AK257) antibodies. Cells were infected with P12 wild-type in the presence of the indicated compounds following protocol layouts like in A), and analyzed via Western blot (WB).

C) Analysis of co-culture supernatants derived from B) for IL-8 secretion via sandwich ELISA. All values were normalized to the IL-8 values found in the supernatants of infected but untreated cells, and are indicated as mean values with standard error of the mean from two independent infections.

D) Growth analysis of *H. pylori* in the presence of LLH-1 and LLH-2. OD_{550} was recorded every 5 min for at least 16 h and experiments were independently repeated two times. The figure depicts a representative growth curve.

3.5 Screening of the NCL library

3.5.1 Screening with the TEM-CagA translocation assay

Next, another natural compound library (NCL; from Helmholtz Centre for Infection Research, Braunschweig) was screened for CagA translocation inhibition. This library comprised 259 purified myxobacterial compounds, that are known for their unique structures as well as numerous described bioactivities in the nanomolar range [207]. Hence, only a low concentration of 4 µM was employed in the screening. Figure 33A gives an overview of the influence of every single compound on translocation.

A)

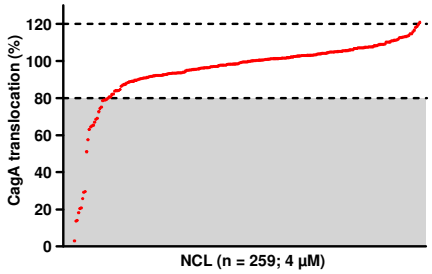

B)

Compound	CagA translocation (%)	Activity spectrum	Mode of action
NCL-1a	13.7	antifungal, cytotoxic	Eukaryotic respiratory chain inhibitor
NCL-1b	20.7		
Aurachin A	18.3	antibacterial, antifungal, cytotoxic	Known antibacterial & respiratory chain inhibitor
Aurachin B	78.9		
Aurachin C	25.8		
Aurachin variant	14.0		
Chondramide A	83.8	antifungal, cytotoxic	Eukaryotic cell modulator (inhibits actin polymerisation)
Chondramide B	67.0		
Chondramide D	51.1		
Chondramide F	68.6		
Cruentaren A	2.9	cytotoxic	Eukaryotic respiratory chain inhibitor (inhibits F-ATPase)
Elansolid A2	72.6	antibacterial	Known antibacterial
Icumazole A	20.4	antifungal	Eukaryotic respiratory chain inhibitor
Myxalamid PI	79.9	antibacterial, antifungal, cytotoxic	Known antibacterial & respiratory chain inhibitor
Myxovalargin A	69.1	antibacterial	Known antibacterial (inhibits protein synthesis)
Myxovalargin B	57.5		
Myxovalargin C	65.0		
Pellasoren A	63.0	antifungal, cytotoxic	
Thiangazole A	29.3	antifungal, cytotoxic	Eukaryotic respiratory chain inhibitor
Thiangazole B	29.6		
Tubulysin A	64.4	cytotoxic	Eukaryotic cell modulator (inhibits tubulin polymerisation)
Tubulysin B	78.9		
Tubulysin G	65.3		

Figure 33: Summary of NCL library screening
A) Screening for CagA translocation inhibition using the TEM-CagA assay. Each dot represents the effect of a compound on translocation at 4 µM.
B) Overview of compound hits exhibiting a translocation rate lower than 80% as well as chondramide A. In addition, a summary of activity spectra and modes of action is indicated. See text for further information.

In total, 9 compounds were able to inhibit translocation by more than 50%. All compounds with translocation rates below 80% are listed in Figure 33B. Of importance, most of the substances that influenced translocation belonged to the same compound class. Thereby, the

detected natural compounds could be classified into three groups: eukaryotic cellular modulators, known antibacterials, and exclusively eukaryotic respiratory chain inhibitors. The compounds targeting cellular structures comprised four variants of chondramides, known for their ability to inhibit the actin cytoskeleton [208] as well as for a cytostatic and antifungal activity [209], and three representatives of tubulysins, named after their property to inhibit tubulin polymerization [210]. Among the known antibacterials, there were three myxovalargins that exhibit a general antibiotic effect against gram-positive bacteria and at high concentrations also against gram-negatives [211] due to inhibition of protein synthesis and membrane disruption [212]. In addition, a derivative of the antibacterial elansolid was detected, although this compound has so far only been described to be active against gram-positive bacteria [213]. Moreover, four variants of aurachins and myxalamid PI were discovered. Both classes have been reported to be active against gram-positive bacteria, yeast and molds [214, 215], as well as to inhibit the eukaryotic respiratory chain [216], whereas aurachins were also shown to inhibit the *E. coli* respiratory chain. The last group comprised described antifungal and/or cytotoxic substances, namely NCL-1a/b, cruentaren A [217, 218], icumazole A [219], two thiangazoles [220] and pellasoren A [221]. Except for the unknown bioactivity of the latter, all of these compounds were reported to inhibit eukaryotic respiration. Above all, these compounds exhibited higher inhibitory potential on translocation than the other two groups. Follow-up studies investigated the interaction of *H. pylori* with representative compounds of all three groups and are described in the following chapter.

3.5.2 Follow-up studies

To determine whether the substances interact with *H. pylori*, the cells or both components, TEM-CagA translocation analysis was performed using the protocol layouts described in Figure 28 (BAC-, CELL- and SCREENapproach). As representatives for eukaryotic cellular modulators, the substances with the highest inhibitory capabilities, chondramide D and tubulysin A, were analyzed (see Figure 34A&B). Effects on translocation in the SCREENapproach (equal to screening conditions) could reproduce the results of the screening, albeit relatively weak for tubulysin A. No inhibition was observed using the BACapproach, but strong effects (only ~30% translocation) were detectable applying the CELLapproach, suggesting that translocation reduction relied on modification of the AGS cell cytoskeleton. Moreover, these results were confirmed via tyrosine phosphorylation assays (data not shown). As the actin polymerization inhibitory activity of chondramides has been described to be comparable to cytochalasin D [208], and tubulysins target the same structure

as nocodazole [210], the observed effects are in accordance with the results already described in Chapter 2.6.1. Nevertheless, to validate the BACapproach, growth analysis in the presence of chondramide D and tubulysin A was conducted (see Figure 34C&D) and no anti-*H. pylori* effect was observed, as expected.

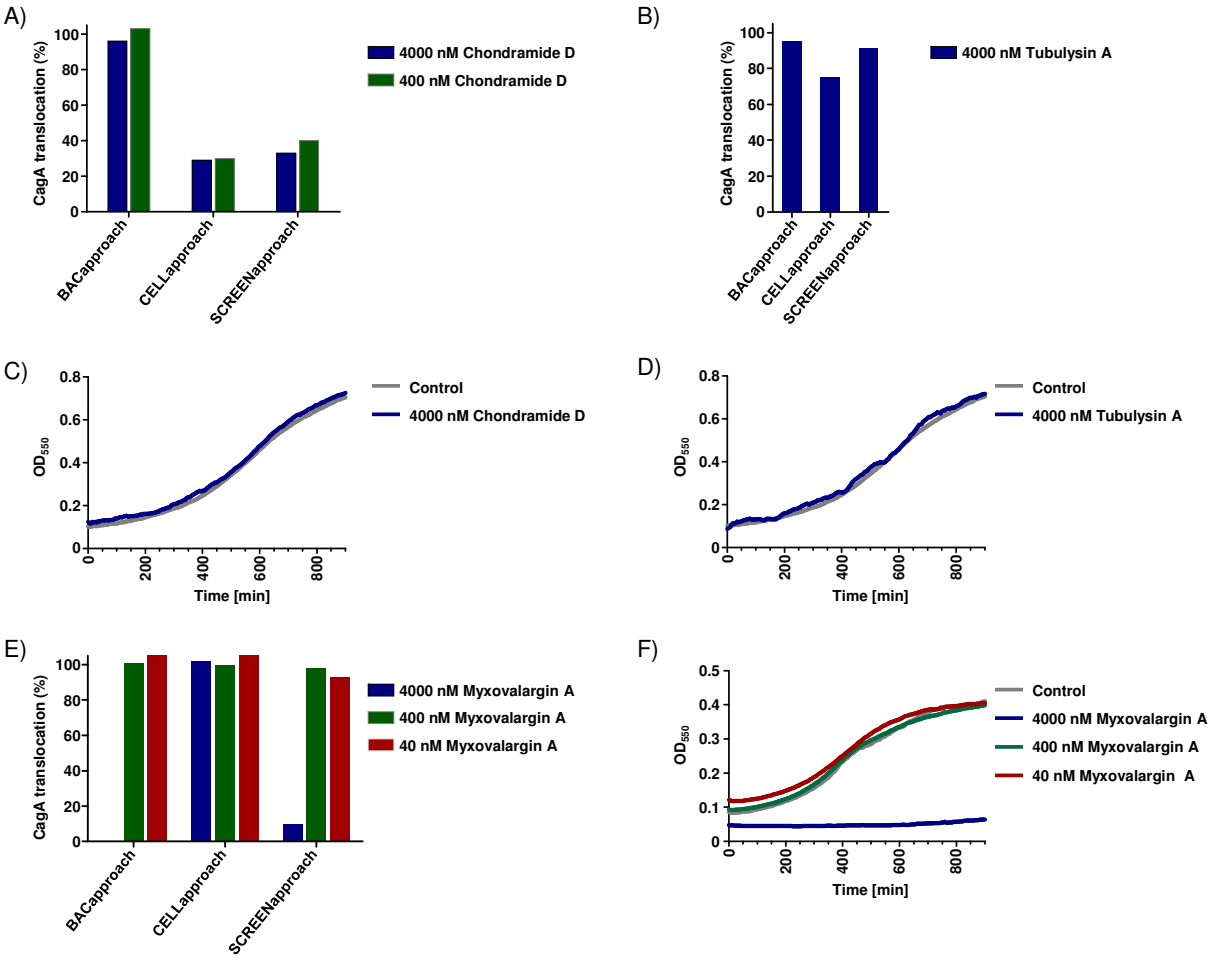

Figure 34: Follow-up studies of cell modulatory and antibacterial NCL hit compounds
A) Quantification of TEM-CagA translocation by plate reading in the presence of chondramide D. AGS cells were infected with P12[TEM-CagA] according to the protocol layouts described in Figure 28. The average blue-to-green ratios were normalized to the mean ratio of untreated P12[TEM-CagA]-infected cells.
B) Quantification of TEM-CagA translocation by plate reading in the presence of tubulysin A. Experiments were performed as described in A).
C) Growth analysis of *H. pylori* in the presence of chondramide D. OD_{550} was recorded every 5 min for at least 16 h and experiments were independently repeated at least 3 times. The figure depicts a representative growth curve.
D) Growth analysis of *H. pylori* in the presence of tubulysin A. Experiments were performed as described in C).
E) Quantification of TEM-CagA translocation rates by plate reading in the presence of myxovalargin A. Experiments were performed as described in A).
F) Growth analysis of *H. pylori* in the presence of myxovalargin A. Experiments were performed as described in C).

As a representative for the known antibacterials detected within the screening, myxovalargin A was further examined (see Figure 34E&F). TEM-CagA translocation analysis revealed a complete inhibition in the BACapproach at 4 µM and a very strong

influence (~10% translocation) in the SCREENapproach. No effect was observed for the CELLapproach (Figure 34E), indicating an antibacterial effect of the compound against *H. pylori*. To verify this, *H. pylori* growth was monitored in the presence of myxovalargin A and similar to the CagA inhibition, a growth deficiency was detected at 4 µM (Figure 34F). In line with this, myxovalargins were reported to act at high concentrations against gram-negative bacteria [211]. Similar observations were made for myxalamid PI and also concluded for elansolid A2, so that these substances were excluded to be useful as specific type IV secretion inhibitors.

As the antibacterial aurachins showed a very strong influence on translocation and were reported to inhibit the bacterial as well as the eukaryotic respiratory chain, these substances were tested together with the other respiration inhibitors detected in the screening. Results are summarized in Figure 35A. Following the protocol layouts explained in Figure 28, concentrations needed for 50% translocation inhibition (IC_{50}) were determined by non-linear regression analysis, and the titration of icumazole A is depicted in Figure 35B as example. For the BAC- and SCREENapproaches, IC_{50} values were constantly lower than IC_{50} values of the CELLapproach, indicating strong effects on *H. pylori*, although effects on cells could not be excluded due to the known cytotoxic properties of the compounds. Importantly, IC_{50} values were in the nanomolar range, revealing a very high potential of the substances. Nevertheless, growth analysis of *H. pylori* P12 in the presence of these compounds exhibited remarkable anti-*H. pylori* effects. These observations lead to the conclusion that effects on CagA translocation were possibly caused by an antibacterial action on *H. pylori* instead of a specific type IV secretion system inhibition. However, the compounds seemed to be very interesting for further studies because of their rather undescribed antibacterial activities (except very weak ones against gram-positive bacteria reported for NCL-1a, aurachins [215] and cruentaren A [218]). Thus, MICs (minimal inhibitory concentrations) and IC_{50} values regarding *H. pylori* growth inhibition were determined (see Figure 35A), and again yielded very low effective concentrations in the nanomolar range. To rule out any strain-specific effects, *H. pylori* B8 and TIGR were additionally tested, and similar inhibitory potentials were detected (see Figure 35C with pellasoren A as example). For examination of a general antibacterial effect, three further bacterial species were cultured in the presence of the natural compounds: *C. jejuni* as the closest relative of *H. pylori*, *E. coli* as a further representative for gram-negative bacteria, and *S. aureus* as a representative for gram-positive bacteria (see Figure 35A&C with aurachin A as example). No antibacterial effect was observed for NCL-1a, pellasoren A as well as thiangazoles, and small effects were detected for *C. jejuni* and

S. aureus in the presence of aurachins, cruentaren A and icumazole A. However, these effects were only obtained applying 4 µM compound concentration and solely delayed growth. In contrast, 4 µM substances were by far sufficient to completely suppress growth of *H. pylori*.

A)

Compound	IC_{50} CagA translocation (nM)			Growth inhibiton of *H. pylori* P12 (nM)		Effect on growth (at 4000 nM)		
	BACapproach	CELLapproach	SCREENapproach	MIC	IC_{50}	*C. jejuni*	*E. coli*	*S. aureus*
NCL-1a	46	>4000	86	3.9	1.5	no	no	no
Aurachin A	72	1469	94	125	25.7	yes	no	weak
Aurachin B	512	>4000	893	1000	160.2	no	no	yes
Aurachin C	169	>4000	91	62.5	14.15	no	no	yes
Cruentaren A	27	>4000	144	31.25	5.0	yes	no	weak
Icumazole A	23	175	22	62.5	10.4	yes	no	weak
Pellasoren A	16	1874	76	125	40.33	no	no	no
Thiangazole A	37	183	8	15.6	4.2	no	no	no
Thiangazole B	6	247	6	7.8	2.4	no	no	no

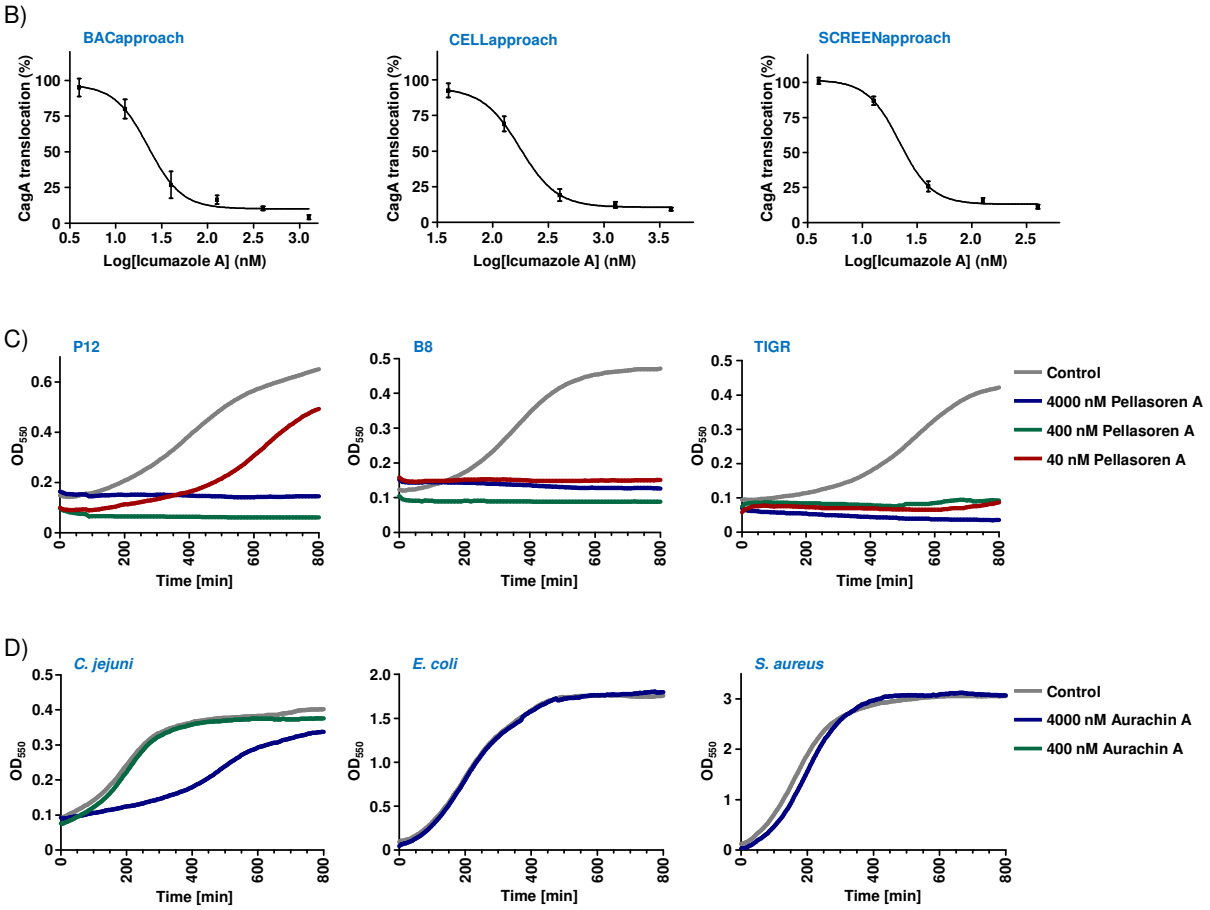

Figure 35: Follow-up studies of respiration-inhibitory NCL hit compounds

A) Table summarizing the influence of the indicated compounds on CagA translocation and bacterial growth. Translocation was quantified using the TEM-CagA assay according to the protocol layouts described in Figure 28. Values depict mean IC_{50} values (concentration for 50% inhibition) of CagA translocation (nM) from at least four independent experiments, calculated by non-linear regression analysis. MIC (minimal inhibitory concentrations) and IC_{50} of growth (nM) were determined analyzing growth curves of *H. pylori* P12, and calculations were based on at least five independent experiments. Effects on *C. jejuni*, *E. coli* and *S. aureus* were monitored via growth curves in the presence of 4000 nM. Observations were based on at least three independent experiments.

B) IC_{50} CagA translocation titration curves of icumazole A as example.

C) Growth curves of *H. pylori* strains P12, B8 and TIGR in the presence of pellasoren A as example.

D) Growth curves of *C. jejuni*, *E. coli* and *S. aureus* in the presence of aurachin A as example.

Taken together, the screening of the NCL library did not reveal promising candidates for specific type IV secretion system inhibition. However, interesting compounds were discovered that seem to be highly effective against *H. pylori*, but not against other bacteria. As these small molecules have been reported to mainly inhibit respiration, an effect on the *H. pylori* respiratory chain was assumed as well, as will be investigated in more detail in Chapter 4.

3.6 Screening of SPECS libraries

3.6.1 Screening with the TEM-CagA translocation assay

Hitherto, natural compounds and commercially available pharmaceuticals were examined. In addition, also a library from the company SPECS, comprising 2240 uncharacterized chemically synthesized small molecules, was screened for CagA translocation inhibition. The library is split into two sub-libraries: SPECS-selected (n = 1120) and SPECS-random (n = 1120) (see Figure 36A). The SPECS-selected library contained exclusively substances with chemical structures (e.g. regarding hydrophobicity) considered to be more prone to enter gram-negative bacteria. Thus, the probability to detect biological activities in *H. pylori* should be enhanced. In contrast, SPECS-random comprised randomly selected substances from the company library. Both libraries were screened at a concentration of 35 µM using the TEM-CagA translocation assay. Screening results of the SPECS-selected library are summarized in Figure 36B and those of the SPECS-random library in Figure 36C. Surprisingly, the SPECS-selected library revealed two compounds that were able to suppress CagA translocation below 50%, whereas the SPECS-random library comprised ten substances with a translocation inhibition of more than 50%. The single hits are listed in Figure 36D and were numbered successively SLH1 to SLH12, where SLH1 and SLH2 were derived from the SPECS-selected and SLH3-12 from the random library. Of these, SLH2 turned out to be a false-positive hit in follow-up studies (data not shown), and SLH5 exhibited virtually no loading with CCF4, indicating a cytotoxic activity of this small molecule against AGS cells which might be the reason for the reduced CagA translocation. In conclusion, the design of the SPECS-selected library failed with regard to its hit rate, as the control library with randomly selected compounds clearly revealed a higher rate (1 versus 9 compounds).

It should be noted that the compounds of the first two plates of the SPECS-random library displayed a wide scattering of translocation efficiencies (see Figure 36C). These barely convincing results are derived from the plates already mentioned in Chapter 3.2 (Figure 29C),

that exhibited low Z´-factors (~0.2). Considering this, some potential hit compounds might not have been detected during the screening of these two plates.

As a next step, SPECS hit compounds (except SLH2 and SLH5) were investigated in follow-up studies, and are described in the following chapter.

A)

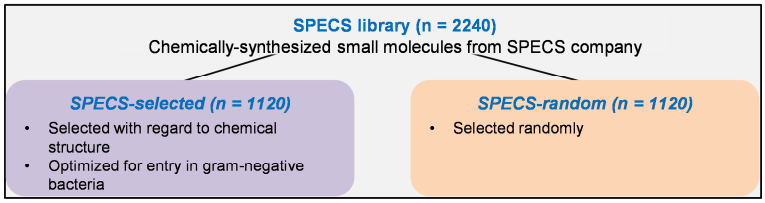

B)

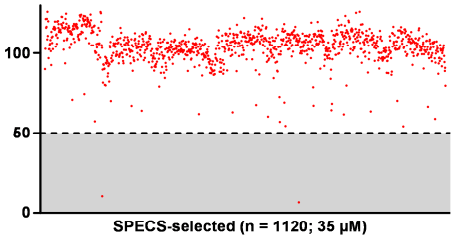

C)

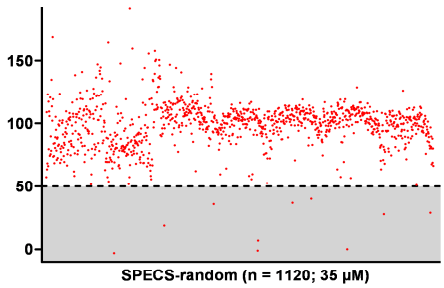

D)

Compound	Chemical name	CagA translocation (%)	Comment
SLH1	N-{3-[4-(2-furoyl)-1-piperazinyl]-1,4-dioxo-1,4-dihydro-2-naphthalenyl}acetamide	6.7	
SLH2	1-allyl-2-{4-[(methoxyacetyl)amino]phenyl}imidazo[1,2-a]pyridin-1-ium	10.5	*false-positive*
SLH3	1-methyl-3-phenylpyrazino[1,2-a]benzimidazole	28.8	
SLH4	N,N-dibenzyl-N-(5-phenyl[1,2,4]triazolo[1,5-a]pyrimidin-7-yl)amine	27.7	
SLH5	6-amino-3-tert-butyl-4-[2-(trifluoromethyl)phenyl]-1,4-dihydropyrano[2,3-c]pyrazole-5-carbonitrile	0	*cytotoxic*
SLH6		40	
SLH7	4-(4-fluorophenyl)-N-[4-(trifluoromethoxy)phenyl]-1-piperazinecarboxamide	36.7	
SLH8		7	
SLH9	2-(2,4-dichlorophenoxy)-5-nitro-1,3-thiazole	-1.1	
SLH10	3-[(1H-benzimidazol-2-ylmethyl)sulfanyl]propyl phenyl ether	35.8	
SLH11	3-(2-methyl-1,3-dithiolan-2-yl)-1H-indole	18.8	
SLH12	N-[4-({5-nitro-1,3-thiazol-2-yl}oxy)phenyl]acetamide	-3	

Figure 36: Summary of SPECS library screenings
A) Overview of the SPECS-selected and the SPECS-random library.
B) Screening of the SPECS-selected library for CagA translocation inhibition using the TEM-CagA assay. Each dot represents the effect of a compound on translocation at 35 µM.
C) Screening of the SPECS-random library for CagA translocation inhibition using the TEM-CagA reporter assay. Each dot represents the effect of a compound on translocation at 35 µM.
D) Overview of compound hits exhibiting a translocation rate below 50%. SLH1 and SLH2 were derived from SPECS-selected and SLH3 – 12 from SPECS-random.

3.6.2 Follow-up studies

A summary of SPECS follow-up studies is presented in Figure 37. All values presented with an approximately sign (~) refer to estimations from three independent measurements due to limitations in compound availability, while all other values were determined following statistical standards. At first, to evaluate the impact of the SPECS compounds on bacteria, cells or both, the TEM-CagA translocation assay was applied following different protocol

layouts described in Figure 28, and IC_{50} values were determined by non-linear regression analysis (summarized in Figure 37). All substances showed lower IC_{50} values for the BACapproach than for the SCREENapproach, while no effect in the CELLapproach was observed at 35 µM (except for SLH4), suggesting that the substances specifically target the bacteria. Growth analysis of *H. pylori* in the presence of SPECS substances showed clear anti-*H. pylori* effects (presented as MIC and IC_{50} values, Figure 37) that correlated with the observed translocation inhibition. In conclusion, no specific CagA translocation inhibition could be inferred. But encouraged by the specific anti-*H. pylori* effects of the NCL hit compounds (Chapter 3.5.2), the effect of SPECS substances on *C. jejuni*, *E. coli* and *S. aureus* was examined at 35 µM. Only SLH12 showed an activity against all three bacteria. Indeed, SLH4, 6, 8, 10 and 11 did not exhibit general antibacterial activities, and only weak effects were observed for SLH1, 3, 7 and 8, suggesting a specific action of some SPECS compounds against *H. pylori*.

In summary, no specific type IV translocation inhibitor was identified, as all compounds displayed clear anti-*H. pylori* effects. Nevertheless, as for the NCL library, most of the substances seemed to have a higher effectivity against *H. pylori* than against other bacteria. For various NCL library hits, a bioactivity as respiratory chain inhibitor was reported (described in Chapter 3.5). Following this, it was hypothesized that the rather undescribed SPECS substances might also target the *H. pylori* respiratory chain. Hence, the SPECS hits together with promising NCL respiratory chain inhibitors were investigated in individual follow-up studies presented in the following section.

Compound	IC_{50} CagA translocation (µM)			Growth inhibiton of *H. pylori* P12 (µM)		Effect on growth (at 35 µM)		
	BACapproach	CELLapproach	SCREENapproach	MIC	IC_{50}	*C. jejuni*	*E. coli*	*S. aureus*
SLH1	~ 0.98	>35	~ 1.4	0.35 – 3.5	*n.d.*	very weak	no	no
SLH3	~ 2.9	>35	~ 8.2	3.5 - 35	*n.d.*	very weak	no	no
SLH4	0.069	~35	0.46	0.5	0.15	no	no	no
SLH6	0.43	>35	5.6	16	3.7	no	no	no
SLH7	~ 1.7	>35	~ 6.6	0.35 – 3.5	*n.d.*	no	no	weak
SLH8	0.21	>35	1.2	1	0.25	no	no	no
SLH9	~ 0.69	>35	~ 0.97	3.5 - 35	*n.d.*	no	no	yes
SLH10	~ 4.7	>35	~ 30	3.5 - 35	*n.d.*	no	no	no
SLH11	~ 35	>35	>35	~35	*n.d.*	no	no	no
SLH12	~ 0.43	>35	~ 1.3	3.5 - 35	*n.d.*	yes	weak	yes

Figure 37: Follow-up studies of SPECS library hits
Summary of the influence of the indicated compounds on CagA translocation and bacterial growth. Translocation was quantified using the TEM-CagA assay according to the protocol layouts described in Figure 28. Values indicate mean IC_{50} values (concentration for 50% inhibition) of CagA translocation (nM) from at least four independent experiments, calculated by non-linear regression analysis. MIC (minimal inhibitory concentrations) and IC_{50} of growth (nM) were determined analyzing growth curves of *H. pylori* P12, and calculations were based on at least five independent experiments. Values presented with an approximately sign (~) are estimations from three independent experiments. Effects on *C. jejuni*, *E. coli* and *S. aureus* were monitored via growth curves in the presence of 35 µM of the respective compound. Observations were based on at least three independent experiments.

4. Characterization of novel respiratory chain inhibitors in *H. pylori*

Screenings of the NCL (Chapter 3.5) and SPECS libraries (Chapter 3.6) for specific type IV secretion system inhibitors revealed a set of small molecules that exhibited strong antibacterial effects against *H. pylori*, but not against other bacteria. Concerning the NCL hits, these observations are also confirmed by previous studies, where the compounds were not recognized as antibacterials, but as highly effective eukaryotic respiratory chain inhibitors, especially NCL-1a, cruentaren A [217, 218], icumazole A [219] and thiangazoles [220]. None of these studies tested effects on *H. pylori*. Hence, it was suspected that these substances might also target respiration of *H. pylori*. This hypothesis was also extended to the rather uncharacterized chemically synthesized SPECS substances. Following this, several efforts were made to demonstrate the action of the NCL and SPECS compounds on *H. pylori* respiration, which are described in the following chapters.

4.1 Comparison of NCL and SPECS hits with known inhibitors

Despite recent efforts [222], the respiratory chain of *H. pylori* has not been fully characterized, which hampers investigations to identify individual proteins as antibacterial targets. As a first step, more familiar respiratory chain inhibitors, namely antimycin A and rotenone, were examined. Both compounds were reported to inhibit *H. pylori* respiration [223-225], but as the NCL hits, antimycin A as well as rotenone are more prominent as eukaryotic respiratory chain inhibitors, targeting complex III (cytochrome bc_1 complex) and complex I (NADH-ubiquinone oxidoreductase), respectively. Thus, as for the NCL and SPECS hits, IC_{50} of CagA translocation, *H. pylori* growth inhibition (MIC and IC_{50}) as well as the effect on other bacterial species was determined for antimycin A and rotenone (summarized in Figure 38). As for the NCL and SPECS hits, effects on CagA translocation were highest in the BAC- and SCREENapproach, and *H. pylori* growth was completely inhibited at relatively low concentrations (8 µM and 0.5 µM, respectively). In contrast, no effects were observed for other bacteria even at concentrations as high as 50 µM (see Figure 38). Overall, the magnitude of antimycin A effects was similar to that of SLH6, while rotenone was more potent and comparable to effects of SLH4 (see Figure 37).

The main purpose of the respiratory chain is the generation of a proton motive force (PMF) that drives the production of ATP (oxidative phosphorylation). Thereby, the PMF can be independently destroyed by ionophores. To take also into account that NCL and SPECS hits

might act as ionophores and not as specific respiratory chain inhibitors, effects of the known ionophore CCCP on CagA translocation and bacterial growth were analyzed for comparison. Indeed, treatment of *H. pylori* with CCCP resulted in similar patterns regarding CagA translocation and growth inhibition as for the known respiratory chain inhibitors or NCL and SPECS hits (e.g. MIC of 2 µM, Figure 38). In contrast to these substances, however, also growth of *C. jejuni*, *S. aureus* and *E. coli* was completely inhibited or strongly affected at CCCP concentrations that were effective against *H. pylori*. Since the known respiratory inhibitors as well as NCL and SPECS hits displayed a high specificity towards *H. pylori*, an action as ionophores seemed very unlikely for these compounds.

Taken together, inhibitory profiles of known *H. pylori* respiration inhibitors exhibited similar profiles to NCL and SPECS hits by means of translocation inhibition and antibacterial effects, while this was not the case for the rather unspecifically acting ionophore CCCP.

Compound	IC_{50} CagA translocation (µM)			Growth inhibiton of *H. pylori* P12 (µM)		Effects on growth (50 µM antimycin A/rotenone; 10 µM CCCP)		
	BACapproach	CELLapproach	SCREENapproach	MIC	IC_{50}	*C. jejuni*	*E. coli*	*S. aureus*
Antimycin A	0.55	>100	6.1	8	2.9	no	no	no
Rotenone	0.15	27.4	0.45	0.5	0.083	no	no	no
CCCP	1.9	181.4	3.8	2	0.67	inhibition	yes	inhibition

Figure 38: Effects of known respiratory chain inhibitors and CCCP on *H. pylori*
Summary of the influence of antimycin A, rotenone (both known *H. pylori* respiratory chain inhibitors) and CCCP (carbonyl cyanide *m*-chlorophenyl hydrazone, ionophore) on CagA translocation and bacterial growth. Translocation was quantified using the TEM-CagA assay according to the protocol layouts described in Figure 28. Values depict mean IC_{50} values (concentration for 50% inhibition) of CagA translocation (µM) from at least four independent experiments, calculated by non-linear regression analysis. MIC (minimal inhibitory concentrations) and IC_{50} of growth (µM) were determined analyzing growth curves of *H. pylori* P12, and calculations were based on at least five independent experiments. Effects on *C. jejuni*, *E. coli* and *S. aureus* were monitored via growth curves in the presence of the indicated concentrations. Observations were based on at least three independent experiments.

4.2 Impact of NCL and SPECS hits on membrane potential and permeability

Because the comparison with known respiration inhibitors regarding translocation and growth inhibition properties provides only indirect parameters of respiration blockage, several parameters that are directly affected by respiratory inhibition were elucidated.

At first, the influence of the compounds on membrane potential was investigated. The membrane potential is a component of the PMF, and thus collapses in response to respiratory chain inhibition. *H. pylori* was incubated for 3 h with NCL and SPECS hits as well as controls, and effects were evaluated using $DiOC_2(3)$ (3,3′-diethyloxacarbocyanine iodide), that exhibits a shift from red to green fluorescence in response to membrane potential destruction. Corresponding outcomes of the highest concentrations applied are summarized in

Figure 39A, and flow cytometry analysis of pellasoren A, SLH8 and rotenone are exemplarily depicted in Figure 39B.

A)

Compound	Concentration	Influence on membrane potential	Influence on membrane permeability
NCL-1a	4 µM	yes	no
Aurachin A	4 µM	yes	no
Aurachin B	4 µM	yes	no
Aurachin C	4 µM	yes	slight
Cruentaren A	4 µM	yes	no
Icumazole A	4 µM	yes	no
Pellasoren A	4 µM	yes	no
Thiangazole A	4 µM	yes	no
Thiangazole B	4 µM	yes	no
SLH1	35 µM	yes	?
SLH3	35 µM	yes	no
SLH4	35 µM	yes	no
SLH6	35 µM	yes	no
SLH7	35 µM	yes	no
SLH8	35 µM	yes	no
SLH9	35 µM	yes	no
SLH10	35 µM	yes	no
SLH11	35 µM	no	no
SLH12	35 µM	yes	slight
Antimycin A	10 µM	yes	*n.d.*
Rotenone	10 µM	yes	no

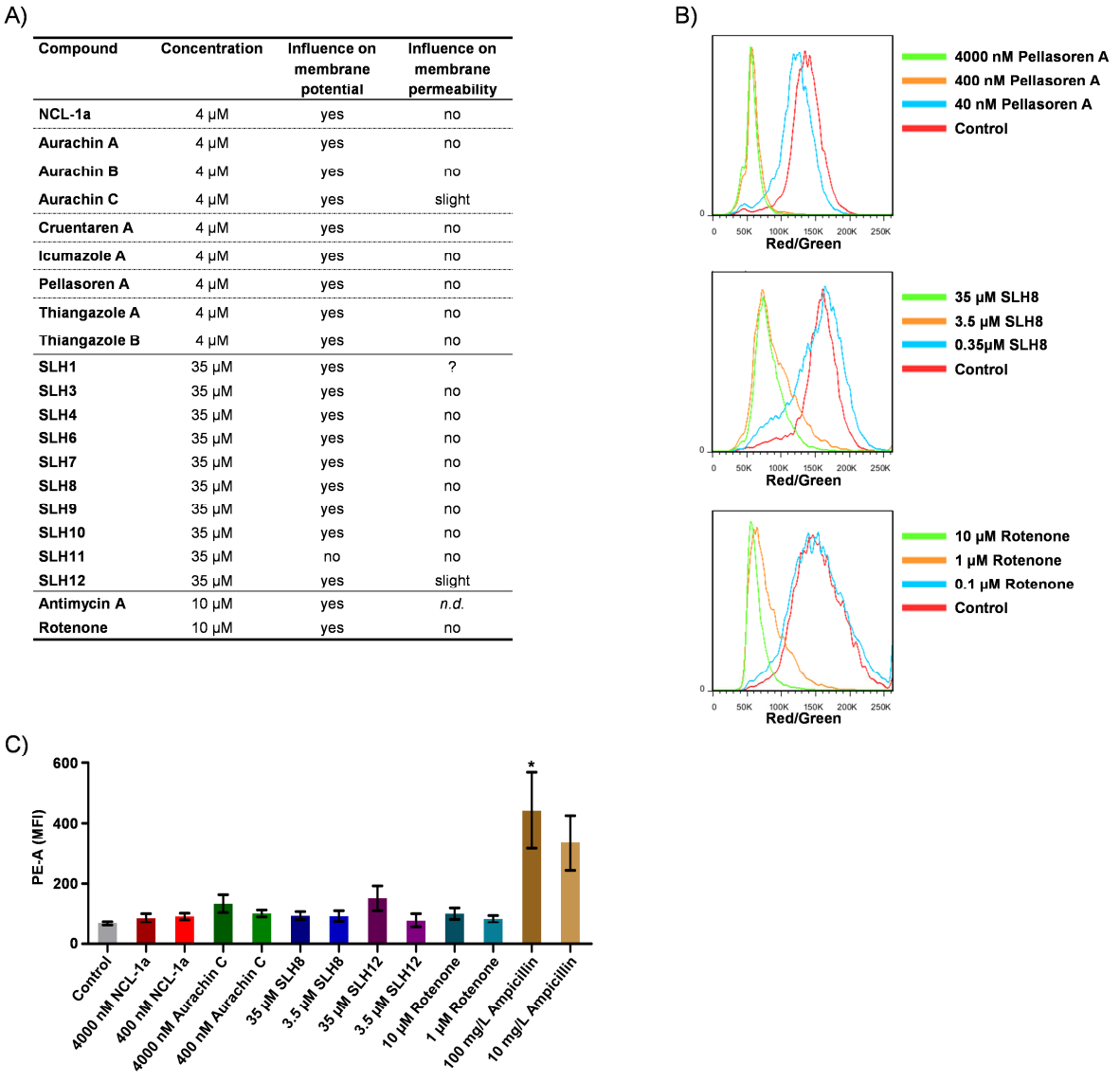

Figure 39: Effect of NCL and SPECS hits on membrane potential and permeability
A) Table summarizing the effects of the indicated substances on membrane potential and permeability at the highest concentrations applied. *H. pylori* was incubated for 3 h with the respective substances, and membrane potential and permeability was evaluated with $DiOC_2(3)$ (3,3′-diethyloxacarbocyanine iodide) or PI (propidium iodide), respectively. Experiments were repeated at least three times.
B) Influence on membrane potential in the presence of pellasoren A, SLH8 and rotenone expressed as red-to-green fluorescence ratio.
C) Influence on membrane permeability in the presence of selected substances or rotenone. Ampicillin was applied as a positive control for membrane disintegration. Values presented are mean values of MFI (median fluorescence intensity) of four independent experiments with standard errors of the mean. ANOVA (one-way, Tukeys post hoc test) referring to untreated control, *: $p<0.05$.

A clear membrane depolarization was observed for all substances, except for SLH11. This substance also showed comparatively weak effects on CagA translocation and *H. pylori* growth (see Figure 37) and thus, the used concentration might have been too low to induce a

potential collapse. But more plausibly, SLH11 might have another target in *H. pylori* and might not interfere with the membrane potential.

The membrane potential can also be destroyed when membrane integrity is disturbed by, for example, pore-forming agents or antibiotics like ampicillin. To exclude such rather unspecific effects, the influence of the compounds on membrane permeability was additionally determined. For this purpose, propidium iodide was applied, that only enters permeabilized *H. pylori* cells and can be detected in the red fluorescence channel by flow cytometry. Ampicillin was used as a positive control as it leads to disintegration of the bacterial membrane (shown in Figure 39C). Unfortunately, the effect of SLH1 could not be evaluated as its red color interfered with the measurement. Apart from that, no significant influence on permeability could be observed for any of the other substances (Figure 39A). Only a slight increase of red fluorescence could be observed for aurachin C and SLH12 (see also examples in Figure 39C). Concerning SLH12, the previously determined inhibitory parameters (see Figure 37) also showed effects on other bacteria and indicated, together with a slight influence on permeability, an unspecific antibacterial effect rather than specific *H. pylori* respiratory chain inhibition.

In conclusion, all NCL hits caused a specific membrane potential inhibition, while from the SPECS hits, SLH11 and SLH12 were excluded as potential *H. pylori* respiratory chain inhibitors. In the following experiments, only SLH4, SLH6 and SLH8 were investigated as these compounds exhibited the most promising and specific anti-*H. pylori* inhibitory profile (compare also Figure 37). As the membrane potential is a component of the PMF, it is intimately involved in oxidative phosphorylation which was focused on next.

4.3 Influence of NCL and SPECS hits on cellular ATP content

A functional respiration is necessary for energy conservation in form of ATP production (oxidative phosphorylation). Hence, cellular ATP levels after incubation with NCL and selected SPECS hits were examined. For this purpose, *H. pylori* was shortly exposed to the respective substances (only 5 min), and ATP concentrations were determined via a luciferase-dependent reaction in the plate reader. Corresponding percental ATP concentrations are summarized in Figure 40.

Overall, bacterial ATP contents rapidly decreased in a concentration-dependent manner for all NCL hits (Figure 40A), SPECS hits (Figure 40B) as well as for antimycin A and rotenone as controls (Figure 40C). Of importance, concentrations causing a 50% decrease were close to the MICs for *H. pylori* growth (compare Figure 35 and Figure 37), except for SLH4 where

only a 50% reduction in ATP content was detected at 35 µM. To rule out any general antibacterial effects, experiments were also repeated with several antibiotics (Figure 40D). Although lethal concentrations were applied, no effect on bacterial ATP concentration could be observed under these assay conditions. In conclusion, the reduced ATP levels evoked by NCL and SPECS hit compounds were supposed to arise from direct respiration inhibition.

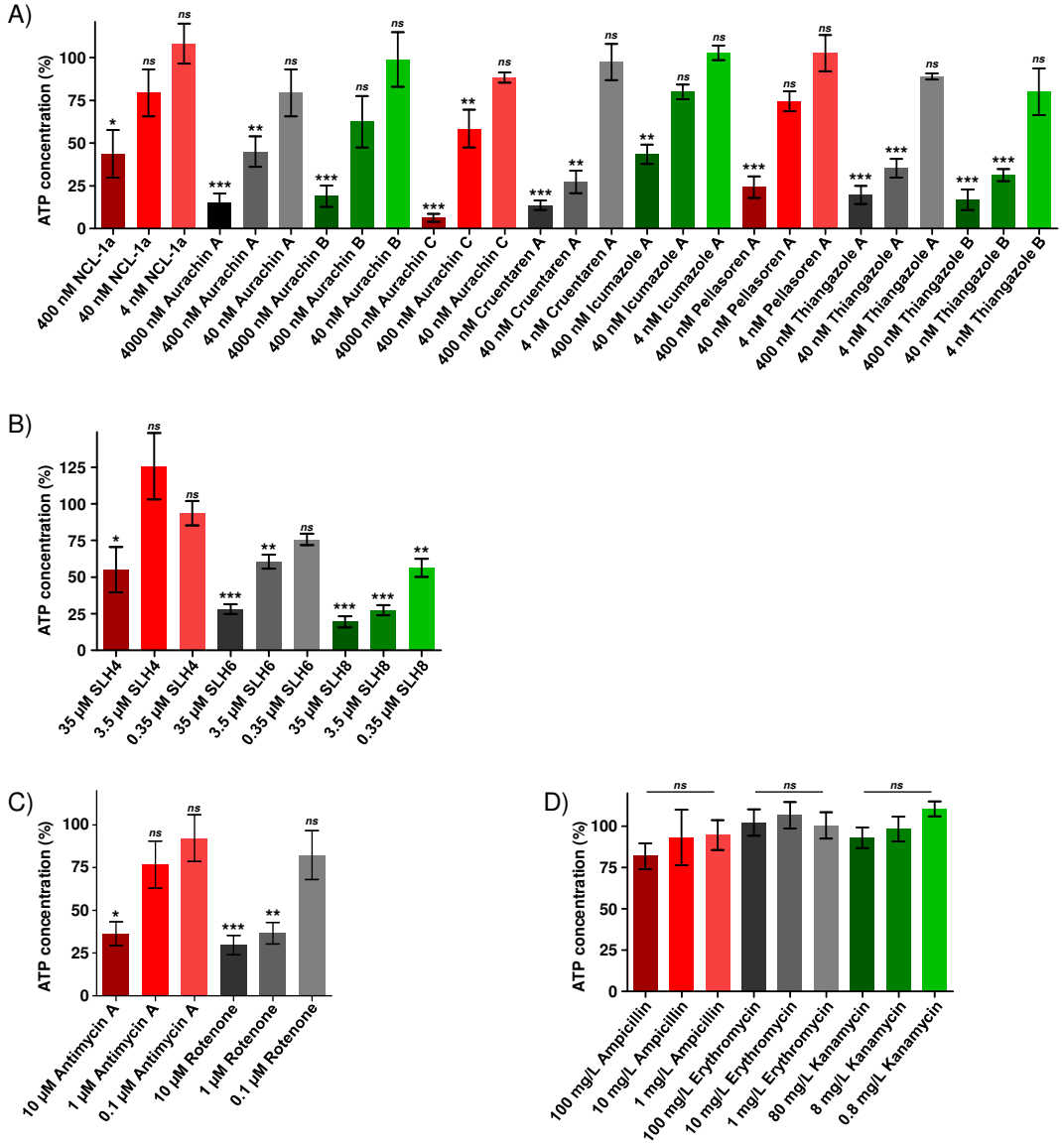

Figure 40: Influence of NCL and SPECS hits on cellular ATP concentration
H. pylori was incubated for 5 min with the indicated substances, and ATP content was quantified following a luciferase-catalyzed reaction. Values were normalized to an untreated control, and are indicated as mean values with standard errors of the mean from at least three independent measurements. ANOVA (one-way, Tukey post hoc test) referring to untreated controls, *: $p<0.05$, **: $p<0.01$, ***: $p<0.001$, *ns*: no significant difference.
A) Effects of NCL hits on bacterial ATP concentration.
B) Effects of SPECS hits on bacterial ATP concentration.
C) Effects of known respiration inhibitors on bacterial ATP concentration.
D) Effects of antibiotics on bacterial ATP concentration.

4.4 Impact of NCL and SPECS hits on oxygen consumption

Oxygen consumption is stringently coupled to respiration in an obligate aerobic bacterium. Hence, this parameter was directly measured when *H. pylori* was exposed to NCL and SPECS hit compounds in Oxoplates, which contain an integrated fluorescence-sensitive oxygen detector. As *H. pylori* mainly oxidizes organic acids as an energy source [226], pyruvate and lactate were added to *H. pylori* suspensions, which were exposed to respective compounds in nutrient-free buffer, and the resulting oxygen consumption was monitored. Results for pyruvate as an energy source are summarized in Figure 41 and for lactate in Figure 42, and the arrows designate the injection of the respective organic acid.

As expected, in the presence of rotenone and antimycin A, oxygen consumption was blocked with pyruvate (Figure 41A) or lactate (Figure 42A) as an energy source, with rotenone inhibiting respiration more efficiently than antimycin A. Consistently, the inhibitory potential of rotenone against *H. pylori* growth was also higher (compare Figure 38). Besides these controls, oxygen levels were also examined in the presence of various antibiotics to exclude any unspecific read-out (Figure 41B & Figure 42B). Although these compounds usually exhibit antibacterial effects against *H. pylori*, no influence on oxygen consumption was observed, strengthening the validity of this measurement. Next, NCL-1a, cruentaren A and icumazole A were examined (Figure 41C & Figure 42C). NCL-1a and icumazole A both inhibited respiration to the same level as rotenone. In addition, NCL-1a still blocked oxygen consumption at a lower concentration which is in accordance with its overall high impact on *H. pylori* (compare Figure 37). In contrast, no respiration inhibition was monitored for cruentaren A, although a drastic reduction in bacterial ATP content was shown in the previous chapter (4.3). One possible explanation would be that cruentaren A specifically inhibits the bacterial F_0F_1-ATPase, which leads to strongly reduced ATP levels but does not influence electron transport within the respiratory chain. Accordingly, cruentaren A has been shown to have an inhibitory effect on mitochondrial ATPase activity in eukaryotic cells [217, 218]. Examination of respiration in the presence of aurachins (Figure 41D & Figure 42D) showed an inhibitory potential of aurachin A and C on the level of rotenone and less effects of aurachin B, which is consistent with the effectivity against *H. pylori* growth and CagA translocation (compare with Figure 35). Strikingly, aurachin C exhibited an even higher inhibition than rotenone for lactate respiration. Respiration inhibition by pellasoren A and thiangazoles revealed blockage to the same extent as by rotenone (Figure 41E & Figure 42E). Similar results were also detected for the SPECS hits (Figure 41F & Figure 42F) that inhibited oxygen consumption similarly to *H. pylori* growth or CagA translocation (compare

Figure 37).

Results observed with α-ketoglutarate and succinate as energy sources were basically similar to those described above, although oxygen consumption after injection was only weakly induced (data not shown).

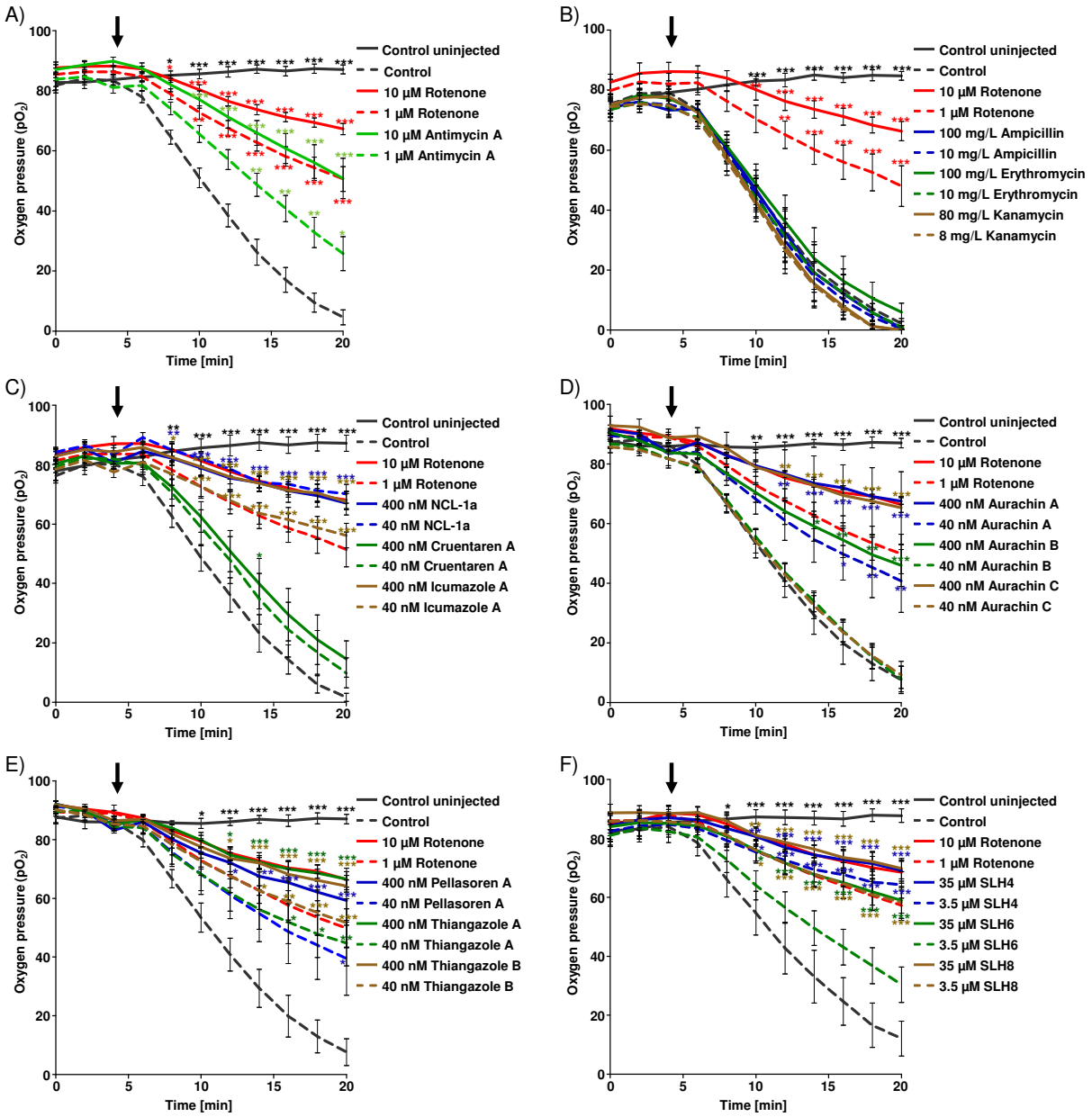

Figure 41: Influence of NCL and SPECS hits on oxygen consumption with pyruvate as substrate
H. pylori was incubated with the indicated compounds in nutrient-free buffer (PBS), 7 mM pyruvate was injected after 4 minutes (indicated by an arrow), and oxygen consumption was monitored. Experiments were performed in Oxoplates that have integrated fluorescence-sensitive oxygen detectors. Values indicate mean values of at least three independent measurements with standard error of the mean. ANOVA referring to untreated controls (two-way, Bonferroni post hoc test), *: $p<0.05$, **: $p<0.01$, ***: $p<0.001$.
A) Influence of known respiratory chain inhibitors on oxygen consumption as control.
B) Influence of antibiotics on oxygen consumption as control.
C) Influence of NCL-1a, cruentaren A and icumazole A on oxygen consumption.
D) Influence of aurachins on oxygen consumption.
E) Influence of pellasoren A and thiangazoles on oxygen consumption.
F) Influence of selected SPECS hits on oxygen consumption.

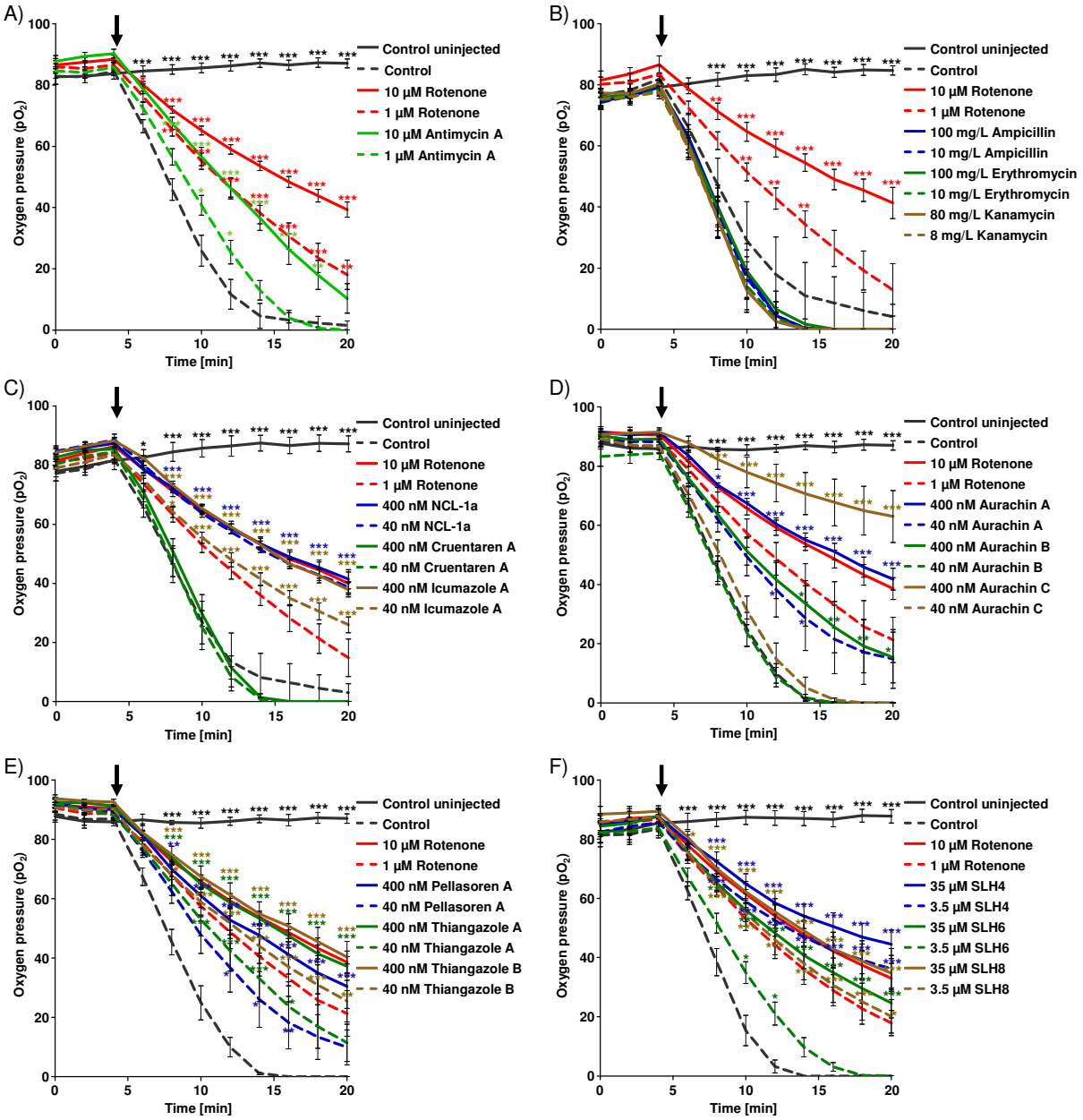

Figure 42: Influence of NCL and SPECS hits on oxygen consumption with lactate as substrate
H. pylori was incubated with the indicated compounds in nutrient-free buffer (PBS), 7 mM lactate was injected after 4 minutes (indicated by an arrow), and oxygen consumption was monitored. Experiments were performed in Oxoplates that have integrated fluorescence-sensitive oxygen detectors. Values indicate mean values of at least three independent measurements with standard error of the mean. ANOVA referring to untreated controls (two-way, Bonferroni post hoc test), *: $p<0.05$, **: $p<0.01$, ***: $p<0.001$.
A) Influence of known respiratory chain inhibitors on oxygen consumption as control.
B) Influence of antibiotics on oxygen consumption as control.
C) Influence of NCL-1a, cruentaren A and icumazole A on oxygen consumption.
D) Influence of aurachins on oxygen consumption.
E) Influence of pellasoren A and thiangazoles on oxygen consumption.
F) Influence of selected SPECS hits on oxygen consumption.

In general, effects were comparable between pyruvate and lactate, although with the latter substrate, oxygen was consumed much faster. This effect can be explained by the conversion of lactate to pyruvate by *H. pylori* lactate dehydrogenase [227]. Within this reaction, additional reduction equivalents are produced and fed into the electron transport chain,

leading to higher respiratory rates.

Since the inhibitory concentrations for respiration of the investigated NCL and SPECS hits were similar to those for CagA translocation and growth inhibition (compare Figure 35 and Figure 37), these anti-*H. pylori* effects were suspected to result from respiration inhibition.

4.5 Determination of cytotoxicity and evaluation as potential drug candidates

The data obtained in the previous chapter strongly indicated an action of the investigated NCL and SPECS hits on the *H. pylori* respiratory chain. As various anti-*H. pylori* effects were present applying only very low concentrations, the respective substances could be potential therapeutic drug candidates to treat *H. pylori* infection. Hence, the most promising candidates were examined regarding their cytotoxicity against eukaryotic cells.

The most effective and specific anti-*H. pylori* compounds from the NCL library comprised NCL-1a, pellasoren A and thiangazoles. However, highly cytotoxic effects (in the nanomolar range) of pellasoren A [221] and thiangazoles [228, 229] have been described in prior studies, while no exact cytotoxic concentration for NCL-1a has been recorded. Thus, NCL-1a as well as the most potent SPECS hits (SLH4, SLH6, SLH8) were tested for their cytotoxic effects in mouse fibroblasts (L929), as summarized in Figure 43.

Compound	Cytotoxicity	Growth inhibiton of *H. pylori*		Therapeutic index
	IC_{50}	MIC	IC_{50}	Cytotoxicity (IC_{50}) / Growth inhibition (IC_{50})
NCL-1a	1800 nM	3.9 nM	1.5 nM	1200
SLH4	26.1 µM	0.5 µM	0.15 µM	174
SLH6	>100 µM	16 µM	3.7 µM	>27
SLH8	>100 µM	1 µM	0.25 µM	>400

Figure 43: Determination of cytotoxicity and therapeutic indices
Cytotoxicity in L929 cells was determined via an MTT assay. Experiments were repeated three times and IC_{50} values were calculated by non-linear regression analysis. Values highlighted in grey are derived from Figure 35 and Figure 37 and serve as an orientation for effectivity against *H. pylori*. The therapeutic index (right column) was calculated by dividing the toxicity IC_{50} values by the IC_{50} of *H. pylori* growth inhibition.

The most potent cytotoxic effects were detected for NCL-1a (IC_{50} of 1.8 µM), followed by SLH4 (IC_{50} of 26.1 µM), whereas the IC_{50} values for SLH6 and SLH8 were out of the determined range (>100 µM). Although cytotoxicity of NCL-1a seemed to be relatively high, the compound also exhibited very strong effects on *H. pylori* CagA translocation and growth (data on growth also summarized in Figure 43). To better compare the substance concentration needed to cause a therapeutic effect (inhibition of *H. pylori*) to the concentration that causes cytotoxicity, therapeutic indices were calculated referring to the IC_{50}

values of growth inhibition (right column, Figure 43). In this regard, NCL-1a showed a broad therapeutic window when comparing the cytotoxic concentration with that needed for growth inhibition. In addition, SLH8 exhibited the highest therapeutic indices, as compared to SLH4 and SLH6. Following this, NCL-1a and SLH8 are highly recommended to be further investigated in future studies including more detailed target identification examinations, additional cytotoxicity determinations as well as animal studies to evaluate the *in vivo* effects of compounds for eradication of *H. pylori* infection.

IV. DISCUSSION

The bacterial pathogen *H. pylori* colonizes the gastric mucosa of half of the world´s population and is the causative agent of gastritis, peptic ulcers as well as gastric adenocarcinoma. Due to increasing antibiotic resistance rates, therapeutic treatment of *H. pylori* infection becomes a major challenge to public health. One key event in the induction of the above-mentioned malignant disorders is the delivery of the oncogenic CagA protein via type IV secretion into host cells. Hence, studying the exact mechanism of CagA translocation is relevant to find possibilities to inhibit this process and to prevent CagA-induced pathogenesis. Hitherto, the analysis of CagA translocation was time-consuming as well as labor-intensive. During this work a novel reporter assay, based on a β-lactamase (TEM-1) fusion to CagA (TEM-CagA), has been developed which overcomes these limitations. This TEM-CagA assay was applied to study various aspects of CagA translocation dynamics and recognition processes by the Cag type IV secretion machinery. Moreover, this assay was downscaled to screen various small compound libraries to identify potential CagA secretion blockers. Besides two promising specific Cag-T4SS inhibitors, these screenings revealed various eukaryotic respiratory chain inhibitors with high efficacy and specificity against *H. pylori* growth, which were further analyzed for their action on *H. pylori* respiration.

1. The novel TEM-CagA reporter assay: fast, specific and quantitative analysis

CagA is delivered into host cells via a type IV secretion-mediated process. Once inside, CagA gets phosphorylated immediately at distinct tyrosine residues (EPIYA motifs) by cellular kinases [74-76]. For many years, CagA translocation has been routinely determined via Western blot analysis of this specific phosphorylation event. But this method is labor- and time-intensive, and thus not suitable for high-throughput applications. During this work, a novel phosphorylation-independent CagA translocation reporter has been developed. This new assay is based on fusion of an *E. coli* β-lactamase (TEM-1) to the N-terminus of the CagA protein. After translocation of the respective TEM-CagA fusion protein into target cells, the enzymatic activity of TEM-1 is measured via conversion of the fluorescent β-lactam derivative CCF4. The cleavage product of CCF4 differs in its fluorescence signal from the intact substrate, resulting in a shift from green to blue fluorescence (see detailed description in Figure 8). During this work, it could be convincingly demonstrated that the blue-to-green

fluorescence ratio corresponds to translocated TEM-CagA protein. Hence, various cell lines infected with TEM-CagA-expressing mutants exhibited high and reproducible blue-to-green fluorescence ratios. Moreover, it could be shown that TEM-CagA is translocated by a T4SS-mediated process, such that a mutant, which is deficient in the Cag-T4SS but expressing TEM-CagA, did not evoke a blue-to-green fluorescence signal increase, even after over-night incubation with the CCF4 substrate. In addition, co-expression of wild-type CagA and the TEM-CagA fusion resulted in mutually reduced translocation of both proteins, suggesting a competitive recognition by the Cag-T4SS. The high specificity of the assay was further proven by the fact that treatment of host cells with TEM-CagA lysates did not result in a blue-to-green fluorescence increase, providing evidence for CCF4 conversion exclusively by translocated TEM-CagA inside the host cytosol. The high sensitivity of the assay was highlighted by detecting very low translocation rates of distinct CagA variants, which was not verifiable via CagA phosphorylation analysis in prior studies. In addition, translocation was observable after infection at low multiplicities of infection (~6), as well as after very short infection durations (about 15 min). In previous studies, CagA phosphorylation was visible after 20 to 30 minutes and increased over time, but quantification by immunoblotting is complicated [230-232]. Therefore, various aspects demonstrated the applicability of the TEM-CagA assay as a quantitative tool, and the blue-to-green fluorescence ratio correlated with the amount of translocated CagA protein. The fluorescence ratio increased dependent on infection duration as well as on MOI, finally resulting in a signal saturation. In addition, a gradual decrease of TEM-CagA translocation after sequential truncation of the CagA C-terminal secretion signal was maintained, in compliance with the CagA phosphorylation analysis presented here, or as previously reported [131]. The blue-to-green signal strengths observed in different cell lines, for example in Kato III and J774.1, were also in accordance with the lower CagA phosphorylation levels in J774A.1 compared to Kato III cells reported elsewhere [233]. Finally, the assay was suitable to titrate the dose-dependency of various inhibitors on CagA translocation, supporting the quantificability of the method. In line with this, a reliable correlation of translocated TEM-1 and CCF4 turn-over was demonstrated by the delivery of TEM-1 fusion proteins via the *Legionella pneumophila* Dot/Icm T4SS [234]. The principle of using TEM-1 fusions for secretion analysis has been originally adapted from Charpentier *et al.*, who applied the assay to type III secretion analysis of *E. coli* [174]. Since then, the reporter system was adapted to study bacterial effectors of type III secretion, for example in *Yersinia pestis* [185], as well as of type IV secretion of the Dot/Icm T4SS of *L. pneumophila*, as already mentioned above [186, 235]. For the Cag-T4SS, Suzuki *et al.* applied TEM-CagA

fusions to study translocation of CagA variants. However, these TEM-CagA variants were plasmid-encoded and not evaluated for quantitative analysis [236]. Previously applied *cagA* complementation plasmids often yielded variable or low CagA expression levels [131]. In contrast, within the work presented here, a chromosomal *cagA* reconstitution system was used which allowed stable (TEM)-CagA expression as well as the expression of diverse variants with only introducing minimal changes compared to the wild-type situation. Hence, quantitative translocation analysis of these TEM-CagA variants was achieved in a fast and reproducible manner.

The TEM-CagA-mediated conversion of fluorescent CCF4 was measurable by various fluorescence-assisted devices, including flow cytometry or fluorescence photometry. While FACS analysis enables precise quantification of secretion on a single-cell level, plate reader applications offer the advantage to be less labor-intensive, because measurements are conducted directly in CCF4 solution and do not require washing steps. This raised the possibility to miniaturize the assay to a 384-well format and to use it for medium-throughput screening of various compound libraries. In this respect, the Z´-factor, a widespread measure for the quality or power of a high-throughput screening (HTS) assay [200], confirmed a high validity of the TEM-CagA assay for HTS applications. This is in agreement with prior studies, which successfully applied the same reporter principle to identify type III or type IV secretion system inhibitors in other bacteria [234, 237], and advocates usage of the TEM-CagA assay in further, ideally automatized, compound library screenings.

As emphasized above, the novel TEM-CagA assay outperforms the validity of the tyrosine phosphorylation assay. During the studies presented here, the analysis of CagA phosphorylation of distinct variants was hampered by the common blot background which complicates analysis of putative phosphorylation bands, especially of weakly expressed CagA variants. This finally distorted phosphorylation rates compared to the TEM-CagA assay results in some cases (see as an example Figure 21). Moreover, the TEM-CagA assay is phosphorylation-independent, which permitted analysis of TEM-CagA variants lacking the EPIYA region as well as in the presence of kinase inhibitors. The tyrosine phosphorylation analysis might additionally misjudge or overestimate CagA translocation rates, because phosphorylation does not follow a linear process but is rather dependent on a multistep activation of the Src and c-Abl kinases, and more than one EPIYA motif can be phosphorylated simultaneously [232]. In addition, human gastric epithelial cell lines exhibit different expression and activation levels of Src and c-Abl kinases, which influences the

intensity of CagA phosphorylation [238]. In order to avoid an EPIYA motif-dependent analysis, a phosphorylatable GSK-tag was fused to CagA in prior studies [131]. But the subsequent immunoblotting still constituted a labor- and time-intensive procedure with limited sensitivity and quantifiablity. Comparing IL-8 induction analysis to the TEM-CagA assay, CagA-mediated IL-8 induction did not detect minor changes in translocation rates, although IL-8 measurement guaranteed a reliable proof for T4SS functionality (e.g. for the sequential C-terminal truncations, see Figure 18). As for CagA phosphorylation analysis, IL-8 secretion is influenced by host cell-specific factors that vary depending on the cell line [238]. Moreover, CagA-induced IL-8 secretion depends on the *H. pylori* strain [189]. In conclusion, the read-out of the TEM-CagA assay directly reflects the CagA translocation rate and is not influenced by cellular effects in comparison to CagA phosphorylation and IL-8 secretion analysis.

Nevertheless, the TEM-CagA assay should not be applied for interaction studies of CagA with host cellular proteins or respective signal transduction analysis. Although TEM-CagA induced IL-8 secretion was comparable to that induced by wild-type CagA, no hummingbird phenotype was observed upon infection. Induction of this phenotype is dependent on phosphorylation of at least two EPIYA motifs [135, 232], and indeed, tyrosine phosphorylation of TEM-CagA was difficult to detect. This might be due to the generally low expression level of TEM-CagA, or the phosphorylation efficiency might be disturbed by a steric hindrance of tyrosine kinase interaction with CagA because of the TEM-1 portion. Such a spatial obstruction could also be imagined for a complex formation of TEM-CagA with other cellular target proteins, e.g. those that are critical for hummingbird phenotype induction as the SHP-2 phosphatase [142, 144].

Apart from that, the TEM-CagA assay offers novel possibilities to decipher Cag type IV secretion activity. Up to date, CagA is the only translocated effector protein of the Cag-T4SS. Fusion of TEM-1 to other putative translocated proteins might lead to the identification of further effector proteins, and the discovery of various type IV secretion bacterial effector proteins was achieved by fusion of TEM-1 to candidate proteins [239-242]. Moreover, FACS analysis allows investigation on a per-cell basis and in this regard, infected cells shifted depending on the amount of injected CagA protein. Hence, cells could be classified into high and low CagA-injected populations. Performing this principle for *Y. pestis* type III secretion, mutants could be characterized that did not only affect the translocation rate of Yops (*Yersinia* outer proteins), but also the fidelity of Yop secretion [243]. Another application constitutes

the transfer of the assay to *in vivo* animal models, as previously reported for *Y. pestis* type III secretion [185]. In this study, mice were infected with *Yersinia* strains carrying TEM-1 fusions of Yops. Afterwards, different cell types derived from these animals were analyzed for TEM-1-mediated conversion of CCF4. In this way, it was discovered that *Y. pestis* primarily targets cells of the innate immune system. Since then, this technique was extended for *in vivo* secretion analysis of various bacteria [235].

In summary, lots of information can be obtained from previous bacterial translocation studies applying TEM-1 fusions. The TEM-CagA assay established here enables investigation of Cag-T4SS activity in more detail, as well as various *in vivo* applications.

2. Type IV secretion-mediated CagA translocation: new functional insights

Applying the novel TEM-CagA reporter system, various aspects of Cag type IV secretion system functionality and requirements for substrate recognition were investigated, and are discussed in the following sections.

2.1 Contribution of specific Cag components to type IV secretion system functionality

The Cag-T4SS is evolutionarily related to the *A. tumefaciens* VirB/VirD4 T4SS and composed of various Vir homologues which are likely to fulfil similar tasks. However, the Cag-T4SS harbors many further Cag-specific components whose functions are only partly clarified. Up to date, functional insights are mainly derived from studies analyzing the influence of respective Cag deletion mutants on CagA phosphorylation, IL-8 induction and bacterial pilus formation (see also Table 1) [87, 88]. This knowledge was extended by analyzing the direct influence of partially uncharacterized Cag-specific components (CagH, CagG and CagP) on CagA translocation via the TEM-CagA assay. Because the Cag-specific component CagI was intensively studied before and shown to be indispensable for CagA phosphorylation, IL-8 secretion as well as pilus production [103, 106], a *cagI* deletion mutant was used as a translocation-deficient control. As expected, the *cagI* deletion mutant did not reveal a translocation signal applying the TEM-CagA assay. Investigation of an isogenic *cagH* deletion mutant also exhibited a deficient TEM-CagA translocation, which was in accordance with prior studies where no CagA phosphorylation was observable with a *cagH*

mutant [115, 116]. As previously reported [103], lack of CagH caused a hyperpiliated phenotype with elongated and thickened pili compared to the wild-type. However, these abnormal pili did not seem to fulfil a functional role since an abolishment of IL-8 induction could also be observed in the *cagH* deletion mutant [103]. It has been speculated that CagH might regulate pilus dimensions by terminating pilus assembly. Indeed, CagH is involved in a subassembly with CagI and the putative integrin ligand CagL, both involved in pilus biogenesis, and the complex has been localized on the bacterial surface [103]. However, pilus location could only be demonstrated for CagL, but not for CagI and CagH, so far [113]. Apart from that, CagH is supposed to be integrated in the inner cytoplasmic membrane [93] and thought to interact with the membrane-associated CagI as well as CagL at the periplasmic face. Moreover, this CagH-CagI-CagL subcomplex was suggested to be important for later stages of pilus assembly [106]. The *cagG* gene is genetically organized together with *cagH*, *cagI* and *cagL* [121], and a functional connection between the gene products has been proposed [106]. CagG contains an N-terminal signal peptide and is thus supposed to be transported to the periplasm, and an interaction of CagG with multiple Cag proteins has been observed in yeast-two hybrid screening approaches [94]. Moreover, *cagG* deletion decreased CagI and CagL protein levels [106], supporting an interplay with the periplasmic CagI, CagL and CagH subcomplex. In a prior study, CagG has been revealed to fulfil functions as a supportive component as its absence attenuated CagA phosphorylation as well as the IL-8 phenotype [115]. Applying the TEM-CagA assay, a clear reduction in CagA translocation could be confirmed upon *cagG* deletion, further proposing a role of CagG for Cag type IV secretion activity. Besides, deletion of *cagG* partially abolished gastric inflammation via reduced colonization of Mongolian gerbils [244]. Another rather understudied component is the CagP protein. Upon *cagP* deletion, the TEM-CagA translocation rate dropped to approximately 10%. This is in discrepancy to prior data, where full CagA phosphorylation was observed, although *cagP* was deleted [115]. However, in the prior study a different *H. pylori* strain was used, and just recently a strain dependency of CagP function was discovered (K.T. Pham, F. Schindele, E. Weiss, R. Haas, W. Fischer; unpublished data). Of note, the predominant gene product of the *cagP* locus is an upstream non-coding RNA, the CncR1 sRNA [121, 122]. CncR1 transcript levels correlated negatively with bacterial motility and positively with adhesion, attributing to this sRNA a major regulatory role [122]. It was even supposed that the CagP protein itself is not expressed at all, because *cagP* mRNA transcription levels were very low [122]. Nevertheless, the TEM-CagA/Δ*cagP* deletion mutant used in this work still harbored the CncR1 sRNA and exerted an effect on CagA

translocation efficiency. Moreover, this mutant exhibited reduced expression of CagI and CagL proteins (data not shown), which might be an indirect reason for the decreased translocation rate. The particular role of CagP has to be elucidated, though it seems to have a regulatory rather than a structural function. For many other Cag-specific compounds, no specific function is known, although Cag-T4SS activity is reduced (e.g. CagN). Intriguingly, some Cag components only have accessory functions and their absence does not affect Cag-T4SS function, e.g. Cagζ or CagS. These proteins might be different translocated effector substrates and could be addressed in future studies by fusion with the TEM-1 reporter tag.

2.2 Recruitment of CagA to the translocation machinery

In many T4SS, chaperones serve as interaction partners for effector protein stabilization as well as for efficient binding by the coupling protein. During this process, secretion substrates might undergo partial unfolding to expose secretion signals for recognition and also to fit through the translocation channel [77]. For the Cag-T4SS, CagF has been identified as the stabilizing chaperone of CagA. Consequently, the TEM-CagA fusion protein was significantly less expressed in the *cagF* deletion mutant compared to the wild-type, as previously described [119]. CagA and CagF are both located at the inner membrane, and it is proposed that CagF assists CagA with recognition by the Cag-T4SS. Hence, lack of CagF abolishes CagA phosphorylation [118, 119], and as expected, no TEM-CagA translocation was observed in the *cagF* deletion mutant. Early studies identified a tight interaction of CagF with an N-terminal CagA fragment [118] and with a region adjacent to the C-terminal secretion signal [119]. Recently, Bonsor *et al.* reported that CagF binds five different domains of CagA with high affinity, creating a broad interaction surface. It was suggested that multiple copies of CagF form these contacts to maintain the labile CagA in a translocation-competent, protease-resistant conformation [120]. Hence, the removal of the N-terminal CagA D1 domain drastically decreased the strength of the CagA-CagF interaction, as shown by co-immunoprecipitation experiments, and in consequence, significantly reduced the CagA translocation efficiency. The CagA-CagF interaction surface contains the EPIYA region as well, but the co-immunoprecipitation analysis performed here showed no decrease of CagF binding to the CagAΔEPIYA variant, and the expression level of the CagA variant was comparable to the wild-type protein. In addition, full translocation of a TEM-CagA variant lacking the EPIYA region was observed. Hence, the stabilizing CagF function seems to be compensated by the remaining interaction surface. Furthermore, a competition of CagF binding to different CagA molecules is suggested by the experiments with mutants co-

producing TEM-CagA and a translocation-deficient CagA variant (CagAΔ20C). The TEM-CagA of this mutant was initially expected to be translocated with an efficiency of 100% but the actual rate reached only 74%. Hence, it can be speculated about a competitive CagF binding by the two CagA variant proteins. Likewise, a competition for recognition by the coupling complex could be assumed. This recognition complex is supposed to be composed of the coupling protein homologue Cagβ together with CagZ [95]. Within this assembly, CagZ stabilizes Cagβ, and the cytoplasmic part of Cagβ interacts and recognizes CagA. Accordingly, both coupling components fulfil, as the CagF chaperone, a function in CagA recruitment to the T4SS, because the absence of each single component only affects CagA translocation but not Cag-T4SS system functionality [115, 116]. Generally, coupling proteins confer substrate specificity to their cognate translocation system as these proteins recognize distinct areas of the effector proteins. For type IV secretion systems, signals in the C-terminus have been identified to be relevant for recognition [77]. For example, VirB/D4 substrates of *A. tumefaciens* (e.g. VirF) are dependent on C-terminal clusters of positively charged arginine residues [190], and substrates of the *L. pneumophila* Dot/Icm T4SS (e.g. RalF) on C-terminal hydrophobic residues or blocks of acidic residues [191, 245]. Also, for the Cag-T4SS, a prior study could demonstrate that deletion of the last 20 amino acids rendered the CagA protein translocation-deficient [131]. In the work presented here, various efforts were made to further characterize this C-terminal secretion signal. Substitution of lysine residues with alanines within the last 20 amino acids did not exert an effect on the translocation rate. Furthermore, a CagA variant with exchange of all charged amino acids within the last 20 amino acids still exhibited a translocation rate of 77%. Hence, a substantial role of C-terminal charged amino acid residues onto translocation, as described for other T4SS, could not be demonstrated, confirming the results of a prior study [131]. Whereas *A. tumefaciens* VirF or *L. pneumophila* RalF do not tolerate the removal of more than two C-terminal amino acids [190, 245], the elimination of up to six C-terminal amino acids did not affect CagA translocation at all. A complete abrogation of translocation was only achieved after removal of the last ten C-terminal amino acids (CagAΔ10C). Intriguingly, CagA translocation could be reconstituted after fusion of arbitrary tags to CagAΔ10C. In a previous study, exchange of the last twenty amino acids with the C-termini of VirB/VirD4 *A. tumefaciens* effectors or T4SS-associated relaxase motifs (conferring substrate specificity in conjugation systems) reconstituted CagA translocation as well, whereas exchange with rather arbitrary CagF, CagS and CagO C-terminal amino acid residues did not result in translocation competence. Hence, it was speculated that a common conserved secretion signal beyond T4SS reconstituted CagA

delivery [131]. However, these prior data were generated via CagA phosphorylation analysis, and in the context of the translocation of TEM-CagAΔ10C extended with arbitrary tags (e.g. TEM-CagAΔ10C-Myc), it is likely that translocation of the reconstituted C-terminal CagF, CagS and CagO extensions were below the detection limit of Western blotting. Consequently, for recognition by the Cag-T4SS, not a defined C-terminal amino acid composition seems crucial but rather a minimal length of the C-terminal tail. Even so, exchange of the last 10 amino acids of CagA with diverse tags reconstituted translocation with different efficiencies, and site-specific exchange of C-terminal charged amino acids significantly reduced the translocation rate. This still suggests an impact of the amino acid composition though not of specific residues. It is tempting to speculate that binding of the intrinsically disordered CagA C-terminus to the coupling protein or to the CagF chaperone confers a secondary structure to the C-terminus. Respective variations in the C-terminal amino acid composition might modulate this induced conformation, hindering recognition by the coupling protein complex, and ultimately have a different impact on translocation efficiency. In compliance with a previous study, C-terminal elongation of full length CagA with arbitrary tags was tolerated as well [131]. Notably, the C-terminal extensions in the study presented here reduced the translocation rate to the same extent, although the amino acid composition of the distinct tags clearly differed. The C-terminal elongations may not directly participate in the recognition process, but modulate the proposed C-terminal secondary structure similarly, leading to an equally decreased CagA translocation rate.

However, TEM-1 solely fused to the last 195 amino acids of CagA was not translocated (TEM-CagAC195, data not shown), suggesting that the C-terminus alone is not sufficient for CagA translocation, which was also concluded previously [131]. In contrast, merely 19 C-terminal amino acids of VirF (*A. tumefaciens*) and 15 C-terminal amino acids of RalF (*L. pneumophila*) enabled reporter protein translocation [190, 245]. One reason for the translocation deficiency of TEM-CagAC195 might be the necessity for other N-terminal or internal recognition motifs in addition to the C-terminal secretion signal. Prior data indicated a contribution of the foremost CagA N-terminus to translocation, and various N-terminal deletion mutants did not exhibit a CagA phosphorylation signal [131]. However, the data presented here convincingly demonstrated that neither the first 17 N-terminal amino acids, nor the N-terminal D1 domain or the internal EPIYA region are needed for CagA delivery. These contradictory results might be caused by the detection limit of prior CagA phosphorylation analysis in comparison to the highly sensitive TEM-CagA translocation reporter. Moreover, previous CagA variants were only weakly expressed, further questioning

the results of phosphorylation analysis [131]. No predicted signal sequence is present in N-terminal CagA, e.g. for sec-dependent secretion across the inner membrane. Accordingly, the full translocation ability of CagA lacking the first 17 amino acids clearly proved the absence of an N-terminal secretion signal. Nevertheless, after removal of the N-terminal D1 domain, CagA translocation efficiency was strongly affected. This decline in CagA delivery was mainly contributed to the lacking CagF stabilization for CagA [120]. Besides, the N-terminal D1 domain may be important for interaction with host cell proteins rather than being required for translocation. According to the CagA structure, the D1 domain forms a single compact domain [127, 130], and various studies showed direct interaction of D1 with host cell proteins causing the degradation of tumor suppressors [148, 149]. In addition, the first 200 N-terminal amino acids of CagA act as another membrane-binding site, which targets CagA to different cell compartments and regulates CagA activity [246, 247].

Notably, the TEM-CagA variant lacking the N-terminal D2 and D3 domains (TEM-CagAΔD2-D3-EPIYA) was defective for translocation. It could be speculated that this N-terminal part of CagA constitutes a supportive second recognition sequence for docking to the translocation channel. Such a recognition mechanism has been described for translocation of Beps (Bartonella-translocated effector proteins) by the *Bartonella* VirB/VirD4 T4SS. Beps contain a bipartite secretion signal, which is composed of a positively charged C-terminus and at least one internal "BID" (Bep intracellular delivery) domain [248]. Moreover, the structural fold of the N-terminal CagA domain could contribute to substrate recognition as previously described for various relaxases. For example, the $TraI_{R1}$ relaxase requires an intact C-terminus together with specific internal motifs, only present in the folded protein, for T4SS-mediated DNA transfer [249]. Another explanation for the involvement of both the N- and C-terminus for CagA translocation could be a two-step delivery mechanism. Type IV secretion is often considered as a one-step transport process, where the substrate is directly delivered through a channel spanning both membranes [82]. Indeed, this route has been biochemically shown for the T-DNA transfer through the *A. tumefaciens* VirB/D4 T4SS [83]. Of note, recent structural analysis of the T4SS core complex from plasmid R388 of *E. coli* revealed no continuous transfer channel [86]. Hence, a two-step translocation mechanisms could be imagined as well, where substrates would access the secretion chamber from the periplasm. This mechanism is also supposed for the pertussis toxin of the *B. pertussis* Ptl T4SS or some substrates of the *A. tumefaciens* VirB/D4 T4SS [250, 251], which enter the periplasm via sec-dependent systems or Vir components, and traverse the outer membrane in a second step. Accordingly, the core complex VirB9 component of *A. tumefaciens* seems to harbor a substrate recognition domain

for crossing the outer membrane [252]. Following such a theory, the C-terminal signal sequence of the CagA protein would be required for recruitment to the inner membrane complex and subsequent transfer across the inner membrane, while the N-terminus would be recognized in a second step by outer membrane components for translocation. Whether CagA accumulates in the periplasm has not been shown yet. Moreover, both one- and two-step mechanisms might work in parallel.

The most obvious reasons for the translocation deficiency of TEM-CagAΔD2-D3-EPIYA might be additional aspects, which are decisive for CagA transfer. These include an overall reduced interaction surface with the stabilizing CagF chaperone [120], no interplay with the putative host cell $\alpha_5\beta_1$ integrin receptor via the D2 single layer β-sheet [114, 127] as well as a missing host cell phosphatidylserine association of CagA via the D2 domain [129]. Taking the host cell receptor and host membrane interplay into account, a mechanism can be assumed in which the delivery of CagA across the host cell membrane requires the N-terminus for physical target cell contact, whereas the C-terminal secretion signal is exclusively responsible for the initial recruitment and delivery through the Cag-T4SS.

2.3 Impact of active bacterial and cellular processes

Monitoring TEM-CagA translocation provided novel insights into Cag-T4SS translocation dynamics. In time-course experiments CagA translocation stopped after approximately two hours irrespective of the MOI applied. Although these observations might be biased in comparison to the situation *in vivo*, it could be assumed that CagA translocation is a self-limiting process to protect the host cell from the pathophysiological effects of CagA to a certain degree. CagA translocation was visible after very short infection durations, which indicates that, immediately after addition to the cell culture, the bacteria swim to the cells and initiate CagA translocation. As direct host cell contact is required for T4SS-mediated transfer of CagA, one could assume that adhesion to the cells triggers assembly of the Cag-T4SS and/or initiates translocation. Intriguingly, a regulatory sRNA encoded by the *cag*PAI, the CncR1 transcript mentioned above, constitutes a switch between motility and adhesion to the cells [122]. Moreover, observations from the work presented here suggest a major role of *de novo* protein synthesis for CagA translocation competence. First, a CagA and TEM-CagA co-producing mutant translocated both CagA proteins to the same extent, although basal CagA expression levels differed significantly. Second, translocation was immediately inhibited upon protein synthesis blockage, which further supports a model in which only freshly synthesized

CagA is recruited by the Cag-T4SS. In addition, it could be assumed that the Cag apparatus itself has to be newly synthesized. Host cell contact might activate the expression of *H. pylori* T4SS components, as it has been reported for the type III secretion system in *Yersinia* species [253]. In contrast, activity of the *Legionella* Dot/Icm T4SS is independent of *de novo* protein synthesis [234]. Reliance on freshly synthesized protein might be specific for the Cag-T4SS, but not for the functionality of type IV secretion systems in general.

Data presented here suggests that only a small proportion of the CagA protein pool is injected into the host cell, which is in accordance with a recent study [193]. However, the CagA protein is highly abundant also without host cell contact [254]. One explanation would be that the high basal CagA expression level is caused by the *in vitro* culture conditions and does not reflect CagA amounts present *in vivo*. Another possibility could be that CagA fulfils a physiological role. In fact, expression of *cagA* is upregulated upon iron starvation without any host cell contact [255]. Moreover, *in vitro* iron depletion induced coccoid morphologies in strains lacking *cagA* [195]. *H. pylori* usually exhibits an elongated and spiral morphology, while coccoid phenotypes are induced in context of environmental stress, proposing a major role of CagA in iron acquisition. Hence, under iron-limiting conditions, *cagA* deletion mutants showed a reduced ability to colonize Mongolian gerbils [256]. Further data from animal and epidemiological studies indicated an inverse correlation of iron levels and the severity of *H. pylori*-induced diseases [125]. The same study could demonstrate that the Cag-T4SS assembly as well as CagA expression levels increased upon iron limitation, which resulted in an augmented translocation rate and higher IL-8 induction levels [125]. It was proposed that iron limitation induces, in addition to higher CagA expression levels, an increased CagA translocation for proper iron acquisition, facilitating colonization. Within the work presented here, this iron limitation was aimed to be modeled by using an iron chelating reagent. But an augmented TEM-CagA translocation in response to iron sequestration could not be observed. Reasons for this discrepancy might be that in the experiments presented here, incubation times to achieve iron depletion were relatively short and the iron concentration in the media may be too high to be complexed by the chelating agent. In contrast, the prior study investigated strains that were either isolated from iron-depleted animals or long-term cultured under iron-limiting conditions [125]. An influence on bacterial translocation competence has also been reported upon zinc depletion. In response to bacterial infection, *in vivo* zinc sequestration is mediated by calprotectin, a neutrophil-produced metal ion chelator. Infection of calprotectin-deficient mice with *H. pylori* resulted in lower bacterial burdens and an increased inflammation compared to wild-type animals. It was concluded that calprotectin

represses the pro-inflammatory activity of the Cag-T4SS *in vivo*, hence contributing to bacterial immune evasion and establishment of the chronic infection [126]. Consistently, sequestration of zinc by the metal ion chelator TPEN significantly reduced CagA phosphorylation, IL-8 induction as well as Cag-T4SS pilus biogenesis in the prior study [126]. In this work, zinc depletion via TPEN also resulted in a reduced TEM-CagA translocation, but this inhibition clearly correlated with an anti-*H. pylori* growth effect. Contrarily, the effects on Cag-T4SS activity in the prior study were observed applying a non-antibacterial TPEN concentration. These discrepant results could be caused by different culture conditions, but a reduced fitness of *H. pylori* upon zinc depletion, which resulted in less Cag-T4SS activity, seems obvious as well. However, regarding the simulation of zinc and iron depletion, the expected effects on TEM-CagA translocation might have been overlooked, because the complexity of the gastric environment and interactions with host responses were not included in these *in vitro* experiments.

The energy requirement for Cag-T4SS activity is another aspect which is poorly understood. In general, energy conserved in the form of ATP seems to be indispensable for type IV secretion functionality, and the Cag-T4SS incorporates three proteins with a putative ATPase activity: the coupling protein Cagβ and the inner membrane complex-associated components CagE and Cagα [87, 88]. Although a catalytic activity has been experimentally proven only for Cagα so far [96], the absence of Cagβ leads to CagA translocation deficiency and lack of CagE as well as Cagα completely abrogates Cag-T4SS functionality. Hence, it is assumed that these ATPases convert energy for the translocation process and for biogenesis of the Cag apparatus or pilus, respectively. Here, additional evidence for this ATP dependency was obtained by the high susceptibility of *H. pylori* towards various respiratory chain inhibitors, which were detected during the screenings for CagA translocation inhibitors. The respiratory chain generates a gradient across the bacterial inner membrane, called the proton motive force (PMF), which drives ATP generation (oxidative phosphorylation). The PMF is composed of two components: an electrical gradient ($\Delta\psi$ or membrane potential) and a proton concentration gradient (ΔpH). As expected, exposure of *H. pylori* to the respiration inhibitors induced a shutdown of the membrane potential and a drastic drop in bacterial ATP content, which resulted in a translocation inhibition. However, the subsequent growth inhibition of *H. pylori* could also be indirectly responsible for this effect. In addition to ATP hydrolysis, transport across membranes often requires the PMF in biological systems [257]. For example, the PMF is necessary for the activity of the flagellar type III secretion system (T3SS) apparatus, which functions as a proton-driven protein exporter [258]. As a result, CCCP (a

proton carrier discharging both the electric potential and the concentration component of the PMF) inhibited *Y. enterocolitica* flagellar T3SS (motility) as well as the Ysc T3SS (Yop secretion) [259]. TEM-CagA translocation levels were also drastically reduced upon direct inhibition of the PMF via CCCP, or indirectly via the above-mentioned respiratory chain inhibitors. However, it is difficult to conclude that the PMF is required for CagA translocation, because breakdown of the PMF was immediately coupled to decreased ATP levels (data for CCCP not shown). The essentiality of ATP for general physiological processes might disturb Cag-T4SS activity as a secondary effect, and, as mentioned above, the CagA translocation process itself seems to depend on ATP. Charpentier *et al.* investigated the influence of the PMF on the Dot/Icm T4SS of *L. pneumophila*, and detected an effector translocation inhibition upon CCCP treatment was well [234]. As this inhibition was reversible and the bacterial ATP pool was only slightly reduced, the authors speculated about a partial contribution of the PMF to the ATP-dependent translocation process. This may be the case for T4SS in general, but deciphering a relative involvement of PMF and the directly linked ATP levels is highly sophisticated.

Apart from the ATP-dependent CagA delivery via the Cag-T4SS machinery, energy-dependent host cellular processes are also involved in CagA uptake into the host cytosol [129]. Hence, upon depletion of ATP from the host cell, via exposure to various respiratory chain inhibitors or CCCP (CELLapproach), the levels of translocated CagA were reduced, which is in agreement with previous experiments [129]. Furthermore, the contribution of the eukaryotic cytoskeleton on CagA translocation was examined. Upon inhibition of the actin cytoskeleton, the CagA translocation rate was clearly reduced, consistent with prior data [129]. This effect was not only observed applying common actin polymerization inhibitors, but also with natural products of the chondramide class [208], which were thus detected during the screening for CagA translocation inhibitors. For the first time, a slight influence of the eukaryotic microtubule system on CagA delivery could also be demonstrated. This impact was also proven with a common microtubule system inhibitor and with the so-called tubulysins [210], which were also identified during the translocation inhibitor screenings. Although the cytoskeleton seems to have a major role in CagA uptake, a prior study showed that no classical endocytotic processes are involved [129]. In addition, cholesterol in lipid rafts (microdomains in the eukaryotic membrane) is important for efficient CagA translocation, and cholesterol sequestration decreased CagA phosphorylation [114, 129, 197]. The data presented here extended prior findings by demonstrating that inhibitory effects on translocation were strongest when cholesterol was constantly depleted from the lipid rafts

during infection (SCREENapproach). Of note, the putative target receptor of the Cag-T4SS, the $\alpha_5\beta_1$ integrin, is raft-associated as well [113, 114], and a constant raft dissociation by cholesterol depletion might be the reason for the strong translocation decline. Moreover, *H. pylori* has been shown to actively recruit lipid raft components to the sites of its host cell attachment and to metabolize host cholesterol, which has been additionally linked to Cag-T4SS-associated activities and CagA-mediated signaling [260]. Besides, binding of CagA to host membrane phosphatidylserine (PS) is crucial for its uptake. Interestingly, PS are transiently externalized to the outer leaflet of the plasma membrane at the site of bacterial attachment, which represents a further contribution of active host processes to CagA translocation [129]. Although the exact mechanisms of CagA cellular uptake are unknown, one can speculate that upon binding of CagA or the T4SS to the host cell membrane – either via lipid raft and integrin interaction, phosphatidylserine binding or everything in parallel – a structure originates (e.g. a membrane pore or channel), which requires specific actin and tubulin rearrangements.

3. In search of a pathoblocker: specific CagA translocation inhibition

CagA, once inside the host cell, exhibits a tremendous pathophysiological activity leading to gastric diseases including cancer development. Hence, for treatment of *H. pylori* infection, inhibition of CagA translocation would be a promising issue. During this work more than 4000 compounds were tested for inhibition of CagA translocation, using the TEM-CagA assay. Finally, two chemically related compounds, LLH-1 and LLH-2, were identified in follow-up studies to specifically inhibit CagA translocation.

The TEM-CagA assay proved to be a valuable tool for high-throughput applications. However, in the primary screening procedure various unspecific CagA translocation inhibitors were detected, and showed that several follow-up studies are necessary to confirm a specific action on translocation. As a bactericidal compound activity directly correlates with CagA translocation competence, such a secondary inhibitory effect could be quickly identified by a subsequent secondary screening monitoring bacterial growth. For hit confirmation of the primary TEM-CagA assay screening, three different washing protocols (BAC, CELL, SCREENapproach) enabled a precise analysis whether compounds act on *H. pylori*, the eukaryotic cells, or the interplay of both. Hence, substances that unspecifically caused translocation blockage due to a cytotoxic effect (e.g. chondramides) could be

identified. Finally, the orthogonal CagA phosphorylation assay provided an independent demonstration of translocation inhibition. This proof was of major importance, as some substances had an impact on the TEM-1 reporter system resulting in false-positive hits (e.g. cinnachinon-hydroxymethyl). Although the exact inhibition mechanisms on the TEM-1 reporter system were not clarified, those false-positive hits might have acted as CCF4 fluorescence quencher, or exhibited an autofluorescence or inhibited the enzymatic activity of the TEM-1 β-lactamase. However, the observed compound-mediated blocking of CCF4-AM loading of cells (e.g. by cantharidin) allowed a quick identification of cytotoxic activities, and compounds could be immediately excluded from further studies.

The source of the libraries screened in this work covered a broad spectrum ranging from chemically synthesized substances to various secondary metabolites. As natural products generally exhibit a higher bioactivity and increased hit rates in HTS compared to synthetic compounds, the applied concentration of natural compound libraries was lower in the screening [261]. Even so, the compound concentrations in the screenings were fixed beforehand, and future studies should adapt the hit output by a preceding concentration optimization [200]. The two identified CagA translocation inhibitors with activities in the µM range, LLH-1 and LLH-2, belong to the same class of chemically synthesized substances. Speculating about a mechanism of LLH-1/2-mediated inhibition, a specific impairment of the CagA delivery process itself is likely, because Cag-T4SS functionality, as determined by IL-8-inducing capability, was maintained in the presence of the compounds. Moreover, the inhibitory effects were only detectable when LLH-1/2 were present during infection, and neither pre-treatment of bacteria nor of cells diminished CagA translocation, which suggests either a reversible inhibition or a direct blockage of the bacteria-host interaction.

Generally, monitoring CagA translocation inhibition in a cell culture infection model is a promising screening approach. Using such a read-out, various possibilities to inhibit the translocation process are covered, including the Cag-T4SS assembly per se, various protein-protein interactions (e.g. CagH-CagI-CagL) or general enzymatic activities relevant for the translocation process (e.g. Cagα), as well as obstruction of *H. pylori*-host interaction. Experimental approaches, where the read-out was based on *in vitro* or even *in silico* inhibition of enzymatic activities or protein assemblies, regularly yielded highly active substances, which exhibited a specific inhibition without off-target activity (e.g. antibacterial). But subsequent application of those hit compounds in living organisms often produced no effect because the substances were simply not delivered to their targets (e.g. due to a failure in

compound uptake or due to metabolic conversion). Such a scenario was the case for a set of highly potent imidazo[1,2-α]pyrazines. These compounds inhibited the Cagα ATPase *in vitro* [262], but did not affect CagA phosphorylation when tested in a cell culture infection experiment (W. Fischer, personal communication). The TEM-CagA screening mode overcomes the limitations of those experimental settings.

Secretion systems are used by various bacteria to exert pathogenic effects, and hence are favored targets for development of anti-virulence drugs. Screening approaches, as presented here, serve as a valuable tool to increase the chance of detecting specific inhibitors. Substantial efforts have been made for blocking type III secretion, leading to the identification of compounds targeting a relatively broad range of pathogens including *Yersinia*, *Salmonella* and *Pseudomonas* species. Nonetheless, successful eradication of pathogens in animal models due to a specific T3SS inhibition has not been shown yet [167, 168]. HTS were applied to identify inhibitors of the *Brucella abortus* T4SS assembly factor VirB8 [263], *E. coli* T4SS-mediated conjugation [264], as well as the *H. pylori* Cag-T4SS relevant Cagα ATPase [265]. Similar to the above-mentioned study [262], the latter study of Hilleringmann *et al.* initially investigated the inhibition of *in vitro* enzymatic activity of purified Cagα. But in this study, a series of thiadiazolidine-3,5-diones was discovered showing an *in vivo* activity as well [265]. The most potent compound CHIR-1 reduced Cag-T4SS function including an abrogation of CagA phosphorylation and diminished gastric colonization of *H. pylori* in a mouse model. However, pre-treatment of bacteria with CHIR-1 was necessary for these effects, excluding the compound as a potential therapeutic pathoblocker. Recently, Shaffer *et al.* identified two synthetic small molecules, C10 and KSK85, which disrupted Cag-T4SS activity [123]. Both compounds contained a central peptidomimetic 2-pyridone motif and were previously reported to inhibit type I pilus biogenesis in *E. coli* [266]. The work of Shaffer *et al.* proposed that KSK85 inhibited biogenesis of the Cag-T4SS pilus, while C10 interfered with Cag-T4SS activity without affecting pilus assembly [123]. However, no animal studies were presented to demonstrate an *in vivo* effect of the two small compounds. For the applicability of LLH-1/2 as pathoblockers, various investigations have to be conducted as well. According to the data presented here, a specific translocation inhibition can be assumed, but the exact mechanism of action has to be elucidated. Moreover, a structure-activity relationship of LLH-1/2 and further related compounds as well as a detailed cytotoxicity determination has to be performed. Ultimately, the efficacy of the most potent LLH-1/2 derivatives against CagA-induced pathologies and gastric colonization success in an *in vivo* model of infection has to be investigated.

Apart from the role of T4SS machineries in translocation of proteins, these systems mediate the spread of virulence factors and antibiotic resistances via T4SS-mediated conjugation among bacteria. Especially the dissemination of antibiotic resistances is a major threat to public health, and leads to increasing treatment failures, also regarding *H. pylori* infection. In addition, the selection pressure by excessive antibiotic usage even accelerates this process [267]. Specific T4SS inhibitors are expected to stop this antibiotic resistance spread and impose only a weak selective pressure at the same time. Consequently, a perfect Cag-T4SS inhibitor would target a broad spectrum of T4SS including other *H. pylori*-expressed T4SS. In particular, besides T4SSs enabling conjugation [78], *H. pylori* encodes another T4SS for exogenous DNA import [79]. Hence, a general T4SS inhibition would also diminish the high adaptability of *H. pylori*. Accordingly, future studies should also investigate the inhibitory capabilities of LLH-1/2 against other T4SS. The Cag-T4SS inhibitors discovered by Shaffer *et al.* blocked interbacterial T4SS-mediated DNA transfer in *E. coli* and T-DNA delivery by VirB/D4 T4SS of *A. tumefaciens* [123]. However, both compounds were not demonstrated to inhibit DNA transfer or uptake by further *H. pylori* T4SSs. Additionally, various unsaturated fatty acids, shown to inhibit conjugative systems of various pathogens (*Escherichia*, *Salmonella*, *Pseudomonas* and *Acinetobacter spp*. [264, 268]), could be tested for their action against *H. pylori* T4SSs.

Most people tolerate *H. pylori* infection without any adverse effects, and after establishment of a therapeutic Cag-T4SS inhibitor, only persons at high risk for developing malignancies should be treated. Moreover, *H. pylori* infection might protect against allergies and other chronic inflammations [14, 166]. Hence, potential beneficial effects of *H. pylori* infection could be preserved applying a personalized treatment with specific Cag-T4SS pathoblockers. In addition, the gut microbiota would be preserved in comparison to treatment with antibiotics. Inhibition of CagA translocation might reduce the bacterial load in the stomach, as it has been proposed that injection of CagA into host cells provides a colonization advantage for *H. pylori*. Translocated CagA allows *H. pylori* to exploit the surface of gastric cells as a replicative niche and for provision with iron [256, 269]. Furthermore, a functional Cag-T4SS has been shown to be relevant for successful colonization in a rodent model of infection [152]. But *cag*PAI-negative strains colonize the human stomach as well, although causing milder pathologies. Thus, Cag-T4SS inhibitors are not expected to induce a bacterial clearance, and a life-time medication with the translocation inhibitor would be required for therapeutic treatment. However, combination therapies of antibiotics with T4SS inhibitors

could be imagined to increase the efficacy of antibiotics as well as to decrease resistance development. Various highly specific *H. pylori* respiratory chain inhibitors were identified using the screening method described in this thesis, and the validity of these possibly novel antibiotics will be discussed in the next section.

4. The *H. pylori* respiratory chain: a potential drug target?

During the screenings for a CagA translocation inhibitor, various compounds were discovered, which exerted specific and efficient inhibition of *H. pylori* growth, presumably by inhibiting respiration. This section discusses whether these compounds could serve as novel specific anti-*H. pylori* antibiotics with respiration as target. For a better understanding, the *H. pylori* respiratory chain is briefly introduced (reviewed in [222, 270]), and a respective schematic is presented in Figure 44.

Bacterial respiratory chains are generally composed of different complexes that transfer electrons while pumping protons from the cytoplasm to the periplasm. In a first step, reduced substrates are oxidized via various membrane-bound or membrane-associated dehydrogenases. *H. pylori* possesses a dehydrogenase with homology to the mitochondrial complex I (NADH-ubiquinone oxidoreductase), the NDH-1 dehydrogenase. Despite a quinone reductase activity and a proton pumping function, NDH-1 lacks the region involved in oxidizing NADH, and the nature of the electron donor to NDH-1 has yet to be identified. Accordingly, the complex is rotenone-insensitive for NADH oxidation, but Nagata *et al.* showed that the overall respiration was sensitive to rotenone, indicating a rotenone-sensitive complex I-like structure in *H. pylori* [223]. Interestingly, *H. pylori* exhibits higher respiration rates for NADPH than NADH, suggesting NADPH as the physiological electron donor, from which electrons might be transferred via an intermediate to the respiratory chain. Recent data also suggests flavodoxin as the main reductive equivalent [271]. Moreover, *H. pylori* possesses an integral Ni-Fe-type hydrogenase (Hyd) which extracts electrons from molecular hydrogen, and various further dehydrogenases (Dehyd), e.g. a D-lactate dehydrogenase, malate-quinone dehydrogenase, or the recently identified D-amino-acid dehydrogenase [272, 273]. From all these (de)hydrogenases, reducing equivalents are fed into the quinone pool, which is located in the lipid bilayer of the inner membrane and consists exclusively of menaquinone-6 in *H. pylori*. Electrons are then transferred via intermediate electron carriers, the integral cytochrome bc_1 complex and the periplasmic cytochrome c_{553}, to a single terminal *cb* (*cbb*$_3$)-type cytochrome c oxidase, for which oxygen is the electron acceptor. Accordingly,

H. pylori is an obligate microaerophilic bacterium. However, there is also evidence for anaerobic respiration with a fumarate reductase (Frd) catalyzing electron transfer from menaquinone to fumarate as terminal acceptor. In addition, *H. pylori* encodes a cytochrome c_{551} peroxidase and S- or N-oxide reductases, indicating hydrogen peroxide and N- or S-oxides, respectively, as further terminal electron acceptors (not depicted in Figure 44). The established proton gradient across the inner membrane, the proton motive force (PMF), is converted via an F_0F_1-ATP synthase into ATP (oxidative phosphorylation). Notably, when *H. pylori* is exposed to the low stomach pH, the periplasmic pH is strictly regulated and buffered by urease activity to a pH of 6.2. This allows *H. pylori* to maintain an optimum pH gradient across the membrane and preserve the essential PMF [274].

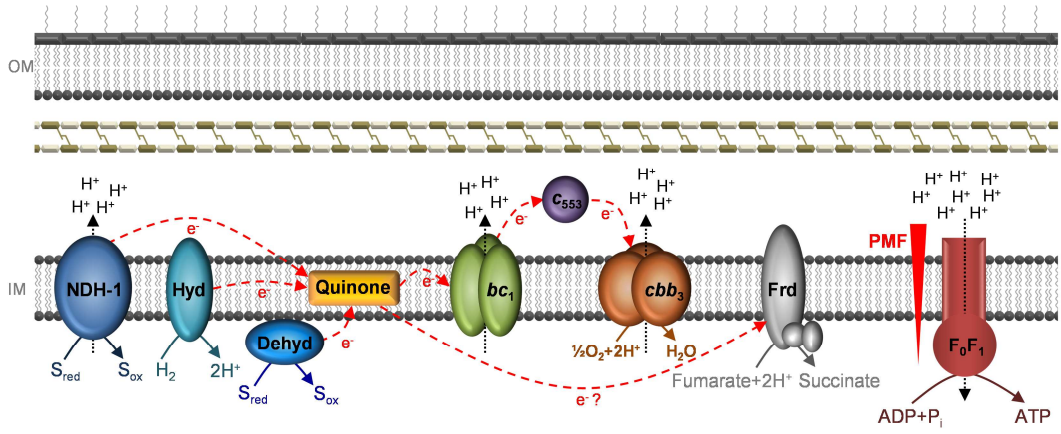

Figure 44: Overview of the *H. pylori* respiratory chain
Dashed red arrows depict electron flow, dashed black arrows the proton flow. bc_1: cytochrome bc_1 complex, c_{553}: cytochrome c_{553}, cbb_3: *cb*-type cytochrome *c* oxidase, Dehyd: dehydrogenase, F_0F_1: F_0F_1-ATP synthase, Frd: fumarate reductase, Hyd: Ni-Fe-type hydrogenase, IM: inner membrane, NDH-1: NADH-ubiquinone-like oxidoreductase complex, OM: outer membrane, PMF: proton motive force. Adapted from [222, 270].

Within this work, several efforts were made to confirm the action of various compounds on *H. pylori* respiration. These included determination of their impact on the PMF (measured as membrane potential), the bacterial ATP content, as well as oxygen consumption in response to the substances. As concentrations for *H. pylori* growth inhibition correlated with those detected for effects on respiration, a specific inhibition of the respiratory chain was assumed. In addition, many of these compounds exhibited a specific growth inhibition of *H. pylori*, but did not affect growth of *E. coli*, *S. aureus* or *C. jejuni*. Besides natural compounds derived from myxobacteria (NCL-1a, aurachins, cruentaren A, icumazole A, pellasoren A and thiangazoles) also partially uncharacterized chemically synthesized compounds derived from the SPECS library (SLH4, SLH6 and SLH8) were discovered to target *H. pylori* respiration. Most of the myxobacterial products were described earlier as respiration inhibitors, and more efficient in inhibiting *H. pylori* respiration than the chemically synthesized compounds. This

is in line with expectations, as compounds derived from myxobacteria are known for their bioactivities in the nanomolar range, and an important source for potent lead structures in drug discovery [207]. The work presented here is not the first study which reports on respiration inhibition of *H. pylori*. For example, Nagata *et al.* demonstrated inhibition of respiration by the proton pump inhibitor lansoprazole in a similar action to rotenone [223]. Additionally, a preceding study showed a specific inhibition of *H. pylori* by lansoprazole and analogues while 27 further bacterial species were not affected [275], which is in accordance with the inhibitory pattern detected for the respiration inhibitors here. But why does *H. pylori* exhibit such a high sensitivity towards respiration inhibitors? Unusually for a bacterium, *H. pylori* possesses a rather simple respiratory chain and a single terminal oxidase, whereas most aerobic or microaerophilic bacteria contain branched respiratory chains with a variety of electron donors and alternative electron acceptors [222, 270, 276]. The overall arrangement of the *H. pylori* respiratory chain is very similar to mitochondrial respiration. As mentioned above, *H. pylori* possesses a rotenone-sensitive NDH-1 dehydrogenase which is a homologue to the mitochondrial complex I. In contrast, other bacteria encode up to three different types of such NADH dehydrogenases. The complex III-like cytochrome bc_1 complex is sensitive for antimycin A, which targets mitochondrial complex III as well, and further pinpoints a similarity. The only terminal oxidase of *H. pylori* is related to mitochondrial complex IV, while other bacteria, e.g. *C. jejuni*, have additional terminal oxidases of classes specific for prokaryotic electron transport chains. This simple arrangement and homology to mitochondrial respiration might be the reason, why *H. pylori* turned out to be highly sensitive to (eukaryotic) respiration inhibitors during this work. In addition, *H. pylori* exhibited a general sensitivity towards small compounds, and for example various antibiotics against gram-positive bacteria also influenced *H. pylori* growth. The relatively high *in vitro* susceptibility of *H. pylori*, compared even to closely related bacteria such as *Campylobacter* ssp., has been described earlier [277]. This high responsiveness might be due to various unspecific transport systems of *H. pylori*, which the bacterium presumably encodes to overcome its limited capacity for biosynthesis [28]. One descriptive example for this is rotenone, which inhibited *H. pylori* in a highly specific and efficient manner, while *E. coli* growth was not affected. Interestingly, rotenone has been shown to inhibit the purified complex I of *E. coli* [278]. This suggests that rotenone is not able to enter *E. coli* and reach its target. Furthermore it could be assumed, that the highly branched respiratory chain of *E. coli* can compensate for the blockage by rotenone while the rather simplified electron transfer of *H. pylori* cannot.

For most of the myxobacterial respiration inhibitors, a strong cytotoxic effect was described before. Finally, solely NCL-1a revealed a potential therapeutic window as a drug candidate, exhibiting a slight cytotoxicity, but with potent and specific action against *H. pylori* growth. Among the SPECS library hit compounds, SLH8 had the best inhibitory profile without a cytotoxic effect within the determined range and specific anti-*H. pylori* activity. For the chemically synthesized SPECS hits earlier descriptions on activities are lacking and preclude speculations on a defined target within the respiratory chain. The identified myxobacterial products were studied before, and hence, possible targets in *H. pylori* together with their therapeutic potential will be discussed next. The most promising compound, NCL-1a, was previously shown to inhibit mitochondrial complex I in the micromolar range, comparable to the cytotoxic activity against L929 mouse fibroblast within this study. In contrast, *H. pylori* respiration and growth was inhibited in the nanomolar range. Speculating that the substance also targets *H. pylori* NDH-1, it seems to do this with much higher effectivity than for mitochondrial complex I, which justifies the application of NCL-1a as a therapeutic inhibitor. In addition, NCL-1a specifically inhibited *H. pylori* growth with high efficiency, but did not affect the growth of other bacteria, although minor activities against fungi and gram-positive bacteria were previously reported. Also, various aurachins were characterized to have a major impact on *H. pylori* respiration. Aurachins exhibited not only strong anti-*H. pylori* effects, but also *S. aureus* growth was inhibited, which is in accordance with a prior study [215]. In addition, *C. jejuni* growth was influenced by aurachin A. Regarding the target, aurachins have been shown to inhibit mitochondrial and bacterial complex I, mitochondrial complex III in an antimycin-like manner as well as the bacterial *cb*-type cytochrome *c* terminal oxidase [216, 278, 279]. In the case of *H. pylori* all three complexes might be targeted by aurachins. Due to the rather unspecific effects and the variety of targets that seem to affect eukaryotic cells and other bacteria, aurachins were omitted as potential drug candidates. The class of thiangazoles specifically inhibited *H. pylori* within these studies, and a general inactivity against bacterial growth is known from prior studies [220]. Thiangazoles were reported to inhibit mitochondrial as well as purified bacterial complex I, and this blockage was at similar concentrations observed for *H. pylori* in the work presented here [220, 278]. Thus, an action on the *H. pylori* NDH-1 complex is likely. However, an application as a therapeutic drug is excluded because prior studies revealed an extremely high cytotoxicity due to mitochondrial inhibition in the nanomolar range [228, 229]. Interestingly, aurachins and thiangazoles, as described above for rotenone, have been shown to inhibit the complex I of *E. coli* [278], but also for these compounds, no growth inhibition of *E. coli* has been observed during this work

as well as in prior reports [215, 220]. This indicates, as for rotenone, that *H. pylori* seems to be more prone for substance uptake and/or fails in compensating the inhibition of complex I. The definition of a distinct target for icumazole A is rather speculative. Prior data ascribed an antifungal action to this compound, due to mitochondrial NADH oxidation inhibition [219], and here, a high efficiency against *H. pylori* growth as well as weak activities against *C. jejuni* and *S. aureus* were observed. Moreover, icumazole A exerted strong effects on CagA translocation when only cells were in contact with the compound (CELLapproach), which also implies a major activity against human cells. Hence, a rather conserved target within the respiratory chain might be responsible for the icumazole A effects, which excludes the substance as a potential drug. No specific mode of action has been described yet for pellasoren A. However, Jahns *et al.* discovered a highly cytotoxic activity against human colon cancer cells at nanomolar concentrations, comparable to those active against *H. pylori* respiration [221]. This indicates the same bacterial and mitochondrial target but restricts the usage of pellasoren A as an anti-infective at the same time. Cruentaren A was described earlier as a potent inhibitor of mitochondrial F_0F_1-ATP synthase, but restricted to eukaryotes because no effect on a purified *E. coli* F_0F_1-ATP synthase was observable [217, 218]. In contrast, the data presented here in fact indicates an inhibition of *H. pylori* F_0F_1-ATP synthase because cruentaren A drastically reduced the bacterial ATP concentration while the oxygen consumption, which is independent of ATP synthase activity, was not affected. Accordingly, IC_{50} values of mitochondrial F_0F_1-ATP synthase inhibition were in the same range as inhibition of *H. pylori* ATP content, which suggests a similarity of this component to those in mitochondria. Intriguingly, the membrane potential of *H. pylori* was also inhibited by cruentaren A. This suggests that the *H. pylori* F_0F_1-ATP synthase has an ATPase function, thus operating reversely as an ATP-driven proton pump as well. This seems reasonable, as a strict regulation of proton import and export in or from the periplasm is required to maintain the afore-mentioned pH homeostasis for PMF preservation in the acidic stomach niche [274]. Indeed, a functional F_0F_1-ATP synthase was reported to be essential for *H. pylori* for survival at low pH [280]. However, due to its high cytotoxic potential, cruentaren A has no drug potential [217, 218], and, in this study, exerted weak effects on *C. jejuni* and *S. aureus* as well.

According to the data presented here, inhibitors targeting *H. pylori* respiration often exerted major effects on human respiration due to a similar electron transport chain arrangement. Thus, the question arises whether the respiratory chain is a suitable therapeutic target at all. Potential targets of *H. pylori* antimicrobials have to fulfill four requirements: they have to be

essential *in vivo*, constitutively expressed, present in all strains and to have unique characteristics different from those of the host [281]. Respiration components match the first three preconditions, the latter reflects again the doubtful suitability of *H. pylori* respiration inhibition. Hence, drugs have to target either unique components or target the respiratory complexes at sites that differ from those in mitochondria. General suggestions for the inhibition of respiration in pathogenic bacteria are energetic machines where no mammalian homologue exists, such as NDH-2 (not encoded by *H. pylori*), cytochrome *bd* oxidase (not encoded by *H. pylori*), or a hydrogenase [276]. Indeed, as mentioned above, *H. pylori* possesses such a hydrogenase (HydABC), and H_2 oxidation is proposed to be responsible for a large proportion of electron flux through the respiratory chain [282]. Moreover, this hydrogenase is essential for virulence, further suggesting it as a potential drug target [276]. Another suitable target might be the putative terminal electron acceptor fumarate reductase (Frd), which has been shown to be essential for colonization of the mouse stomach and is absent in mitochondria [283]. Targeting the quinone pool or even inhibiting biosynthesis of menaquinones might be also a promising approach [276]. Accordingly, the quinone analogue ibedenone specifically inhibited *H. pylori* growth by acting on respiration [284]. As the inhibition of *H. pylori* was accompanied by ibedenone reduction, it was suggested that the analogue sequestrated electrons more efficiently than the intrinsic menaquinone. In this work, NCL-1a and SLH-8 constituted the most promising candidates with only minor cytotoxic effects. Although for NCL-1a an inhibition of the NDH-1 complex seems likely, the exact inhibitory activity of both compounds cannot be concluded from this data. Hence, further studies have to confirm a specific target, for example by examining the compound effects in a cell-free system with purified respiration complex components, as described elsewhere [273]. In addition, a metabolome analysis of *H. pylori* upon exposure to the inhibitors could be conducted. In this case, besides the elucidation of a distinct target, further insights in the rather understudied respiration of *H. pylori* might be obtained. Finally, an *in vivo* activity of NCL-1a and SLH8 against *H. pylori* should be verified.

New drug targets are urgently needed to address the emergence of drug-resistant *H. pylori* strains and the associated treatment failures. One major advantage of a specific respiration inhibition of *H. pylori* would be constituted by a decreased risk for resistance development. Antibiotic resistances often develop by mutation of the genes encoding the bacterial target, but it is challenging to modify the respiratory chain, as this functional entity has evolved to a high complexity. Accordingly, no resistances could be identified upon long-term exposure of aurachins and rotenone to *H. pylori* within this work (data not shown). In addition, potent

respiration inhibitors were found to specifically inhibit *H. pylori* with high efficiency, which might enable a preservation of the gut microbiota upon treatment. Although targeting *H. pylori* respiration is critical due to putative toxic effects, a prior study demonstrated that the quinone 1,4-di-hydroxy-2-naphthoic acid abolished *H. pylori* infection in mice without exerting adverse effects on the host [285]. This demonstrates that respiration inhibitors could be successfully applied for *H. pylori* eradication. Interestingly, bismuth compounds, which have been used in the bismuth quadruple therapy for decades, also exert an inhibition on *H. pylori* respiration [224]. Thus, respiration inhibitors might have been used for years for *H. pylori* treatment but only with minor attention.

5. Conclusion and Outlook

This work presents a novel Cag-T4SS reporter, the TEM-CagA assay, which allows fast, sensitive and quantitative analysis of CagA translocation. Applying this assay, the impact of partially uncharacterized Cag-T4SS components on the translocation rate was quantified, and the stabilizing effect of CagF on CagA reconfirmed. With respect to the signal recognition mechanism of CagA, it was shown that the C-terminal secretion signal is more dependent on a minimal length than on its amino acid composition for efficient recruitment by the Cag-T4SS. While an influence of utter N-terminal regions on CagA translocation was excluded, several internal N-terminal regions are of further importance for CagA delivery. It was demonstrated that CagA translocation is dependent on a functional protein synthesis machinery, and moreover, efficient CagA uptake is strongly influenced by active host cellular processes. Besides, the TEM-CagA assay was successfully applied for identification of specific CagA translocation inhibitors, which will serve as valuable tools to investigate T4SS-functionality, assembly and delivery mechanisms. Transfer of the TEM-CagA assay into animal models of infection will enable analysis of Cag-T4SS activity *in vivo*.

In addition, two novel strategies to treat *H. pylori* infection were investigated. First, two specific CagA translocation inhibitors were identified, which could prevent CagA-triggered carcinogenesis, and also hold the potential to block the T4SS-mediated spread of antibiotic resistances. Second, respiration inhibitors of *H. pylori* were discovered, which are promising future antibiotics due to their high and specific efficiency. Future studies have to further evaluate these hit candidates as therapeutic drugs, and an ultimate determination of an *in vivo* action against *H. pylori* infection would be a big step towards the usage as a new medication. Importantly, both approaches overcome the disadvantages of the current antibiotic treatment and would preserve the gut microbiota as well as exhibit a low risk for resistance

development. As *H. pylori* is the major risk factor for development of gastric cancer due to the oncogenic CagA activity and *H. pylori* eradication increasingly fails, new strategies to combat infection are urgently required. This work did not only contribute to basic research of Cag-T4SS activity, but also made promising steps towards future ways for treatment of *H. pylori* infection.

List of Abbreviations

*	*Denotes the addition of protease inhibitors to a buffer*
AF	Accessory factor
AlpA/B	Adherence associated lipoproteins A and B
AP	Alkaline phosphatase
APS	Ammonium peroxide sulfate
ATP	Adenosine triphosphate
BabA	Blood group antigen-binding adhesin
BB	Brucella broth
BB/FCS	BB supplemented with 10% FCS
BCIP	5-Bromo-4-chloro-3-indolyl phosphate
Beps	Bartonella-translocated effector proteins
BID	Bep intracellular delivery
bp	Base pair
cag	Cytotoxin-associated gene
CagA	Cytotoxin-associated gene product A
CagA-P	CagA phosphorylation
*cag*PAI	*cag* pathogenicity island
Cag-T4SS	Cag Type IV Secretion System
CBS	C-terminal binding sequence
CCCP	Carbonyl cyanide *m*-chlorophenyl hydrazone
CD	Cluster of differentiation
CEA / CEACAM	Carcinoembryonic antigen related cell adhesion molecule
cfu	Cell forming unit
CM	Cytoplasmic membrane
Cm^R	Chloramphenicol resistance
C-terminus	Carboxyl terminal end of a protein
ddH_2O	Ultrapure water
Dehyd	Dehydrogenase
dH_2O	Distilled water
$DiOC_2(3)$	3,3′-Diethyloxacarbocyanine iodide
DMEM	Dulbecco´s Modified Eagle media
DMSO	Dimethyl sulfoxide
DNA	Deoxyribonucleic acid
dNTP	Deoxynucleotide triphosphate
DPBS	Dulbecco's PBS without calcium and magnesium
EDTA	Ethylenediaminetetraacetic acid
ELISA	Enzyme Linked Immunosorbent Assay
EPIYA	Protein motif: glutamate-proline-isoleucine-tyrosine-alanine
Erm^R	Erythromycin resistance
FACS	Flow cytometry
FCS	Fetal calf serum
Frd	Fumarate reductase
FRET	Fluorescence Resonance Energy Transfer
FSC	Forward scatter
gDNA	Genomic DNA
GGT	γ-glutamyl transpeptidase
Gln	L-glutamine
GSK	Glycogen synthase kinase

HTS	High-throughput screening
Hyd	Ni-Fe-type hydrogenase
I-	Inner-
IC_{50}	Concentration for 50% inhibition
ID	Identifier
IgG	Immunoglobulin G
IL-8	Interleukin-8
IM	Inner membrane
IMC	Inner membrane complex
IP	Immunoprecipitation
Kan^R	Kanamycin resistance
kb	Kilo base
kDa	Kilodalton
LB	Luria-Bertani broth
Le^b	Lewis b
LJ	Left junction
LPS	Lipopolysaccharide
M	Molar, mol/L
MALT	Mucosa-associated lymphoid tissue
MFI	Median fluorescence intensity
MIC	Minimal inhibitory concentration
MKI	MARK kinase inhibitor motif
MOI	Multiplicity of infection
MW	Molecular weight
NAD(P)H	Nicotinamide adenine dinucleotide (phosphate)
NBS	N-terminal binding sequence
NBT	Nitro blue tetrazolium
N-Terminus	Amino terminal end of a protein
O-	Outer-
OD_x	Optical density at a wavelength of x nm
OM	Outer membrane
OMC	Outer membrane complex
OMP	Outer membrane protein
PAGE	Polyacrylamide gel electrophoresis
PAMPs	Pathogen-associated molecular patterns
PBS	Phosphate-buffered saline
DPBS/FCS	DPBS supplemented with 10% FCS
PCR	Polymerase chain reaction
PG	Peptidoglycan
PI	Propidium iodide
PMF	Proton motive force
PMSF	Phenylmethylsulfonyl fluoride
PMT	Photomultiplier tube
POX	Horseradish peroxidase
PPI	Proton pump inhibitor
PRR	Pattern recognition receptors
PS	Phosphatidylserine
PTyr	Tyrosine phosphorylation
PVDF	Polyvinylidene fluoride
RE	Restriction enzyme

RGD	Protein motif: arginine, glycine, aspartate
RIPA	Radioimmunoprecipitation
RJ	Right junction
RLU	Relative light unit
RNA	Ribonucleic acid
rpm	Revolutions per minute
RT	Room temperature
S/B	Signal to background
S/N	Signal to noise
SA	Secretion apparatus component
SabA	Sialic acid-binding adhesin
SAP	Shrimp alkaline phosphatase
SC	Supportive component
SDS	Sodium dodecyl sulfate
SH-2	Src homology 2
SLB	Single layer β-sheet
sp.	Species
spp.	Species pluralis
SRK	Src family kinases
SSC	Side-scatter
ssp.	Subspecies
T3SS	Type III secretion system
T4SS	Type IV secretion system
TAE	Tris-acetate-EDTA
TBS(T)	Tris-buffered saline (with Tween)
TEM / TEM-1 / BlaM	*E. coli* β-lactamase
TEM-CagA	TEM-1 fused to the CagA protein
TEMED	Tetramethylethylenediamine
TF	Translocation factor
Th	T-helper
TLR	Toll-like receptor
TPEN	N,N,N',N'-tetrakis(2-pyridylmethyl) ethylenediamine
Tris	Tris(hydroxymethyl)aminomethane
UV	Ultraviolet
v/v	Volume to volume ratio
VacA	Vacuolating cytotoxin A
WB	Immunoblot/Western blot(ting)
w/v	Weight to volume ratio
wt	Wild-type
x g	x-fold gravitational acceleration
Yops	*Yersinia* outer proteins
α	Anti
Δ	Deletion *or* difference

List of Figures

List of Tables

Literature

1. Warren JR & Marshall B (1983) Unidentified curved bacilli on gastric epithelium in active chronic gastritis. *Lancet* 321(8336):1273-1275.
2. Marshall B & Warren JR (1984) Unidentified curved bacilli in the stomach of patients with gastritis and peptic ulceration. *Lancet* 323(8390):1311-1315.
3. Marshall BJ, Armstrong JA, McGechie DB, & Glancy RJ (1985) Attempt to fulfil Koch's postulates for pyloric *Campylobacter*. *Med J Aust* 142(8):436-439.
4. Brown LM (2000) *Helicobacter pylori*: epidemiology and routes of transmission. *Epidemiol Rev* 22(2):283-297.
5. Malaty HM (2007) Epidemiology of *Helicobacter pylori* infection. *Best Pract Res Clin Gastroenterol* 21(2):205-214.
6. Falush D*, et al.* (2003) Traces of human migrations in *Helicobacter pylori* populations. *Science* 299(5612):1582-1585.
7. Moodley Y*, et al.* (2012) Age of the association between *Helicobacter pylori* and man. *PLoS pathog* 8(5):e1002693.
8. Linz B*, et al.* (2007) An African origin for the intimate association between humans and *Helicobacter pylori*. *Nature* 445(7130):915-918.
9. Dixon MF (2001) Pathology of gastritis and peptic ulceration. In: *Helicobacter pylori*: physiology and genetics, ed Mobley HLT, Mendz GL & Hazell SL. *Washington (DC): ASM Press* Chapter 38.
10. Dooley CP*, et al.* (1989) Prevalence of *Helicobacter pylori* infection and histologic gastritis in asymptomatic persons. *N Engl J Med* 321(23):1562-1566.
11. Suerbaum S & Michetti P (2002) *Helicobacter pylori* infection. *N Engl J Med* 347(15):1175-1186.
12. El-Omar EM*, et al.* (2000) Interleukin-1 polymorphisms associated with increased risk of gastric cancer. *Nature* 404(6776):398-402.
13. Blaser MJ & Atherton JC (2004) *Helicobacter pylori* persistence: biology and disease. *J Clin Invest* 113(3):321-333.
14. Atherton JC & Blaser MJ (2009) Coadaptation of *Helicobacter pylori* and humans: ancient history, modern implications. *J Clin Invest* 119(9):2475-2487.
15. Wotherspoon A*, et al.* (1993) Regression of primary low-grade B-cell gastric lymphoma of mucosa-associated lymphoid tissue type after eradication of *Helicobacter pylori*. *Lancet* 342(8871):575-577.
16. Atherton JC (2006) The pathogenesis of *Helicobacter pylori*-induced gastro-duodenal diseases. *Annu Rev Pathol* 1(1):63-96.
17. Plummer M, Franceschi S, Vignat J, Forman D, & de Martel C (2015) Global burden of gastric cancer attributable to *Helicobacter pylori*. *Int J Cancer* 136(2):487-490.
18. Peek RM & Blaser MJ (2002) *Helicobacter pylori* and gastrointestinal tract adenocarcinomas. *Nat Rev Cancer* 2(1):28-37.
19. Fox JG & Wang TC (2007) Inflammation, atrophy, and gastric cancer. *J Clin Invest* 117(1):60-69.
20. Leung W*, et al.* (2004) Factors predicting progression of gastric intestinal metaplasia: results of a randomised trial on *Helicobacter pylori* eradication. *Gut* 53(9):1244-1249.
21. Hansson L-E*, et al.* (1996) The risk of stomach cancer in patients with gastric or duodenal ulcer disease. *N Engl J Med* 335(4):242-249.
22. Torre LA*, et al.* (2015) Global cancer statistics, 2012. *CA Cancer J Clin* 65(2):87-108.
23. Parsonnet J*, et al.* (1991) *Helicobacter pylori* infection and the risk of gastric carcinoma. *N Engl J Med* 325(16):1127-1131.
24. Uemura N*, et al.* (2001) *Helicobacter pylori* infection and the development of gastric cancer. *N Engl J Med* 345(11):784-789.
25. IARC Working Group on the Evaluation of Carcinogenic Risks to Humans (2012) Biological agents. Volume 100 B. A review of human carcinogens. *IARC Monogr Eval Carcinog Risks Hum* 100(Pt B):1-441.
26. Wroblewski LE, Peek RM, & Wilson KT (2010) *Helicobacter pylori* and gastric cancer: factors that modulate disease risk. *Clin Microbiol Rev* 23(4):713-739.
27. Cover TL (2016) *Helicobacter pylori* diversity and gastric cancer risk. *MBio* 7(1):e01869-15.
28. Tomb J-F*, et al.* (1997) The complete genome sequence of the gastric pathogen *Helicobacter pylori*. *Nature* 388(6642):539-547.

29. Kavermann H, *et al.* (2003) Identification and characterization of *Helicobacter pylori* genes essential for gastric colonization. *J Exp Med* 197(7):813-822.
30. Baldwin DN, *et al.* (2007) Identification of *Helicobacter pylori* genes that contribute to stomach colonization. *Infect Immun* 75(2):1005-1016.
31. Salama NR, Hartung ML, & Muller A (2013) Life in the human stomach: persistence strategies of the bacterial pathogen *Helicobacter pylori*. *Nat Rev Micro* 11(6):385-399.
32. Marshall B, Barrett L, Prakash C, McCallum R, & Guerrant R (1990) Urea protects *Helicobacter* (*Campylobacter*) *pylori* from the bactericidal effect of acid. *Gastroenterology* 99(3):697-702.
33. Celli JP, *et al.* (2009) *Helicobacter pylori* moves through mucus by reducing mucin viscoelasticity. *Proc Natl Acad Sci U S A* 106(34):14321-14326.
34. Sycuro LK, *et al.* (2012) Multiple peptidoglycan modification networks modulate *Helicobacter pylori*'s cell shape, motility, and colonization potential. *PLoS Pathog* 8(3):e1002603.
35. Eaton K, Suerbaum S, Josenhans C, & Krakowka S (1996) Colonization of gnotobiotic piglets by *Helicobacter pylori* deficient in two flagellin genes. *Infect Immun* 64(7):2445-2448.
36. Ottemann KM & Lowenthal AC (2002) *Helicobacter pylori* uses motility for initial colonization and to attain robust infection. *Infect Immun* 70(4):1984-1990.
37. Schreiber S, *et al.* (2005) Rapid loss of motility of *Helicobacter pylori* in the gastric lumen *in vivo*. *Infect Immun* 73(3):1584-1589.
38. Terry K, Williams SM, Connolly L, & Ottemann KM (2005) Chemotaxis plays multiple roles during *Helicobacter pylori* animal infection. *Infect Immun* 73(2):803-811.
39. Schreiber S, *et al.* (2004) The spatial orientation of *Helicobacter pylori* in the gastric mucus. *Proc Natl Acad Sci U S A* 101(14):5024-5029.
40. Rolig AS, Shanks J, Carter JE, & Ottemann KM (2012) *Helicobacter pylori* requires TlpD-driven chemotaxis to proliferate in the antrum. *Infect Immun* 80(10):3713-3720.
41. Aihara E, *et al.* (2014) Motility and chemotaxis mediate the preferential colonization of gastric injury sites by *Helicobacter pylori*. *PLoS Pathog* 10(7):e1004275.
42. Alm RA, Bina J, Andrews BM, Doig P, & Hancock RE (2000) Comparative genomics of *Helicobacter pylori*: analysis of the outer membrane protein families. *Infect Immun* 68(7):4155-4168.
43. Ilver D, *et al.* (1998) *Helicobacter pylori* adhesin binding fucosylated histo-blood group antigens revealed by retagging. *Science* 279(5349):373-377.
44. Odenbreit S, Till M, Hofreuter D, Faller G, & Haas R (1999) Genetic and functional characterization of the *alpAB* gene locus essential for the adhesion of *Helicobacter pylori* to human gastric tissue. *Mol Microbiol* 31(5):1537-1548.
45. Senkovich OA, *et al.* (2011) *Helicobacter pylori* AlpA and AlpB bind host laminin and influence gastric inflammation in gerbils. *Infect Immun* 79(8):3106-3116.
46. Lu H, *et al.* (2007) Functional and intracellular signaling differences associated with the *Helicobacter pylori* AlpAB adhesin from Western and East Asian strains. *J Biol Chem* 282(9):6242-6254.
47. Mahdavi J, *et al.* (2002) *Helicobacter pylori* SabA adhesin in persistent infection and chronic inflammation. *Science* 297(5581):573-578.
48. Rossez Y, *et al.* (2014) The lacdiNAc specific adhesin LabA mediates adhesion of *Helicobacter pylori* to human gastric mucosa. *J Infect Dis* 210(8):1286-1295.
49. Suerbaum S & Josenhans C (2007) *Helicobacter pylori* evolution and phenotypic diversification in a changing host. *Nat Rev Micro* 5(6):441-452.
50. Suerbaum S, *et al.* (1998) Free recombination within *Helicobacter pylori*. *Proc Natl Acad Sci U S A* 95(21):12619-12624.
51. Baltrus DA, Guillemin K, & Phillips PC (2008) Natural transformation increases the rate of adaptation in the human pathogen *Helicobacter pylori*. *Evolution* 62(1):39-49.
52. Israel DA, *et al.* (2001) *Helicobacter pylori* genetic diversity within the gastric niche of a single human host. *Proc Natl Acad Sci U S A* 98(25):14625-14630.
53. Solnick JV, Hansen LM, Salama NR, Boonjakuakul JK, & Syvanen M (2004) Modification of *Helicobacter pylori* outer membrane protein expression during experimental infection of rhesus macaques. *Proc Natl Acad Sci U S A* 101(7):2106-2111.
54. Talarico S, Whitefield SE, Fero J, Haas R, & Salama NR (2012) Regulation of *Helicobacter pylori* adherence by gene conversion. *Mol Microbiol* 84(6):1050-1061.
55. Perez-Perez GI, Dworkin BM, Chodos JE, & Blaser MJ (1988) *Campylobacter pylori* antibodies in humans. *Ann Intern Med* 109(1):11-17.

56. Moran AP, Lindner B, & Walsh EJ (1997) Structural characterization of the lipid A component of *Helicobacter pylori* rough-and smooth-form lipopolysaccharides. *J Bacteriol* 179(20):6453-6463.
57. Cullen TW, *et al.* (2011) *Helicobacter pylori* versus the host: remodeling of the bacterial outer membrane is required for survival in the gastric mucosa. *PLoS Pathog* 7(12):e1002454.
58. Andersen-Nissen E, *et al.* (2005) Evasion of Toll-like receptor 5 by flagellated bacteria. *Proc Natl Acad Sci U S A* 102(26):9247-9252.
59. Rad R, *et al.* (2009) Extracellular and intracellular pattern recognition receptors cooperate in the recognition of *Helicobacter pylori*. *Gastroenterology* 136(7):2247-2257.
60. Cover TL & Blanke SR (2005) *Helicobacter pylori* VacA, a paradigm for toxin multifunctionality. *Nat Rev Microbiol* 3(4):320-332.
61. Boquet P & Ricci V (2012) Intoxication strategy of *Helicobacter pylori* VacA toxin. *Trends Microbiol* 20(4):165-174.
62. Cover TL & Blaser M (1992) Purification and characterization of the vacuolating toxin from *Helicobacter pylori*. *J Biol Chem* 267(15):10570-10575.
63. Szabò I, *et al.* (1999) Formation of anion-selective channels in the cell plasma membrane by the toxin VacA of *Helicobacter pylori* is required for its biological activity. *EMBO J* 18(20):5517-5527.
64. Cover TL, Krishna US, Israel DA, & Peek RM (2003) Induction of gastric epithelial cell apoptosis by *Helicobacter pylori* vacuolating cytotoxin. *Cancer Res* 63(5):951-957.
65. Zheng PY & Jones NL (2003) *Helicobacter pylori* strains expressing the vacuolating cytotoxin interrupt phagosome maturation in macrophages by recruiting and retaining TACO (coronin 1) protein. *Cell Microbiol* 5(1):25-40.
66. Molinari M, *et al.* (1998) Selective inhibition of Ii-dependent antigen presentation by *Helicobacter pylori toxin* VacA. *J Exp Med* 187(1):135-140.
67. Sewald X, *et al.* (2008) Integrin subunit CD18 is the T-lymphocyte receptor for the *Helicobacter pylori* vacuolating cytotoxin. *Cell Host Microbe* 3(1):20-29.
68. Gebert B, Fischer W, Weiss E, Hoffmann R, & Haas R (2003) *Helicobacter pylori* vacuolating cytotoxin inhibits T lymphocyte activation. *Science* 301(5636):1099-1102.
69. Schmees C, *et al.* (2007) Inhibition of T-cell proliferation by *Helicobacter pylori* γ-glutamyl transpeptidase. *Gastroenterology* 132(5):1820-1833.
70. Wüstner S, *et al.* (2015) *Helicobacter pylori* γ-glutamyltranspeptidase impairs T-lymphocyte function by compromising metabolic adaption through inhibition of cMyc and IRF4 expression. *Cell Microbiol* 17(1):51-61.
71. Oertli M, *et al.* (2013) *Helicobacter pylori* γ-glutamyl transpeptidase and vacuolating cytotoxin promote gastric persistence and immune tolerance. *Proc Natl Acad Sci U S A* 110(8):3047-3052.
72. Yokoyama K, *et al.* (2005) Functional antagonism between *Helicobacter pylori* CagA and vacuolating toxin VacA in control of the NFAT signaling pathway in gastric epithelial cells. *Proc Natl Acad Sci U S A* 102(27):9661-9666.
73. Oldani A, *et al.* (2009) *Helicobacter pylori* counteracts the apoptotic action of its VacA toxin by injecting the CagA protein into gastric epithelial cells. *PLoS Pathog* 5(10):e1000603.
74. Odenbreit S, *et al.* (2000) Translocation of *Helicobacter pylori* CagA into gastric epithelial cells by type IV secretion. *Science* 287(5457):1497-1500.
75. Stein M, Rappuoli R, & Covacci A (2000) Tyrosine phosphorylation of the *Helicobacter pylori* CagA antigen after *cag*-driven host cell translocation. *Proc Natl Acad Sci U S A* 97(3):1263-1268.
76. Backert S, *et al.* (2000) Translocation of the *Helicobacter pylori* CagA protein in gastric epithelial cells by a type IV secretion apparatus. *Cell Microbiol* 2(2):155-164.
77. Alvarez-Martinez CE & Christie PJ (2009) Biological diversity of prokaryotic type IV secretion systems. *Microbiol Mol Biol Rev* 73(4):775-808.
78. Fischer W, *et al.* (2010) Strain-specific genes of *Helicobacter pylori*: genome evolution driven by a novel type IV secretion system and genomic island transfer. *Nucleic Acids Res* 38(18):6089-6101.
79. Hofreuter D, Odenbreit S, & Haas R (2001) Natural transformation competence in *Helicobacter pylori* is mediated by the basic components of a type IV secretion system. *Mol Microbiol* 41(2):379-391.
80. Llosa M, Roy C, & Dehio C (2009) Bacterial type IV secretion systems in human disease. *Mol Microbiol* 73(2):141-151.
81. Bhatty M, Laverde Gomez JA, & Christie PJ (2013) The expanding bacterial type IV secretion lexicon. *Res Microbiol* 164(6):620-639.

82. Christie PJ, Whitaker N, & González-Rivera C (2014) Mechanism and structure of the bacterial type IV secretion systems. *Biochim Biophys Acta* 1843(8):1578-1591.
83. Cascales E & Christie PJ (2004) Definition of a bacterial type IV secretion pathway for a DNA substrate. *Science* 304(5674):1170-1173.
84. Chandran V*, et al.* (2009) Structure of the outer membrane complex of a type IV secretion system. *Nature* 462(7276):1011-1015.
85. Fronzes R*, et al.* (2009) Structure of a type IV secretion system core complex. *Science* 323(5911):266-268.
86. Low HH*, et al.* (2014) Structure of a type IV secretion system. *Nature* 508(7497):550-553.
87. Fischer W (2011) Assembly and molecular mode of action of the *Helicobacter pylori* Cag type IV secretion apparatus. *FEBS J* 278(8):1203-1212.
88. Backert S, Tegtmeyer N, & Fischer W (2015) Composition, structure and function of the *Helicobacter pylori cag* pathogenicity island encoded type IV secretion system. *Future Microbiol* 10(6):955-965.
89. Censini S*, et al.* (1996) *cag*, a pathogenicity island of *Helicobacter pylori*, encodes type I-specific and disease-associated virulence factors. *Proc Natl Acad Sci U S A* 93(25):14648-14653.
90. Olbermann P*, et al.* (2010) A global overview of the genetic and functional diversity in the *Helicobacter pylori cag* pathogenicity island. *PLoS Genet* 6(8):e1001069.
91. Terradot L & Waksman G (2011) Architecture of the *Helicobacter pylori* Cag-type IV secretion system. *FEBS J* 278(8):1213-1222.
92. Aras RA*, et al.* (2003) Plasticity of repetitive DNA sequences within a bacterial (type IV) secretion system component. *J Exp Med* 198(9):1349-1360.
93. Kutter S*, et al.* (2008) Protein subassemblies of the *Helicobacter pylori* Cag type IV secretion system revealed by localization and interaction studies. *J Bacteriol* 190(6):2161-2171.
94. Busler VJ*, et al.* (2006) Protein-protein interactions among *Helicobacter pylori* Cag proteins. *J Bacteriol* 188(13):4787-4800.
95. Jurik A*, et al.* (2010) The coupling protein Cagβ and its interaction partner CagZ are required for type IV secretion of the *Helicobacter pylori* CagA protein. *Infect Immun* 78(12):5244-5251.
96. Savvides SN*, et al.* (2003) VirB11 ATPases are dynamic hexameric assemblies: new insights into bacterial type IV secretion. *EMBO J* 22(9):1969-1980.
97. Buhrdorf R, Förster C, Haas R, & Fischer W (2003) Topological analysis of a putative *virB8* homologue essential for the *cag* type IV secretion system in *Helicobacter pylori*. *Int J Med Microbiol* 293(2):213-217.
98. Gopal GJ, Pal J, Kumar A, & Mukhopadhyay G (2015) C-terminal domain of CagX is responsible for its interaction with CagT protein of *Helicobacter pylori* type IV secretion system. *Biochem Biophys Res Commun* 456(1):98-103.
99. Pinto-Santini DM & Salama NR (2009) Cag3 is a novel essential component of the *Helicobacter pylori* Cag type IV secretion system outer membrane subcomplex. *J Bacteriol* 191(23):7343-7352.
100. Frick-Cheng AE*, et al.* (2016) Molecular and structural analysis of the *Helicobacter pylori cag* type IV secretion system core complex. *MBio* 7(1):e02001-15.
101. Rohde M, Puls J, Buhrdorf R, Fischer W, & Haas R (2003) A novel sheathed surface organelle of the *Helicobacter pylori cag* type IV secretion system. *Mol Microbiol* 49(1):219-234.
102. Tanaka J, Suzuki T, Mimuro H, & Sasakawa C (2003) Structural definition on the surface of *Helicobacter pylori* type IV secretion apparatus. *Cell Microbiol* 5(6):395-404.
103. Shaffer CL*, et al.* (2011) *Helicobacter pylori* exploits a unique repertoire of type IV secretion system components for pilus assembly at the bacteria-host cell interface. *PLoS pathog* 7(9):e1002237.
104. Andrzejewska J*, et al.* (2006) Characterization of the pilin ortholog of the *Helicobacter pylori* type IV *cag* pathogenicity apparatus, a surface-associated protein expressed during infection. *J Bacteriol* 188(16):5865-5877.
105. Johnson EM, Gaddy JA, Voss BJ, Hennig EE, & Cover TL (2014) Genes required for assembly of pili associated with the *Helicobacter pylori cag* type IV secretion system. *Infect Immun* 82(8):3457-3470.
106. Pham KT*, et al.* (2012) CagI is an essential component of the *Helicobacter pylori* Cag type IV secretion system and forms a complex with CagL. *PLoS One* 7(4):e35341.
107. Zahrl D*, et al.* (2005) Peptidoglycan degradation by specialized lytic transglycosylases associated with type III and type IV secretion systems. *Microbiology* 151(Pt 11):3455-3467.

108. Bourzac KM, Satkamp LA, & Guillemin K (2006) The *Helicobacter pylori cag* pathogenicity island protein CagN is a bacterial membrane-associated protein that is processed at its C terminus. *Infect Immun* 74(5):2537-2543.

109. Gorrell RJ, *et al.* (2013) A novel NOD1-and CagA-independent pathway of interleukin-8 induction mediated by the *Helicobacter pylori* type IV secretion system. *Cell Microbio* 15(4):554-70.

110. Guillemin K, Salama NR, Tompkins LS, & Falkow S (2002) *Cag* pathogenicity island-specific responses of gastric epithelial cells to *Helicobacter pylori* infection. *Proc Natl Acad Sci U S A* 99(23):15136-15141.

111. Viala J, *et al.* (2004) Nod1 responds to peptidoglycan delivered by the *Helicobacter pylori cag* pathogenicity island. *Nat Immunol* 5(11):1166-1174.

112. Kaparakis M, *et al.* (2010) Bacterial membrane vesicles deliver peptidoglycan to NOD1 in epithelial cells. *Cell Microbio* 12(3):372-385.

113. Kwok T, *et al.* (2007) *Helicobacter* exploits integrin for type IV secretion and kinase activation. *Nature* 449(7164):862-866.

114. Jiménez-Soto LF, *et al.* (2009) *Helicobacter pylori* type IV secretion apparatus exploits β1 integrin in a novel RGD-independent manner. *PLoS pathog* 5(12):e1000684.

115. Fischer W, *et al.* (2001) Systematic mutagenesis of the *Helicobacter pylori cag* pathogenicity island: essential genes for CagA translocation in host cells and induction of interleukin-8. *Mol Microbiol* 42(5):1337-1348.

116. Selbach M, Moese S, Meyer TF, & Backert S (2002) Functional analysis of the *Helicobacter pylori cag* pathogenicity island reveals both VirD4-CagA-dependent and VirD4-CagA-independent mechanisms. *Infect Immun* 70(2):665-671.

117. Cendron L, *et al.* (2009) The *Helicobacter pylori* CagD (HP0545, Cag24) protein is essential for CagA translocation and maximal induction of interleukin-8 secretion. *J Mol Biol* 386(1):204-217.

118. Couturier MR, Tasca E, Montecucco C, & Stein M (2006) Interaction with CagF is required for translocation of CagA into the host via the *Helicobacter pylori* type IV Secretion System. *Infect Immun* 74(1):273-281.

119. Pattis I, Weiss E, Laugks R, Haas R, & Fischer W (2007) The *Helicobacter pylori* CagF protein is a type IV secretion chaperone-like molecule that binds close to the C-terminal secretion signal of the CagA effector protein. *Microbiology* 153(Pt 9):2896-2909.

120. Bonsor DA, *et al.* (2013) Characterization of the translocation-competent complex between the *Helicobacter pylori* oncogenic protein CagA and the accessory protein CagF. *J Biol Chem* 288(46):32897-32909.

121. Sharma CM, *et al.* (2010) The primary transcriptome of the major human pathogen *Helicobacter pylori*. *Nature* 464(7286):250-255.

122. Vannini A, Roncarati D, & Danielli A (2016) The *cag*-pathogenicity island encoded CncR1 sRNA oppositely modulates *Helicobacter pylori* motility and adhesion to host cells. *Cell Mol Life Sci* 73(16):3151-3168.

123. Shaffer CL, *et al.* (2016) Peptidomimetic small molecules disrupt type IV secretion system activity in diverse bacterial pathogens. *MBio* 7(2):e00221-16.

124. Belogolova E, *et al.* (2013) *Helicobacter pylori* outer membrane protein HopQ identified as a novel T4SS-associated virulence factor. *Cell Microbiol* 15(11):1896-1912.

125. Noto JM, *et al.* (2013) Iron deficiency accelerates *Helicobacter pylori*-induced carcinogenesis in rodents and humans. *J Clin Invest* 123(1):479-492.

126. Gaddy JA, *et al.* (2014) The host protein calprotectin modulates the *Helicobacter pylori cag* type IV secretion system via zinc sequestration. *PLoS Pathog* 10(10):e1004450.

127. Kaplan-Türköz B, *et al.* (2012) Structural insights into *Helicobacter pylori* oncoprotein CagA interaction with β1 integrin. *Proc Natl Acad Sci U S A* 109(36):14640-14645.

128. Barrozo RM, *et al.* (2013) Functional plasticity in the type IV secretion system of *Helicobacter pylori*. *PLoS Pathog* 9(2):e1003189.

129. Murata-Kamiya N, Kikuchi K, Hayashi T, Higashi H, & Hatakeyama M (2010) *Helicobacter pylori* exploits host membrane phosphatidylserine for delivery, localization, and pathophysiological action of the CagA oncoprotein. *Cell Host Microbe* 7(5):399-411.

130. Hayashi T, *et al.* (2012) Tertiary structure-function analysis reveals the pathogenic signaling potentiation mechanism of *Helicobacter pylori* oncogenic effector CagA. *Cell Host Microbe* 12(1):20-33.

131. Hohlfeld S, *et al.* (2006) A C-terminal translocation signal is necessary, but not sufficient for type IV secretion of the *Helicobacter pylori* CagA protein. *Mol Microbiol* 59(5):1624-1637.

132. Woon AP, *et al.* (2013) Conformational analysis of isolated domains of *Helicobacter pylori* CagA. *PLoS One* 8(11):e79367.

133. Stein M, Ruggiero P, Rappuoli R, & Bagnoli F (2013) *Helicobacter pylori* CagA: from pathogenic mechanisms to its use as an anti-cancer vaccine. *Front Immunol* 4:328.

134. Higashi H, *et al.* (2005) EPIYA motif is a membrane-targeting signal of *Helicobacter pylori* virulence factor CagA in mammalian cells. *J Biol Chem* 280(24):23130-23137.

135. Stein M, *et al.* (2002) c-Src/Lyn kinases activate *Helicobacter pylori* CagA through tyrosine phosphorylation of the EPIYA motifs. *Mol Microbiol* 43(4):971-980.

136. Tammer I, Brandt S, Hartig R, König W, & Backert S (2007) Activation of Abl by *Helicobacter pylori*: a novel kinase for CagA and crucial mediator of host cell scattering. *Gastroenterology* 132(4):1309-1319.

137. Hatakeyama M (2004) Oncogenic mechanisms of the *Helicobacter pylori* CagA protein. *Nat Rev Cancer* 4(9):688-694.

138. Higashi H, *et al.* (2002) Biological activity of the *Helicobacter pylori* virulence factor CagA is determined by variation in the tyrosine phosphorylation sites. *Proc Natl Acad Sci U S A* 99(22):14428-14433.

139. Argent RH, *et al.* (2004) Determinants and consequences of different levels of CagA phosphorylation for clinical isolates of *Helicobacter pylori*. *Gastroenterology* 127(2):514-523.

140. Basso D, *et al.* (2008) Clinical relevance of *Helicobacter pylori cagA* and *vacA* gene polymorphisms. *Gastroenterology* 135(1):91-99.

141. Ferreira RM, Machado JC, Leite M, Carneiro F, & Figueiredo C (2012) The number of *Helicobacter pylori* CagA EPIYA C tyrosine phosphorylation motifs influences the pattern of gastritis and the development of gastric carcinoma. *Histopathology* 60(6):992-998.

142. Higashi H, *et al.* (2002) SHP-2 tyrosine phosphatase as an intracellular target of *Helicobacter pylori* CagA protein. *Science* 295(5555):683-686.

143. Mohi MG & Neel BG (2007) The role of Shp2 (PTPN11) in cancer. *Curr Opin Genet Dev* 17(1):23-30.

144. Segal ED, Cha J, Lo J, Falkow S, & Tompkins LS (1999) Altered states: involvement of phosphorylated CagA in the induction of host cellular growth changes by *Helicobacter pylori*. *Proc Natl Acad Sci U S A* 96(25):14559-14564.

145. Suzuki M, *et al.* (2009) *Helicobacter pylori* CagA phosphorylation-independent function in epithelial proliferation and inflammation. *Cell Host Microbe* 5(1):23-34.

146. Saadat I, *et al.* (2007) *Helicobacter pylori* CagA targets PAR1/MARK kinase to disrupt epithelial cell polarity. *Nature* 447(7142):330-333.

147. Nešić D, *et al.* (2010) *Helicobacter pylori* CagA inhibits PAR1-MARK family kinases by mimicking host substrates. *Nat Struct Mol Biol* 17(1):130-132.

148. Tsang YH, *et al.* (2010) *Helicobacter pylori* CagA targets gastric tumor suppressor RUNX3 for proteasome-mediated degradation. *Oncogene* 29(41):5643-5650.

149. Nešić D, Buti L, Lu X, & Stebbins CE (2014) Structure of the *Helicobacter pylori* CagA oncoprotein bound to the human tumor suppressor ASPP2. *Proc Natl Acad Sci U S A* 111(4):1562-1567.

150. Backert S, Tegtmeyer N, & Selbach M (2010) The versatility of *Helicobacter pylori* CagA effector protein functions: the master key hypothesis. *Helicobacter* 15(3):163-176.

151. Graham DY, Lu H, & Yamaoka Y (2007) A report card to grade *Helicobacter pylori* therapy. *Helicobacter* 12(4):275-278.

152. Rieder G, Merchant JL, & Haas R (2005) *Helicobacter pylori cag*-type IV secretion system facilitates corpus colonization to induce precancerous conditions in Mongolian gerbils. *Gastroenterology* 128(5):1229-1242.

153. Franco AT, *et al.* (2008) Regulation of gastric carcinogenesis by *Helicobacter pylori* virulence factors. *Cancer Res* 68(2):379-387.

154. Ohnishi N, *et al.* (2008) Transgenic expression of *Helicobacter pylori* CagA induces gastrointestinal and hematopoietic neoplasms in mouse. *Proc Natl Acad Sci U S A* 105(3):1003-1008.

155. Neal JT, Peterson TS, Kent ML, & Guillemin K (2013) *H. pylori* virulence factor CagA increases intestinal cell proliferation by Wnt pathway activation in a transgenic zebrafish model. *Dis Model Mech* 6(3):802-810.

156. Blaser MJ, *et al.* (1995) Infection with *Helicobacter pylori* strains possessing *cagA* is associated with an increased risk of developing adenocarcinoma of the stomach. *Cancer Res* 55(10):2111-2115.
157. Parsonnet J, Friedman G, Orentreich N, & Vogelman H (1997) Risk for gastric cancer in people with CagA positive or CagA negative *Helicobacter pylori* infection. *Gut* 40(3):297-301.
158. Backert S, *et al.* (2004) Functional analysis of the *cag* pathogenicity island in *Helicobacter pylori* isolates from patients with gastritis, peptic ulcer, and gastric cancer. *Infect Immun* 72(2):1043-1056.
159. Correa P & Houghton J (2007) Carcinogenesis of *Helicobacter pylori*. *Gastroenterology* 133(2):659-672.
160. Malfertheiner P, *et al.* (2012) Management of *Helicobacter pylori* infection—the Maastricht IV/Florence consensus report. *Gut* 61(5):646-664.
161. Graham DY & Fischbach L (2010) *Helicobacter pylori* treatment in the era of increasing antibiotic resistance. *Gut* 59(8):1143-1153.
162. Megraud F, *et al.* (2013) *Helicobacter pylori* resistance to antibiotics in Europe and its relationship to antibiotic consumption. *Gut* 62(1):34-42.
163. Fallone CA, *et al.* (2016) The Toronto consensus for the treatment of *Helicobacter pylori* infection in adults. *Gastroenterology* 151(1):51-69.e14.
164. Zawahir S, Czinn SJ, Nedrud JG, & Blanchard TG (2013) Vaccinating against *Helicobacter pylori* in the developing world. *Gut microbes* 4(6):568-576.
165. Sutton P & Chionh YT (2013) Why can't we make an effective vaccine against *Helicobacter pylori*? *Expert Rev Vaccines* 12(4):433-441.
166. Arnold IC, Hitzler I, & Müller A (2012) The immunomodulatory properties of *Helicobacter pylori* confer protection against allergic and chronic inflammatory disorders. *Front Cell Infect Microbiol* 2:10.
167. Rasko DA & Sperandio V (2010) Anti-virulence strategies to combat bacteria-mediated disease. *Nat Rev Drug Discov* 9(2):117-128.
168. Heras B, Scanlon MJ, & Martin JL (2015) Targeting virulence not viability in the search for future antibacterials. *Br J Clin Pharmacol* 79(2):208-215.
169. Nägele V (2010) Funktionelle Charakterisierung trimerer Autotransporteradhäsine von *Neisseria meningitidis* (NadA) und *Yersinia enterocolitica* (YadA). *Dissertation Technische Universität München*.
170. Farnbacher M, *et al.* (2010) Sequencing, annotation, and comparative genome analysis of the gerbil-adapted *Helicobacter pylori* strain B8. *BMC genomics* 11(1):335.
171. Schmitt W & Haas R (1994) Genetic analysis of the *Helicobacter pylori* vacuolating cytotoxin: structural similarities with the IgA protease type of exported protein. *Mol Microbiol* 12(2):307-319.
172. Grant SG, Jessee J, Bloom FR, & Hanahan D (1990) Differential plasmid rescue from transgenic mouse DNAs into *Escherichia coli* methylation-restriction mutants. *Proc Natl Acad Sci U S A* 87(12):4645-4649.
173. Hanahan D (1983) Studies on transformation of *Escherichia coli* with plasmids. *J Mol Biol* 166(4):557-580.
174. Charpentier X & Oswald E (2004) Identification of the secretion and translocation domain of the enteropathogenic and enterohemorrhagic *Escherichia coli* effector Cif, using TEM-1 β-lactamase as a new fluorescence-based reporter. *J Bacteriol* 186(16):5486-5495.
175. Püls J, Fischer W, & Haas R (2002) Activation of *Helicobacter pylori* CagA by tyrosine phosphorylation is essential for dephosphorylation of host cell proteins in gastric epithelial cells. *Mol Microbiol* 43(4):961-969.
176. Obert S, O'Connor RJ, Schmid S, & Hearing P (1994) The adenovirus E4-6/7 protein transactivates the E2 promoter by inducing dimerization of a heteromeric E2F complex. *Mol Cell Biol* 14(2):1333-1346.
177. Fischer W & Haas R (2004) The RecA protein of *Helicobacter pylori* requires a posttranslational modification for full activity. *J Bacteriol* 186(3):777-784.
178. Sambrook J & Russell D (2001) Molecular cloning. A laboratory manual. *Cold Spring Harbor Laboratory Press*.
179. Haas R, Meyer TF, & Putten JP (1993) Aflagellated mutants of *Helicobacter pylori* generated by genetic transformation of naturally competent strains using transposon shuttle mutagenesis. *Mol Microbiol* 8(4):753-760.
180. Holmes DS & Quigley M (1981) A rapid boiling method for the preparation of bacterial plasmids. *Anal Biochem* 114(1):193-197.

181. Lundberg KS*, et al.* (1991) High-fidelity amplification using a thermostable DNA polymerase isolated from *Pyrococcus furiosus*. *Gene* 108(1):1-6.
182. Laemmli UK (1970) Cleavage of structural proteins during the assembly of the head of bacteriophage T4. *Nature* 227(5259):680-685.
183. Marshall T & Williams KM (1992) Recovery of protein by coomassie brilliant blue precipitation prior to electrophoresis. *Electrophoresis* 13(11):887-888.
184. Towbin H, Staehelin T, & Gordon J (1979) Electrophoretic transfer of proteins from polyacrylamide gels to nitrocellulose sheets: procedure and some applications. *Proc Natl Acad Sci U S A* 76(9):4350-4354.
185. Marketon MM, DePaolo RW, DeBord KL, Jabri B, & Schneewind O (2005) Plague bacteria target immune cells during infection. *Science* 309(5741):1739-1741.
186. de Felipe KS*, et al.* (2008) *Legionella* eukaryotic-like type IV substrates interfere with organelle trafficking. *PLoS pathog* 4(8):e1000117.
187. Naqvi T & Singh R (2007) A novel chemiluminescent substrate for detecting lactamase. *Mol Biosyst* 3(6):431-438.
188. Zechner EL, Lang S, & Schildbach JF (2012) Assembly and mechanisms of bacterial type IV secretion machines. *Philos Trans R Soc Lond B Biol Sci* 367(1592):1073-1087.
189. Brandt S, Kwok T, Hartig R, König W, & Backert S (2005) NF-κB activation and potentiation of proinflammatory responses by the *Helicobacter pylori* CagA protein. *Proc Natl Acad Sci U S A* 102(26):9300-9305.
190. Vergunst AC*, et al.* (2005) Positive charge is an important feature of the C-terminal transport signal of the VirB/D4-translocated proteins of *Agrobacterium*. *Proc Natl Acad Sci U S A* 102(3):832-837.
191. Huang L*, et al.* (2011) The E Block motif is associated with *Legionella pneumophila* translocated substrates. *Cell Microbio* 13(2):227-245.
192. Schindele F, Weiss E, Haas R, & Fischer W (2016) Quantitative analysis of CagA type IV secretion by *Helicobacter pylori* reveals substrate recognition and translocation requirements. *Mol Microbiol* 100(1):188-203.
193. Jiménez-Soto LF & Haas R (2016) The CagA toxin of *Helicobacter pylori*: abundant production but relatively low amount translocated. *Sci Rep* 6:23227.
194. Chimienti F, Seve M, Richard S, Mathieu J, & Favier A (2001) Role of cellular zinc in programmed cell death: temporal relationship between zinc depletion, activation of caspases, and cleavage of Sp family transcription factors. *Biochem Pharmacol* 62(1):51-62.
195. Noto JM*, et al.* (2014) Regulation of *Helicobacter pylori* virulence within the context of iron deficiency. *J Infect Dis* 211(11):1790-1794.
196. Rodal SK*, et al.* (1999) Extraction of cholesterol with methyl-β-cyclodextrin perturbs formation of clathrin-coated endocytic vesicles. *Mol Biol Cell* 10(4):961-974.
197. Lai CH*, et al.* (2008) Cholesterol depletion reduces *Helicobacter pylori* CagA translocation and CagA-induced responses in AGS cells. *Infect Immun* 76(7):3293-3303.
198. Selbach M, Moese S, Hauck CR, Meyer TF, & Backert S (2002) Src is the kinase of the *Helicobacter pylori* CagA protein *in vitro* and *in vivo*. *J Biol Chem* 277(9):6775-6778.
199. Bae EA, Han MJ, & Kim DH (2001) *In vitro* anti-*Helicobacter pylori* activity of irisolidone isolated from the flowers and rhizomes of *Pueraria thunbergiana*. *Planta Med* 67(2):161-163.
200. Zhang J-H, Chung TDY, & Oldenburg KR (1999) A simple statistical parameter for use in evaluation and validation of high throughput screening sssays. *J Biomol Screen* 4(2):67-73.
201. Taniguchi M*, et al.* (2002) YM-181741, a novel benz[a]anthraquinone antibiotic with anti-*Helicobacter pylori* activity from *Streptomyces* sp. *J Antibiot (Tokyo)* 55(1):30-35.
202. Sato K, Asao N, & Yamamoto Y (2005) Efficient method for synthesis of angucyclinone antibiotics via gold-catalyzed intramolecular [4+ 2] benzannulation: enantioselective total synthesis of (+)-ochromycinone and (+)-rubiginone B2. *J Org Chem* 70(22):8977-8981.
203. Elliott RL*, et al.* (1998) Anhydrolide macrolides. 1. Synthesis and antibacterial activity of 2, 3-anhydro-6-O-methyl 11, 12-carbamate erythromycin A analogues. *J Med Chem* 41(10):1651-1659.
204. Heilman W*, et al.* (1979) Stoffwechselprodukte von Mikroorganismen. 177. Mitteilung. Avilamycin C. *Helv Chim Acta* 62(1):1-6.
205. Zeeck A, Zähner H, & Mardin M (1974) Stoffwechselprodukte von Mikroorganismen, 129[1)] Isolierung und Konstitution der Isochromanchinon-Antibiotica β-und γ-Naphthocyclinon. *Justus Liebigs Ann Chem* 1974(7):1100-1125.

206. Gräfe U, *et al.* (1995) Aurantimycins, new depsipeptide antibiotics from *Streptomyces aurantiacus* IMET 43917. Production, isolation, structure elucidation, and biological activity. *J Antibiot (Tokyo)* 48(2):119-125.

207. Weissman KJ & Müller R (2010) Myxobacterial secondary metabolites: bioactivities and modes-of-action. *Nat Prod Rep* 27(9):1276-1295.

208. Sasse F, Kunze B, Gronewold TMA, & Reichenbach H (1998) The chondramides: cytostatic agents from myxobacteria acting on the actin cytoskeleton. *J Natl Cancer Inst* 90(20):1559-1563.

209. Jansen R, Kunze B, Reichenbach H, & Höfle G (1996) Chondramides A–D, new cytostatic and antifungal cyclodepsipeptides from *Chondromyces crocatus* (myxobacteria): isolation and structure elucidation. *Liebigs Ann* 1996(2):285-290.

210. Khalil MW, Sasse F, Lünsdorf H, Elnakady YA, & Reichenbach H (2006) Mechanism of action of tubulysin, an antimitotic peptide from myxobacteria. *Chembiochem* 7(4):678-683.

211. Irschik H, Gerth K, Kemmer T, Steinmetz H, & Reichenbach H (1983) The myxovalargins, new peptide antibiotics from *Myxococcus fulvus* (myxobacterales). I. Cultivation, isolation, and some chemical and biological properties. *J Antibiot (Tokyo)* 36(1):6-12.

212. Irschik H & Reichenbach H (1985) The mechanism of action of myxovalargin A, a peptide antibiotic from *Myxococcus fulvus*. *J Antibiot (Tokyo)* 38(9):1237-1245.

213. Steinmetz H, *et al.* (2012) Precursor-directed syntheses and biological evaluation of new elansolid derivatives. *Chembiochem* 13(12):1813-1817.

214. Gerth K, *et al.* (1983) The myxalamids, new antibiotics from *Myxococcus xanthus* (myxobacterales). I. Production, physico-chemical and biological properties, and mechanism of action. *J Antibiot (Tokyo)* 36(9):1150-1156.

215. Kunze B, Höfle G, & Reichenbach H (1987) The aurachins, new quinoline antibiotics from myxobacteria: production, physico-chemical and biological properties. *J Antibiot (Tokyo)* 40(3):258-265.

216. Meunier B, Madgwick SA, Reil E, Oettmeier W, & Rich PR (1995) New inhibitors of the quinol oxidation sites of bacterial cytochromes *bo* and *bd*. *Biochemistry* 34(3):1076-1083.

217. Kunze B, Sasse F, Wieczorek H, & Huss M (2007) Cruentaren A, a highly cytotoxic benzolactone from myxobacteria is a novel selective inhibitor of mitochondrial F_1-ATPases. *FEBS lett* 581(18):3523-3527.

218. Kunze B, *et al.* (2006) Cruentaren, a new antifungal salicylate-type macrolide from *Byssovorax cruenta* (myxobacteria) with inhibitory effect on mitochondrial ATPase activity. *J Antibiot (Tokyo)* 59(10):664-668.

219. Barbier J, *et al.* (2012) Isolierung und Totalsynthese der Icumazole und Noricumazole–antimykotische Antibiotika und Kationenkanalblocker aus *Sorangium cellulosum*. *Angew Chem* 124(5):1282-1286.

220. Kunze B, *et al.* (1993) Thiangazole, a new thiazoline antibiotic from *Polyangium* sp. (myxobacteria): production, antimicrobial activity and mechanism of action. *J Antibiot (Tokyo)* 46(11):1752-1755.

221. Jahns C, *et al.* (2012) Pellasoren: structure elucidation, biosynthesis, and total synthesis of a cytotoxic secondary metabolite from *Sorangium cellulosum*. *Angew Chem Int Ed* 51(21):5239-5243.

222. Kelly DJ, Hughes NJ, & Poole RK (2001) Microaerobic physiology: aerobic respiration, anaerobic respiration, and carbon dioxide metabolism. In: *Helicobacter pylori*: physiology and genetics, ed Mobley HLT, Mendz GL & Hazell SL. *Washington (DC): ASM Press* Chapter 10.

223. Nagata K, Sone N, & Tamura T (2001) Inhibitory activities of lansoprazole against respiration in *Helicobacter pylori*. *Antimicrob Agents Chemother* 45(5):1522-1527.

224. Baer W, Koopmann H, & Wagner S (1993) Effects of substances inhibiting or uncoupling respiratory-chain phosphorylation of *Helicobacter pylori*. *Zentralbl Bakteriol* 280(1):253-258.

225. Chen M, Andersen LP, Zhai L, & Kharazmi A (1999) Characterization of the respiratory chain of *Helicobacter pylori*. *FEMS Immunol Med Microbiol* 24(2):169-174.

226. Kelly DJ (1998) The physiology and metabolism of the human gastric pathogen *Helicobacter pylori*. *Adv Microb Physiol* 40:137-189.

227. Iwatani S, *et al.* (2014) Identification of the genes that contribute to lactate utilization in *Helicobacter pylori*. *PLoS One* 9(7):e103506.

228. Jurkiewicz E, *et al.* (1992) Three new potent HIV-1 inhibitors from myxobacteria. *Antiviral Chem Chemother* 3(4):189-193.

229. Wipf P & Venkatraman S (1995) Total synthesis of (-)-thiangazole and structurally related polyazoles. *J Org Chem* 60(22):7224-7229.

230. Odenbreit S, Gebert B, Püls J, Fischer W, & Haas R (2001) Interaction of *Helicobacter pylori* with professional phagocytes: role of the *cag* pathogenicity island and translocation, phosphorylation and processing of CagA. *Cell Microbio* 3(1):21-31.

231. Selbach M*, et al.* (2003) The *Helicobacter pylori* CagA protein induces cortactin dephosphorylation and actin rearrangement by c-Src inactivation. *EMBO J* 22(3):515-528.

232. Mueller D*, et al.* (2012) c-Src and c-Abl kinases control hierarchic phosphorylation and function of the CagA effector protein in Western and East Asian *Helicobacter pylori* strains. *J Clin Invest* 122(4):1553-1566.

233. Bauer B, Moese S, Bartfeld S, Meyer TF, & Selbach M (2005) Analysis of cell type-specific responses mediated by the type IV secretion system of *Helicobacter pylor*i. *Infect Immun* 73(8):4643-4652.

234. Charpentier X*, et al.* (2009) Chemical genetics reveals bacterial and host cell functions critical for type IV effector translocation by *Legionella pneumophila*. *PLoS Pathog* 5(7):e1000501.

235. Pechous RD & Goldman WE (2015) Illuminating targets of bacterial secretion. *PLoS Pathog* 11(8):e1004981.

236. Suzuki M*, et al.* (2011) Attenuated CagA oncoprotein in *Helicobacter pylori* from Amerindians in Peruvian Amazon. *J Biol Chem* 286(34):29964-29972.

237. Pan NJ, Brady MJ, Leong JM, & Goguen JD (2009) Targeting type III secretion in *Yersinia pestis*. *Antimicrob Agents Chemother* 53(2):385-392.

238. Schneider S*, et al.* (2011) Complex cellular responses of *Helicobacter pylori*-colonized gastric adenocarcinoma cells. *Infect Immun* 79(6):2362-2371.

239. De Jong MF, Sun Y-H, Den Hartigh AB, Van Dijl JM, & Tsolis RM (2008) Identification of VceA and VceC, two members of the VjbR regulon that are translocated into macrophages by the *Brucella* type IV secretion system. *Mol Microbiol* 70(6):1378-1396.

240. Carey KL, Newton HJ, Lührmann A, & Roy CR (2011) The *Coxiella burnetii* Dot/Icm system delivers a unique repertoire of type IV effectors into host cells and is required for intracellular replication. *PLoS Pathog* 7(5):e1002056.

241. Marchesini MI, Herrmann CK, Salcedo SP, Gorvel J-P, & Comerci DJ (2011) In search of *Brucella abortus* type IV secretion substrates: screening and identification of four proteins translocated into host cells through VirB system. *Cell Microbio* 13(8):1261-1274.

242. Zhu W*, et al.* (2011) Comprehensive identification of protein substrates of the Dot/Icm type IV transporter of *Legionella pneumophila*. *PLoS One* 6(3):e17638.

243. Dewoody R, Merritt PM, & Marketon MM (2013) YopK controls both rate and fidelity of Yop translocation. *Mol Microbiol* 87(2):301-317.

244. Saito H*, et al.* (2005) Roles of *virD4* and *cagG* genes in the *cag* pathogenicity island of *Helicobacter pylori* using a Mongolian gerbil model. *Gut* 54(5):584-590.

245. Nagai H*, et al.* (2005) A C-terminal translocation signal required for Dot/Icm-dependent delivery of the *Legionella* RalF protein to host cells. *Proc Natl Acad Sci U S A* 102(3):826-831.

246. Bagnoli F, Buti L, Tompkins L, Covacci A, & Amieva MR (2005) *Helicobacter pylori* CagA induces a transition from polarized to invasive phenotypes in MDCK cells. *Proc Natl Acad Sci U S A* 102(45):16339-16344.

247. Pelz C, Steininger S, Weiss C, Coscia F, & Vogelmann R (2011) A novel inhibitory domain of *Helicobacter pylori* protein CagA reduces CagA effects on host cell biology. *J Biol Chem* 286(11):8999-9008.

248. Schulein R*, et al.* (2005) A bipartite signal mediates the transfer of type IV secretion substrates of *Bartonella henselae* into human cells. *Proc Natl Acad Sci U S A* 102(3):856-861.

249. Lang S*, et al.* (2010) Molecular recognition determinants for type IV secretion of diverse families of conjugative relaxases. *Mol Microbiol* 78(6):1539-1555.

250. Pantoja M, Chen L, Chen Y, & Nester EW (2002) *Agrobacterium* type IV secretion is a two-step process in which export substrates associate with the virulence protein VirJ in the periplasm. *Mol Microbiol* 45(5):1325-1335.

251. Locht C, Coutte L, & Mielcarek N (2011) The ins and outs of pertussis toxin. *FEBS J* 278(23):4668-4682.

252. Jakubowski SJ, Cascales E, Krishnamoorthy V, & Christie PJ (2005) *Agrobacterium tumefaciens* VirB9, an outer-membrane-associated component of a type IV secretion system, regulates substrate selection and T-pilus biogenesis. *J Bacteriol* 187(10):3486-3495.

253. Pettersson J*, et al.* (1996) Modulation of virulence factor expression by pathogen target cell contact. *Science* 273(5279):1231-1233.

254. Jungblut P, *et al.* (2000) Comparative proteome analysis of *Helicobacter pylori*. *Mol Microbiol* 36(3):710-725.

255. Merrell DS, *et al.* (2003) Growth phase-dependent response of *Helicobacter pylori* to iron starvation. *Infect Immun* 71(11):6510-6525.

256. Tan S, Noto JM, Romero-Gallo J, Peek Jr RM, & Amieva MR (2011) *Helicobacter pylori* perturbs iron trafficking in the epithelium to grow on the cell surface. *PLoS Pathog* 7(5):e1002050.

257. Alder NN & Theg SM (2003) Energy use by biological protein transport pathways. *Trends Biochem Sci* 28(8):442-451.

258. Paul K, Erhardt M, Hirano T, Blair DF, & Hughes KT (2008) Energy source of flagellar type III secretion. *Nature* 451(7177):489-492.

259. Wilharm G, *et al.* (2004) *Yersinia enterocolitica* type III secretion depends on the proton motive force but not on the flagellar motor components MotA and MotB. *Infect Immun* 72(7):4004-4009.

260. Wang HJ, Cheng WC, Cheng HH, Lai CH, & Wang WC (2012) *Helicobacter pylori* cholesteryl glucosides interfere with host membrane phase and affect type IV secretion system function during infection in AGS cells. *Mol Microbiol* 83(1):67-84.

261. Li JW-H & Vederas JC (2009) Drug discovery and natural products: end of an era or an endless frontier? *Science* 325(5937):161-165.

262. Sayer JR, *et al.* (2014) 2-and 3-substituted imidazo[1, 2-a]pyrazines as inhibitors of bacterial type IV secretion. *Bioorg Med Chem* 22(22):6459-6470.

263. Paschos A, *et al.* (2011) An *in vivo* high-throughput screening approach targeting the type IV secretion system component VirB8 identified inhibitors of *Brucella abortus* 2308 proliferation. *Infect Immun* 79(3):1033-1043.

264. Fernandez-Lopez R, *et al.* (2005) Unsaturated fatty acids are inhibitors of bacterial conjugation. *Microbiology* 151(Pt 11):3517-3526.

265. Hilleringmann M, *et al.* (2006) Inhibitors of *Helicobacter pylori* ATPase Cagα block CagA transport and *cag* virulence. *Microbiology* 152(Pt 10):2919-2930.

266. Pinkner JS, *et al.* (2006) Rationally designed small compounds inhibit pilus biogenesis in uropathogenic bacteria. *Proc Natl Acad Sci U S A* 103(47):17897-17902.

267. Baron C (2010) Antivirulence drugs to target bacterial secretion systems. *Curr Opin Microbiol* 13(1):100-105.

268. Getino M, *et al.* (2015) Synthetic fatty acids prevent plasmid-mediated horizontal gene transfer. *MBio* 6(5):e01032-15.

269. Tan S, Tompkins LS, & Amieva MR (2009) *Helicobacter pylori* usurps cell polarity to turn the cell surface into a replicative niche. *PLoS Pathog* 5(5):e1000407.

270. Myers JD & Kelly DJ (2004) Respiratory electron transport in *Helicobacter* and *Campylobacter*. In: Respiration in archaea and bacteria: diversity of prokaryotic respiratory systems, ed Zannoni D. *Springer Netherlands, Dordrecht* Chapter 3.

271. Weerakoon DR & Olson JW (2008) The *Campylobacter jejuni* NADH:ubiquinone oxidoreductase (complex I) utilizes flavodoxin rather than NADH. *J Bacteriol* 190(3):915-925.

272. Tanigawa M, *et al.* (2009) D-amino acid dehydrogenase from *Helicobacter pylori* NCTC 11637. *Amino Acids* 38(1):247-255.

273. Tanigawa M, *et al.* (2010) Purification of *Helicobacter pylori* NCTC 11637 cytochrome bc_1 and respiration with D-proline as a substrate. *J Bacteriol* 192(5):1410-1415.

274. Rektorschek M, Weeks D, Sachs G, & Melchers K (1998) Influence of pH on metabolism and urease activity of *Helicobacter pylori*. *Gastroenterology* 115(3):628-641.

275. Iwahi T, *et al.* (1991) Lansoprazole, a novel benzimidazole proton pump inhibitor, and its related compounds have selective activity against *Helicobacter pylori*. *Antimicrob Agents Chemother* 35(3):490-496.

276. Cook GM, Greening C, Hards K, & Berney M (2014) Energetics of pathogenic bacteria and opportunities for drug development. *Adv Microb Physiol* 65:1-62.

277. Goodwin CS, Blake P, & Blincow E (1986) The minimum inhibitory and bactericidal concentrations of antibiotics and anti-ulcer agents against *Campylobacter pyloridis*. *J Antimicrob Chemother* 17(3):309-314.

278. Friedrich T, *et al.* (1994) Two binding sites of inhibitors in NADH: ubiquinone oxidoreductase (complex I). *Eur J Biochem* 219(1-2):691-698.

279. Oettmeier W, *et al.* (1990) The aurachins, naturally occurring inhibitors of photosynthetic electron flow through photosystem II and the cytochrome b_6/f-complex. *Z Naturforsch* 45(5):322-328.

280. McGowan CC, Cover TL, & Blaser MJ (1997) Analysis of F_1F_0-ATPase from *Helicobacter pylori*. *Infect Immun* 65(7):2640-2647.

281. Duckworth MJ, Okoli AS, & Mendz GL (2014) Novel *Helicobacter pylori* therapeutic targets: the unusual suspects. *Expert Rev Anti Infect Ther* 7(7):835-867.

282. Olson JW & Maier RJ (2002) Molecular hydrogen as an energy source for *Helicobacter pylori*. *Science* 298(5599):1788-1790.

283. Ge Z (2002) Potential of fumarate reductase as a novel therapeutic target in *Helicobacter pylori* infection. *Expert Opin Ther Targets* 6(2):135-146.

284. Inatsu S, Ohsaki A, & Nagata K (2006) Idebenone acts against growth of *Helicobacter pylori* by inhibiting its respiration. *Antimicrob Agents Chemother* 50(6):2237-2239.

285. Nagata K, *et al.* (2010) The bifidogenic growth stimulator inhibits the growth and respiration of *Helicobacter pylori*. *Helicobacter* 15(5):422-429.

Acknowledgment

At first, I would like to thank Prof. Dr. Rainer Haas for giving me the opportunity to perform my PhD thesis in his group and the transfer of the exciting theme. I especially thank him for his confidence, his scientific guidance as well as for the freedom to work on many interesting topics.

Above all, I want to thank PD Dr. Wolfgang Fischer for his excellent and instructive support. I thank him for his encouragement to turn ideas into action and all the helpful discussions during the creation of my work. His scientific advice and backing helped me to successfully complete this project.

I very much thank Evelyn Weiss for her outstanding technical assistance especially in the generation of various mutants. Her infinite willingness to help as well as her personal support were essentially involved in the success of this work.

I would like to thank all collaboration partners within the German Center of Infection Research (DZIF) for the informative input. I give thanks especially to Prof. Dr. Ursula Bilitewski for providing various substances and any helpful advice.

My sincere thanks also go to all my colleagues of the AG Haas for the enjoyable time in the lab. In particular, I thank Bea, Ben, Eva, Evelyn, Friederike, Lea, Luisa, Verena, Ute, Wolfgang and Qing for all the help and fun from the day I started. I also give thanks to the people for the nice time who joined the group during my PhD including Ciara, Desirée, Gudrun, Ina, Katrin and Kristina. I want to especially thank Ciara for proof-reading the manuscript.

Moreover, I want to thank all employees of the Max von Pettenkofer-Institute for the pleasant working atmosphere.

Finally, I want to thank my family and friends, without whom I could not have done this whole project. Especially, I give thanks to Thomas for his patience, continuous support and understanding.